MICROSTRUCTURAL AND ENVIRONMENTAL EFFECTS ON FRETTING FATIGUE

A Dissertation

presented to

the Faculty of the Graduate School

University of Missouri

In Partial Fulfillment

of the Requirement for the Degree

Doctor of Philosophy

BY

Roger Keith Reeves

May 1977

Dissertation Supervisor Professor David W. Hoeppner

The undersigned, appointed by the Dean of the Graduate Faculty, have examined a thesis entitled

Microstructural And Environmental Effects On Fretting Fatigue

presented by

Roger Reeves

a candidate for the degree of

Doctor of Philosophy

and hereby certify that in their opinion it is worthy of acceptance.

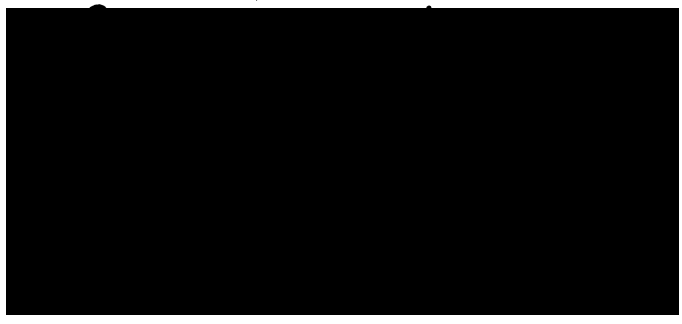

MICROSTRUCTURAL AND ENVIRONMENTAL EFFECTS ON FRETTING FATIGUE

Roger Keith Reeves

Dr. David W. Hoeppner Dissertaion Supervisor

ABSTRACT

One of the primary causes of premature fatigue failures is a phenomenon known as fretting. The research leading to this paper consisted of developing information regarding microstructural and environmental effects on fretting fatique of a .40/.50 carbon steel. Microstructural effects are discussed in terms of stress/life data, crack growth data, and fractographic analysis of two microstructures. The effect of environment is analyzed through data from these two microstructures being tested in lab air and vacuum. The hypothesis developed is that the microstructure plays an important part in the initial stages of fretting damage and that the mechanical damage is responsible for the largest portion of the decrease in fatigue life.

ACKNOWLEDGMENTS

The research leading to this dissertation was completed under the Office of Naval Research contract number ONR N00014-75-C-0670. The support of Dr. David Hoeppner, Dr. Phillip Clarkin of ONR, and the Office of Naval Research is acknowledged as the work could not have been completed without their continuing assistance.

I would like to thank many members of the faculty of the College of Engineering for their patience and determination in the classroom during my coursework, especially Drs. Cenap Oran, Roger Duffield, Paul Braisted, and Donald Creighton.

I would like to acknowledge the outstanding efforts of both the Mechanical Engineering and Science Instruments machine shops at the University of Missouri - Columbia, especially Mr. Larry Clark and Mr. Hugh Maxwell.

A special thanks is extended to Gary Salivar, Art Braun, Gregg Bogucki, Larry Mueller, and John Sweigart for their assistance in the development of the experimental apparatus and techniques.

Most of all, my sincerest appreciation is extended to my wife, Becky, and daughter, Christine, for their personal sacrifices and moral support throughout the period of this research.

TABLE OF CONTENTS

NOMENCLATURE

2a	Crack length. (in)
a_o	Interatomic spacing. (A)
B	Thickness. (in, mm, m)
b	Fatigue strength exponent.
c	Fatigue ductility exponent.
C	Material parameter.
C	Compliance. (in, mm, m)
D	Grain diameter.
da/dt	Crack growth rate based on time.
da/dN	Crack growth rate based on number of cycles.
E	Modulus of elasticity for axial loading (Young's Modulus).
e	Weibull threshold parameter.
e	Engineering strain.
exp	Base of natural logarithms (2.718).
G	Modulus of elasticity in shear (modulus of rigidity).
k	Weibull shape parameter.
K	Stress intensity factor.
K_B	Stress intensity range at unstable crack growth.
K_{Ic}	Plane strain fracture toughness.
K_c	Plane stress fracture toughness.
K_q	Gereralized fracture toughness.
ΔK	Stress intensity range.
K_f	Fatigue stress concentration factor or fatigue strength reduction factor.

K_t	Theoretical stress concentration factor.
ln	Natural logarithm.
log	Logarithm to base 10.
N	Number of cycles.
$2N_f$	Life in number of cycles for strain cycling.
n	Exponent; material parameter.
P	Load or external force.
R	Stress ratio in fatique; radius of curvature.
S_a	Alternating stress ($S_{max} - S_{mean}$).
ΔS	Stress range ($S_{max} - S_{min}$).
S_{max}	Maximum applied stress.
S_{mean}	Mean stress ($[S_{max} + S_{min}]/2$).
S_{min}	Minimum applied stress.
S_e	Fatigue limit or endurance limit for completely reversed loading.
S_y	Yield stress in tension.
S_u	Ultimate tensile strength.
T	Temperature.
t	Time; thickness.
U_E	Elastic strain energy.
U_S	Total surface energy.
V	Weibull characteristic value parameter
W	Width
γ	Shear strain; surface energy.
Δ	Finite change.

δ	Deformation; elongation; deflection; incremental change.
ε	True strain.
$\Delta\varepsilon$	Strain range.
ε'_f	Fatigue ductility coefficient.
λ	Wavelength.
μ	Coefficient of friction.
ν	Poisson's ratio.
ρ	Density.
σ	Stress.
$\sigma_1, \sigma_2, \sigma_3$	Principal stresses.
σ_{max}	Theoretical cohesive strength.
τ	Shear stress.
τ_{max}	Maximum shear stress.

LIST OF TABLES

LIST OF FIGURES

Page

Page

Page

Page

1.0 INTRODUCTION

1.1 OBJECTIVE

The main objective of this study is to establish a better understanding of fretting fatigue and its mechanisms. The objective becomes threefold in nature, viz.:

1. Show that fretting fatigue is dependent upon microstructure and environment.
2. Determine the relative dependence of fretting fatigue life on environmental and mechanical damage.
3. Establish an explanation of why fatigue and fretting fatigue are dependent upon microstructure and environment.

1.2 BACKGROUND

The problem of fatigue is widely recognized today as a major cause of structural failure. In addition to this, it is commonly found that structural members do not live up to their expected fatigue life specifications due to some synergistic effect, frequently not accounted for in the initial design. One of the primary causes of such premature fatigue failures is a phenomenon known as fretting.

The problem of fretting fatigue is rapidly becoming of major imprtance in many structural components. Various fasteners, usually in conjunction with vibrations, provide the majority of fretting fatigue failures. However, the failure of other components such as bearings, rotors, and gears also seems related to fretting damage.

Some information has been made available through various studies pertaining to many of the variables that affect fretting fatigue, however the basic mechanisms by which fretting fatigue occurs are avoided. In order to better prepare for providing information on the basic mechanisms of fretting fatigue, the following sections present a technical discussion of fatigue and fretting fatigue.

2.0 TECHNICAL DISCUSSION

The technical discussion is divided into four parts: a background and discussion of fatigue; a background and discussion of fretting fatigue including hypothesized microstructural and environmental influences; a treatise on fracture mechanics and its application to fretting fatigue; and a discussion of the contact stress problem associated with the various types of wear phenomena.

2.1 FATIGUE

Fatigue is progressive localized failure of a material under repeated loading; the loading being less than that required to cause failure during a single application. Estimates of the amount of service failures due to fatigue are varied but range up to ninety percent (90%). Since the percentage of service failures due to fatigue is large, it seems that the majority of the technical community, working in the area of prevention of service failures, should be concentrating their efforts on and lending their support to uncovering the unknowns of the fatigue porcess. At the present time fatigue is analyzed in three different veins: strain cycling; stress cycling; and crack growth.

The following sections will describe strain cycling, stress cycling, crack growth, and some of the theories of fatigue. Stain cycling aspects of fatigue will be considered only breifly since the results presented in this report deal exculsively with stress cycling

(stress/life) and crack growth.

2.1.1 STRAIN CYCLING

The concept of strain cycling fatigue is based on test methods in which the amount or amplitude of strain is recorded and controlled throughout the life of the test sample. Strain cycling is of little or no use unless the material enters the range of macroscopic plastic deformation. In view of this, strain cycling is usually confined to the realm of "low cycle" fatigue (i.e. the region in which the loads are large enough to cause permanent deformation within the material).

The sequence of events in strain cycling fatigue is usually as follows:

1. The material is trained into its "plastic" range so that it is, "locally", permanently deformed.
2. The strain is released or reversed.
3. The strain is reapplied.

Upon releasing the load it can be seen, Figure 1, that the stress/strain (load/deformation) curve does not reverse itself exactly, but actually follows a new path. When the stress (load) reaches zero, the amount of plastic strain (permanent deformation) can be found for the material. Generally, upon reapplying the load, the yield stress in tension is increased by strain hardening from point A to B and the compressive strength is decreased from point C to D (Figure 1); this phenomenon is known as the Bauschinger effect [1]*.

*Number in brackets refer to references.

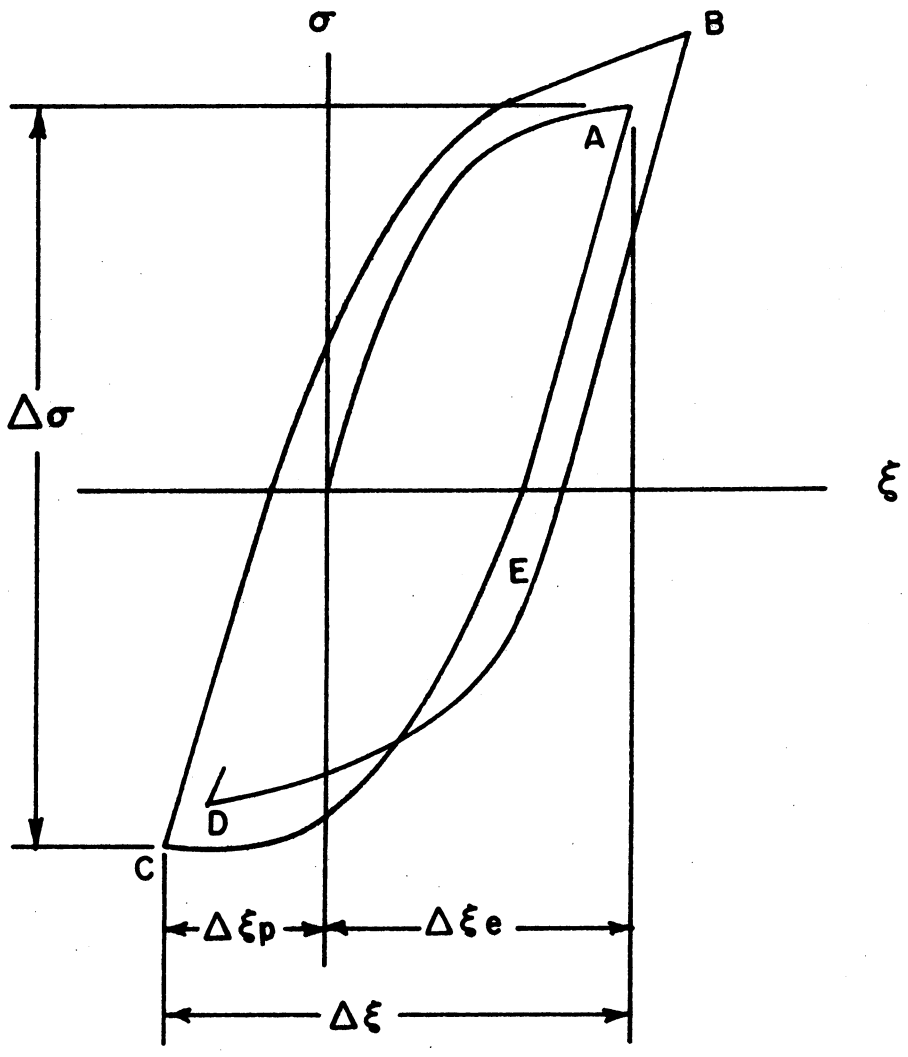

Figure 1. Cyclic Stress-Strain response (hysteresis).

The strain cycling approach to fatigue analysis is claimed by some to have conceptual and computational advantages over a stress cycling approach. Upon initial observation, this claim seems valid since strain is a physical quantity, whereas stress is a derived quantity. The fault of this concept is that an average value of strain (or strain amplitude) due to the applied load is used instead of values of the more important localized strain.

Strain cycling is presented in graphical form by plotting strain range versus number of cycles to failure. A curve of this type is shown in Figure 2 (usually generated from experimental data); as shown, the curve is then expressed "conservatively" by straight lines. An equation [2] can then be applied for computational purposes:

$$\frac{\Delta\varepsilon}{2} = \frac{\sigma'_f}{E} (2N_f)^b + \varepsilon'_f (2N_f)^c \qquad (1)$$

therefore, by knowing the strain amplitude, a prediction can be made for the life, or vice-versa.

Strain cycling analysis of fatigue behavior of materials is useful in the study of the low cycle region; that is the region where strain amplitudes are large and lives are short. In this region the accuracy of the strain measurements is not affected as much as in the long life/ low strain amplitude region. In the long life region, although average strain amplitudes are low, localized strains may be large.

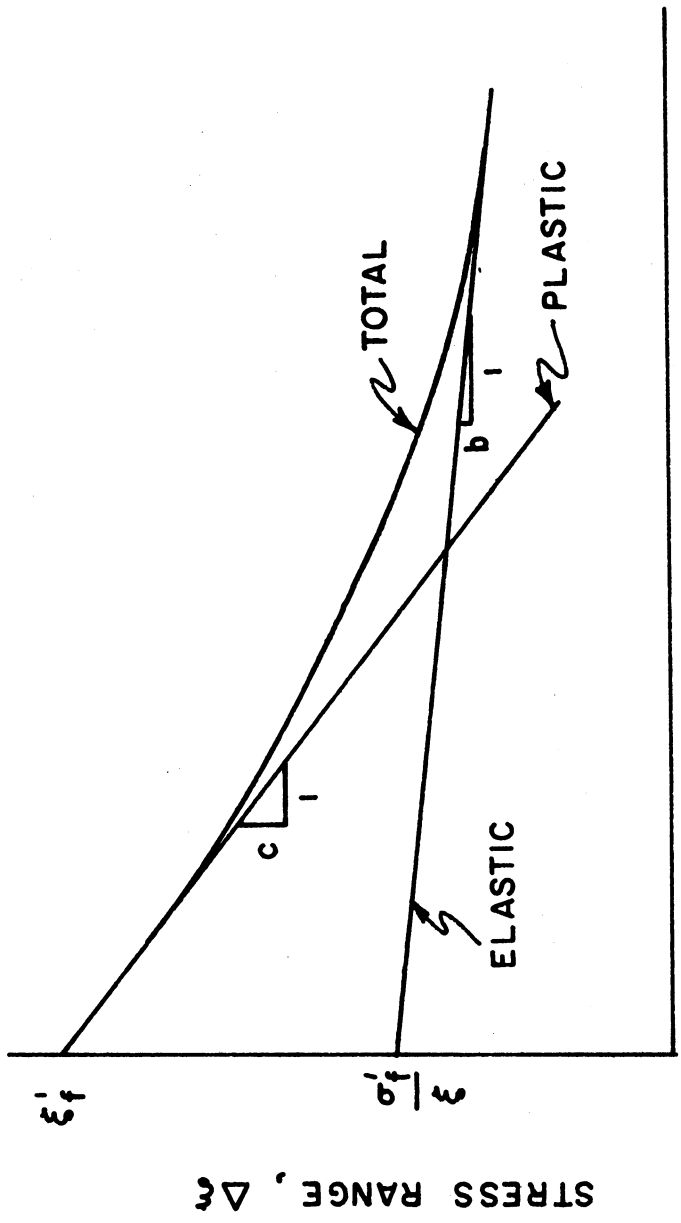

Figure 2. Reversals to failure for given strain amplitudes.

2.1.2 STRESS CYCLING

Stress cycling (stress/life) has been the most widely used approach in studying the problem of fatigue. Much of the data from past stress cycling experiments have been generated on R. R. Moore rotating beam fatigue machines and are presented in the form of stress versus life (S-N) curves.

In the rotating beam tests the applied load or stress is completly reversed from positive to negative as shown in Figure 3. Since this loading often does not nearly simulate actual component loading, the axially loaded fatigue test was devised. In axially loaded fatigue testing the loading takes on the general characteristics shown in Figure 4. Figures 3 and 4 exemplify much of the nomenclature used in stress cycling fatigue. Random load applications can also be made by a computer controlled actuating system and may more nearly represent actual service loads. An example of service loading for a given component is presented in Figure 5.

Ther results presented in this report are from axially loaded fatigue specimens; however the data from each of these tests may be presented in the form of stress/life curves. Stress/life curves normally present the dependence of the life of the specimen on the maximum applied stress. This dependence, as seen in Figure 6, is that the life increases with decreasing applied stress.

The life of a specimen as taken from a stress/life curve is composed of the number of cycles to initiate a crack and the number of cycles to propagate the crack completely through the specimen.

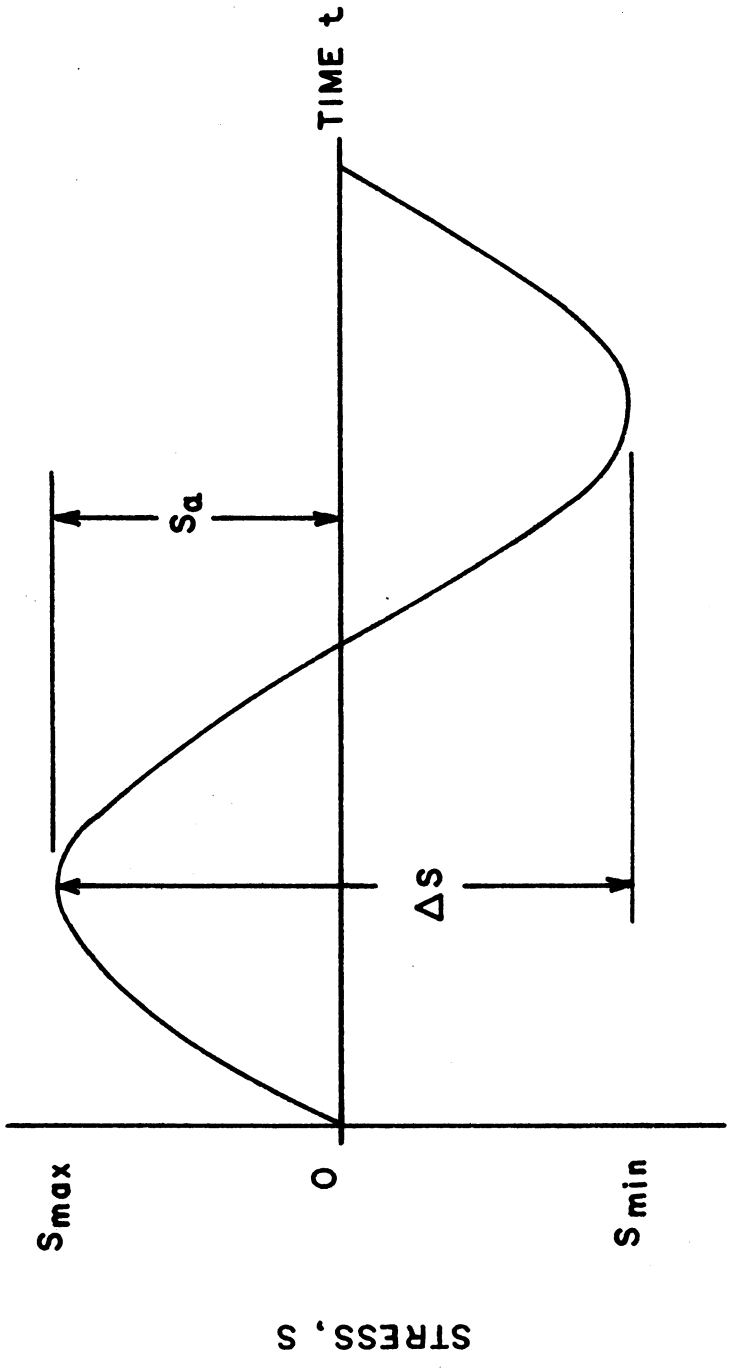

Figure 3. Completely reversed stress cycle.

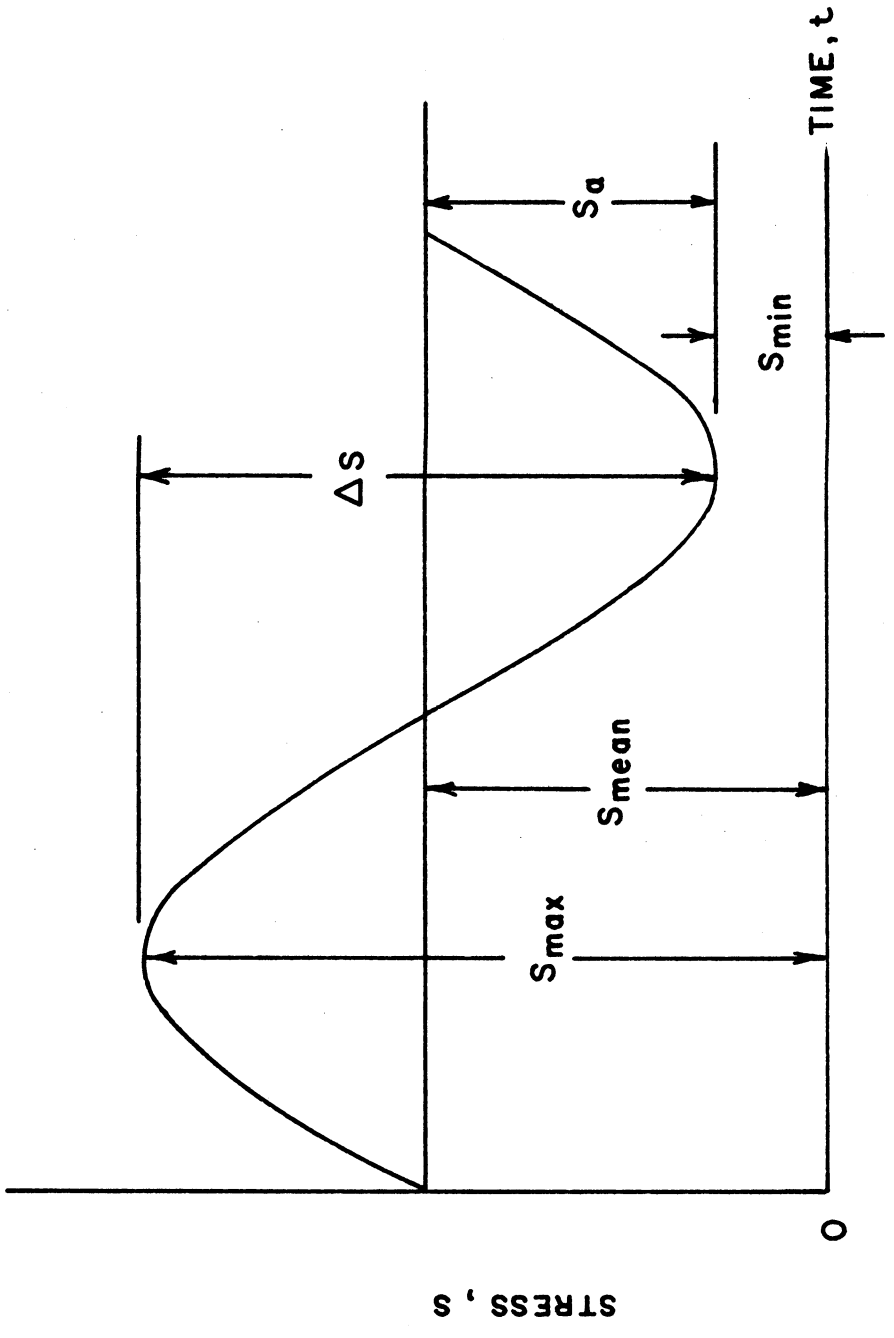

Figure 4. Tension-tension stress cycle.

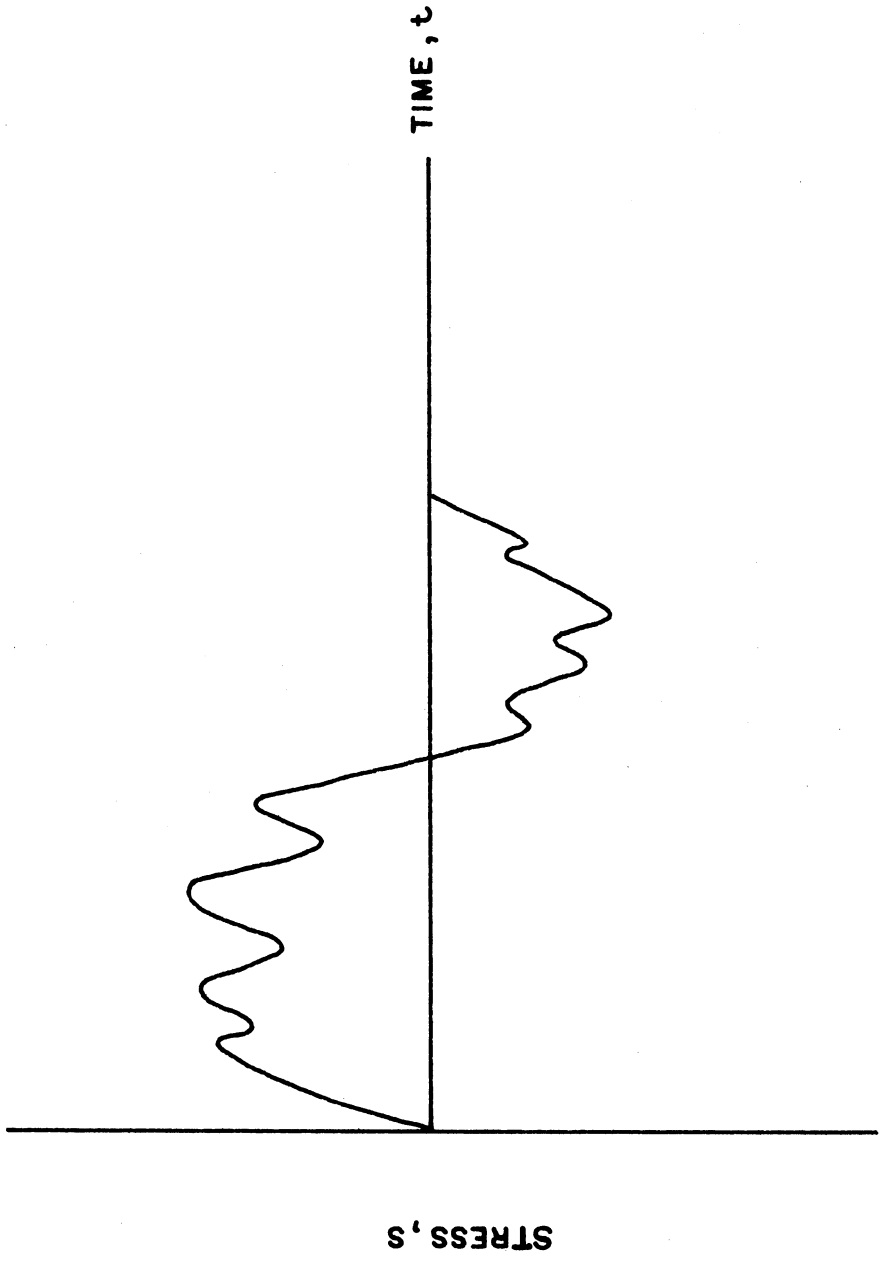

Figure 5. Random stress cycle.

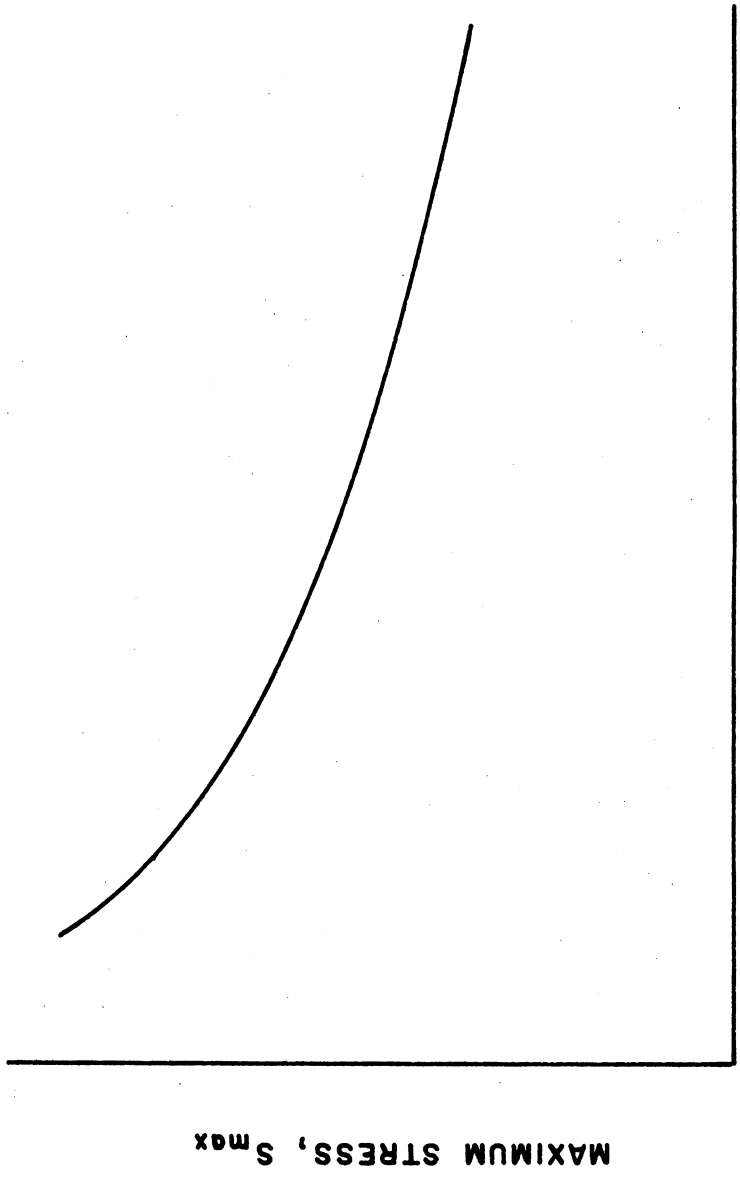

Figure 6. Reversals to failure for given maximum stresses.

Normally a distinction between cycles to initiate a crack and cycles to propagate the crack is not made. From this it can be concluded that stress/life curves, like strain/life curves, frequently treat fatigue as an end event.

The only obvious information obtainable from stress/life curves is how long a component or test specimen can be expected to last under some given conditions. This means of presenting data is particularly useful in comparing various effects on fatigue life.

2.1.3 CRACK GROWTH

Since fatigue is a progressive event, an analysis of crack growth mechanisms is becoming the most popular approach to fatigue design methodology. The fatigue process is broken into three basic regions:

i) Initiation

ii) Propagation

iii) Final Fracture

The separation of these categories remains somewhat obscure, especially between the realms of initiation and propagation.

For the purposes of this report the initiation of a crack will be considered as that portion of the component's life during which the rate of crack extension is zero and has never exceeded zero:

$$da/dt = 0 \qquad (2)$$

(Note: There are times when the rate of crack extension apparently

goes to zero after some crack extension has taken place; when this occurs, it will still be taken as in the region entitled propagation.)

The propagation region consists of that portion of a component's life after the rate of crack extension has taken some finite value:

$$da/dt > 0 \tag{3}$$

This region extends until the crack growth rate becomes unstable (i.e., the rate of crack extension approaches infinity, $da/dt \to \infty$).

The last region of the fatigue process, final fracture, occurs very rapidly. This region consists of that portion of the component's life beginning when the crack growth rate becomes unstable and ending when the component is in two or more pieces. (Frequently a component's "useful" life is over before the final fracture region is ever reached.) Some significance may be attached to the final fracture condition, determined by either the fracture toughness or fracture strength, since this information may lead to an assessment of the damage tolerance of a given material in a given structure.

A typical crack growth curve is shown in Figure 7. Each of the three regions is illustrated in Figure 7 by showing the values of the crack extension rate. Crack growth curves are normally presented as time (or number of cycles) to attain a specific crack size.

It seems intuitively obvious that a method based on a fundamental mechanism such as the extension of a crack (or flaw) would be most desirable in the study of fatigue since fatigue actually involves this

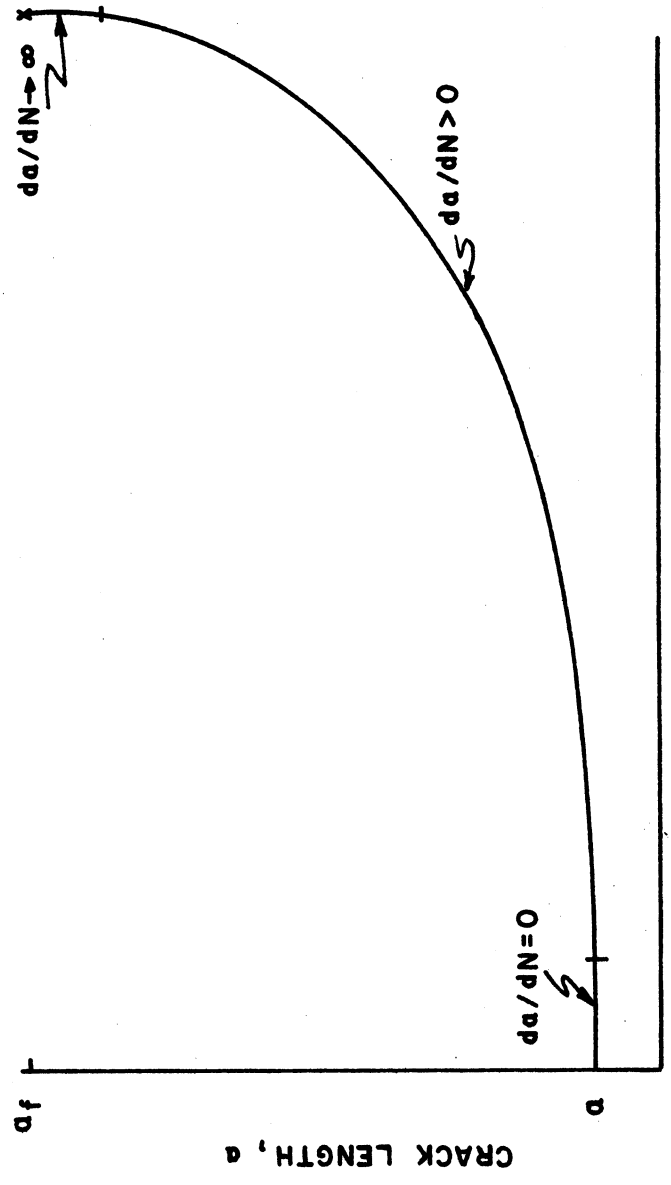

Figure 7. Crack growth curve.

type of progression of events. Thus, explanations contained within this paper will rely heavily on concepts from the crack growth analysis of fatigue with additional references being made to the stress cycling analysis of fatigue.

2.1.4 PHYSICAL BASES OF FATIGUE

Since the beginning of the twentieth century several theories have evolved in an effort to explain the fatigue phenomenon. Although most of these theories have evolved through genuine concern for bringing about a better understanding of fatigue, many have clouded the issue for most engineers. Five theories or physical bases are presented here to give an historical view of the progress made.

Theory of Ewing and Humfrey [3]

The theory of Ewing and Humfrey was developed during their study on the effect of alternating stresses on the structure of metals. They observed the groth of slip bands within the crystals during the fatigue loadings. The slip bands increased in number and size with further fatigue loading. Failure was then attributed to a process of attrition brought about by slipping surfaces becoming increasingly abraded due to the alternating loading. During this process, they noted a decrease in the cohesion between the slipping surfaces until a crack, which spread from crystal to crystal to cause failure, was finally observed.

Theory of Gough and Hanson [4]

The work of Gough and Hanson was an extension of previous work, *such as that of Ewing and Humfrey. They began their work by hypothe*sizing that the appearance of slip bands did not necessarily indicate that the applied range of loading (or stress) was greater than the fatigue range. From this they recognized the fundamental role played by plastic inhomogeneities in fatigue as well as in strain hardening and hysteresis. They further explained that the plastic regions of plastically inhomogeneous materials can become strain hardened by alternating stresses without an overall exteranl strain being detected. They hypothesized that a progressive break-up of the crystal into small fragments would decrease the cohesion of the crystalline planes until finally a crack would appear.

Theory of Orowan [5]

Orowan brought together many of the early works on fatigue and produced one of the earliest accepted explanations regarding the fatigue process. His theory leads to the prediction of the general shape of the stress/life curve, however it does not depend on any specific deformation mechanism other than the concept that fatigue deformation is heterogeneous. Orowan assumes that metals contain small weak regions which may be regions of favorable orientation for slip or high stress concentration. He then assumed that the inhomogeneities in the material can be treated as plastic regions in an elastic matrix. This is brought out through the mechanical analogy given by Orowan as in

Figure 8. The figure illustrates the concept by trating A as a plastic rod, B and B' as the elastic bulk of the specimen, and C as the elastic neighborhood of the plastic region where C is a much weaker spring than B or B'. From this, Orowas explains that the total plastic strain in the weak region may exceed some critical value such that a crack is formed. The crack creates a new plastic inhomogeneity and the process is repeated. This theory is based on a concept of localized strain hardening using up the plasticity of the metal until fracture takes place.

Theory of Wood [6]

Wood's concept of fatigue was one of the first not requiring localized strain hardening for fatigue deformation to occur. He notes that slip bands produced by a fine movement of slip under fatigue loading are smaller than those due to static loading. He leads this into a concept that a large total strain can occur without causing appreciable strain hardening. Slip due to static loading is schematically presented as by Wood in Figure 9. Under fatigue loading the appearance is more that of notches and ridges (Figure 10) due to the back and forth motion of the slip. The intrusions and extrusions of Figure 10 are described as the "starting" of a fatigue crack.

Theory of Hoeppner [7]

Hoeppner presents his theory in three tables dealing with preinitiation, initiation, and propagation. This theory displays the impor-

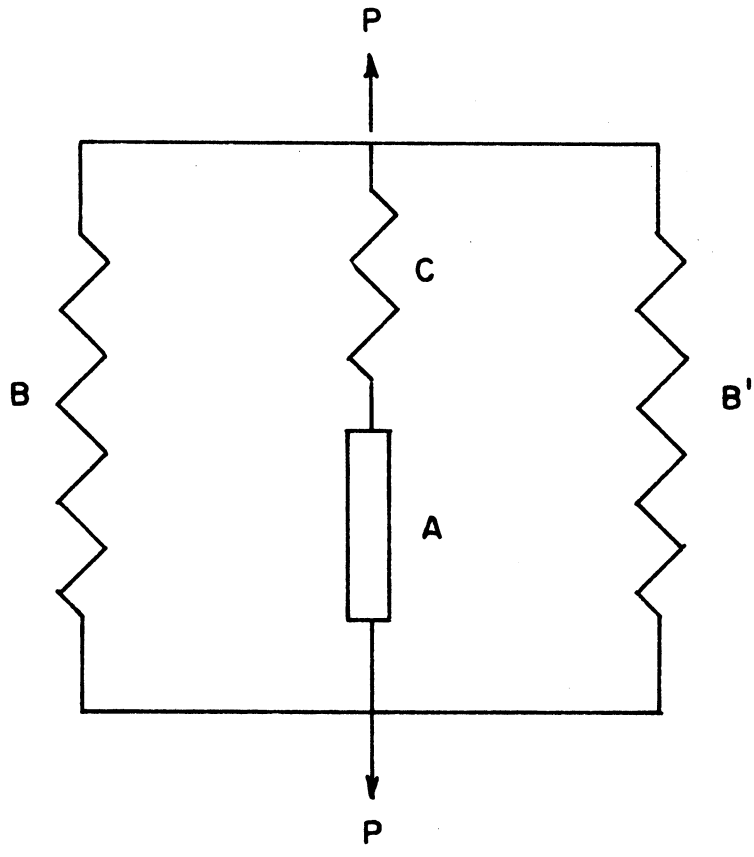

Figure 8. Mechanical model of a plastic inhomogeneity in elastic surroundings.

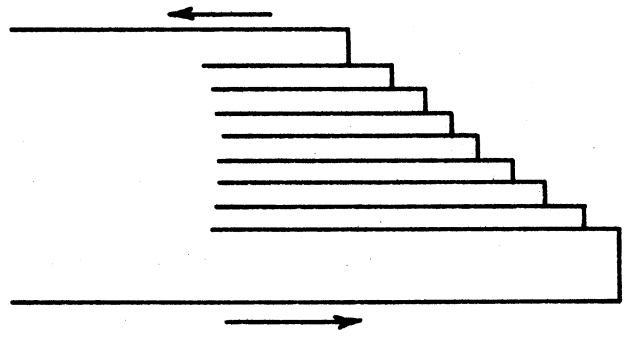

Figure 9. Schematic of slip under static loading.

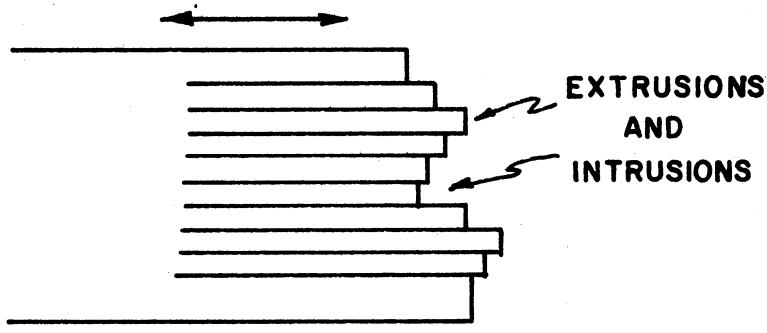

Figure 10. Schematic of slip under fatigue loading.

tance of internal factors on fatigue.

EVENTS LEADING TO FATIGUE CRACK INITIATION

1. Strain hardening or softening takes place.
2. Saturation of strain hardening or softening occurs.
3. Basic tensile properties are changed.
4. Macroscopic strain distribution is altered.
5. Fine slip develops.
6. Intrusions and extrusions form.
7. In some alloys, overaging or resolution of precipitate particles occurs creating local soft spots.
8. Intermetallic constituents crack.
9. Grain boundary cracks develop.
10. Cell structure forms.

INITIATION OF A FATIGUE CRACK

1. Occurs after saturation of hardening or softening.
2. Slip bands develop and "persist".
3. Cracks at intermetallic constituents link up.
4. Local soft spots in some aluminum alloys deform, crack, and cracks link.
5. Pore formation is observed in grain boundaries and cell structure.
6. Initial formation of cracks parallel to slip planes in most cases (also referred to as stage I crack growth).
7. A large portion of the life is used up.

8. Microcracks are influenced greatly by metallurgical discontinuities such as grain boundaries, twin boundaries, inclusions, extrusions, and intrusions.

FATIGUE CRACK PROPAGATION

1. Crack growth takes place perpendicular to the maximum tensile stress.*
2. Cracks are generally transcrystalline but in special circumstances may be intercrystalline.
3. A plastic zone forms at the crack tip, the size and shape of which is influenced by the maximum stress, crack length, and material.
4. Cell structure forms at the tip of the macrocrack.
5. Mechanism of crack propagation in the "macro range" is presumably independent of crystal structure although this point deserves further consideration.
6. Striations are sometimes observed to form on the fracture surface.

From these theories or proposed physical aspects of fatigue, it is readily seen that fatigue is a complicated process that is, even at the present time, not completely understood. The purpose of this research is not to further develop the concepts of fatigue but rather to make use of many of the established practices in establishing a better

*The crack may propagate in the flat (plane strain) mode or the single or double slant (plane stress) mode.

understanding of the effects fretting has on fatigue. Thus, background information and hypothesized effects are presented in the following sections.

2.2 FRETTING FATIGUE

Fretting is normally defined as the damage that occurs when two surfaces in contact, under a normal or clamping load, and nominally at rest experience some relative displacement (Figure 11). When this phenomenon is experienced in conjunction with fatigue the life of the component or test specimen is reduced. The amount of decrease depends on factors ranging from the material involved to the amount of clamping load. It is noted in Figure 12 that the largest decrease in life is at the lower stress levels, thus implying that the decrease in life is directly related to the damage caused by fretting. This relationship has been hypothesized as due to the speed with which a crack is initiated under fretting conditions [8] [9]. As mentioned in section 2.1.2, the stress/life curve is made up of the number of cycles to initiate a crack and the number of cycles to propagate that crack to its final failure. Thus, the major effect of fretting is to eliminate much of the time required to initiate a crack, therefore altering the stress/life curve as in Figure 12.

The incidence of fretting fatigue was first recorded in 1911 when Eden, Rose, and Cunningham reported that they were experiencing failures of their fatigue specimens in the grips of their fatigue machine. They observed at that time that intersurface damage seemed to be

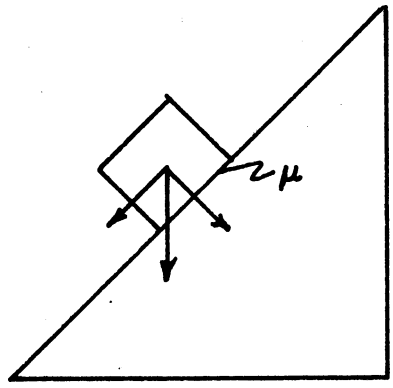

(a)

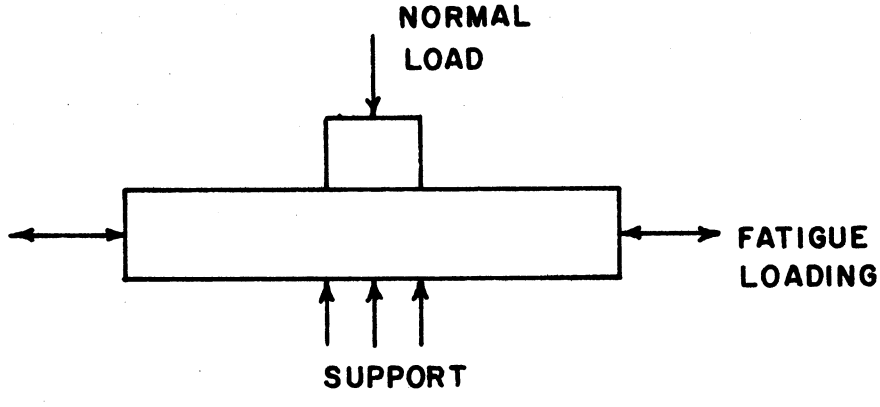

(b)

Figure 11. Friction loading and schematic of fretting fatigue loading.

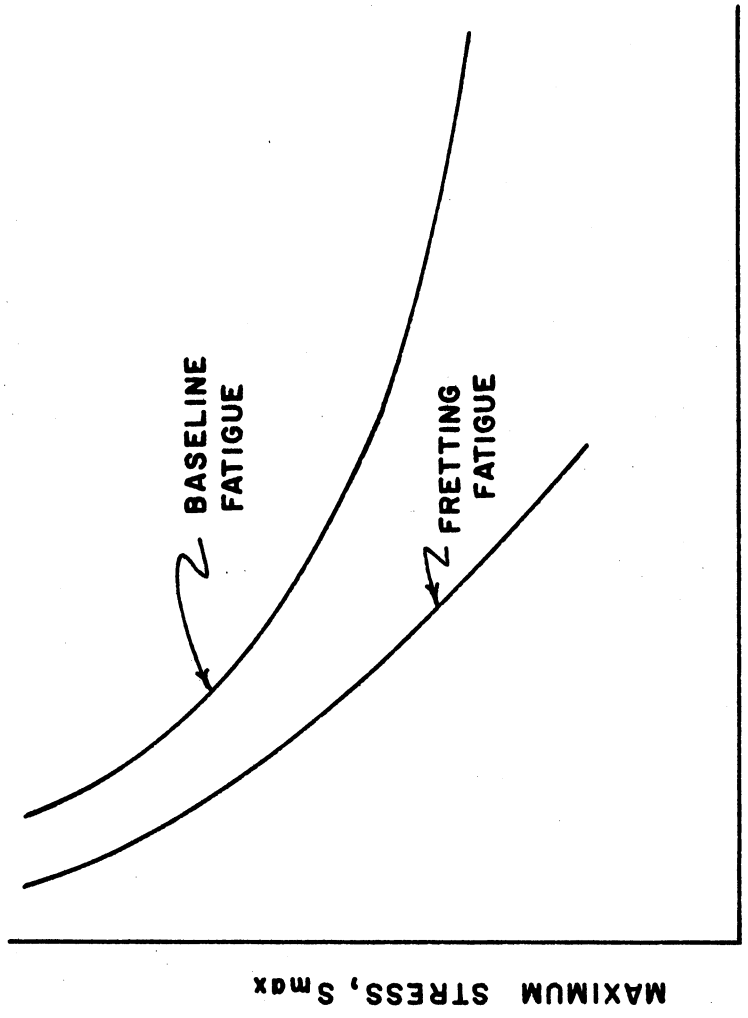

Figure 12. Schematic representation of reduction in fatigue life due to fretting.

associated with the failures. Since this first experience with fretting several theories have evolved [10]:

Theory of Tomlinson

Tomlinson, the first to conduct a systematic study of fretting, hypothesized that fretting resulted from "molecular attrition". He further argued that the cohesive forces between surface molecules resulted in tearing away subsequent oxidation.

Theory of Godfrey et al.

Godfrey et al. employed optical microscopy in attempting to characterize the nature of fretting and establish its mechanism. They concluded that adhesion resulted from contact, and extremely fine particles subsequently were broken loose and oxidized. Another of their findings was that fretting occurs in less than one cycle; consequently, they concluded alternating motion was not a necessary condition for fretting and surface fatigue was not a factor.

Theory of Feng and Rightmire

Feng and Rightmire hypothesized a multi-stage fretting process. It consisted of four stages: (1) Initial stage; (2) transition period; (3) declining stage; and (4) steady state stage.

The process they visualized basically consisted of the breakaway of particles, subsequent oxidation, and abrasion. This process, they believed, reached a steady state (saturation) level when the oxide

layer became very thick.

Theory of Uhlig

Uhlig postulated that both a chemical factor and a mechanical factor are involved in fretting. He further proposed a quantitative expression for fretting damage:

$$W\ (\text{total}) = (k_0 L^{1/2} - K_{1L})\ \frac{C}{f} + k_2 \varepsilon L C \qquad (4)$$

where W is the specimen weight loss, L is the load, C is the number of cycles, f is the frequency, ε is the slip, and k_0, k_1, and k_2 are constants. The equation predicts that the fretting weight loss is a hyperbolic function of frequency.

Theory of Halliday and Hirst

These authors were the first ot employ optical and electron microscopy and electron diffraction to the fretting process. They attempted to define the relationship between fretting and magnitude of slip amplitude. Welding of the surface occurs, according to their observations, and the degree of relative slip influences the result. They showed that fretting was not dependent on the formation of an oxide.

Theory of Waterhouse

Waterhouse, building on concepts expressed earlier by others, believed fretting was much like other wear in that adhesion, the breaking

of welds, and metal transfer occurs. In special cases, oxide play an important part in the process, he believes.

Theory of Wright

Wright, principally through electron microscopic observations, emphasized that oxygen was a principal factor causing fretting damage.

Comyn and Furlani [11] discuss these theories in much greater detail than the above. However, Hoeppner and Goss point out that three principal factors causing fretting are obtained from the above theories:

1. Interaction between contacting surfaces (welding, adhesion, molecular attrition)
2. Oxidation
3. Abrasion

Most of these theories suggest a strong dependence of fretting fatigue on the corrosive action taking place; however this report will suggest that the mechanical surface damage plays a major, if not dominant, role in the fretting fatigue process.

The two main concerns of this investigation are to study the influence of microstructure and environment on fretting fatigue. Microstructural and environmental influences therefore are discussed seperatly from the other variables, the other variables being discussed in section 2.2.3.

2.2.1 MICROSTRUCTURAL INFLUENCES

The effect of microstructure on fatigue has been investigated extensively at the University of Missouri - Columbia over the past two years [12] [13]. The influence of a material's microstructure on its expected fretting fatigue life has been proposed [9] [10], but until now has not been investigated extensively. The microstructural influences on the fretting fatigue process become complex since there are separate influences on fatigue and on fretting.

In the past, it has been observed that, on fretted surfaces, the amount of damage varies over the area of contact [9]. This observation leads to the belief that microstructural orientation has some effect on the amount of damage that can occur. In essence, some portions of the microstructure may be oriented, at the surface, such that the grains are more susceptible to cracking or notching.

During the propagation of cracks under fatigue loading, the orientation of the microstructure influences the ease (or lack thereof) with which the crack may extend. Examples of this are transcrystalline and intercrystalline cracking. The extension of a crack is greatly dependent on the energy required to slip or cleave the material. (This will be discussed more extensively in section 4.3.1).

The microstructure ahead of a crack front will vary in the amount of plastic deformation it will undergo in response to a given loading. Since fatigue is dependent upon loacalized plastic deformation and the amount of localized plastic deformation is dependent upon the orientation of the microstructure with respect to the ensuing crack front, it

appears that fatigue itself is dependent upon the microstructural orientation and the direction of cracking.

The influence of microstructure on fretting fatigue becomes compounded since the initiation of a crack due to the fretting process is hypothesized to be microstructure dependent. This influence is also dependent upon the size of the individual grains in the material. Smaller grain size smaples of a given material tend to have higher strengths than the large grain smaples of the same material at temperatures below the equicohesive temperature. At the same time, however, the higher strength samples are usually more notch sensitive, thus implying that fretting in conjunction with fatigue may reduce the strength of these small grained samples to levels on the order of the large grained samples of the same material.

2.2.2 ENVIRONMENTAL INFLUENCES

It is expected that theintroduction of a corrosive environment to the fretting fatigue process would reduce the life of a component appreciably. The corrosive environment most commonly encountered during experimental procedures is that of laboratory air containing moisture.

Many of the theories of fretting fatigue of section 2.2 suggest a strong dependence on corrosive action. These are, in the main, based on the thoery that surface oxides are produced during the fretting process. This chemical component of fretting takes place when a moving asperity produces a track of clean metal surface which immediately oxidizes or adsorbs gas. This process is repeated over and over by contacting asperities.

To determine the relative importance of the chemical process occurring during fretting fatigue, the corrosive environment must be removed. This may be accomplished by performing experiments in an inert environment, or, as in this research, they may be conducted under vacuum conditions.

2.2.3 VARIABLES AFFECTING FRETTING

Numerous variables play important roles in the fretting fatigue process. Many of these variables have been discussed [9] and are presented in Table 1. These variables are being held constant in the present research to more fully emphasize the microstructural and environmental effects.

2.3 MECHANICS OF FRETTING FATIGUE

Fatigue and fretting commonly occur in service due to vibrational loadings. The desgn engineer normally uses a traditional approach when dealing with fatigue and related phenomena. In many cases this approach is undesirable. In recent years the development of fracture mechanics as an engineering tool has been introduced to the engineering community. This approach has proven extememly useful in the design of components that will experience conditions outside the realm of traditional design philosophies. The following sections will explain the traditional approach to fatigue design, its shortcomings, and a fracture mechanics analysis of fatigue and fretting fatigue.

TABLE 1

FRETTING FATIGUE VARIABLES

Increasing Variable*	Damage	Life (cycles)
Normal Load	increases	decreases
Slip Amplitude	increases	decreases
Frequency	decreases	increases
Temperature	decreases	increases
Hardness	decreases	increases
Surface Finish	increases	decreases

*these variables are not necessarily linear or directly related to damage and/or life.

2.3.1 VIBRATIONAL ASPECTS

Vibrations are the source of many failures or inadequacies of service structures. Fatigue of structures is often directly due to the loading of the structure and the vibrations that cause the loads to fluctuate. In the case of structures that are in fatigue situations simply due to their design, superimposed vibrations make the problem worse, not only from a mechanistic point of view, but also from an analytical or design point of view.

Fretting, being defined by relative displacements between surfaces, can frequently be attributed to vibrations of the system. Components near rotating machinery, for example, may be loaded in a fatige situation and may also experience vibration due to the mechanical and acoustical vibrations of the rotating machinery. In the case of a clamping load, this situation could cause a synergistic effect of fretting imposed on fatigue.

Research is being conducted throughout the engineering community relating to the problems of vibrations. It seems impossible, however, to eliminate vibrations completely, therefore implying that engineering design procedures are necessary for dealing with such matters as fretting fatigue.

2.3.2 TRADITIONAL APPROACH TO FATIGUE DESIGN

In the past, design philosophies have been based on the simple tensile properties of the specific material. Material selection has been based on tensile properties and, to a certain extent, experience

with given materials. For instance, certain materials may be chosen for a particular application because of previous "good luck" with that material.

Fatigue design has been no exception to the above. Modified Goodman diagrams are drawn for a particular material by knowing its ultimate strength and its endurance or fatigue limit in completely reversed loading. These diagrams imply that fatigue life is heavily dependent upon the mean stress. A modified Goodman diagram is shown in Figure 13 illustrating the dependence on ultimate strength, mean stress, and endurance or fatigue limit. Another diagram commonly used contains the modified Goodman line and the Soderberg line, Figure 14. The Soderberg line is based on the material's yield strength instead of its ultimate strength. A modified Goodman diagram is shown in Figure 15 with all of the components of stress normally encountered.

Another commonly used diagram for establishing fatigue loadings is the constant life diagram shown in Figure 16. Constant life diagrams are generated from stress/life data, thus lending more credibility to their results.

Since fretting damage consists of a series of notches on the surface, a traditional notch sensitivity might be used in relation to reducing the endurance or fatigue strength reduction factor, K_f, is defined as:

$$K_f = \frac{\text{fatigue limit of notch free specimen}}{\text{fatigue limit of notched specimen}} \qquad (5)$$

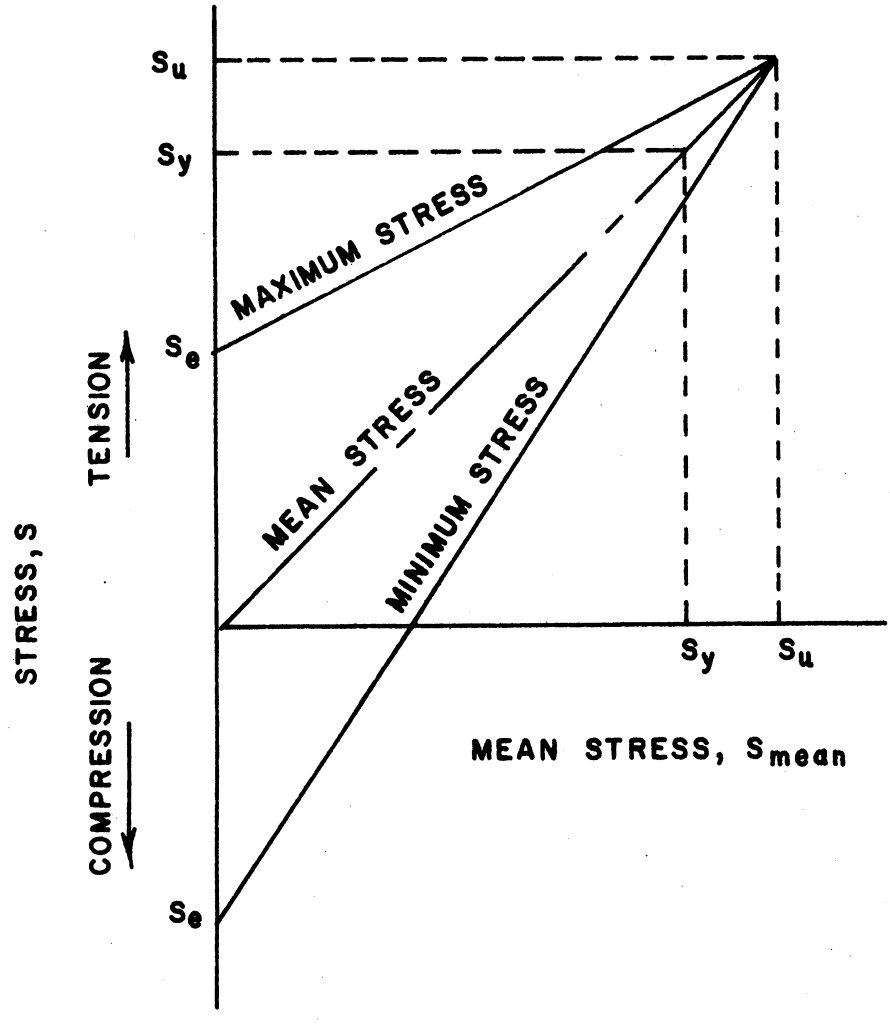

Figure 13. Modified Goodman Diagram.

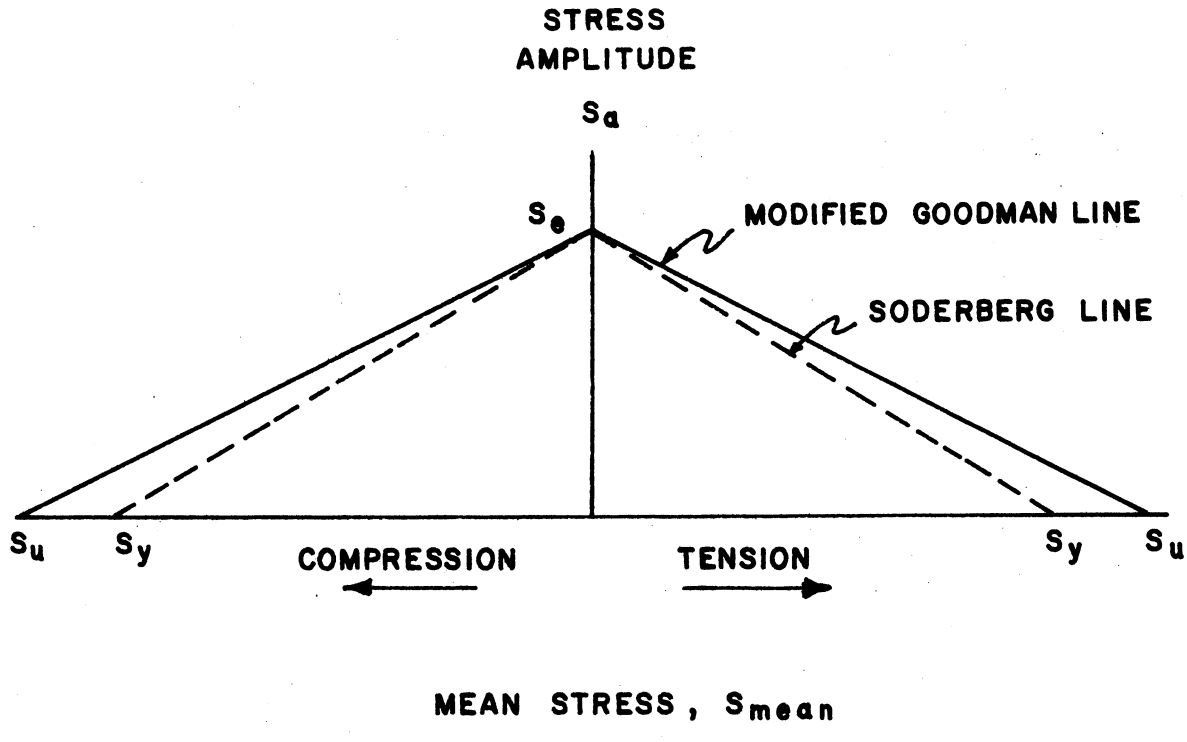

Figure 14. Diagram showing modified Goodman line and Soderberg line.

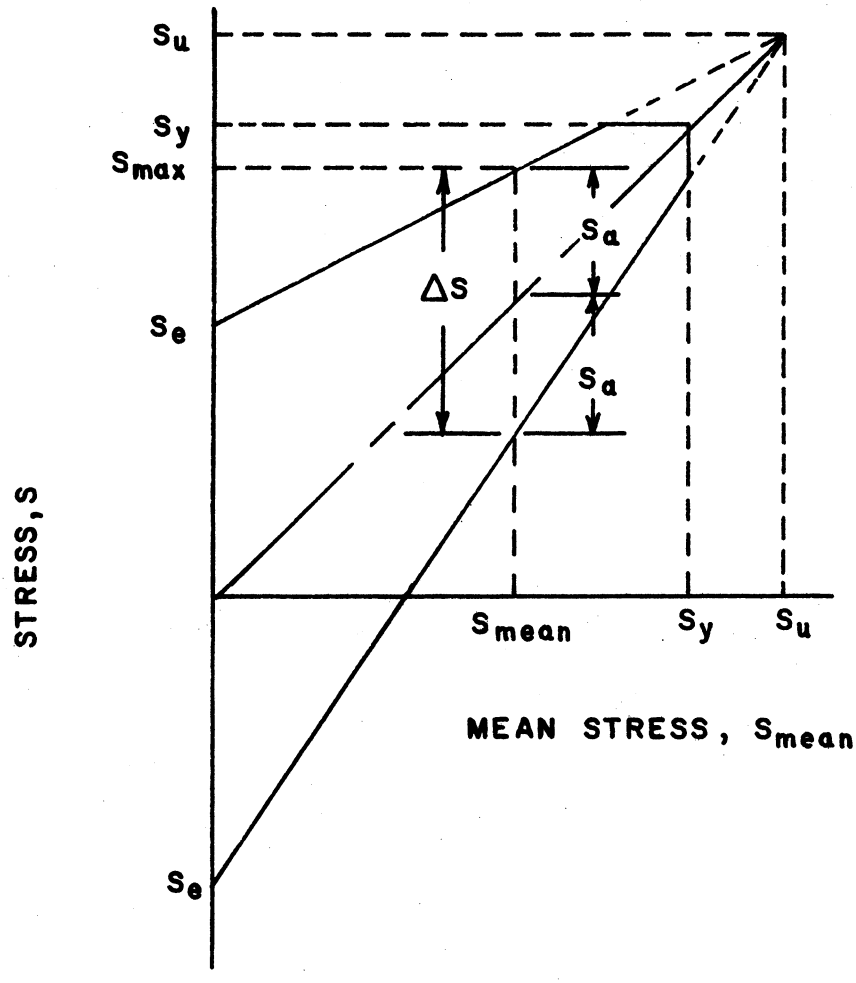

Figure 15. Modified Goodman diagram with all components of stress.

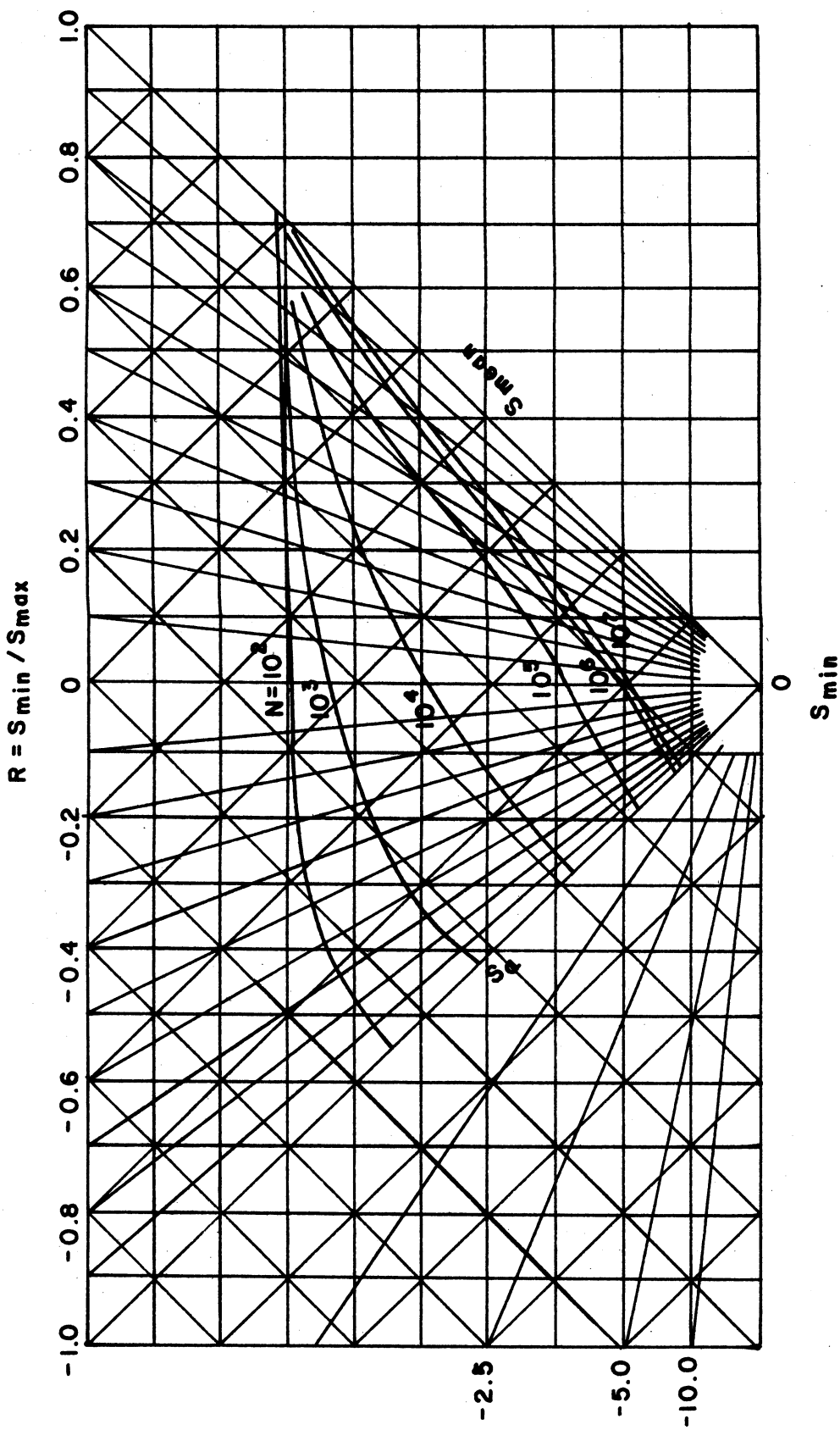

Figure 16. Constant life diagram.

In fretting, it has been illustrated [9] that the fatigue-strength reduction factor must increase with increasing normal or clamping load since the life is further reduced.

A notch sensitivity index, q, is defined as follows:

$$q = \frac{K_f - 1}{K_t - 1} \tag{6}$$

where K_t is determined by the geometry of the specimen or component. Values of the theoretical stress concentration factor, K_t, are tabulated [15].

2.3.3 FRACTURE MECHANICS APPROACH TO FATIGUE AND FRETTING FATIGUE

The fracture mechanics approach to fatigue design is still not completely accepted by the engineering and technical community. It will become obvious in the following sections, however, that this approach has numerous advantages over the traditional approach, especially in the reliability and accuracy of results.

2.3.3.1 FRACTURE MECHANICS - A BACKGROUND

The basis of fracture mechanics was formed from the observation that a material's true fracture strength is much less that its theoretical cohesive strength (Figure 17). The theoretical cohesive strength can be obtained [1] by representing the cohesive force curve by a sine wave, thus giving:

$$\sigma_{max} = \left(\frac{E\gamma}{a_0}\right)^{1/2} \tag{7}$$

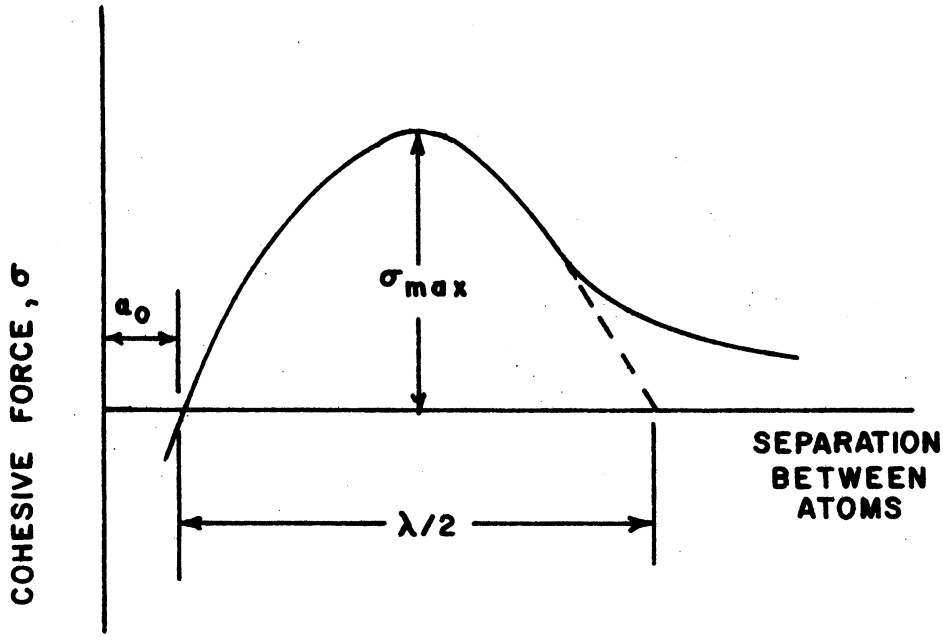

Figure 17. Cohesive force as a function of atomic spacing.

Griffith [16] worked initially with glass, concluding that the theoretical cohesive strength is not attained due to stress concentrations developed by fine cracks or flaws inherent to the material. Griffith proposed a criterion for crack propagation: "A crack will propagate when the elastic strain energy is at least equal to the energy required to create the new crack surface(s)". This criterion has been applied [1] for the Griffith crack model, Figure 18. The elastic strain energy per unit plate thichness is:

$$U_E = \frac{\pi c^2 \sigma^2}{E} \tag{8}$$

where σ is the tensile stress acting normal to the crack of length, 2c. The total surface energy due to the crack is:

$$U_S = 4c\gamma \tag{9}$$

The potential energy due to the creation of the crack is:

$$\Delta U = U_S + U_E \tag{10}$$

This crack will propagate, according to Griffith, when the increased surface energy is compensated by a decrease in elastic strain energy:

$$\frac{d(\Delta U)}{dc} = 0 = \frac{d}{dc}\left(4c\gamma - \frac{\pi c^2 \sigma^2}{E}\right) \tag{11}$$

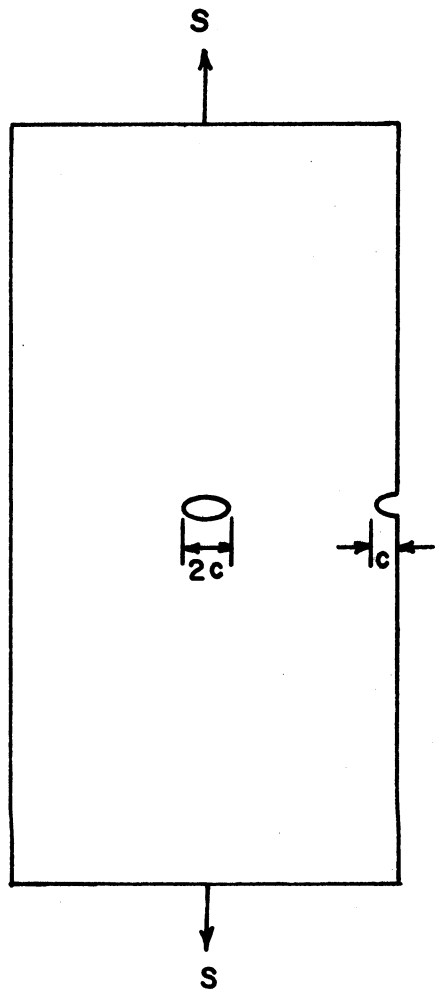

Figure 18. Griffith crack model.

For the case of plane strain (i.e., the plate being much thicker than the crack length) the Griffith equation becomes:

$$\sigma = \left[\frac{2E\gamma}{(1 - \nu)^2 \pi c}\right]^{1/2} \tag{12}$$

The expression for the critical stress to cause brittle fracture [1] is:

$$\sigma = \left(\frac{E\gamma}{4c}\right)^{1/2} \tag{13}$$

The Griffith criterion, therefore, is nothing more than an energy balance; the energy being put into the system or material is elastic strain energy and the energy coming out is in the form of surface energy.

The work of Griffith has been expanded upon for various types of flaws such as given by Irvin [18] for a part-through crack.

At the present time the fracture mechanics approach involves conducting fatigue crack growth tests on various types of specimens. These data are then presented in crack growth curves similar to Figure 7, page 15. Variouw specimen configurations are used as shown in Figure 19 to determine the crack growth characteristics of materials.

For each of the specimen configurations in Figure 19, there are corresponding equations [19] relating the applied stress and crack length to a stress intensity factor, K, or plane strain fracture toughness K_I,:

$$K = f(S,a) \tag{14}$$

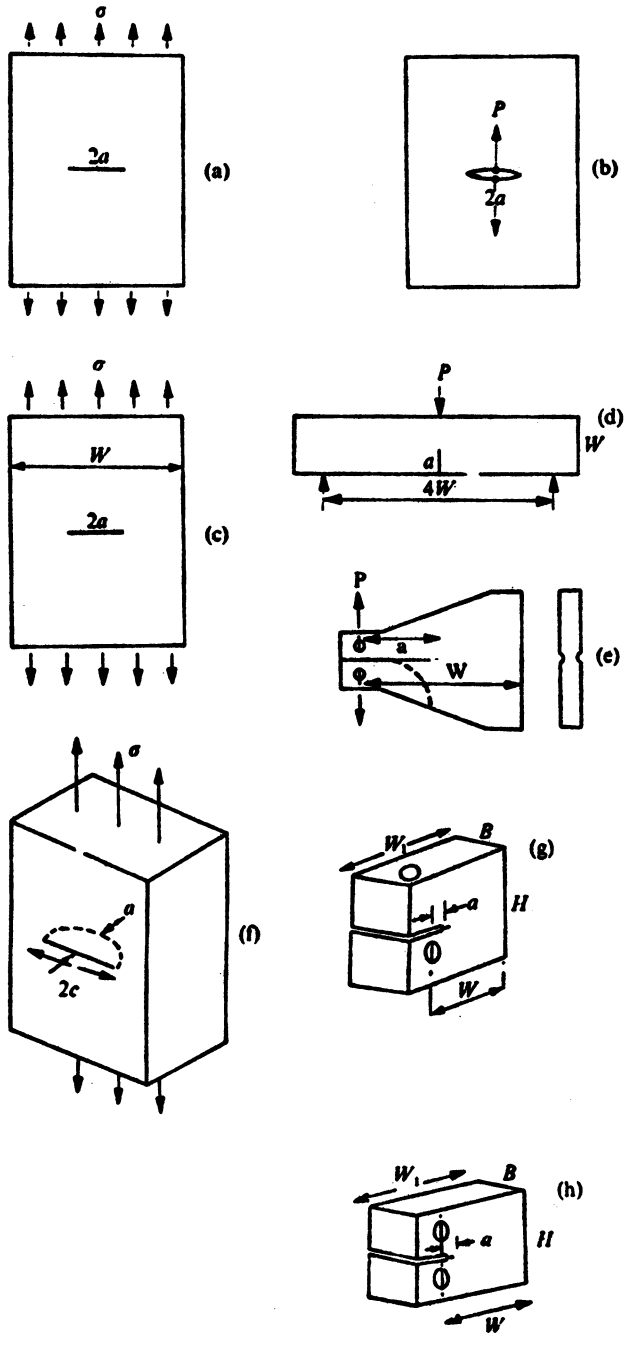

Figure 19. Various specimen configurations for determining crack growth characteristics.

From this, changes in stress intensity, ΔK, may be calculated and presented in curves similar to Figure 20.

Methods of measuring crack length have been tabulated [18] and are presented in Table 2. Certain of these methods have definite advantages to their use.

2.3.3.2 THE EFFECTS OF FRETTING ON FATIGUE

The effects of fretting on fatigue life can be illustrated using the graphical methods of fracture mechanics. Since the main effect is to accelerate the early formation of a crack that will propagate to failure, it is proposed that the notches act as regions of high stress concentrations.

Knowing that the stress concentration at the tip of a fretting induced flaw or crack will change as the flaw or crack increases in size, there is some functional dependence of crack growth rate on the stress intensity range at the tip. This dependence has been given by Paris (1965) as:

$$da/dN = C(\Delta K)^n \qquad (15)$$

where C and n are operating or test parameters over a limited range of interest (The limitations of this functional relationship will be discussed in section 4.3).

The effect of fretting can be described as introducing a flaw or crack in the material early in its life such that the threshold region

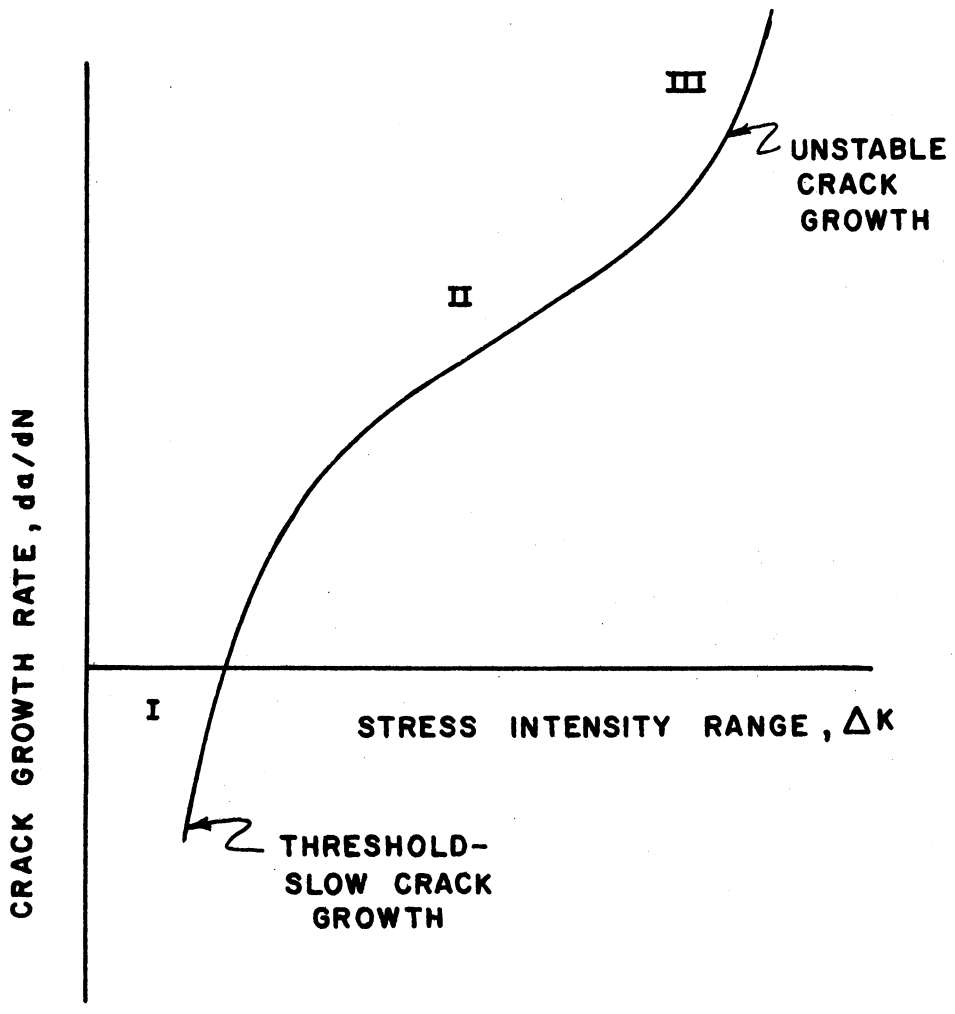

Figure 20. Typical crack growth rate curve.

TABLE 2

CRACK GROWTH MEASUREMENT TECHNIQUES [18]

Method	Usage	Advantages	Disadvantages
Microscopy techniques	Sheet and plate test-pieces. Photography sometimes used	Cheap. Easy installation.	Difficulty of crack tip location without stroboscopic light. Only surface measurements possible during test. Difficult to automate.
Mechanical methods	Rotating bend test pieces. Sheet, plate, and others depending on displacement gauge used	Use of compliance change which can be measured externally away from specimen.	Restricted to tests where compliance calibration (relationship between specimen stiffness and crack length) is known.
Acoustic methods	Applicable to most types of test-piece	Very small probe required, can be mounted easily; useful in low- and high-temperature tests.	Errors due to background noise and calibration is difficult
Electrical techniques	Continuity gauges usually used on sheet and plate samples, could be used for surface measurements on other test-pieces	Electrical signal gives easy automation.	Difficulty of connecting wire and foil gauges. Gauges must break when crack passes. Only surface measurement.
Eddy currents	Used on surface crack monitoring of sheet test-pieces; others should be possible.	Easily adapted to automatic process. Small probe which is not in contact with test-piece.	Not yet used on thicker samples, may only be useful for surface measurement. Expensive.
Electrical resistance or potential measurement	Used on sheet and plate test-pieces	Easily adapted to automatic process. Only four leads attached to specimen, therefore ideally suited for high- or low-temperature tests	Problems of insulating the test-piece. Initial calibration problem thought to be overcome.
Ultrasonics	Ideally suited to compact fracture toughness test-pieces.	Easily adapted to automatic process. Internal measurement of crack front.	Expensive compared to other techniques. Measurements restricted to thicker type test-pieces.

of the crack growth rate curve is eliminated. Figure 21 shows a crack of size a_1, produced by fretting much sooner than its production by normal fatigue in N_1 cycles. The crack growth rate corresponding to this crack, a_1, is shown to be $(da/dN)_j$. This value can be transposed to Figure 22 to illustrate the accelerated crack growth due to fretting.

Another method by which this effect may be seen is combining crack growth curves and stress/life curves. Figure 23 shows typical curves for baseline and fretting fatigue. N_{f1} represents the number of fretting cycles to fail a specimen at some stress, S_2, and N_{b2} is the baseline fatigue life at that same stress level, S_2. The reduction of life due to fretting is: $(N_{b1} - N_{f1})$ at S_1; and $(N_{b2} - N_{f2})$ at S_2. The points in Figure 23 can then be transferred to a crack growth curve as in Figure 24. By realizing that the specimen must reach final failure at some crack size, a_f, crack growth curves can be drawn such that N_{b1} corresponds to a_f at S_1 and N_{b2} corresponds to a_f at S_2. Thus, the quantity $(N_{b1} - N_{f1})$ represents the starting point for fretting fatigue at S_1 and the quantity $(N_{b2} - N_{f2})$ represents the starting point for fretting fatigue at S_2. These quantities correspond to a_{f1} and a_{f2} respectively, implying that the introduction of some relatively large flaws causes a decrease in the initial portion of fatigue life.

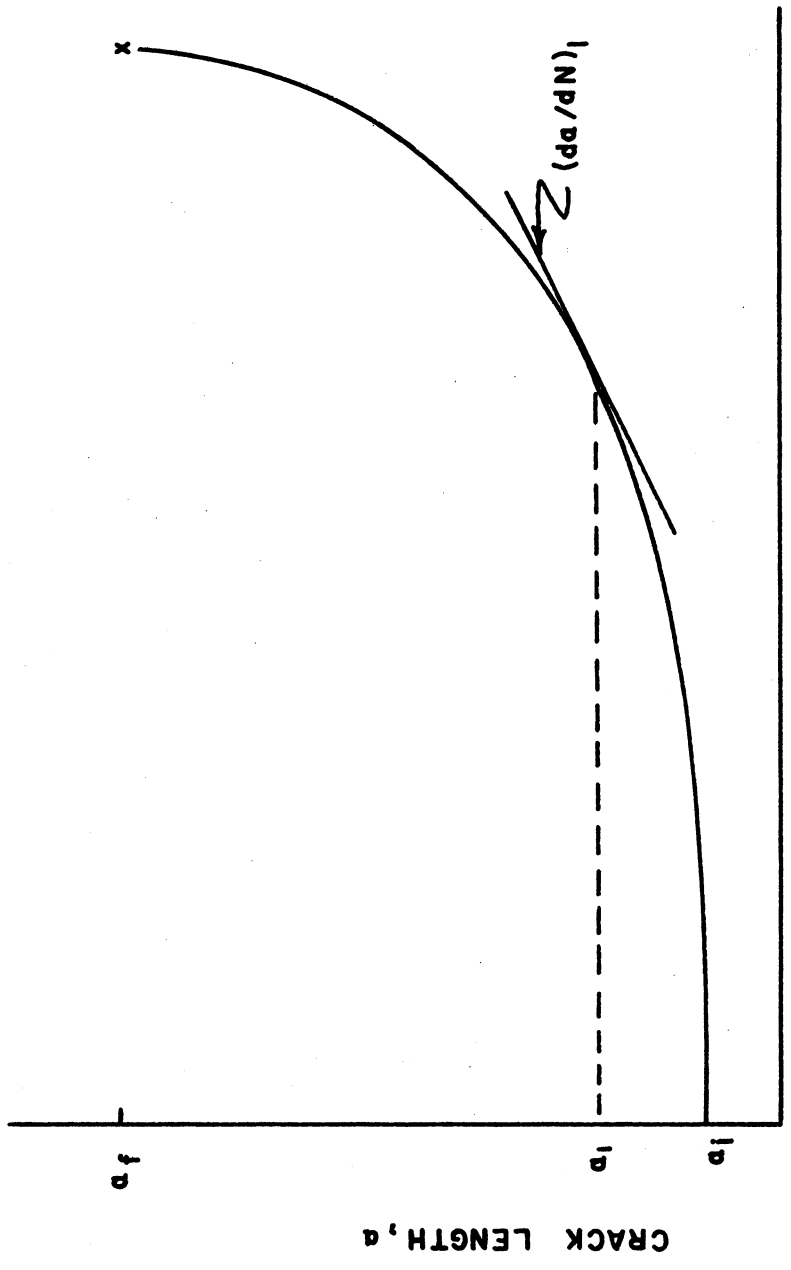

Figure 21. Crack growth curve showing fretting induced crack, a_1, and its corresponding crack growth rate, $(da/dN)_1$.

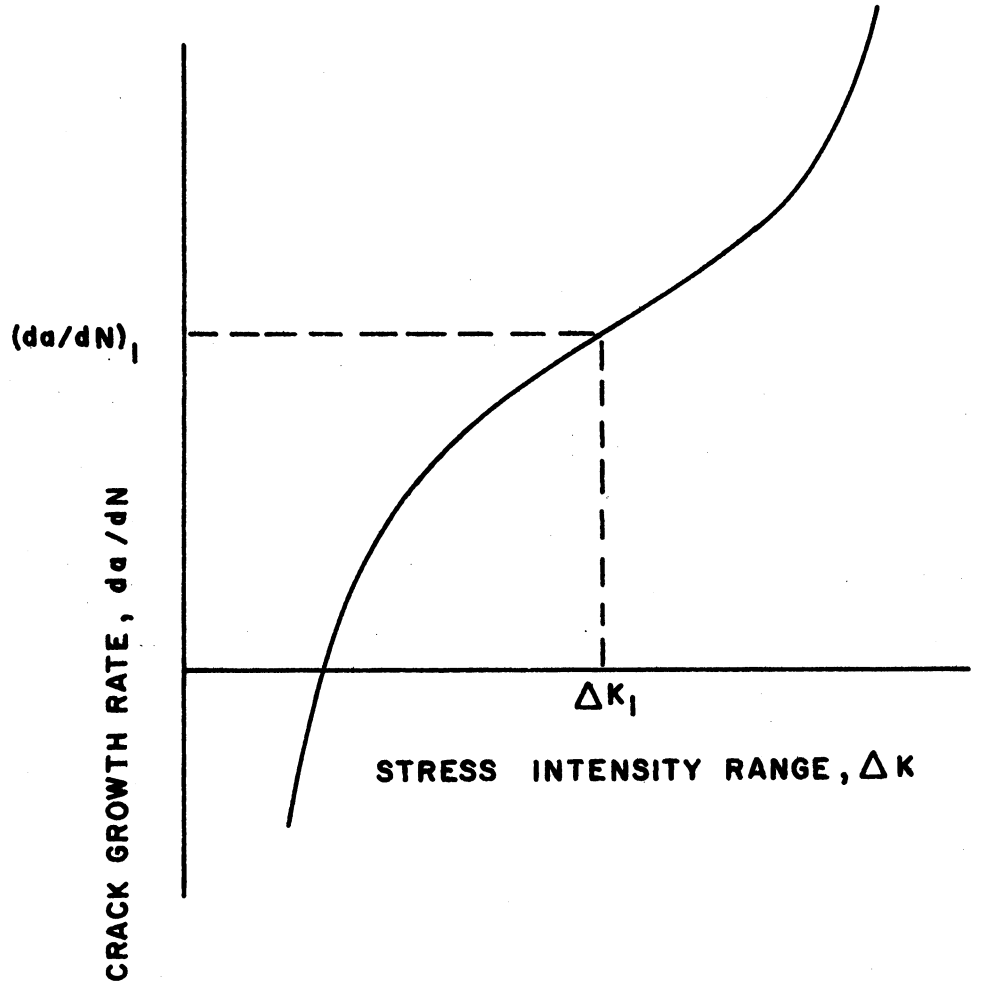

Figure 22. Crack growth rate curve depicting the accelerated crack growth rate due to fretting.

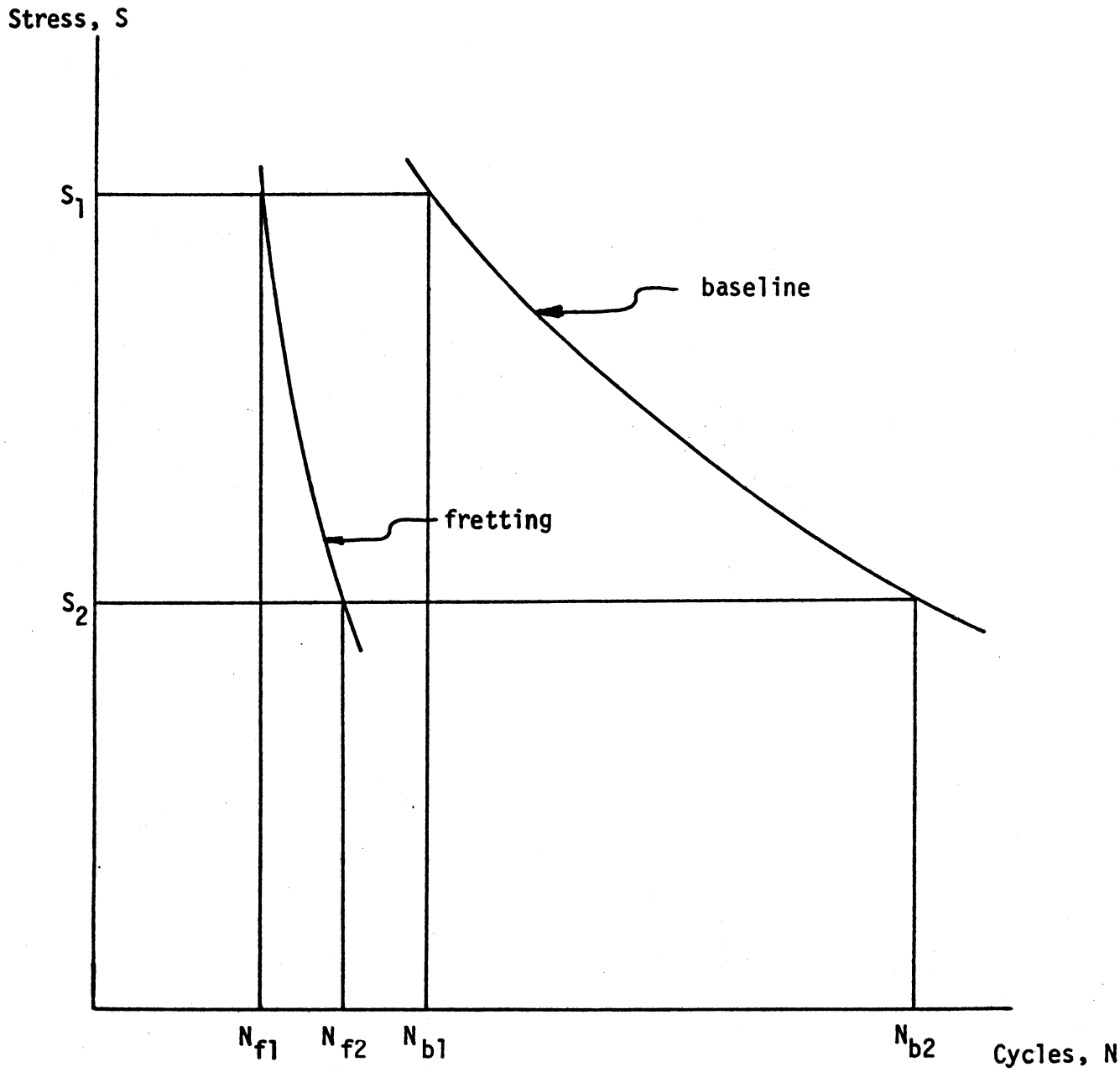

Figure 23. Schematic comparison of fretting and baseline fatigue.

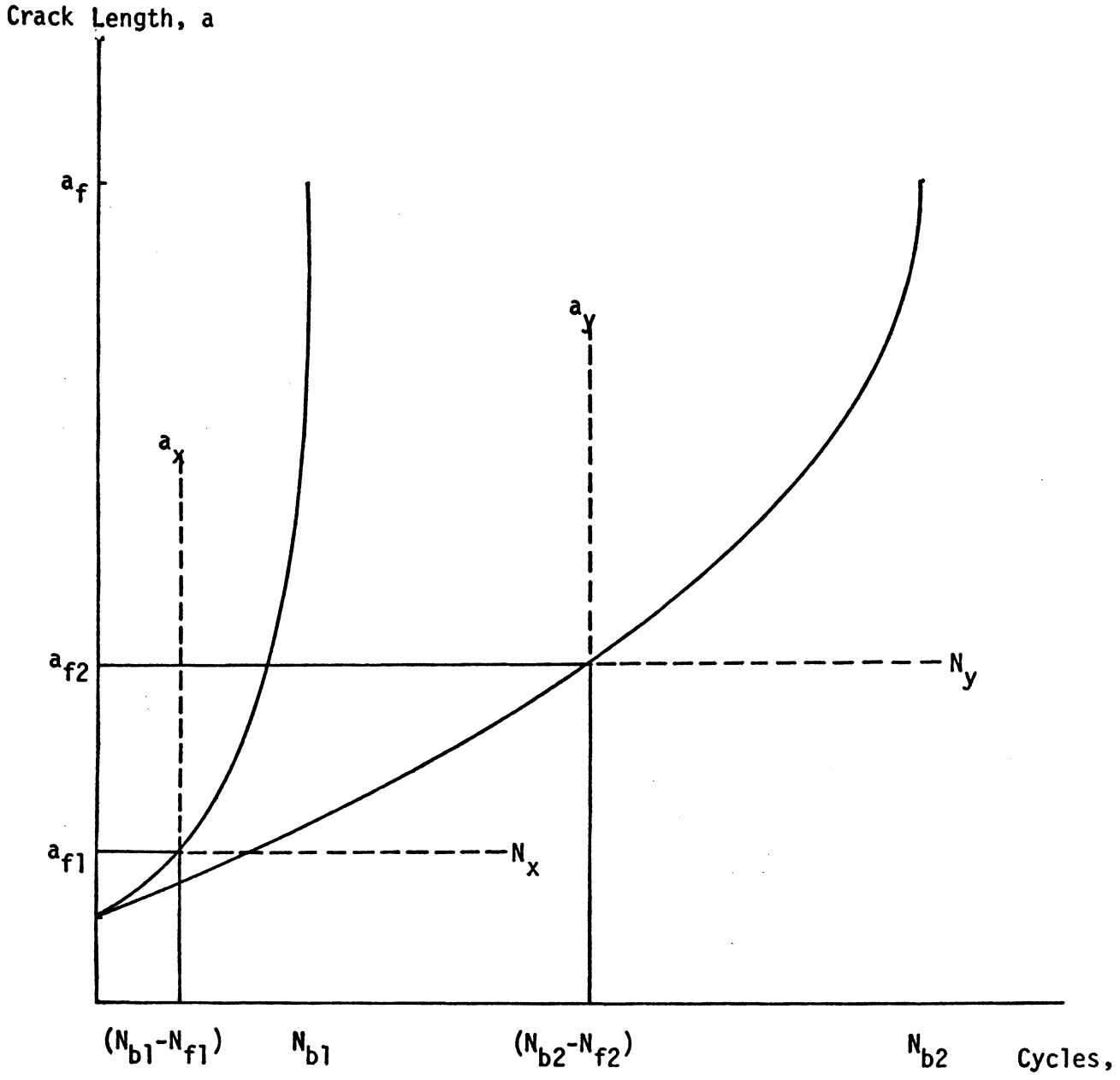

Figure 24. Schematic of crack growth curve with values taken from Figure 23.

2.4 SURFACES IN CONTACT

The matter of surfaces in contact is the main factor in causing the problem of fretting fatigue. A typical representation of sufaces in contact is given in Figure 25. Descriptions of actual contact areas have been written by Waterhouse [20] and Bowden and Tabor [21].

The problem of fretting centers around the effect of the contact stresses due to the clamping or normal forces, the relative motion between the surfaces, and the wear mechanisms. Each of the above is discussed in the following sections as they pertain to the fretting process.

2.4.1 HERTZIAN CONTACT STRESSES

Contact stresses are caused by the pressure of one elastic solid on another at limited areas of contact [22]. Most components are designed according to their ability to withstand stresses through their bodies. When contact stresses are encountered, the stresses through the body of the component may remain largely unchanged, however, the stresses at or near the surface of contact may become quite large. This is due to the large shear stresses developed just below the surface and the triaxiallity of stresses developed near the surface. This is graphically illustrated in Figure 26.

The first satisfactory solution in the determination of values for the stresses due to contact was presented by Heinrich Hertz [23]. Seely and Smith [22] have simplified the Hertz solution and presented it as it applies to two curved sufaces in contact. The values of in-

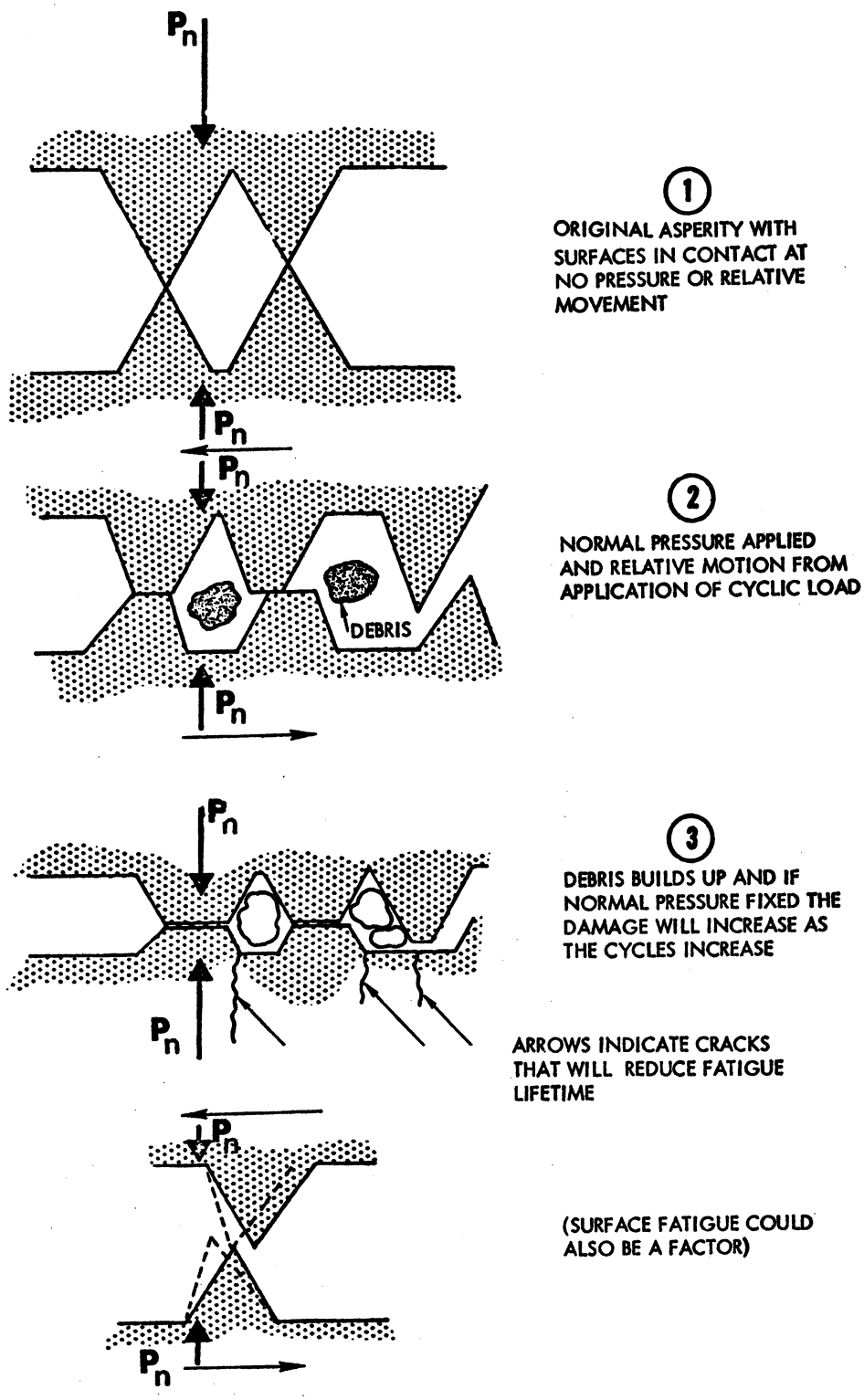

FIGURE 25. Schematic representation of contacting surfaces in fretting fatigue.[11]

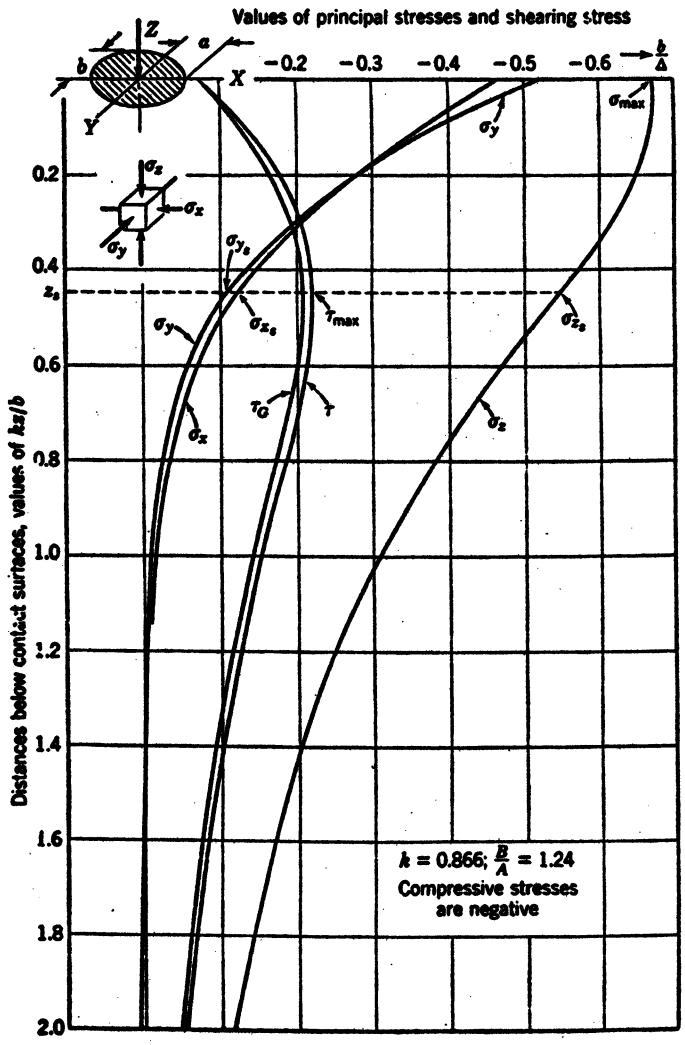

Figure 26. Variation in principal stresses and shear stresses below the contacting surfaces. [21]

terest are the principal stresses and the shearing stresses through the cross section of the body.

Quantities related to the geometric shape and configuration of the two bodies in contact are computed first. For two curved surfaces this becomes:

$$A = 1/4\ (1/R_1 + 1/R_1' + 1/R_2 + 1/R_2') - 1/4\ \{[1/R_1 - 1/R_1') + 1/R_2 - 1/R_2')]^2 - 4(1/R_1 - 1/R_1')(1/R_2 - 1/R_2')\ \sin^2\alpha\}^{1/2} \tag{16a}$$

$$B = 1/4\ (1/R_1 + 1/R_1') + 1/R_2 + 1/R_2') + 1/4\{[(1/R_1 - 1/R_1') + (1/R_2 - 1/R_2')]^2 - 4(1/R_1 - 1/R_1')\ (1/R_2 - 1/R_2')\ \sin^2\alpha\} \tag{16b}$$

where R_1, R_1', R_2, R_2', and α are given in Figure 27. From this, values of Δ, k, k', and b can be found.

$$\Delta = \frac{1}{A + B}\left(\frac{1 - \nu_1^2}{E_1} + \frac{1 - \nu_1^2}{E_2}\right) \tag{17}$$

The quantities, k and $k' = (1 - k^2)^{1/2}$, are found from:

$$\frac{B}{A} = \frac{(\frac{1}{k^2})E(k') - K(k')}{K(k') - E(k')} \tag{18}$$

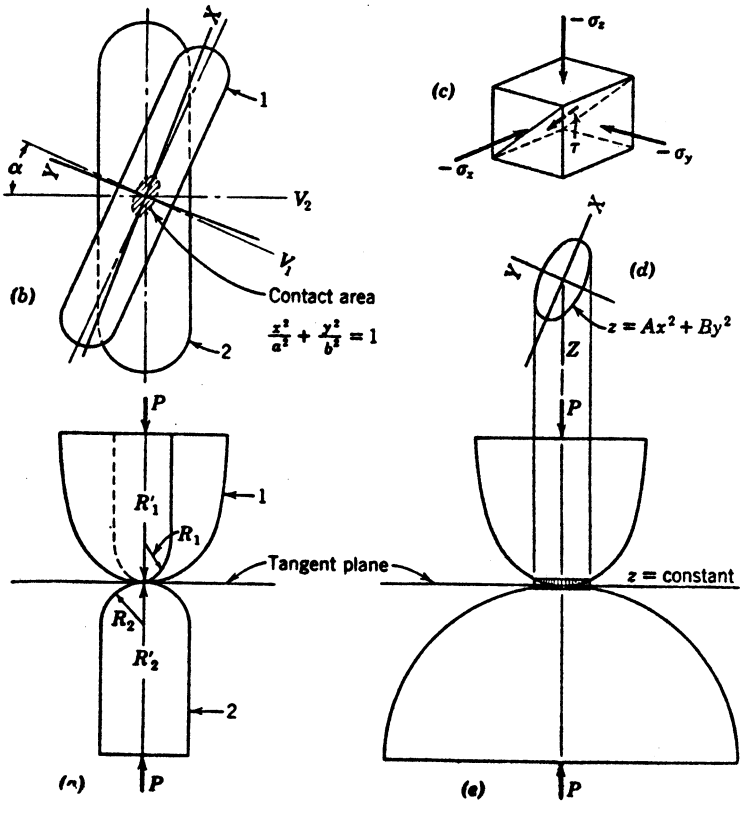

Figure 27. Curved surfaces in contact. (21)

where E(k') and K(k') are:

$$E(k') = \int_0^{\pi/2} (1 - k'^2 \sin^2\theta)^{1/2} d\theta \tag{19}$$

$$K(k') = \int_0^{\pi/2} \frac{d\theta}{(1 - k'^2 \sin^2\theta)^{1/2}} \tag{20}$$

The quantity, b, is then found to be:

$$b = \left[\frac{3kE(k')}{2\pi} P\Delta\right]^{1/3} \tag{21}$$

From these, the principal stresses may be calculated:

$$\sigma_x = [M(\Omega_x + \nu\Omega'_x)] \frac{b}{\Delta} \tag{22a}$$

$$\sigma_y = [M(\Omega_y + \times\Omega'_y)] \frac{b}{\Delta} \tag{22b}$$

$$\sigma_z = -\left[\frac{M}{2} \left(\frac{1}{n} - n\right)\right] \frac{b}{\Delta} \tag{22c}$$

where:

$$M = \frac{2k}{k'^2 E(k')} \tag{23}$$

$$n = \left[\frac{k^2 + k^2(z/b)^2}{1 + k^2(z/b)^2}\right]^{1/2} \tag{24}$$

$$\Omega_x = -\frac{1-n}{2} + k\frac{z}{b}[F(\phi,k') - H(\phi,k')] \tag{25}$$

$$\Omega'_x = -\frac{n}{k^2} + 1 + k\frac{z}{b}[(\frac{1}{k^2})H(\phi,K') - F(\phi,k')] \tag{26}$$

$$\Omega_y = \frac{1}{2n} + \frac{1}{2} - \frac{n}{k^2} + k\frac{z}{b}[\frac{1}{k^2}\,H(\phi,k') - F(\phi,k')] \tag{27}$$

$$\Omega'_y = -1 + n + k\frac{z}{b}[F(\phi,k') - H(\phi,k')] \tag{28}$$

$$F(\phi,k') = \int_0^{\phi} \frac{d\theta}{[1 - k'^2\sin^2\theta]^{1/2}} \tag{29}$$

$$H(\phi,k') = \int_0^{\phi} [1 - k'^2\sin^2\theta]^{1/2} d\theta \tag{30}$$

Finally the maximum shear stress may be calculated as:

$$\tau_{max} = 1/2\ (\sigma_{max} - \sigma_{min}) \tag{31}$$

The results are presented in graphical form as a function of depth below the contacting surface, z, as shown in Figure 26.

Photoelastic contact test are often performed to illustrate isochromatic lines of principal stresses through contacting bodies. From these tests, qualitative judgements can be integrated into the design process.

As can be seen in Figure 26, the principal stresses due to the contact are large at the surface and the maximum shearing stresses are large at a point just below the surface of contact.

These contact stresses in conjunction with the surface wear mechanisms are believed to cause premature crack nucleation as described in section 3.3.2

2.4.2 RELATIVE MOTION

In conjunction with the contact of surfaces, the relative motion provides the damage observed during the fretting fatigue process. This amount of motion depends upon the applied load as well as the material and its rigidity. This motion provides the opportunity for the asperities, shown in Figure 25, to come into contact and cause the various types of wear as discussed in the following section. The effect of the amounts of relative motion between bodies during fretting has been discussed in terms of slip amplitude [24].

2.4.3 THE WEAR PHENOMENA

Several different types of wear exist. Of these, abrasion, adhesion, and corrosion are most commonly associated with explanations in the area of wear and fretting.

2.4.3.1 ABRASIVE WEAR

The abrasion theory of wear proposes that plastic deformation will cause asperities to interlock on a microscopic scale. Abrasive wear is most common, perhaps, in the area of material processing - machining, grinding, polishing, etc.

Tangential forces, necessary in the breaking of interlocking microscopic asperities, cause the shearing off of peaks rather than shearing

along the original interface. The theory in this case is that the interface is strain hardened and strengthened causing breaking in the weaker section of the asperities further from the interface. On the other hand, small particles of debris begin to accumulate in the spaces between high spots after being sheared off and become oxidized. Pits then form in the central region between the high spots due to the stronger abrasive action in that area. As the pits fill, the oxide particles spill into adjoining depressed regions until the entire region becomes covered by the oxidized material. The pits then become fewer in number but deeper and larger in size.

2.4.3.2 ADHESIVE WEAR

Adhesion has been described in fundamental terms as a molecular-kinetic, thermally activated exchange mechanism at a sliding interface [25]. Molecular bonds formed at any instant may be stretched, ruptured, and relaxed an instant later, thus giving rise to a dissipative stick-slip process on a molecular level.

On a macroscopic level, a similar phenomenon referred to as "stick-slip" can be observed experimentally. This stick-slip occurs due to a decreasing friction velocity characteristic, as in Figure 28a. The motion of the simple block mechanism in Figure 28b illustrates the forces occuring in macroscopic stick-slip.

Two types of junctions appear in an adhesion theory: a strong junction leading to metal transfer; or a weak junction leading to loose particle wear. Both types of junctions are formed in the presence of a

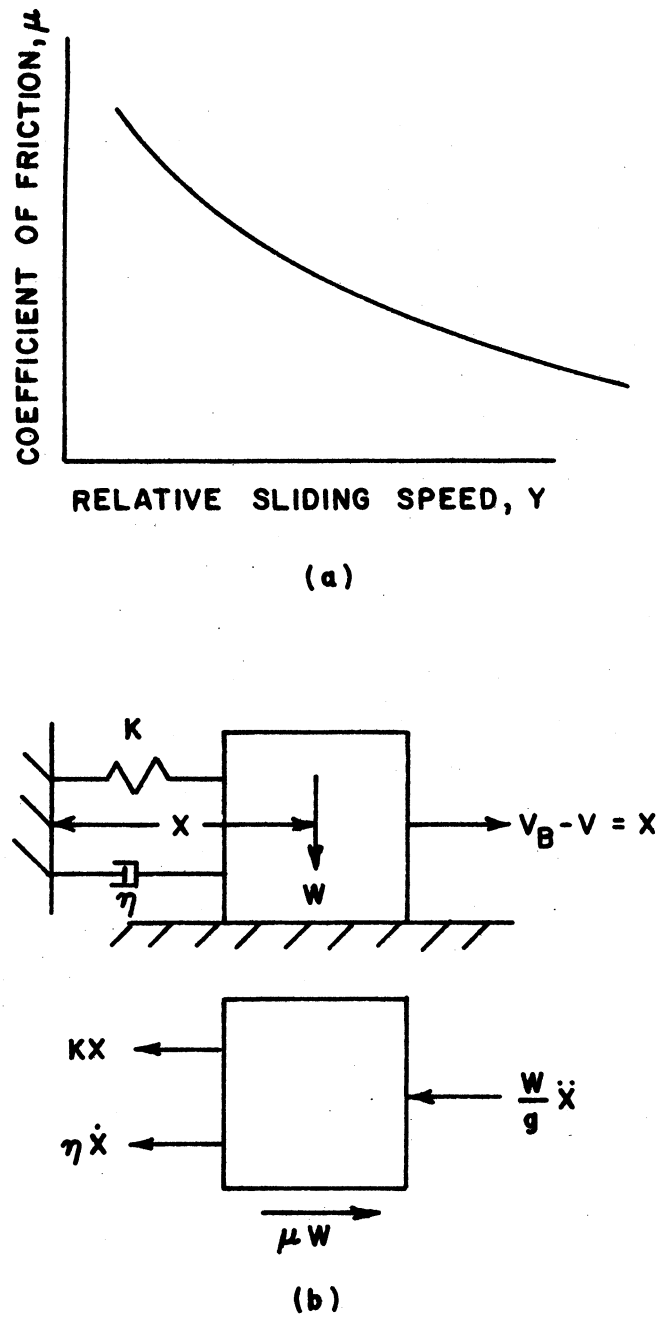

Figure 28. Friction velocity characteristics and stick-slip behavior of a sliding block system.

films may reduce the number of strong junctions because of gases being adsorbed on the surfaces, only strong junctions will occur under vacuum conditions. These strong junctions normally result in metal transfer causing surface ploughing.

2.4.3.3 CORROSIVE WEAR

The corrosion theories of wear indicate that fretting is a combined chemical and mechanical phenomena. The chemical component of fretting occurs when a moving asperity produces a track of clean metal surface which oxidizes or adsorbs gases. According to this theory, the mechanical component occurs when the asperities dig below the surface and cause welding and shearing actions that dislodge metal particles.

2.4.3.4 SURFACE FATIGUE

As the name implies, surface fatigue consists of a component or specimen experiencing larger amounts of deformation (usually plastic) at or near the free surface. A surface fatigue explanation of the frettin/contact problem is useful since fretting causes some definite plastic deformation in the vicinity of the contacting surfaces. The surface asperities coming into contact during fretting fatigue contribute to the surface fatigue problem by causing large amounts of localized plastic deformation. This surface phenomenon may play an important role in the fretting process, especially in conjuction with a delamination theory as discussed in the following section.

2.4.3.5 THE DLAMINATION THEORY OF WEAR

The The delamination theory of wear has been discussed in terms of loose particle formation at the contacting surfaces [26] [27]. The mechnism involved is based on dislocation theory and plastic deformation and fracture of metals near the contacting surfaces.

Suh has based his proposed deamination theory on the following [26]:

(a) During wear, the material at and very near the surface does not have a high dislocation density, due to the elimination of dislocations by the image force acting on those dislocations which are parallel to the surface. Therefore, the material very near the surface cold works less than that of the sub-surface layer.

(b) With continued sliding there will be pile-ups of dislocations a finite distance from the surface. In time, this will lead to the formation of voids. The formation of voids will be enhanced if the material contains a hard second phase for dislocations to pile against. Voids form primarily by plastic flow of matrix around hard particles, when there are large secondary phase particles in the metal.

(c) With time, the voids will coalesce, either by growth or shearing of metal. The end result is a crack parallel to the wear surface.

(d) When this crack reaches a critical length (dependent upon the material) the material between the crack and the surface will

shear, yielding a sheet like particle.

(e) The final observed shape of the particle will be dependent upon its length and internal strains.

He continues by explaining that many dislocations are generated in the contact situation due to plastic deformation of surface asperities. These dislocations become more dense below the surface thus creating more cold work and thus larger amounts of plastic deformation.

Waterhouse and Taylor [27], through microscopic examination, have observed cracks below the surface of materials experiencing contact under fretting conditions. They have noted that the formation of the cracks takes place at right angles to the direction of motion whereupon the cracks propagate parallel to the surface until they join with other cracks.

Under the conditions of fretting fatigue it appears that the delamination process begins much as that proposed by Suh and Waterhouse and Taylor. However, as the voids form, elongate, and become cracks, instead of loose particles forming (or in addition to) some of the cracks begin to propagate due to the fatigue loading. This is illustrated in Figure 29 in its various stages.

Thus the steps of the process become:

(a) Dislocations pile-up (usually at hard particles).

(b) Voids form due to the dislocations.

(c) Voids elongate due to motion and loading.

(d) Cracks emanate from elongated voids and begin propagating due to the fatigue loading.

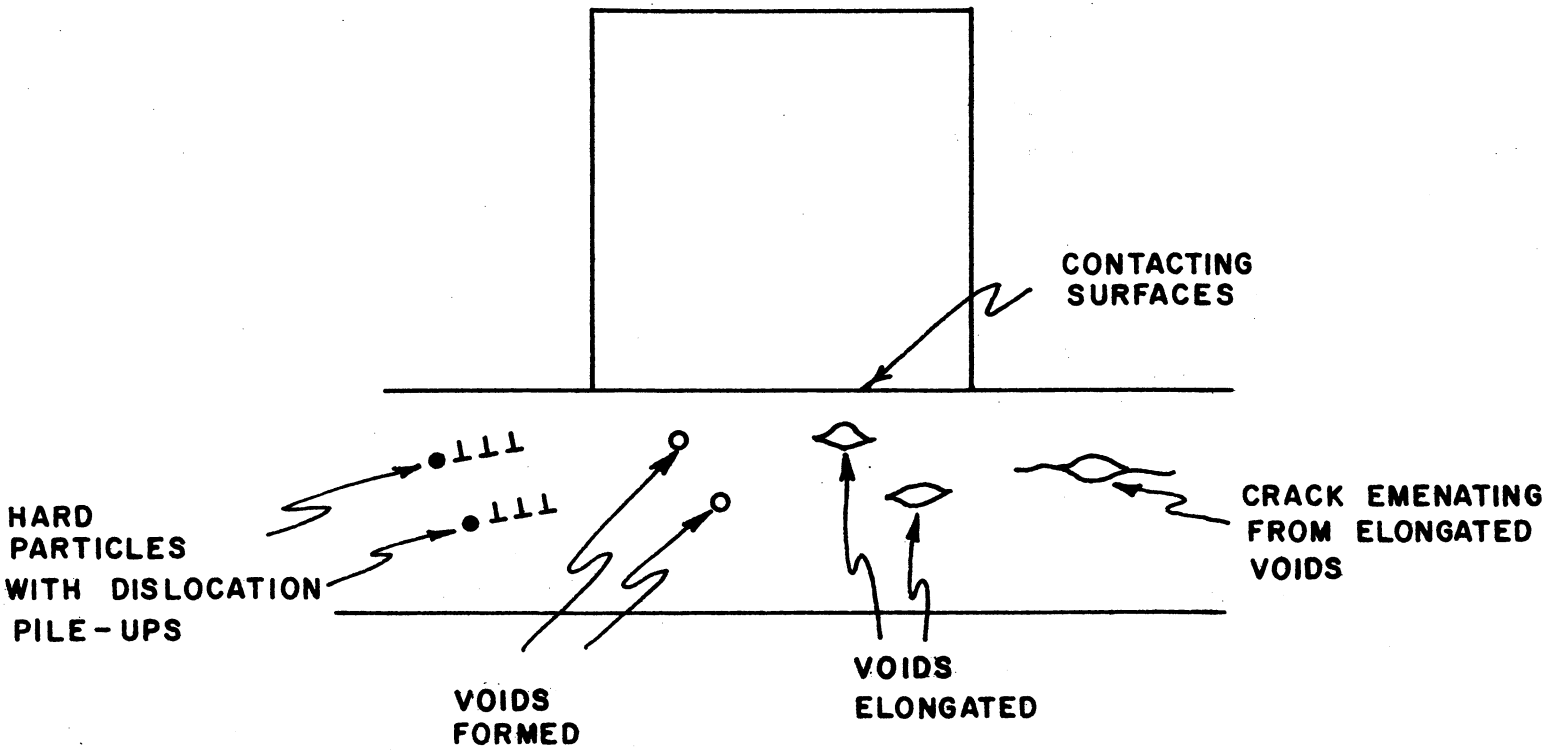

Figure 29. Formation of subsurface cracks in fretting fatigue.

2.4.3.6 COMBINED WEAR

It is obvious that the wear process is not simple and that it may involve more than one mechanism. For example, a certain wear process may be taking place such that the corrosive environment is causing surface oxidation while an abrasive type is superimposed.

It is believed that the combined effects of subsurface delamination in conjunction with surface fatigue (cracking due to contact) and the abrasive action of contacint surfaces play the major role in reduction of life due to fretting fatigue. Corrosion is then believed in certain instances to act as an acclerator in the process. Thus, it seems logical that wear is a combination of phenomena and may be worsened due to synergisms taking place between the different mechanisms involved.

3.0 EXPERIMENTAL METHODS AND PROCEDURE

Since research on fretting fatigue is somewhat uncommon, it was neccessary to design and build the experimental system. For discussion purposes, the experimental system is divided into subsystems: Vacuum Chamber; Hydraulic System; Electronic system; and the Vacuum System.

3.1 DESIGN OF EXPERIMENTAL APPARATUS

3.1.1 VACUUM CHAMBER AND COMPONENTS

The first section of the experimental apparatus to be designed was the vacuum chanber and its individual components.

3.1.1.1 CHAMBER

The chamber is shown in Figure 30. The purpose of the chamber is to provide a sealed volume to be evacuated to eliminate any effects on fretting fatigue life due to the existing environment.

The chamber was machined entirely from a single block of aluminum so that deformation of the fixed support due to fatigue loading and leaks in the chamber itself could be minimized.

The plexiglass plates are attached to the chamber by a series of bolts with an o-ring system being used to prevent air leakage into the chamber. These plates allow continuous visual observation of the experimental specimens during the fatigue process.

A thermocouple vacuum gage is shown in Figure 31 in the position it normally occupies. This gage is within approximately three inches

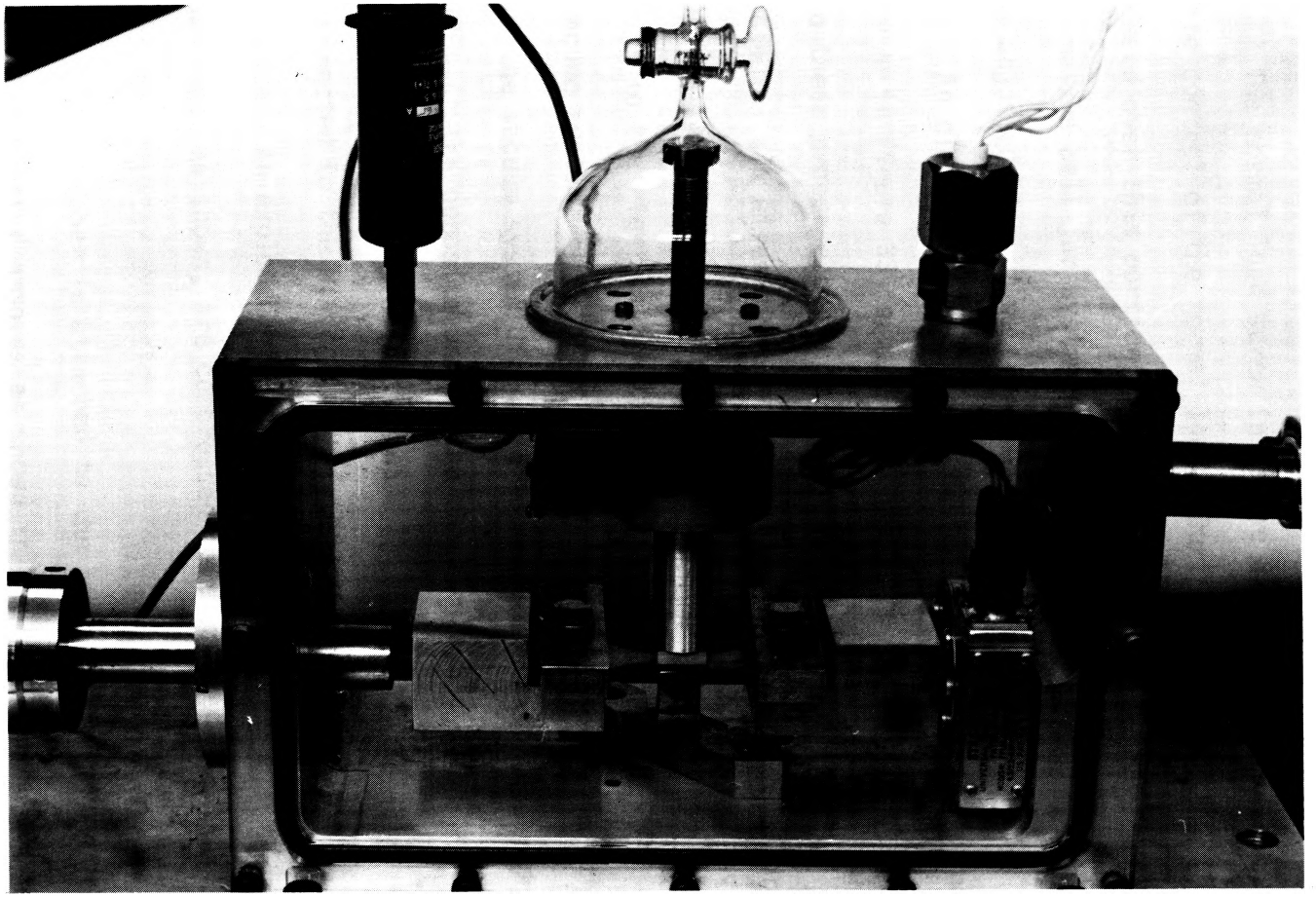

Figure 30. Fretting chamber.

of the specimen surface and provides a method of continuously observing the vacuum readings.

The normal load screw in Figure 32 has an extra fine thread for fine control of the normal load. During vacuum testing a bell jar is placed over this portion of the chamber to prevent air seepage. By using the bell jar system during the test operation, the normal load may be adjusted without severe loss of vacuum.

An electronic feedthrough device at the top of the chamber and shown in Figure 33 is used to connect the load cells within the system to their proper electronic controls. This feedthrough device is composed of six wires surrounded tightly be compressed teflon seals to prevent air seepage.

To the right of the chamber, Figure 30, is the connection to the vacuum system. The connection made here is similar to other connections of the vacuum system discussed in section 5.4 of this report.

At the opposite end of the chamber is the actuator feedthrough mechanism. This provides a means by which the hydraulic actuator is connected to the moving grip of the axial load train without a loss of vacuum. An exploded view of this apparatus is shown in Figure 34. The o-rings, as shown, are compressed so that they fit tightly around the smooth actuator extension.

The chamber is attached to the baseplate by four bolts placed through slotted grooves as shown in Figure 30. The slotted grooves provide slight lateral movement of the camber so that proper alignment may be acheived.

3.1.1.2 GRIPS

Many problems are currently being found in the methodology of the experimental procedures of fatigue testing. One such problem is that of specimens failing in the gripping section. Since experimental start-up in this study was somewhat difficult, this problem was of paramount concern.

The grips are shown in Figure 35. They were made of a 17-4 PH steel for high strength qualities and machined to prevent any high stress concentrations from occurring. A 100 grit silicone carbide paper was glued to those surfaces of the grips coming into contact with the fatigue specimens. This provided frictional type clamping of the specimen ends to prevent slippage.

A lock washer was used in conjunction with the grip bolts to prevent then from coming loose during the experiment. It was found by using this method of gripping that the bolts were as tight after failure of the fatigue specimen as they were during the initial start-up period.

3.1.1.3 NORMAL LOAD TRAIN

The normal load train, shown in Figure 36, is used to apply pressure between the fretting pads and the fatigue specimen. This is acheived by a simple load screw apparatus.

For load control and measurement purposes, a strain gage load cell is placed between the load screw and the fretting pad, thus requiring all loads from the load screw to be transmitted through it to the

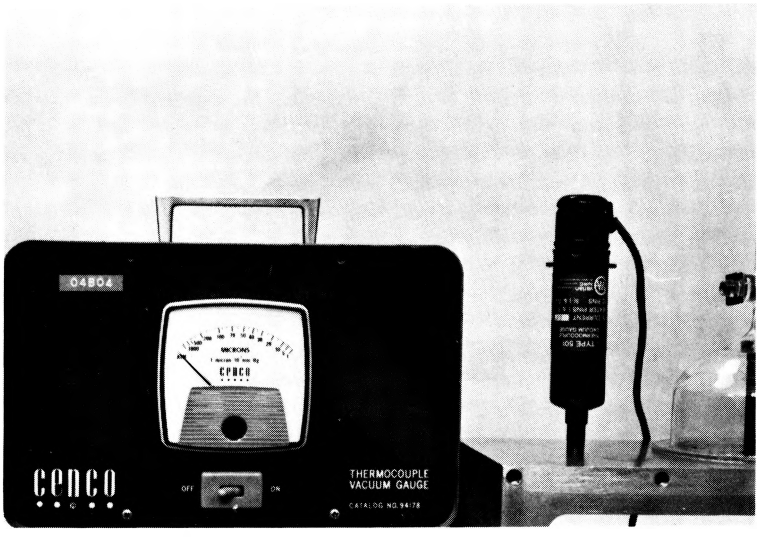

Figure 31. Vacuum gage and readout device.

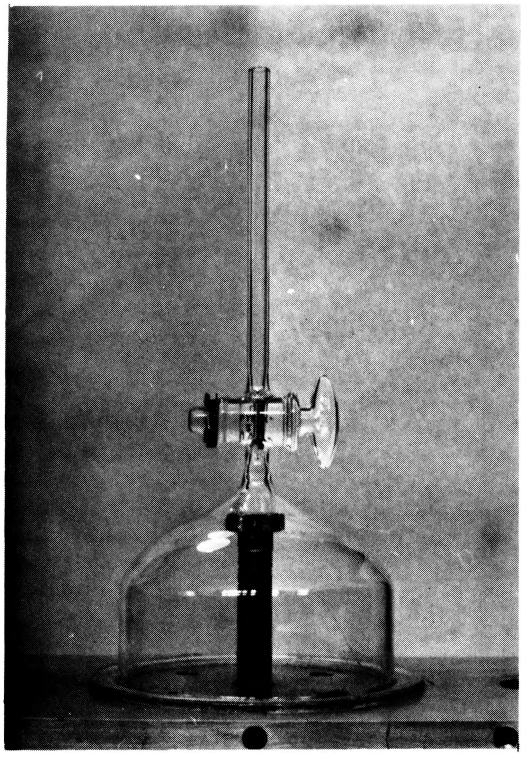

Figure 32.
Normal load screw and bell jar.

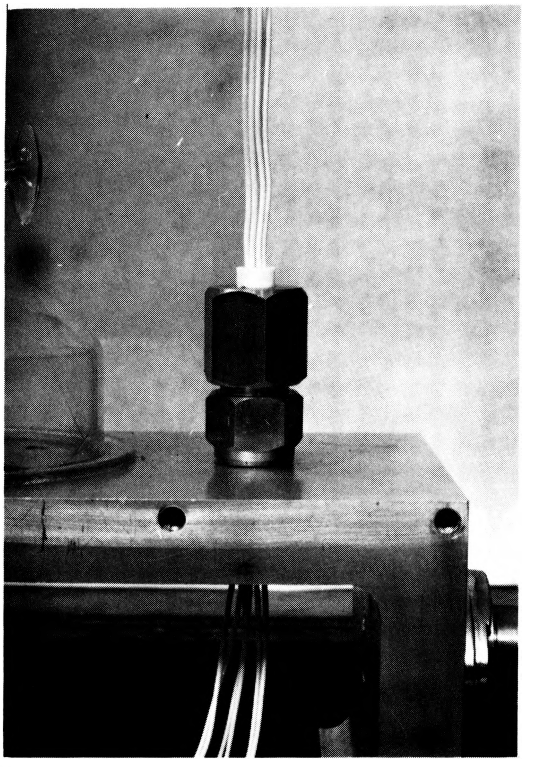

Figure 33.
Electronic feedthrough device.

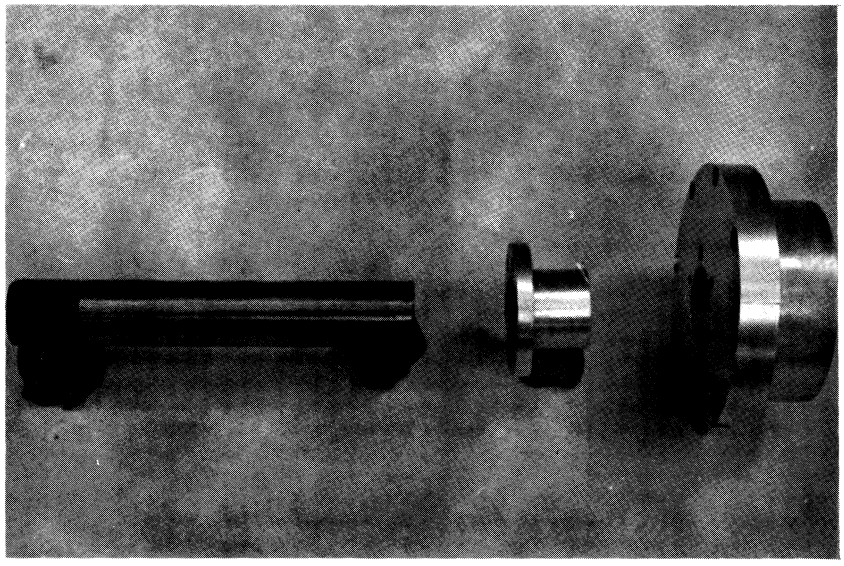

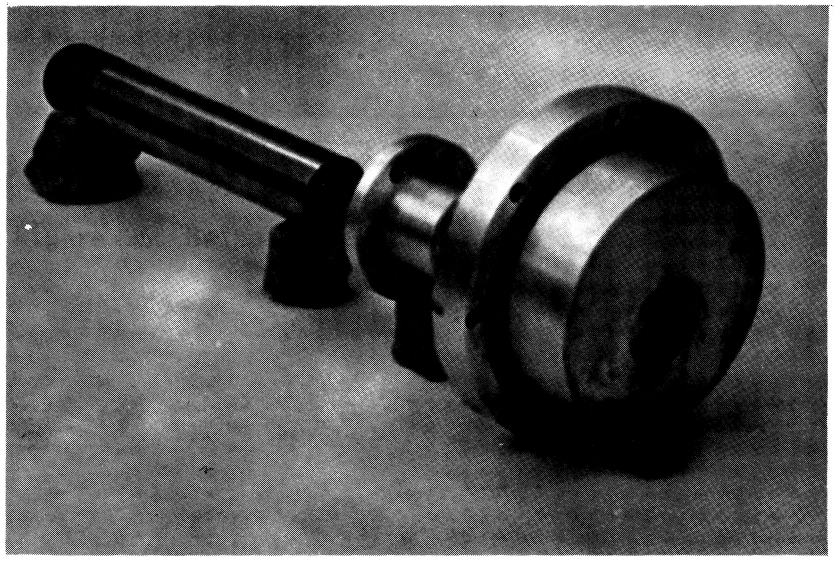

Figure 34. Actuator feedthrough mechanism.

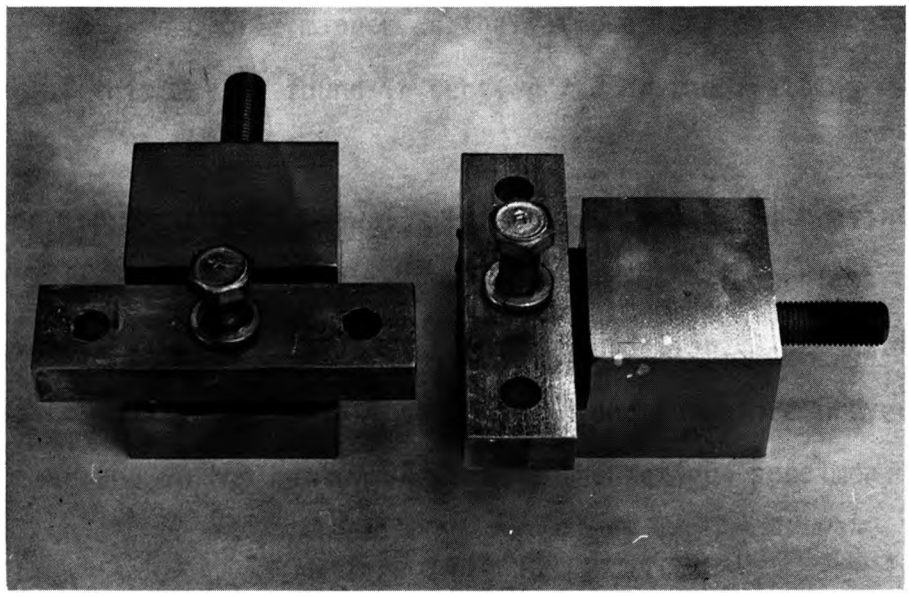

Figure 35. Gripping mechanism.

fretting pad.

This load train is considered to be rigid, thus preventing any large lateral deflections. The vertical spring constant of the normal load train is very large, thus allowing the normal load to vary in exactly the same cyclic manner as the fatigue loading. A detailed discussion of this may be found in section 7.3 on the fretting fatigue tests.

The support block, shown in Figure 37, is used to prevent bending of the fatigue specimen due to the normal load. It consists of a cover cap, two small roller bearings, and the foundation. The bearing allow the cap to move with the fatigue specimen and therefore prevent fretting from occurring on the bottom surface of the fatigue specimen.

3.1.1.4 AXIAL LOAD TRAIN

The azial load train, shown in Figure 38, shows the method by which the fatigue loading is applied and measured. The grips are such that the load is transferred, as nearly as possible, through the fatigue specimen's centerline.

The actuator extension is attached to the hydraulic actuator via the threaded portion, while the strain gage load cell is attached to the wall of the chamber by eight bolts.

3.1.2 HYDRAULIC ACTUATING SYSTEM

A hydrualically powered actuator, Figure 39, was used as the method of applying the fatigue loading. A schematic diagram of the system is

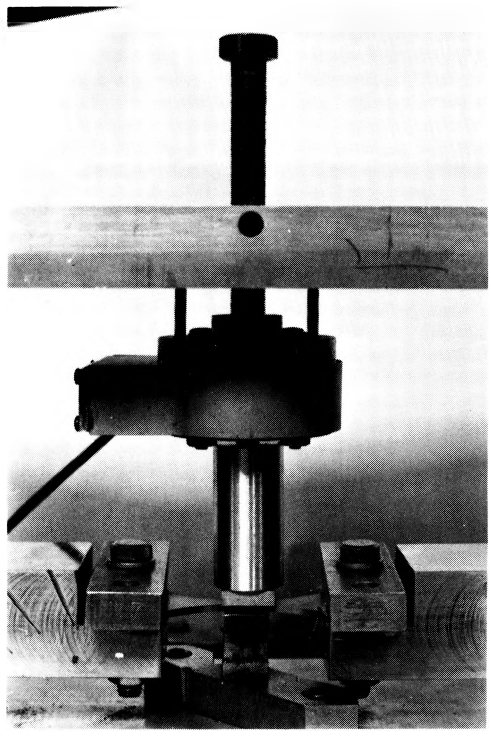

Figure 36. Normal load train.

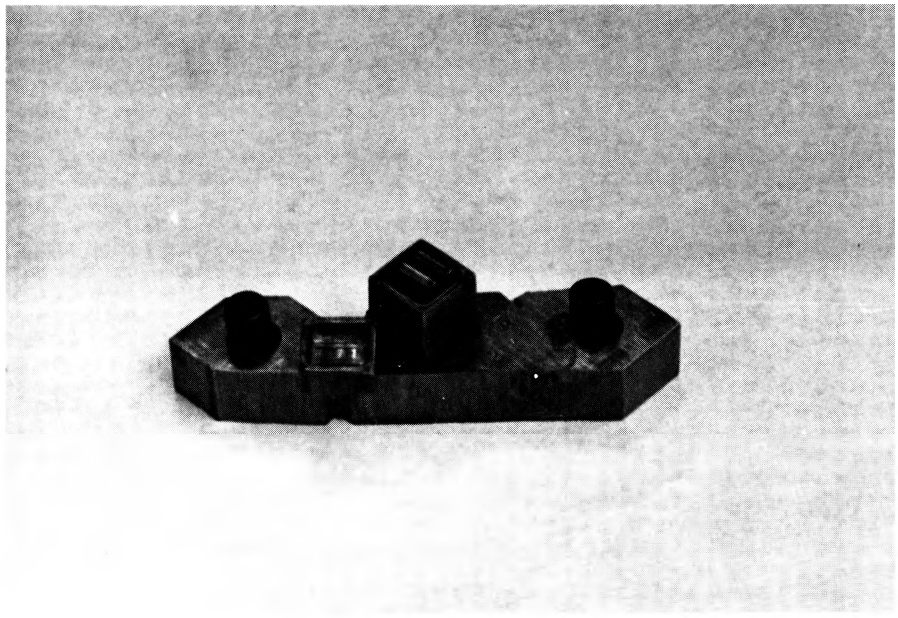

Figure 37. Normal load support block and bearings.

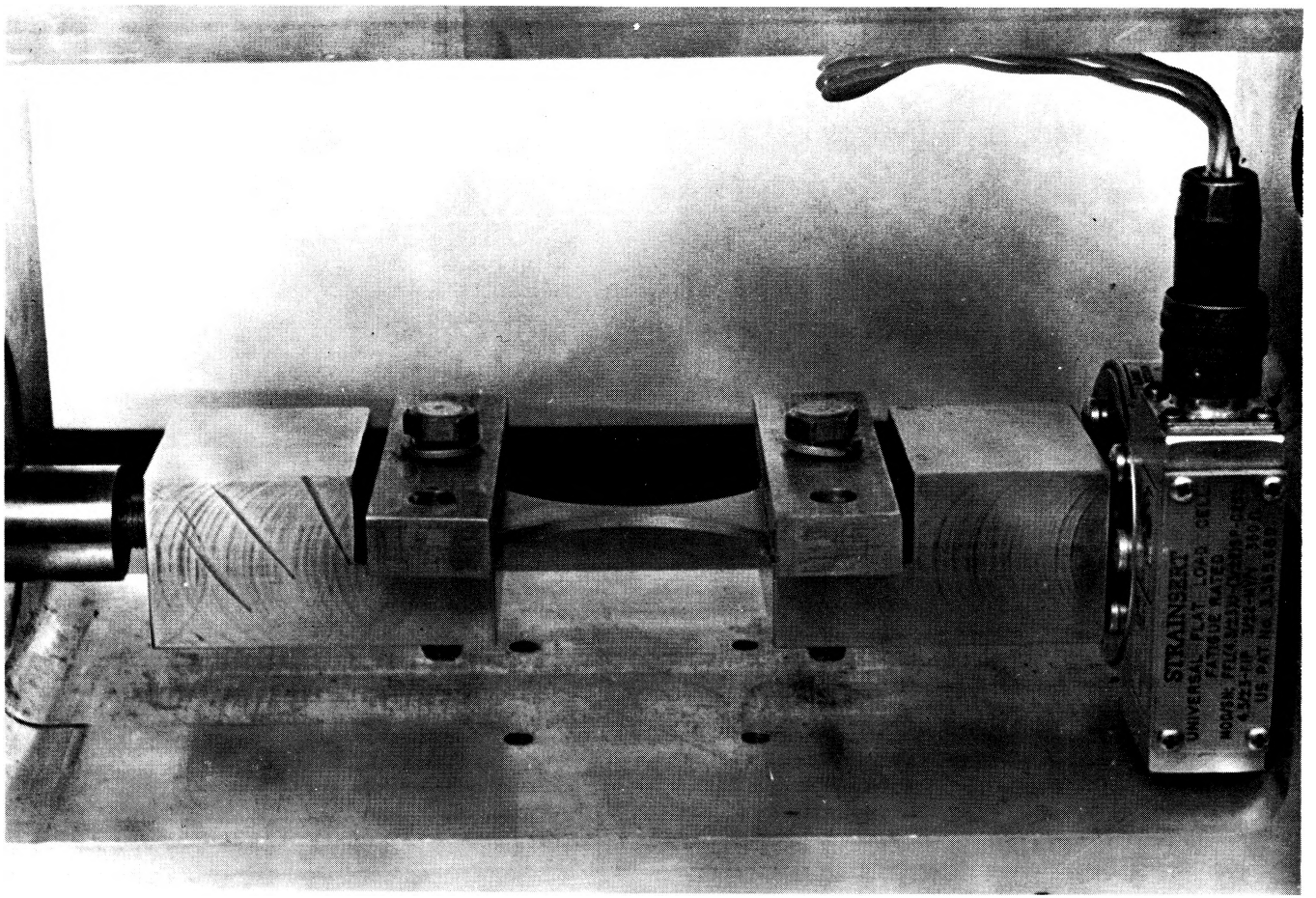

Figure 38. Axial load train.

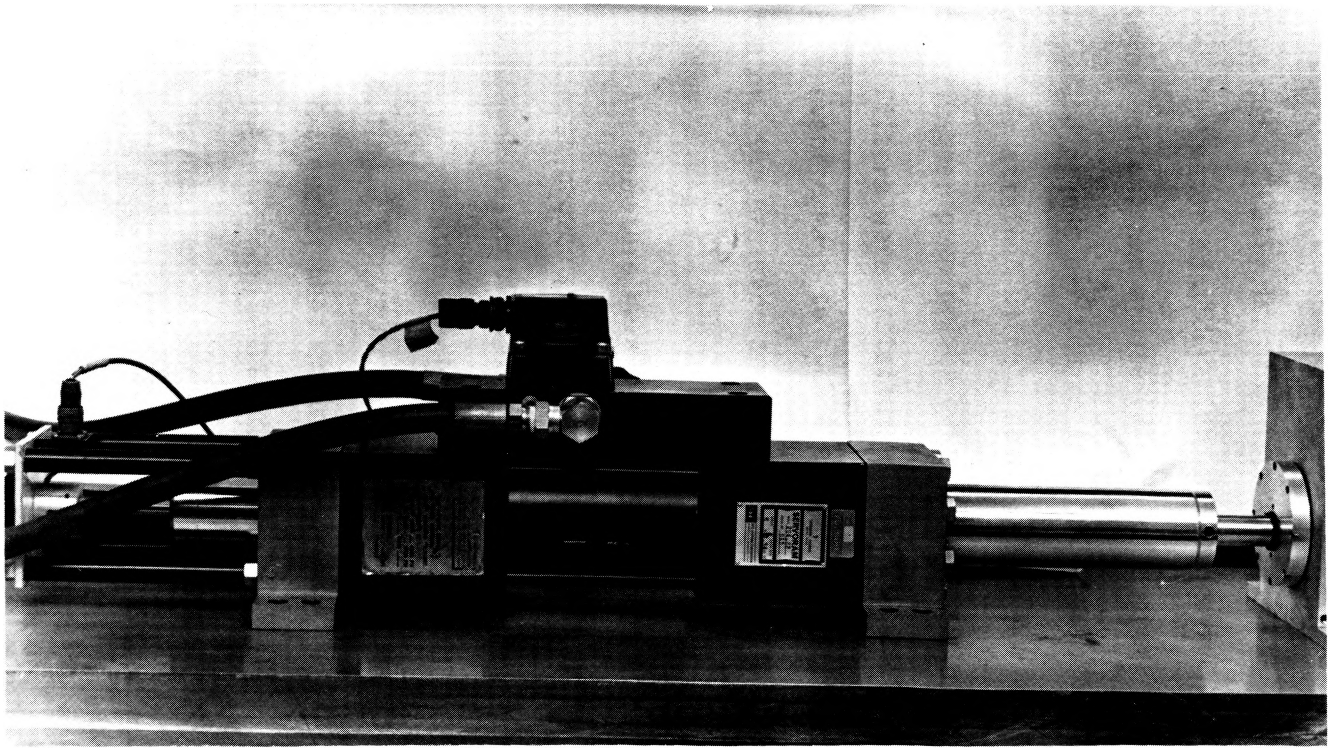

Figure 39. Overall view of actuating device.

presented in Figure 40 with the major components listed in Table 3. The system was designed and built during the course of this investigation specifically for this type project.

The major consideration was to provide the actuator with up to seven gallons per minute (7 gpm) of hydraulic fluid at up to three thousand pounds per square inch (3000 psi) of fluid pressure. This goal was attained using a seven gallon per minute (7 gpm) rated hydraulic gear pump driven by a fifteen horsepower (15 hp) electric motor.

Filters were installed at various positions throughout the system to prevent damage to such elements as the gear pump, the hydraulic actuator, the pressure and return line accumulators and the heat exchanger.

Accumulators were placed in the pressure and return lines of the system to prevent surges of hydraulic fluid to the actuator and heat exchenger respectively. Surges of flow would cause unwanted fluctuations in pressure to the actuator and therefore uncontrollable changes in loading. Surges of flow in heat exchangers have been found to produce fatigue of heat exchanges structural elements and thereby to reduce their effective lives.

The heat exchanger was used to prevent overheating in the system since overheating could cause damage and/or reduced capabilities of various components in the hydraulic system. To surther prevent this type of damage, a temperature and level shutoff switch was installed in the fluid reservoir. If the temperature should rise above some predetermined value or the level fall below some predetermined amount, power

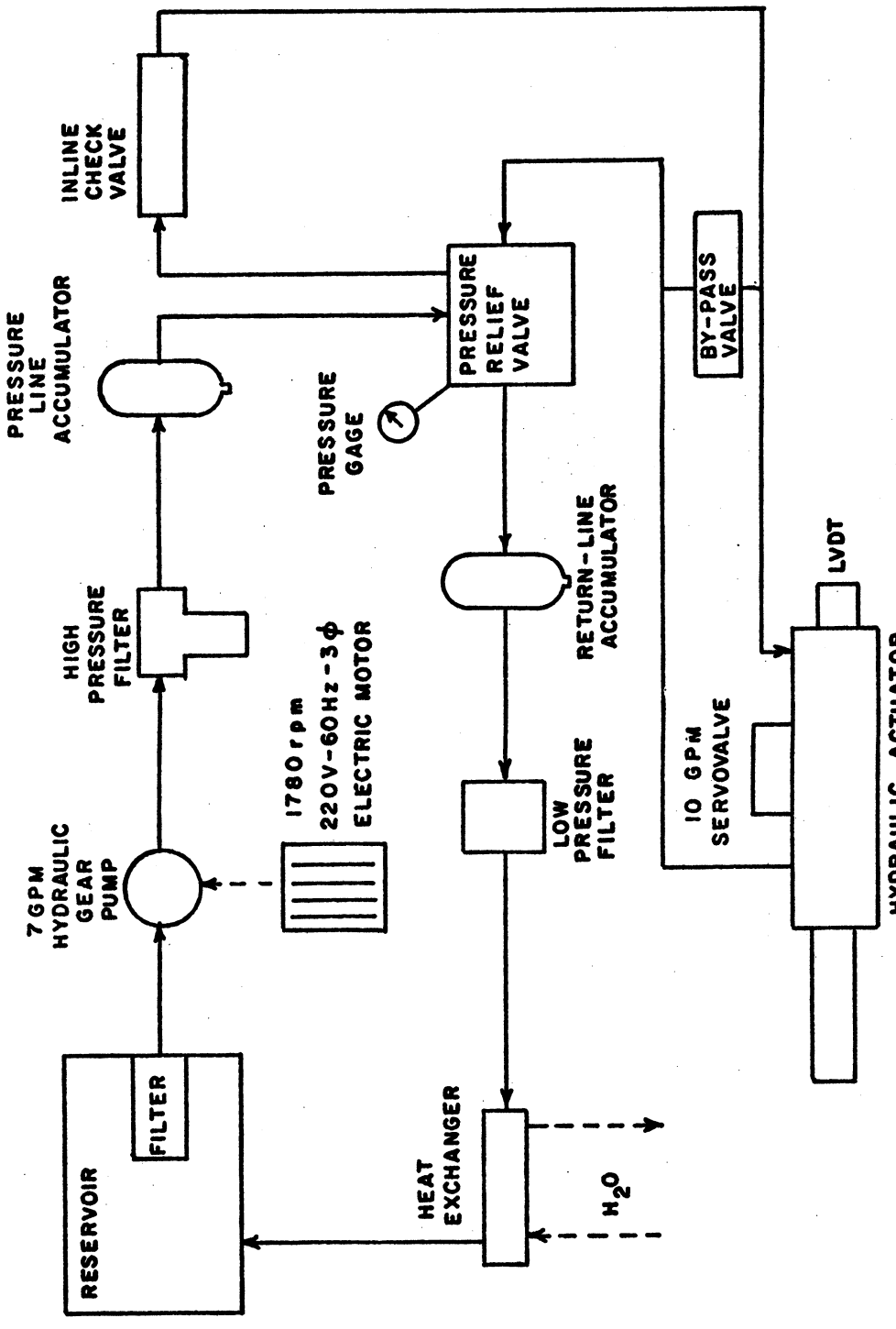

Figure 40. Schematic of hydraulic power supply system.

TABLE 3

COMPONENTS OF THE HYDRAULIC

POWER SUPPLY

Component	Type, Model
Electric Motor (1750 rpm, 15 hp, 220v)	Lincoln, 254T
Hydraulic Gear Pump (7 gpm)	Tyrone, 274P2-45-6D4-D
Return Line Accumulator (1 pint)	Greer, 30A - 1/8A
Pressure Line Accumulator (1 quart)	Greer, 30A - 1/4A
Finned Tube Heat Exchanger (water type)	Modine, TA8656
Inline Check Valve	Double A, DL-06-10A1
Relief Valve	Double A, B-06-10A1
Filters	
Dual Element Suction	Michigan Fluid Power, SU25
10 micron Pressure	Purolator, MS 28720-12
10 micron Return	Gresen, 1551-001
Temperature/Level Shutoff Switch	Gem, LS-800-T
Actuator (9 kip)	MTS, 204.02
Servovalve (10 gpm)	Moog, A076-103
Pressure Gage	MTS, 2½-AD-8719

to the motor is discontinued thereby shutting down completely. A shut down of this type does not damage the experimental specimen in any way, since the load would automatically be released.

A relief valve is used to prevent the hydraulic pressure from exceeding some preset value. In addition to this, a checkvalve prevents any possibility of backflow in the system.

This system is similar in operation to most commercial hydraulically powered testing systems and contains many of the same components. The system provides an economical as well as easily controlled power output and is, therefore, perhaps the most desireable power supply for a fatigue testing system.

3.1.3 ELECTRONIC FEEDBACK CONTROL SYSTEM

The purpose of the electronic feedback control system, Figure 41, is to set the test variables and continuously correct any variations from these predetermined settings. A schematic diagram of this system is presented in Figure 42. A detailed component list is given in Table 4.

The control unit provides manual or automatic control of the electric power, hydraulic pressure, program, and program counting. In addition to these, the control unit also provides interlocks which will stop the programmer and allow the gydraulic pressure to remain.

The function generator can provide sine, square, and triangle waveforms at frequencies from one hundredth (.01) to one hundred thousand (100,000) hertz. Operation of the function generator is controlled

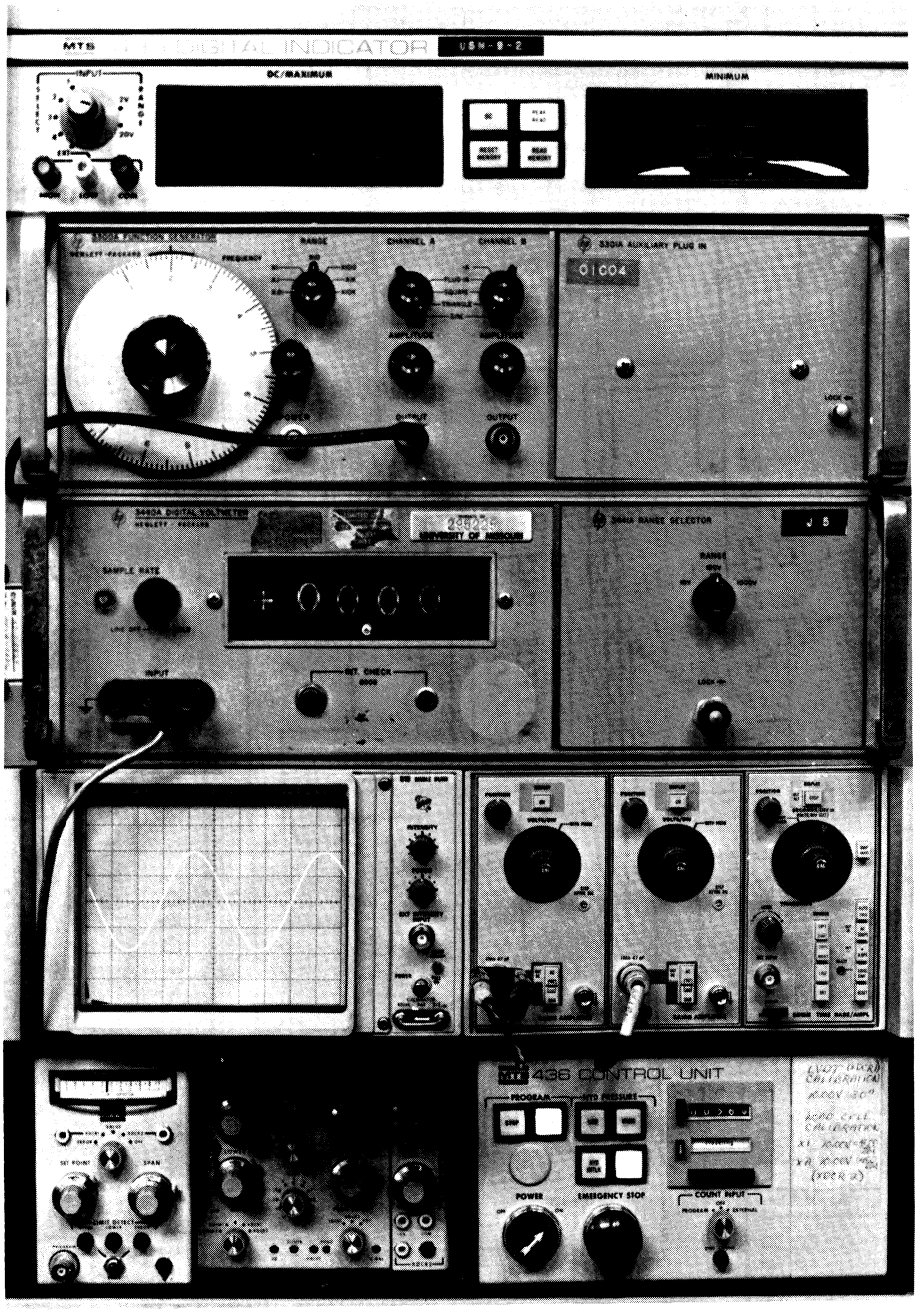

Figure 41. Electronic Console.

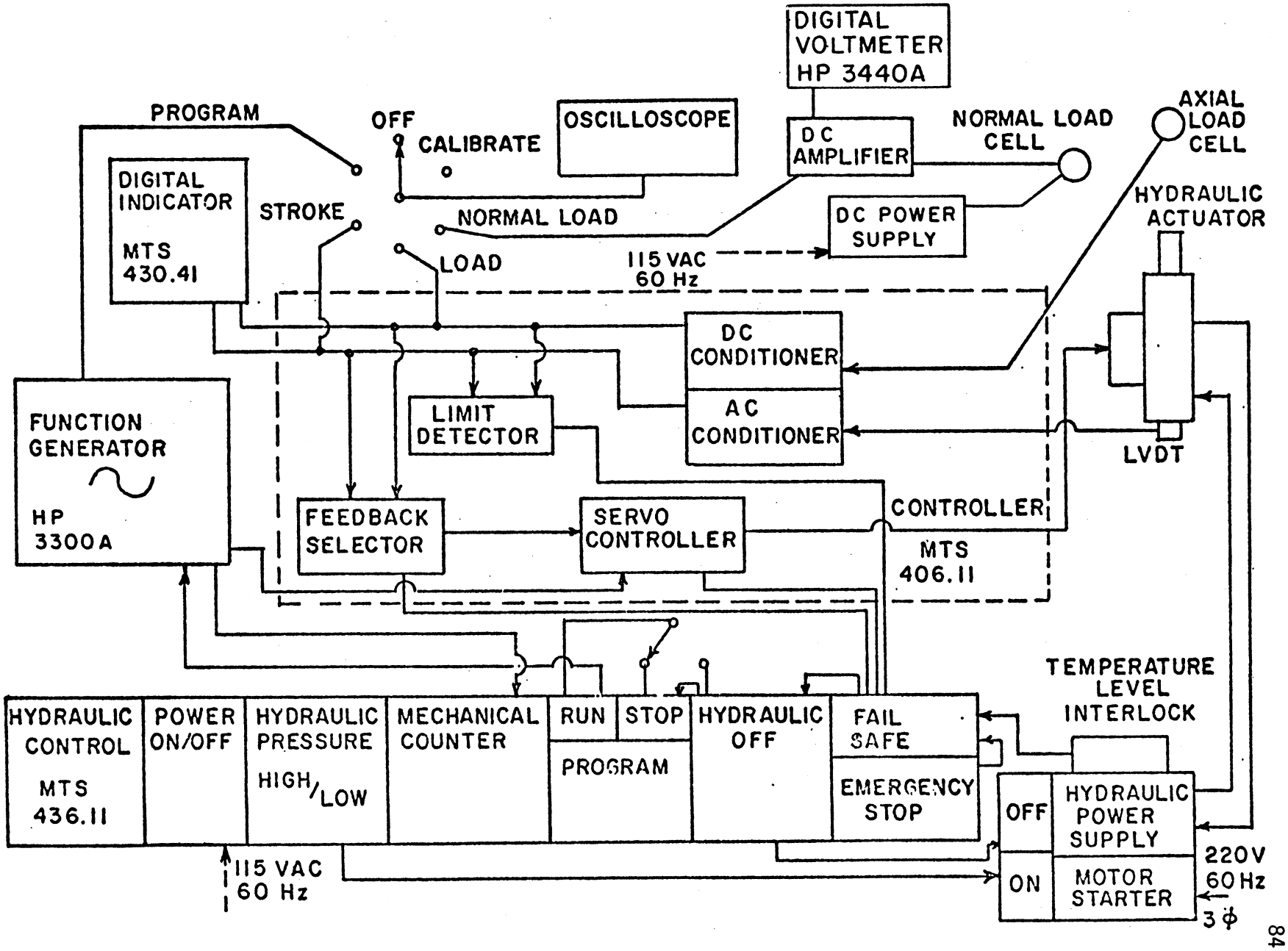

Figure 42. Electro-hydraulic servocontrolled fretting fatigue testing system.

TABLE 4

COMPONENTS OF THE ELECTRONIC

FEEDBACK CONTROL SYSTEM

Component	Type, Model
Control Unit	MTS, 436.11
Function Generator	Hewlett Packard, 3300A
Digital Indicator	MTS, 430.41
Oscilloscope	Tektronix, RM 502 A
Controller	MTS, 406.11
Digital Voltmeter	Hewlett Packard, 3440A
Normal Load Cell	Straincert, 1000 pound
Axial Load Cell	Straincert, 4500 pound (fatigue rated flat load cell)

by the program run of the control unit and in turn controls the counting of the counter panel in the control unit. Commands are sent from the function generator to the oscilloscope for display purposes and to the servo controller for comparison purposes. The servo controller compares the feedback signal with the command signal from the function generator.

The digital indicator is used to continuously monitor and display in digital form the voltage of the axial load cell and the linear variable differential transformer (LVDT) of the stroke control. The digital indicator operates in one of two modes; DC mode or Peak Read mode. The DC mode is selected for static or slowly changing inputs; the input maximum is displayed and updated at periodic intervals. Peak Read is selected for cyclic inputs and maximum and minimum values are displayed. Maximum and minimum values of the various inputs are stored and may be recalled during the experiment.

An oscilloscope is used to provide waveform information. The amount of distortion, if any, can readily be found from the oscilloscope thereby creating a distinct need for this equipment. Channels are reserved on the dual beam oscilloscope for the command signal from the function generator and the feedbacks from the axial and normal load cells as well as feed back of instantaneous position of stroke from the linear variable differential transformer (LVDT).

The controller is an electronic subsystem in itself and contains the servo control, failsafe, and readout functions of the electrohydraulic testing system. The servo controller provides the signal to

the servovalve during operation. When an error, exceeding a preset limit, is detected by the servo controller between the command and feedback signals, the error detector circuit opens a failsafe interlock to stop the test. The limit detector simply monitors the output of the DC and AC conditioners and indicates if the output exceeds some preset upper and lower limit; this can be used to open another fail-safe interlock and stop the test. The controller contains a DC conditioner for load feedback and an AC conditioner for stroke position feedback. The feedback selector may be positioned to provide monitoring of either of these transducer conditioners thus giving "load control" or "stroke control".

A straincent load cell is used to provide monitoring of the applied normal load. The constantly cycling normal load is monitored by a digital voltmeter. The normal load output is completely independent of other parts of the electronic system and is not controlled by an automatic feedback mechanism.

This electronic feedback control system provides excellent control over test variables throughout the period of the test. Ease of operation and good response are the main features of the system.

3.1.4 VACUUM SYSTEM

The vacuum system, Figure 43, provides the means by which the vacuum chamber, Figure 30, is evacuated. A schematic diagram showing the operational characteristics of the vacuum system is given in Figure 44. A list of the major components is presented in Table 5.

The main component of the system is the vapor diffusion pump. The

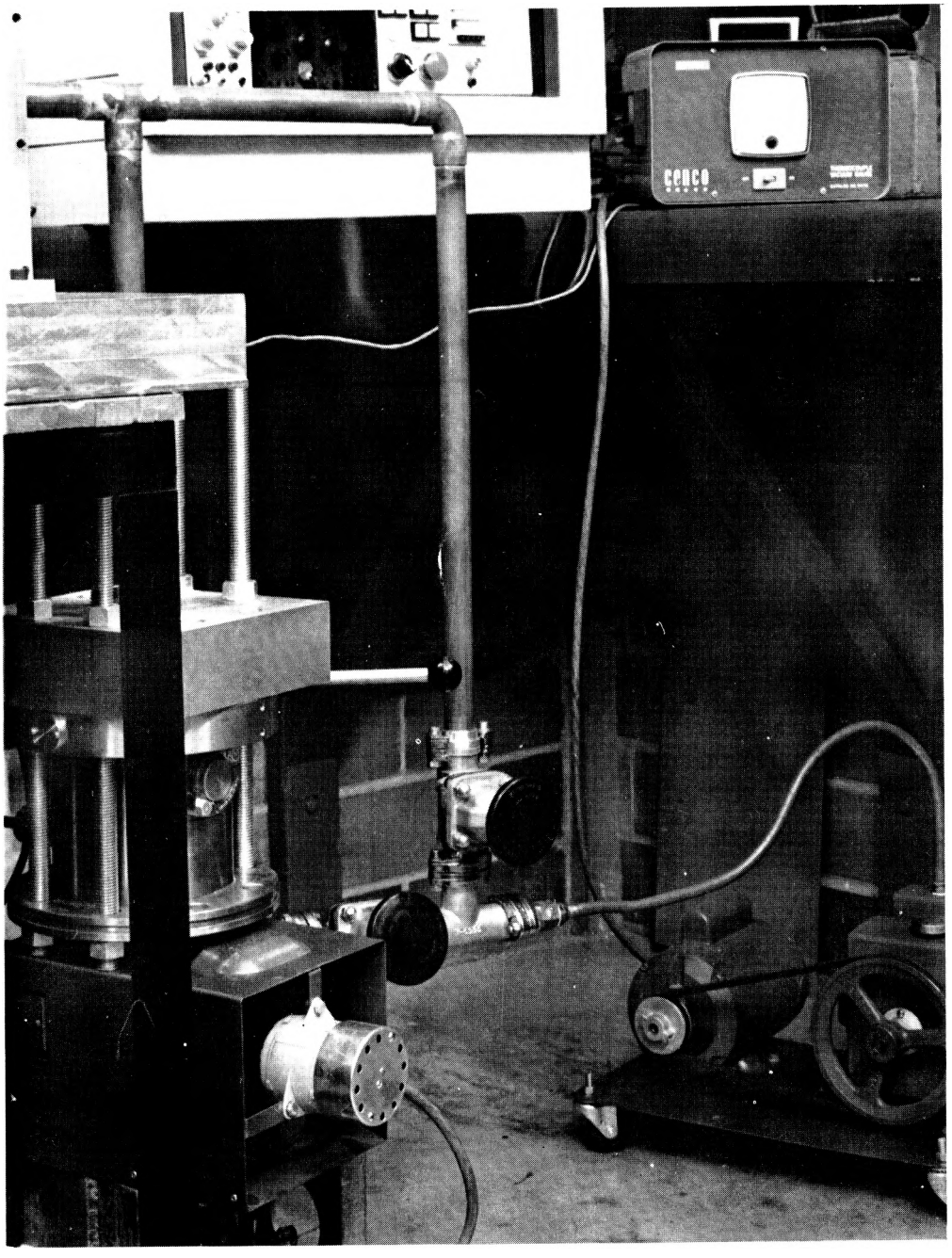

Figure 43. Vacuum system.

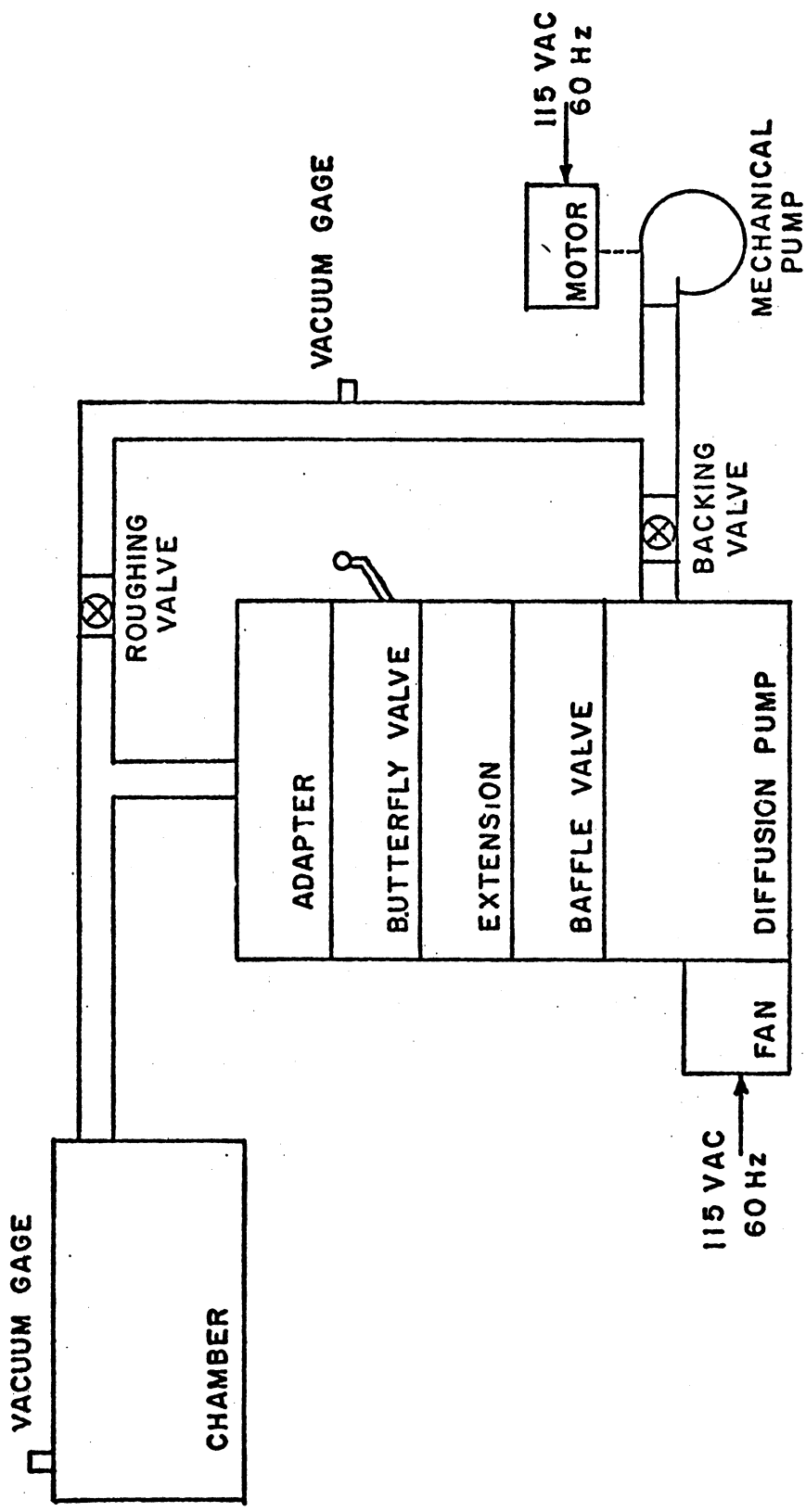

Figure 44. Schematic of vacuum system.

TABLE 5

COMPONENTS OF THE VACUUM SYSTEM

Component	Type, Model
Air Cooled Vapor Diffusion Pump	Edwards, E04
Chevron Baffle Valve	Edwards, CB4A
Quarter Swing Butterfly Valve	Edwards, QV4
Mechanical Pump	Welch, 1400M
Vacuum Gage (thermocouple)	Varian, 501
Vacuum Gage Readout*	Cenco, DO-91

*ranges from 1 atmosphere to 1 micron

(1 micron = 10^{-3}mmHg; 1mmHg = 1 torr)

model used is air cooled and has the capability of reaching as low as one ten millionth of a torr (10^{-7} torr). The diffusion pump is opened to the system by a quarter-swing butterfly valve.

A water cooled baffle valve is used as a cold trap for the system and is placed between the diffusion pump and the butterfly valve. This provides a means by which any outgassed vapors are condensed to prevent contamination, and thus reduced operating efficiency, of the diffusion pump.

Another major component of this system is the mechanical "roughing" and "backing" pump. This pump is used for two purposes:

1. To initially evacuate the chamber to approximately 50 microns (roughing).
2. To continuously evacuate the diffusion pump (backing).

The respective "backing" and "roughing" valves are shown in Figure 43. The method of operation is outlined in detail in section 3.3.3.

The vacuum gage indicates vacuum readings from one atmosphere down to one thousandth of a torr (10^{-7} torr). The gage is placed to that losses of vacuum in the vicinity of the specimen are easily detected. Thus, the system provides the environment required for the program of testing and remains quite simple to operate.

3.2 MATERIAL CHARACTERIZATION/PROPERTIES

A .40/.50 carbon steel (similar in composition to 1045 steel) was selected to be used to determine the effects of microstructure and environment on the fretting fatigue process. This steel contained

sufficient amounts of carbon so that a mixed structure of pearlite and ferrite could be obtained as well as a quenched and tempered structure, without any large secondary effects due to additional alloying elements.

3.2.1 COMPOSITION

The .40/.50 carbon steel used in this research effort was obtained in a hot-rolled sheet, four feet by ten feet by twelve gage. A chemical analysis of the material was performed by the Geology Department of the University of Missouri - Columbia (see Appendix 2). The quantitative results of this analysis are given in Table 6.

3.2.2 HEAT TREATMENT

It was desired to compare two microstructures of the given material for this study. One of the microstructures was that of the as received sheet of .40/.50 carbon steel. The second microstructure was a tempered martensite structure obtained by: austenitizing the material at 1500F (816C) for one hour; quenching the material in still water at room temperature; and tempering at 800F (427C) for one hour before being air cooled to room temperature.

3.2.3 TENSILE PROPERTIES

The tensile properties of both microstructures of the .40/.50 carbon steel were determined by using ASTM standard sheet specimens (see section 3.3). A two inch gage length extensometer was used during the tests to acquire load-extension data. The load was applied axially

TABLE 6

COMPOSITION OF .40/.50

CARBON STEEL SHEET*

Element	Concentration
Carbon	.40 - .50 weight %
Manganese	8230 ± 1900 ppm
Chromium	740 ± 170 ppm
Silicon	1760 ± 480 ppm
Iron	remainder

*See Appendix 2 for detailed analysis.

to the specimen by moving the actuator at a rate of .02 inches per minute. The results of the two tensile tests are given in Table 7. (It is noted from these data that the tempering process performed on the martensite has restored a large amount of ductility to the structure.)

3.2.4 HARDNESS

Rockwell hardness tests were made on the grip ends of several failed fatigue specimens. Ten hardness readings were taken for each microstructure on either the Rockwell "B" or "C" scales. These values were converted to the conventional Brinnel hardness numbers and are presented in Table 8.

3.2.5 MICROHARDNESS

The Vickers microhardness values of the constituents in the two microstructures were determined using a Leitz-Durimet Small Hardness Tester. These tests were performed on the metallurgically prepared specimens of the materials' surface. A standard Vickers indenter was used under a given load. By measuring the diagonals made by the diamond shaped indenter, the Vickers hardness number was calculated from the following equation [27]:

$$HV = 1854\ P/d^2 \tag{32}$$

where

P = load in grams

TABLE 7

TENSILE DATA FOR THE

.40/.50 CARBON STEEL

Property	As Received	Martensite
Ultimate Strength	108.3 ksi (747 MPa)	170.4 ksi (1175 MPa)
.2% offset Yield Strength	80.4 ksi (555 MPa)	151.2 ksi (1043 MPa)
Reduction of Area	28.5%	26.3%
Fracture Strength	131.3 ksi (906 MPa)	188.9 ksi (1303 MPa)
% elongation	14.4%	13.3%

TABLE 8

HARDNESS DATA FOR THE

.40/.50 CARBON STEEL

Microstructure	Mean Value Rockwell Hardness	Standard Deviation	Brinell Hardness
As Received	98.5 (R_B)	± 1.85	231
Martensite	34.7 (R_C)	± 2.57	321

TABLE 9

VICKERS MICROHARDNESS DATA

FOR THE .40/.50 CARBON STEEL

Microstructure	Mean Value, Vickers Microhardness (kg/mm^2)	Standard Deviation
As Received		
Pearlite	388.4	± 56.2
Ferrite	276.5	± 25.5
Martensite	488.0	± 78.1

d = mean diagonal of indentation in μm

Ten values were taken for each constituent. The mean values and standard deviations of the readings are given in Table 9.

3.3 MATERIAL PREPARATION AND EXPERIMENTAL PROCEDURES

The material was received in a hot-rolled sheet. Initial preparation of the material consisted of shearing the sheet into specimen blanks so that the longitudinal axis of the specimen corresponeded to the rolling direction of the sheet. Further preparation as well as testing procedures are given in the following four sections.

3.3.1 GENERAL GRINDING AND POLISHING

In order to minimize the effect that surface condition has on the fretting fatigue process, the fatigue and fretting fatigue specimens were carefully prepared so that repeatable results were readily obtainable. In this study, a "scratch free" surface was to be maintained for the fatigue and fretting fatigue specimens. During specimen machining, each surface was ground to a depth of approximately 0.0125 inches on each side so that the final specimen thickness was 0.100 inches. This was done on an automatic surface grinder. The specimens were then subjected to a series of grinding and polishing steps including the following: 240, 320, 400, and 600 grit silicone carbide abrasive papers; 30, 15, 9, and 3 micron diamond polishes; and a final 0.05 micron aluminum oxide solution polish.

3.3.2 FATIGUE TESTING

The fatigue specimens (see Figure 45) were tested in a feedback mode controlling the loads at a frequency of twenty hertz. A sinusoidal waveform was used with a ratio of minimum to maximum load, R. of one-tenth. Stree/life data were obtained for each of the two microstructures by consecutively testing at lower maximum stress levels until a specimen survived ten million cycles ("runout"). Consecutive tests were also conducted at higher maximum stress levels until a specimen's life became very short (less than ten thousand cycles). These data were used to generate stress/life plots for baseline fatigue of the particular microstructures.

The following procedures were followed in each of the fatigue tests:

1. Measure smallest cross section of a polished specimen with dial calipers.
2. Calculate operating loads (see Appendix 3).
3. Place specimen in grips by positioning the hydraulic actuator (system in feedback mode controlling actuator position or stroke, "stroke control").
4. Preload specimen to five hundred pounds (system in feedback mode controlling load, "load control").
5. Tighten grip bolts to fifty foot-pounds.
6. Adjust load to the calculated mean load.
7. Zero the cycle counter.
8. Start the test program.

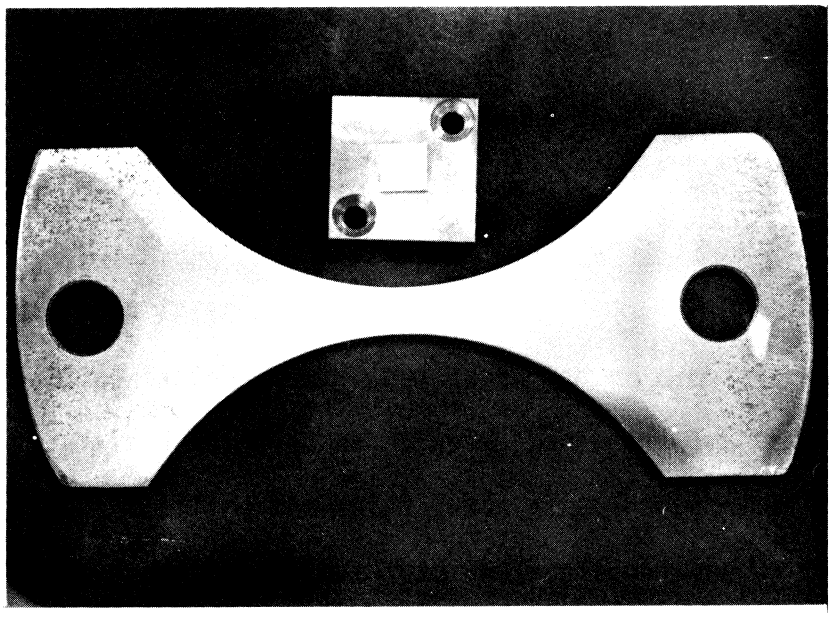

Figure 45. Fatigue specimen.

9. Adjust span setting to proper value from step 3.
10. Record temperature and relative humidity values throughout the specimen's life.
11. Cycle specimen to failure or ten million cycles (runout).
12. Average the values of temperature and relative humidity and record with number of cycles to failure in laboratory notebook.
13. Remove specimen from grips and spray fracture and wear surfaces with acrylic and store in vacuum dessicator for fractographic analysis.

3.3.3 FRETTING FATIGUE TESTING

Fretting fatigue tests were conducted on each microstructure in laboratory air and in vacuum. These specimens were tested in the feedback mode controlling the axial loads at a frequency of twenty hertz while a fixed support normal load was applied. The normal load was applied as shown in section 3.1.1.3 and was observed to fluctuate in correspondence to the axial load fluctuation. The data aquisition in each case was precisely the same as that described in the preceding section with the exception that no "runout" condition was experienced.

The procedure for testing the fretting fatigue specimens in air was slightly different than the procedure for baseline fatigue tests. The procedure used for fretting fatigue in air was as follows:

1. Meausure smallest cross section of a polished specimen with dial calipers.
2. Calculate operating loads (see Appenidx 3).

3. Measure cross section of a polished fretting pad with dial calipers.
4. Calculate normal load (see Appendix 4).
5. Place specimen in grips by positioning the hydraulic actuator (system in feedback mode controlling actuator position or stroke, "stroke control").
6. Preload specimen to five hundred pounds (system in feedback mode controlling the load, "load control").
7. Tighten grip bolts to fifty foot-pounds.
8. Adjust load to the calculate mean load.
9. Position normal load train above the fatigue specimen and apply the calculated normal load.
10. Zero the cycle counter.
11. Start the test program.
12. Adjust span setting to proper value from step 3.
13. Record temperature and relative humidity values throughout the specimen's life.
14. Cycle specimen to failure.
15. Average the values of temperature and relative humidity and record with the number of cycles to failure in laboratory notebook.
16. Remove specimen and spray fracture and wear surfaces with acrylic and store in vacuum dessicator for fractographic analysis.

The procedure used in the fretting fatigue vacuum testing was

slightly different in that steps to secure and evacuate the chamber were included. The procedure used for this type of testing was as follows:

1. through 9. Same as procedure in fretting fatigue in air.
10. Reduce the axial load to zero.
11. Secure the chamber by putting sides and bell jar in place (see section 3.1.4).
12. Open chamber to the mechanical pump until pressure is reduced to approximately fifty microns.
13. Turn on diffusion pump and allow mechanical pump to back the diffusion pump to approximately fifty microns.
14. Close the chamber to the mechanical pump and open to the diffusion pump (pressure will fall rapidly below one micron).
15. Adjust axial load to the calculated mean load.
16. Zero the cycle counter.
17. Start the test program.
18. Adjust span setting to proper value from step 3.
19. Cycle specimen to failure.
20. Record number of cycles to failure in laboratory notebook.
21. Close chamber to diffusion pump.
22. Open valve on bell jar to allow air into the chamber and remove chamber sides.
23. Remove specimen and spray fracture and wear surfaces with acrylic and store in vacuum dessicator for fractographic analysis.

24. Turn off diffusion and mechanical pumps unless another test immediately follows.

3.3.4 CRACK GROWTH TESTING

In order to establish the cracking characteristics of each microstructure, crack growth tests were conducted using center cracked panels macined from the same sheet of material as the fatigue and fretting fatigue specimens. Figure 46 shows the general appearance of the center cracked panels used in this study.

A jeweler's saw with an "extra fine" blade was used to introduce notches from a one sixteenth inch diameter hole in the center of the specimen. The total distance from notch tip to notch tip was between 0.135 and 0.185 inches. No difficulties were incurred by the notches as the fatigue cracks grew in a manner approximately perpendicular to the loading. It was also noted that the crack fronts from each notch remained in approximately the same plane.

Priliminary tests were made to determine proper loads and stress intensities by making several compliance measurements. An explanation of the method by which compliance measurements are used to calculate stress intensity is given in Appendix 5.

From these analyses, it was determined that a maximum load of 1750 pounds would be applied to the as received microstructure and a maximum load of 2000 pounds would be applied to the martensite microstructure. As in the fatigue and fretting fatigue test, a sinusoidal wave form was used at a frequency of twenty hertz and a ratio of minimum to maximum

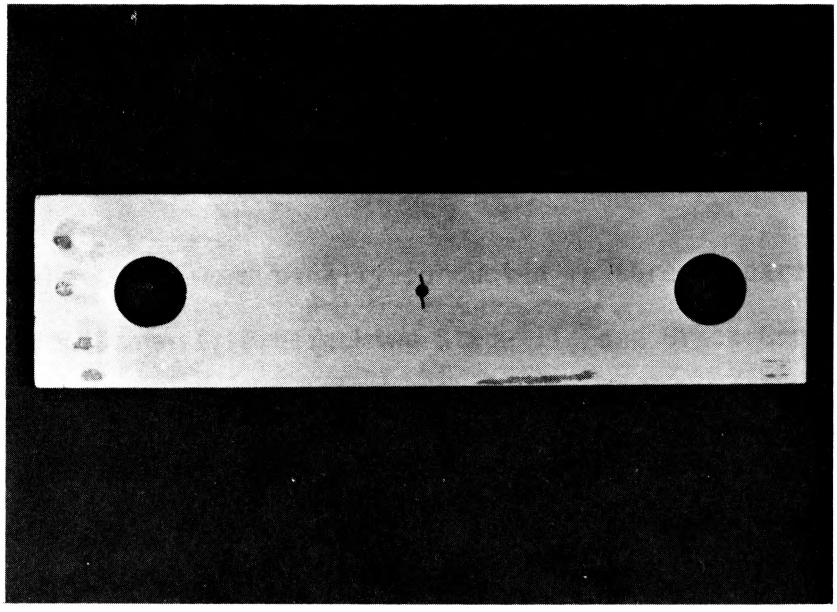

Figure 46. Center cracked panel.

load, R, of one tenth (this method was applied for all stages of the crack growth tests). The maximum applied load was held constant throughout the life of the specimen (to eliminate any effects due to changing load levels) and readings were made optically at various cyclic intervals. The method of measurement of crack length was by means of a travelling microscope attached to the load frame. The measurement intervals varied from once every ten thousand cycles to once every five hundred cycles, depending upon the rate at which the crack was extending.

The tests were usually conducted in three separate stages: Precracking Stage I; Precracking Stage II; and Crack Growth. Precracking Stage I involved initiating cracks from the ends of the notches and applying enough cycles to extend the crack length, 2a, to a value of approximately 0.200 inches. This stage was performed at a load higher than the load used for the actual crack growth testing in order to extend the cracks through any zone of residual stresses due to the notching. Precracking Stage II was used primarily to extend the cracks through any plastic zones created by the precracking in stage I. This stage was performed at a load less than the load used in the crack growth testing to as to minimize any plastic zones at the beginning of the crack growth test. This stage involved extending the crack length, 2a, to a value of approximately 0.225 inches. The crack growth portion involved setting the maximum load at the desired value and measuring crack lengths at various increments. From this the curves shown in section 4.2 were developed.

4.0 DATA ANALYSIS

The research discussed in this paper contains two basic types of data: stress/life data; and crack growth data (these data are tabulated in Appendix 6 and 7 respectively). While these types of data may be correlated to formulate needed information pertaining to a material's fatigue characteristics, the methods of analysis are somewhat different. The following three sections illustrate the methods used in this research effort to analyze the stress/life and crack growth characteristics of the .40/.50 carbon steel. Graphical representations of the data using the analyses are given in section 6.0.

4.1 STRESS/LIFE DATA

As outlined in the procedures section 3.3.2, the stress/life data was generated by choosing various maximum stress values and cycling the fatigue specimens until failure. These data were then plotted as number of cycles to failure for a given maximum stress level. An example of this type data is given in Figure 47. Since repetitive fatigue tests at various maximum stress levels were not conducted, a mathematical method of data analysis is not applied.

The method of data analysis for the stress/life data, therefore, is confined to visual observation of plotted data points. Since the material's characteristics are statistical in nature, the data points obtained in this research effort are contained within some unknown scatter. With this in mind, some conclusions may be drawn by visual

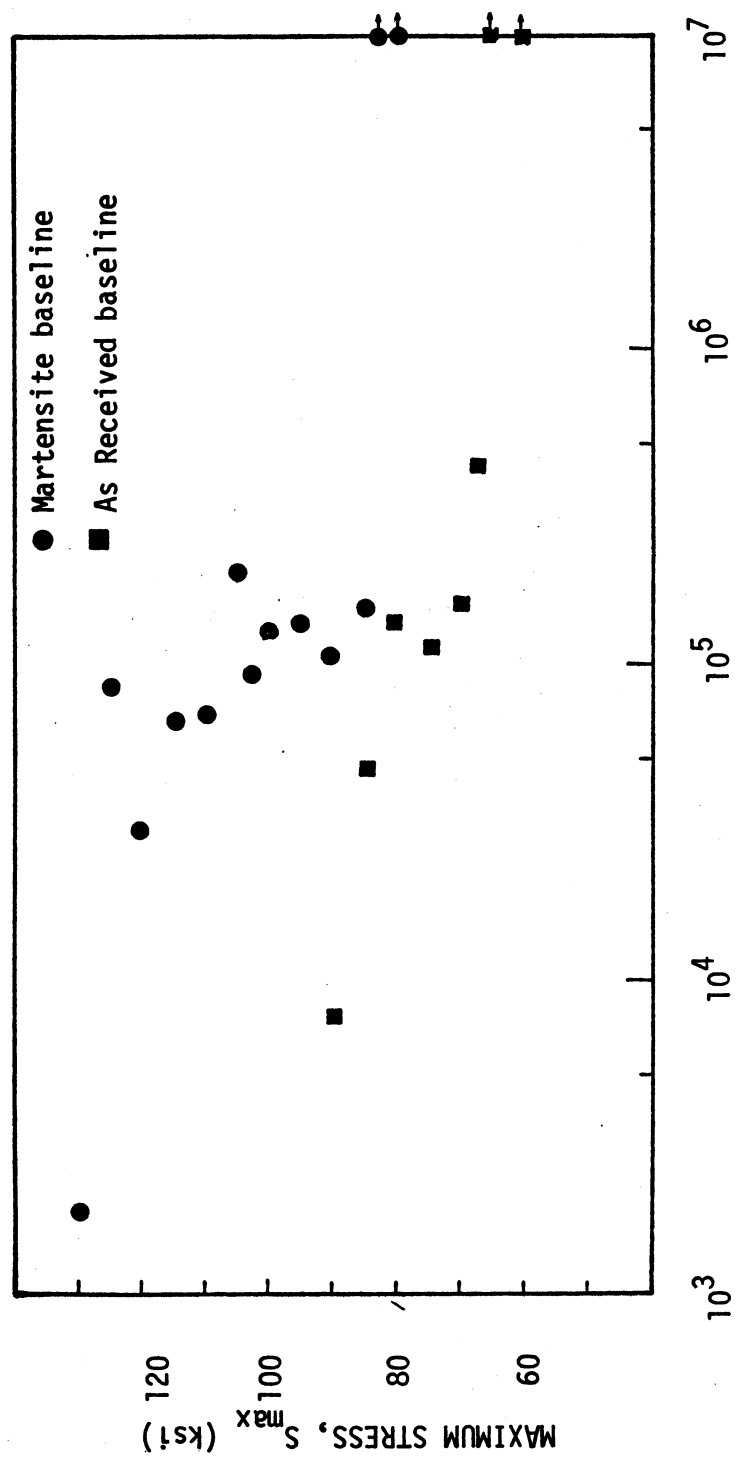

Figure 47. Comparison of as received and martensite baseline data.

observation of a limited number of data points. Even though, as in this case, a true prediction of the expected life at some given maximum stress cannot be made from this data, this visual technique may be used in comparing data sets. Trends may then be predicted from this type of analysis. Further discussions of each curve and the significance of their observed trends are contained in section 6.0.

4.2 CRACK GROWTH DATA

The actual crack growth data are given by the crack lengths in a center cracked panel after various numbers of fatigue cycles. Mathematical methods of analyzing these data are not needed since data points are located so close to each other. By plotting these data, a curve takes shape without the aid of fitting or numerical techniques.

The analysis of these data again is visual in that two crack growth tests were conducted of each microstructure so that a comparison of general shape and variance could be made. These comparisons, as those of the previous section, will be made in the discussion of the experimental results in section 6.0.

The statistical nature of the crack growth data is dealt with in the analysis of the crack growth rate data. These two types of data, crack growth and crack growth rate, are closely associated and cannot be completely separated. Thus, the statistical treatment used in the following section may also apply, indirectly, to the so-called crack growth characteristics generally associated with crack growth data.

4.3 CRACK GROWTH RATE DATA*

As mentioned in section 2.3.3.2, the functional dependence of crack growth rate on stress intensity range as given by Paris,

$$da/dN = C(\Delta K)^n \qquad (33)$$

is greatly limited. As evidenced by observed data sets of crack growth rate versus stress intensity range, the type of functional dependence illustrated in the equation proposed by Paris does not typify the actual data throughout the range of the data. At best, this equation may be used to illustrate some mean value of the data. The equation in no way represents the data in either region I, the threshold crack growth region, or region III, the unstable crack growth region. Thus, the type of functional relationship in equation 33 would not provide evidences of shifts in data sets in either regions I or III. These regions prove to be of utmost importance in determining the effects on fatigue crack growth characteristics of variables such as frequency, waveform, environment, stress ratio, and loading spectrum. Therefore, some form of curve fitting is needed which will formally represent the entire data set.

The functional relationships used in this study for relating the non-dimensional compliance to the normalized crack lenght (see Appendix 5) and the crack growth rate to the stress intensity range are [28]:

*A complete description of the computer techniques used in this analysis is given in Appendix 5.

$$(1 - 2a/W) = \exp(-(\frac{CEB - e}{v - e})^k) \quad (34)$$

$$(1 - \Delta K/K_B) = \exp(-(\frac{da/dN - e}{v - e})^k) \quad (35)$$

The non-dimensional compliance relationship with normalized crack length of equation 34 is of the form of a three parameter Weibull survivorship function. In this case the parameters are: k, the shaping parameter; e, the threshold parameter; and v, the characteristic value parameter. Similarly, the crack growth rate relationship with stress intensity range of equation 35 is of the form of a four parameter Weibull survivorship function. The additional parameter in equation 35 is K_B which takes on the value of the stress intensity range in the region of unstable crack growth.

The analysis of the crack growth rate data is dependent on an accurate analysis of compliance for the given material. Thus, for this analysis, compliance data for each microstructure is needed to define the relationship of equation 34. The method of establishing this relationship is given in Appendix 5. The values of the stress intensity range corresponding to various crack lenghts may be found using the analysis as outlined in Appendix 5. In addition, using the methods of regression analysis, corresponding values of crack growth rate may be used in conjunction with the calculated stress intensity range values to determine the four parameters: k, e, v, and K_B. By evaluating these parameters, an equation is established relating crack growth rate and stress intensity range for a given data set.

The procedural outline for the crack growth rate data analysis is given in Table 10.

TABLE 10

CRACK GROWTH RATE DATA ANALYSIS PROCEDURE*

1. Obtain compliance values at numerous crack lenghts for the given material, microstructure, etc.
2. Non-dimensionalize the compliance and mormalize the crack lengths.
3. Determine the expression for the stress intensity coefficient from the equation:

$$Y = \left[.5\left(\frac{1}{2a/W}\right)\frac{d(CEB)}{d(2a/W)}\right]^{1/2} \qquad (36)$$

4. Determine the expression for the stress intensity using the stress intensity coefficient of equation 36:

$$K = \frac{P\sqrt{2a}}{BW} Y \qquad (37)$$

5. Use regression analysis of crack growth rate versus stress intensity range data to determine the parameters used in equation 35.
6. Determine scatter of data about proposed equation using regression analysis.

* See Appendix 5 for complete information on these procedures.

5.0 METALLOGRAPHIC AND FRACTOGRAPHIC ANALYSIS

Metallography and fractography are important in determining the characteristics of a material and the failure modes to which it is susceptible. Metallography is an important tool in determining the general microscopic structure of a given material thus explained the randomness of many of its properties. Fractographic analysis of controlled experimental specimens is useful in illustrating the change in general failure mechanisms for different experimental conditions. Thus, fractographic analysis may be useful in explaining the effects various conditions have on a given material. The following two sections will illustrate the use of these analysis methods for this study.

5.1 METALLOGRAPHY

The photomicrographs of the as received and martensite microstructures are shown in the following figures. Lhese figures clearly illustrate that the material is not isotropic, homogeneous, continuous material as is commonly assumed in mathematical analyses. It is noted that the as received microstructure seems somewhat more random in its nature than the martensite microstructure.

Figures 48 and 49 show the microstructural configurations of the surfaces of the as received and martensite microstructures respectively in the condition as they were fatigue (i.e., after machining, grinding, and polishing procedures). These figures may be compared to those of Figures 50 and 51 before any machining operations. This comparison

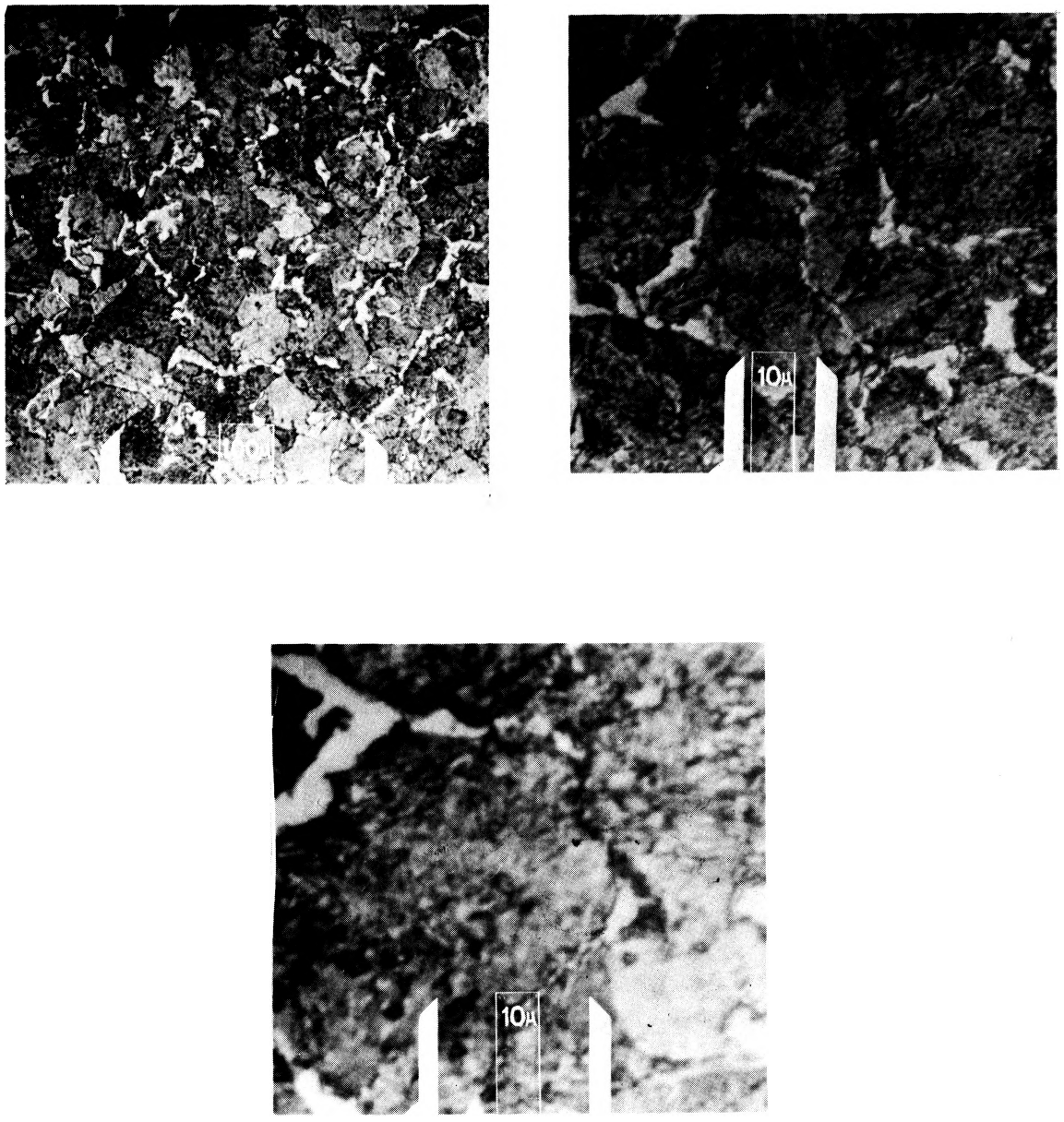

Figure 48. Surface of a typical specimen of the as received microstructure after machining.

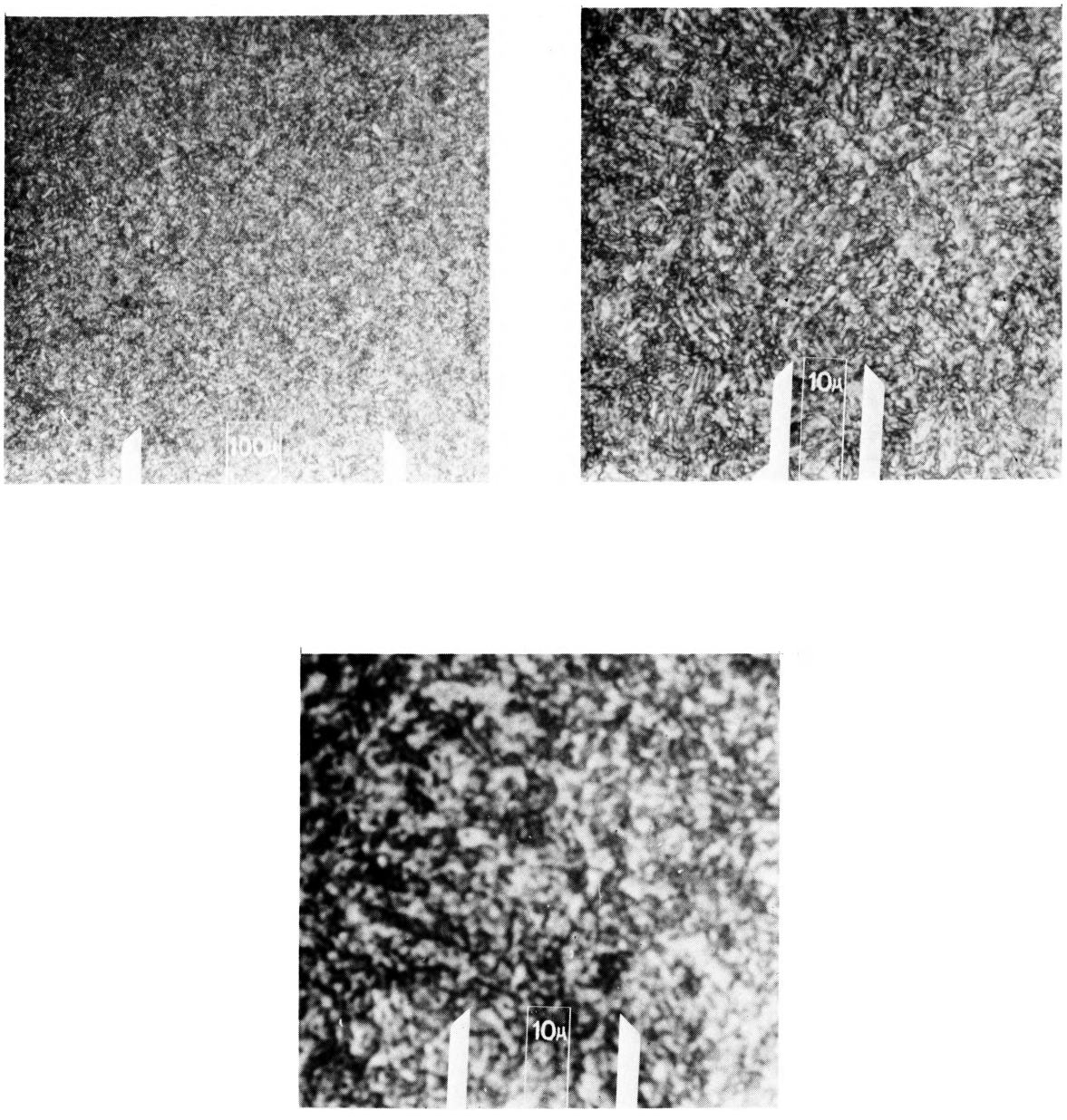

Figure 49. Surface of a typical specimen of the martensitic microstructure after machining.

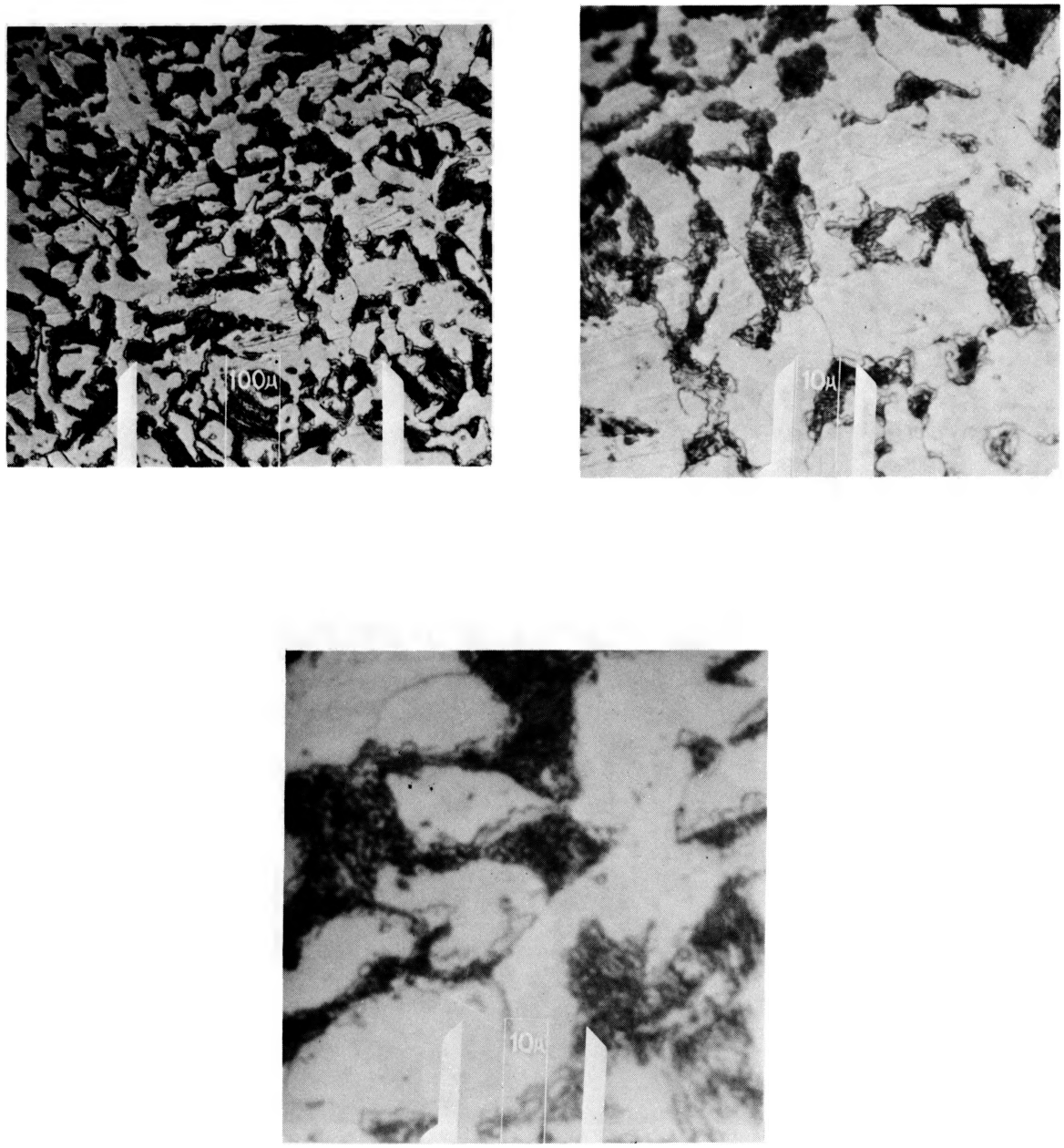

Figure 50. Surface of a typical specimen of the as received microstructure before machining.

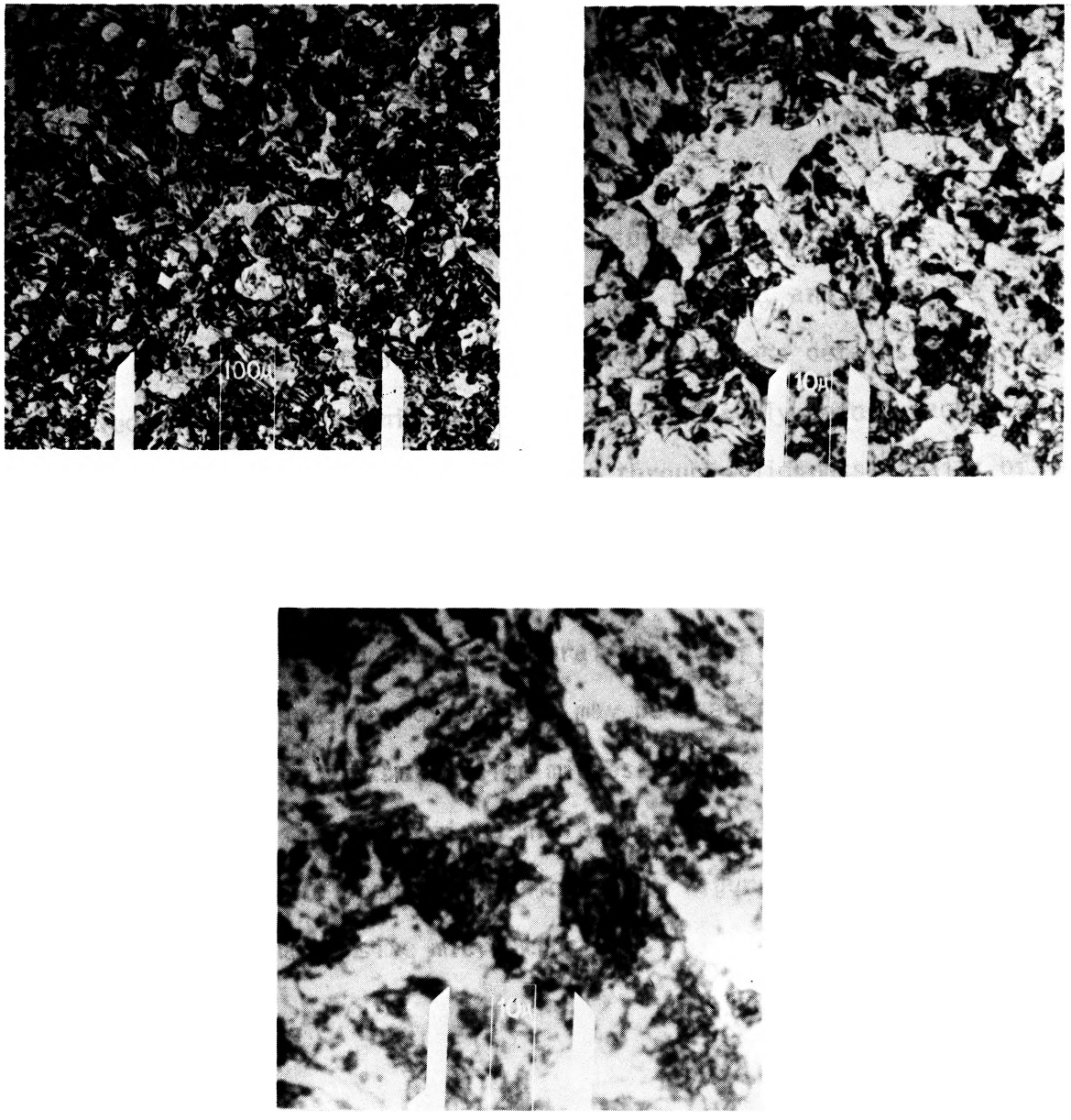

Figure 51. Surface of a typical specimen of the martensitic microstructure before machining.

illustrates that unwanted surface conditions from rolling and heat treatment operations are eliminated.

To further establish that unwanted surface conditions are removed during the machining processes, Figures 52, 53, 54, and 55 may be compared. Figures 52 and 53 show the through-thickness details of the as received and martensite microstructures respectively before machining operations. Figures 54 and 55 show the through-thickness details of the as received and martensite microstructures respectively after machining.

The differences in microstructural characteristics between the normal and axial specimen directions may be seen in Figures 56 and 57 for the as received and martensite microstructures respectively. Figure 56 compares the as received microstructure at the specimen's surface and through the specimen's thickness. Figure 57 compares the same details for the martensite microstructure.

5.2 FRACTOGRAPHY

The fractographic analysis consists of both macroscopic examination of typical fracture and wear surfaces and microscopic examination of the same surfaces. The macroscopic views are simply enlargements made in conjunction with close-up photography. The microscopic views are images obtained from scanning electron microscopy.

5.2.1 MACRO FRACTOGRAPHY

To illustrate the macroscopic differences in fracture character-

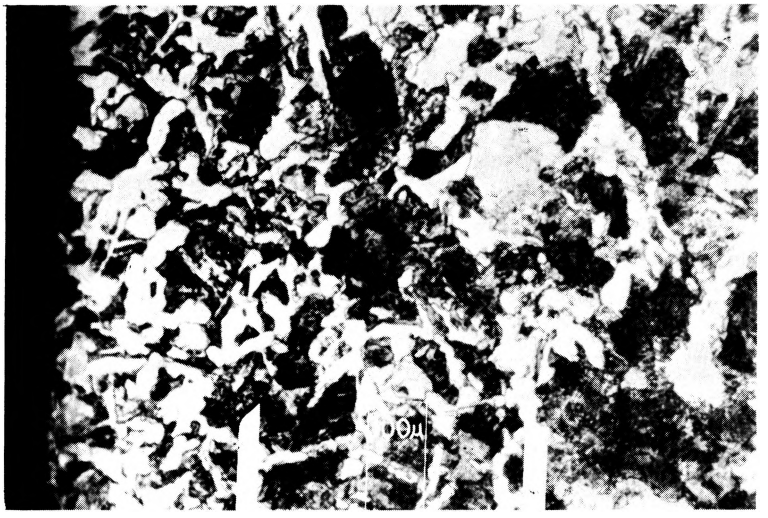

(a)

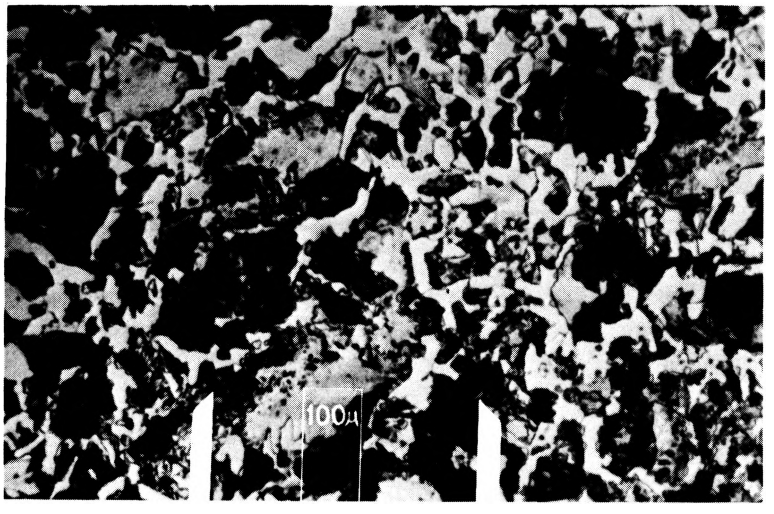

(b)

Figure 52. Comparison of the as received microstructure through the specimen's thickness before machining; (a) at the surface, and (b) midway through the thickness.

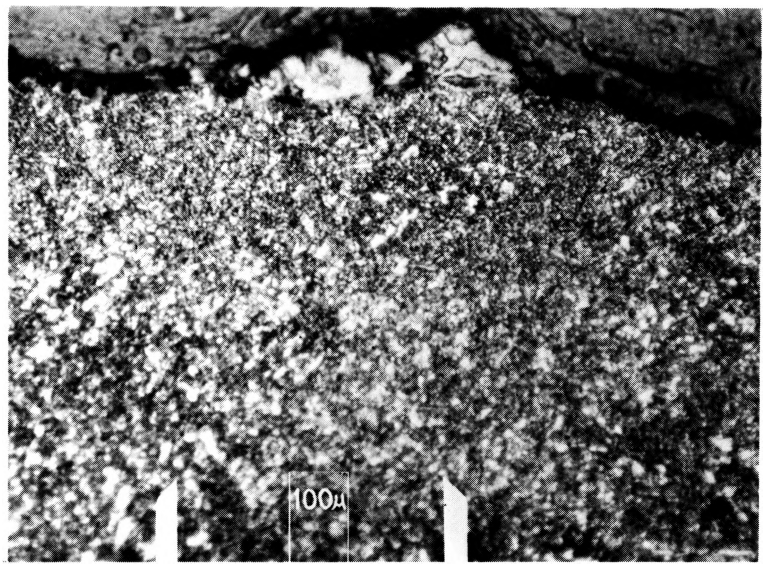

(a)

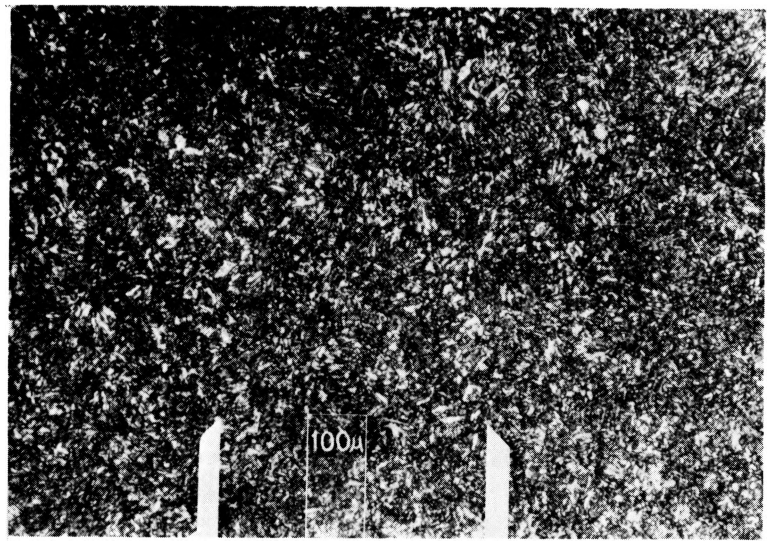

(b)

Figure 53. Comparison of the martensite microstructure through the specimen's thickness before machining; (a) at the surface, and (b) midway through the thickness.

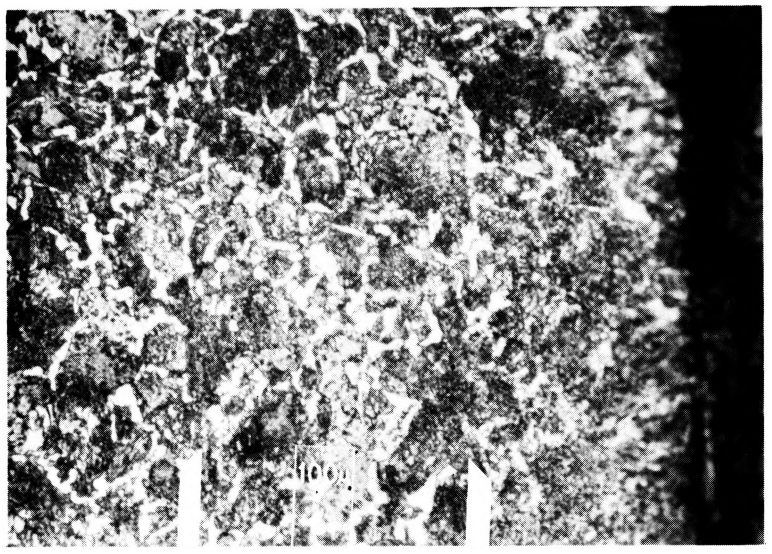

(a)

(b)

Figure 54. Comparison of the as received microstructure through the specimen's thickness after machining; (a) at the surface, and (b) midway through the thickness.

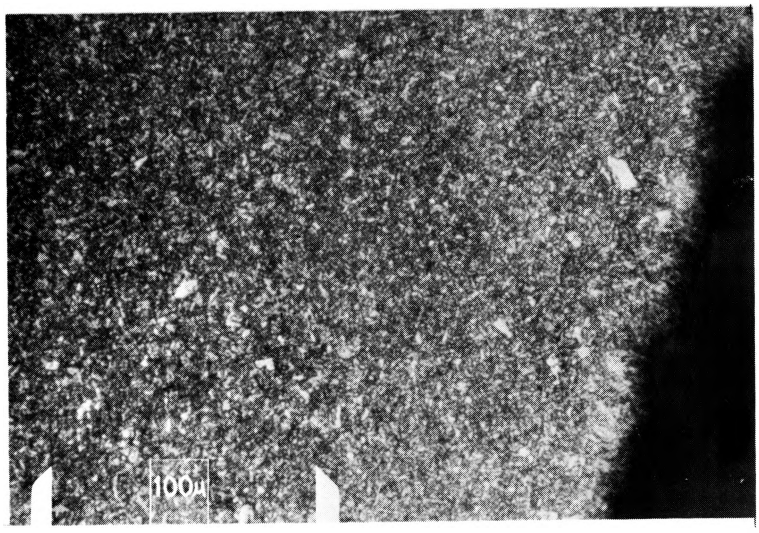

(a)

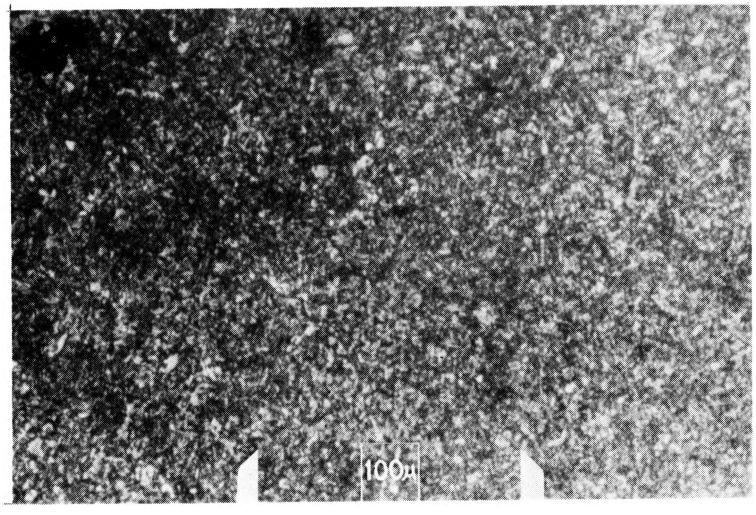

(b)

Figure 55. Comparison of the martensite microstructure through the specimen's thickness after machining; (a) at the surface, and (b) midway through the thickness.

(a)

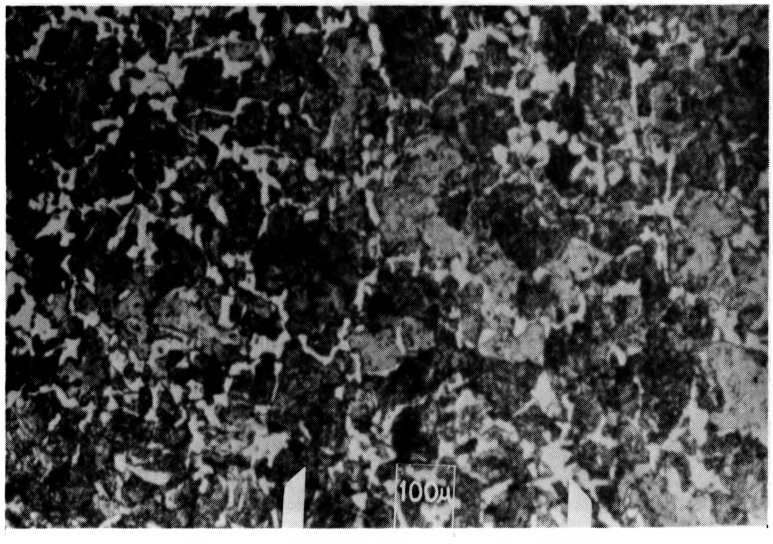

(b)

Figure 56. Comparison of (a) the surface and (b) through thickness as received microstructures after machining.

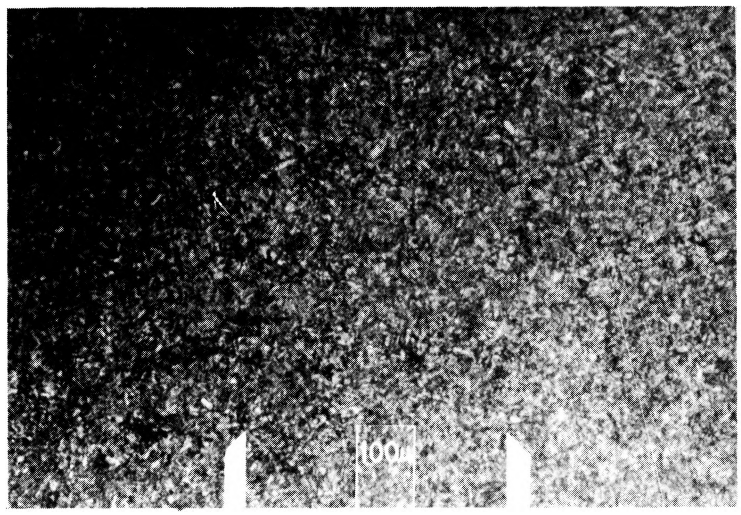

(a)

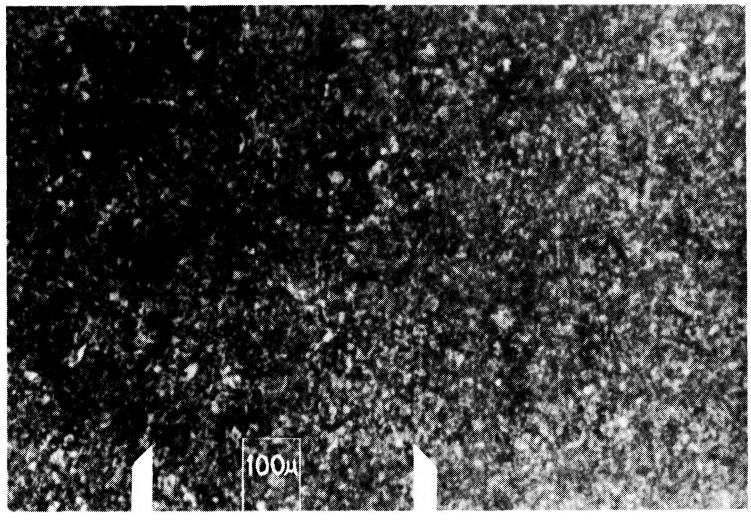

(b)

Figure 57. Comparison of (a) the surface and (b) through thickness martensite microstructures after machining.

istics, a number of figures are presented. Figures 58, 59, and 60 show typical long and short life failures of the as received microstructures for the baseline, fretting, and vacuum fretting fatigue specimens. Likewise, Figures 61, 62, and 63 illustrate these same types of failures for the martensite microstructure. Note that specimen 3-33 of Figure 61 survived over ten million cycles or "run-out", Figure 64 shows both the as received and martensite crack growth specimens. These figures illustrate slight differences by which the test conditions cause failures.

Macro views of the various fracture surfaces are presented in Figures 65 through 72. With the exception of the crack growth fracture surfaces of Figures 71 and 72, all of the macrophotographs are at ten times their actual size. The crack growth fracture surfaces are at three times their actual size. The figures illustrate, in general, the macro failure characteristics for the various test conditions.

5.2.2 MICRO FRACTOGRAPHY

The micro fractography involves microscopic examination of fracture and wear surfaces of both the as received and martensite microstructures. In additions, systematic views of the crack growth specimens' fracture surfaces of these microstructures are presented. The system for presenting the crack growth microscopic vies is presented in Figure 73 and Table 11.

An as received wear surface is shown in Figure 74. This figure exemplifies the type of wear surface found on an as received fretting fatigue specimen tested in laboratory air. Figure 75 illustrates the

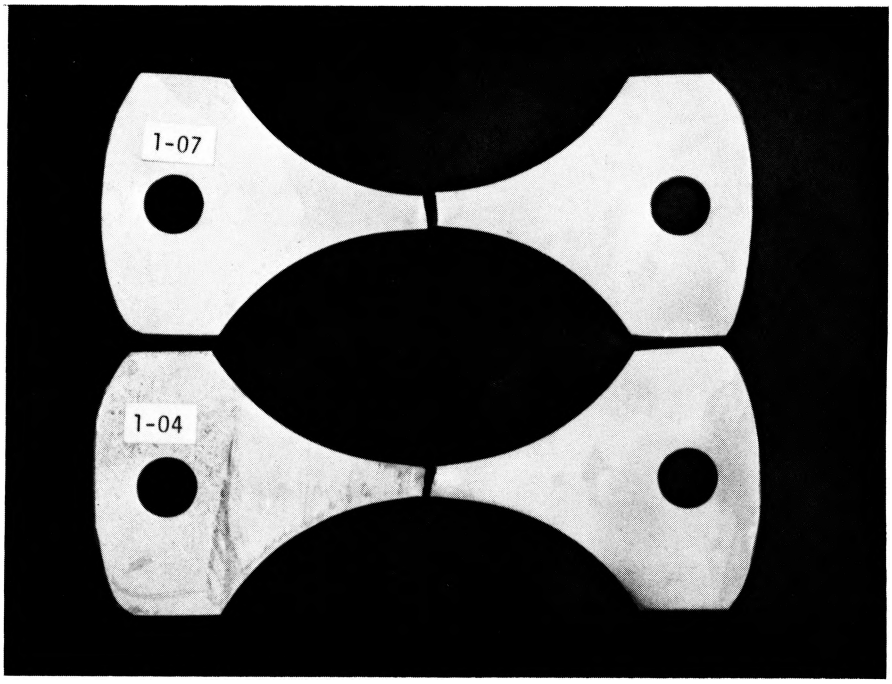

Figure 58. Comparison of long life (1-07; 427,900 cycles) and short life (1-04; 7,640 cycles) as received baseline fatigue specimens.

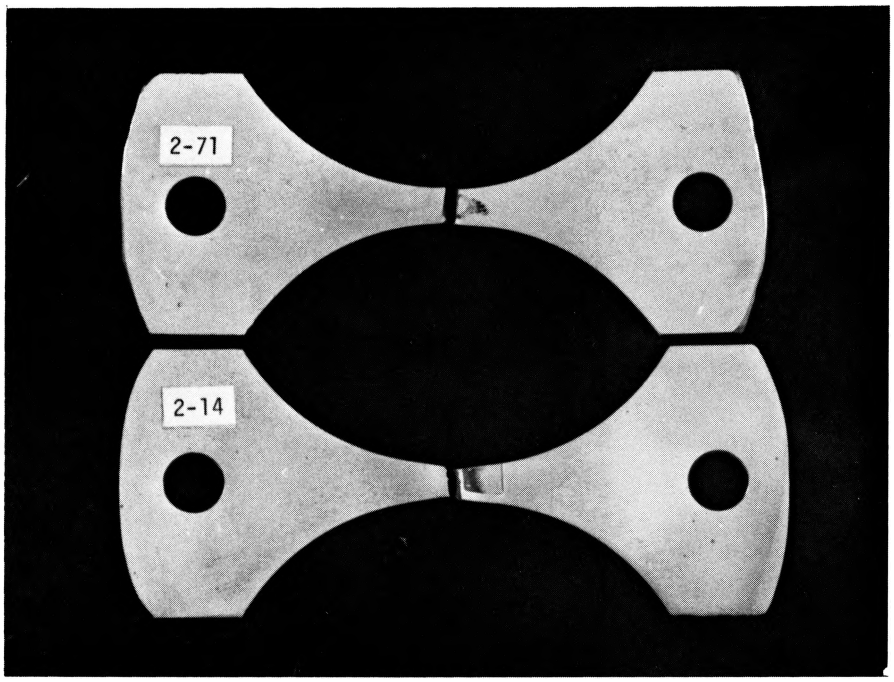

Figure 59. Comparison of long life (2-71; 733,590 cycles) and short life (2-14; 6,120 cycles) as received fretting fatigue specimens.

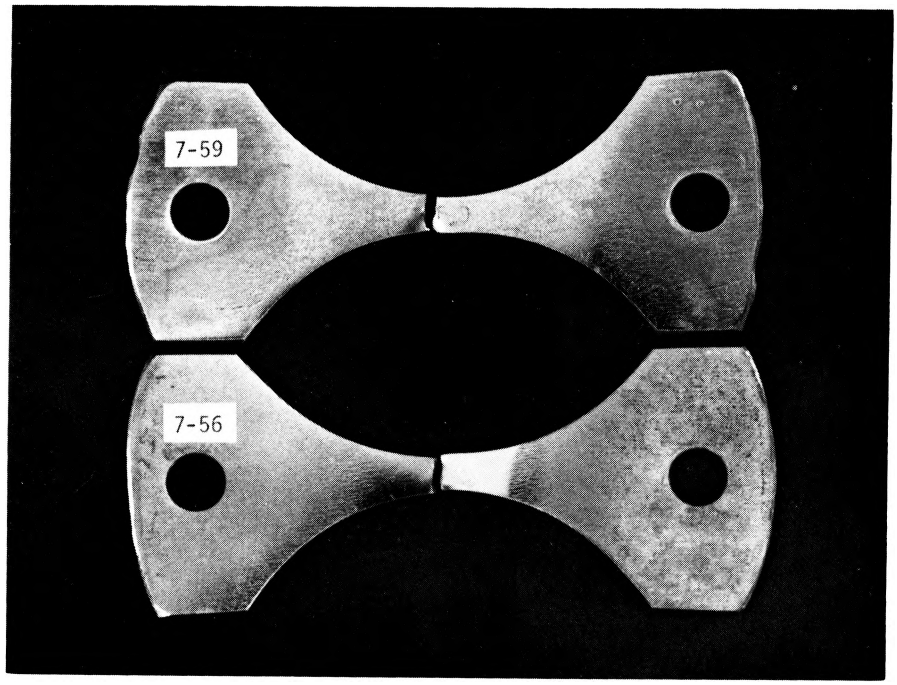

Figure 60. Comparison of long life (7-59; 2,371,090 cycles) and short life (7-56; 87,360 cycles) as received vacuum fretting fatigue specimens.

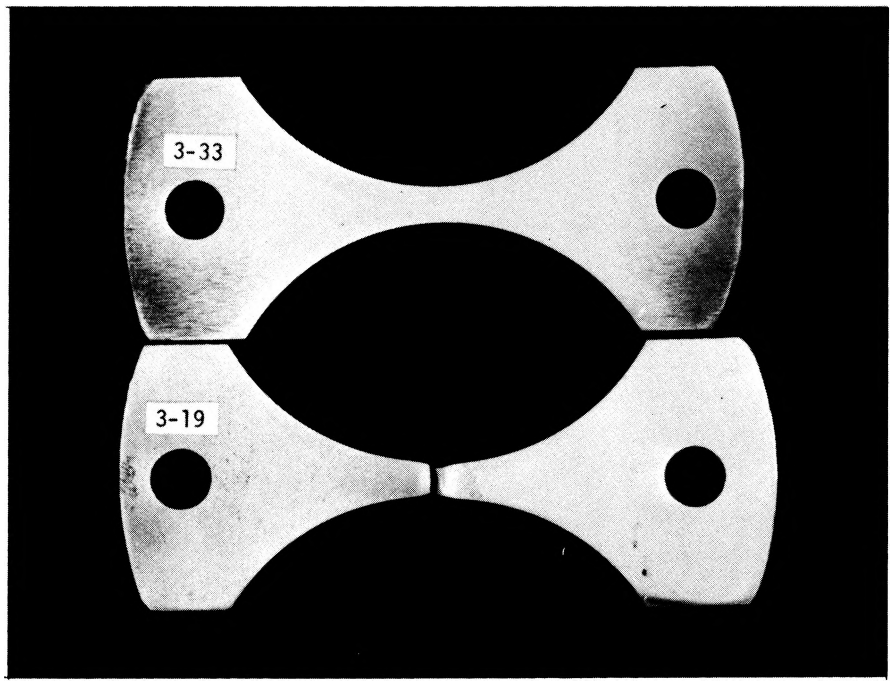

Figure 61. Comparison of long life (3-33; 10,000,000+ cycles) and short life (3-19; 1,790 cycles) martensite baseline fatigue specimens.

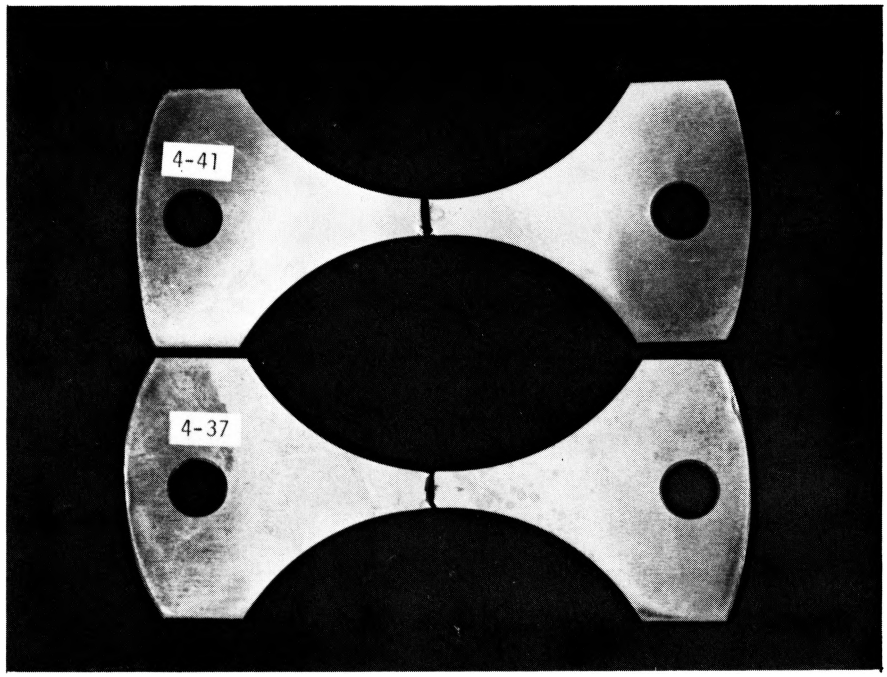

Figure 62. Comparison of long life (4-41; 1,034,640 cycles) and short life (4-37; 45,510 cycles) martensite fretting fatigue specimens.

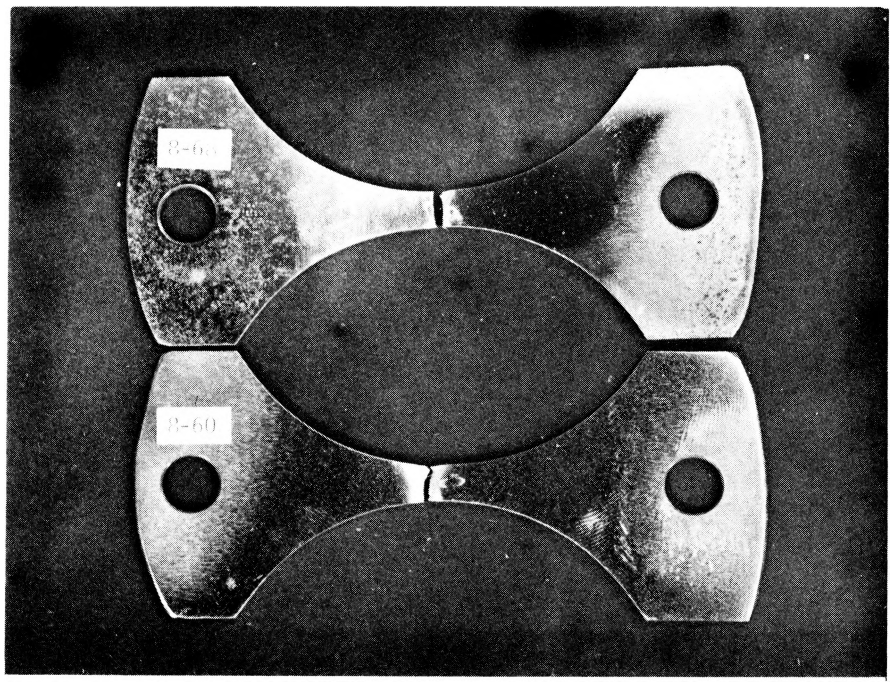

Figure 63. Comparison of long life (8-68; 2,813,990 cycles) and short life (8-60; 260,570 cycles) martensite vacuum fretting fatigue specimens.

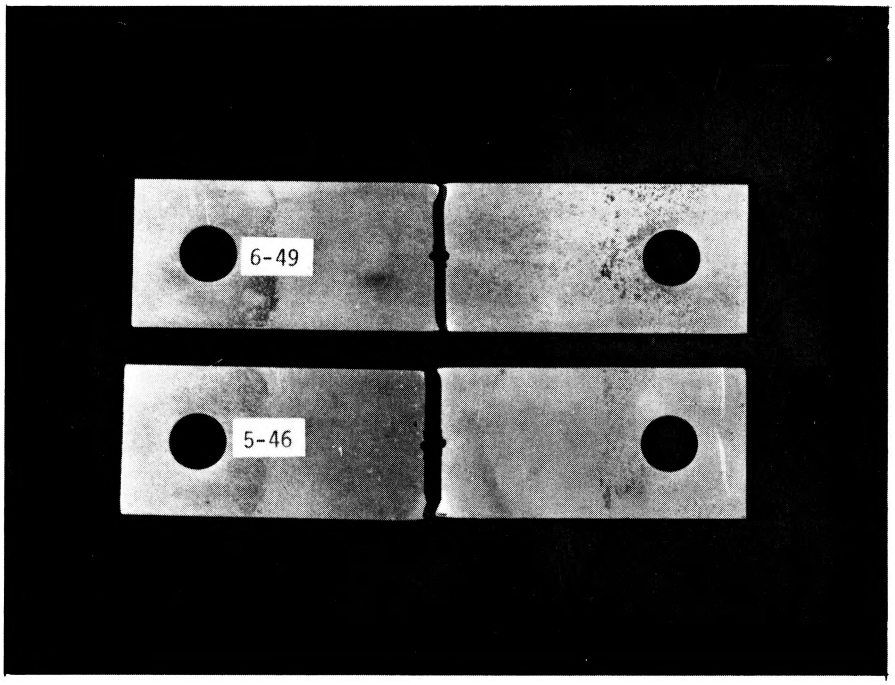

Figure 64. Crack growth specimens of martensite (6-49) and as received (5-46) microstructures.

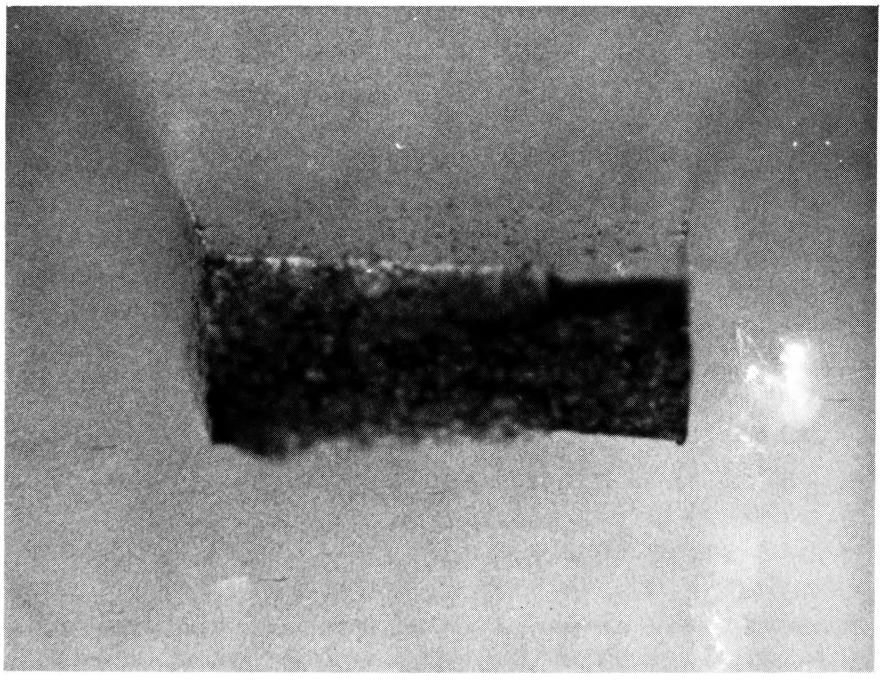

Figure 65. Fracture surface of as received baseline fatigue specimen 1-04 (7,640 cycles).

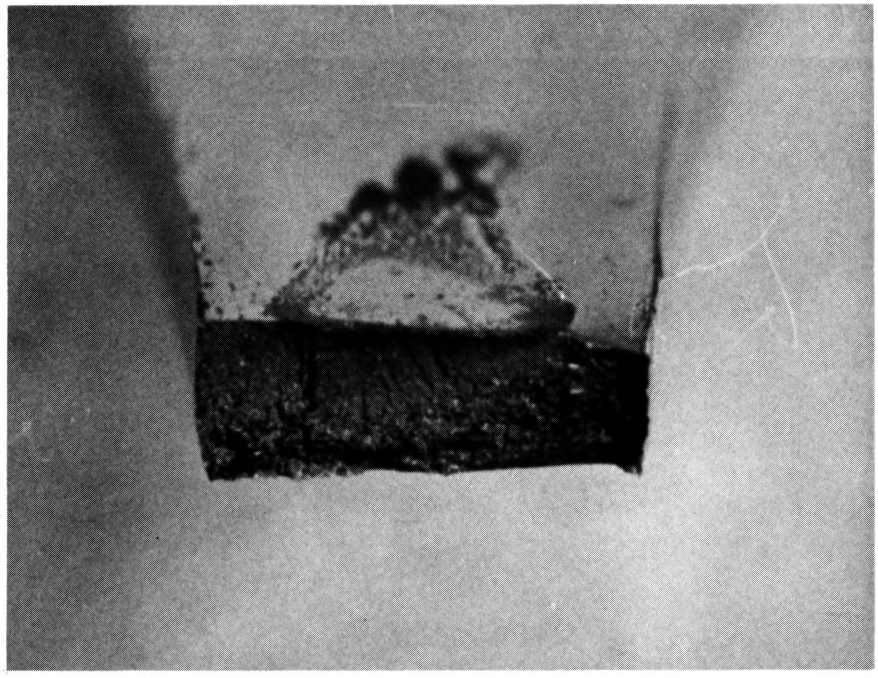

Figure 66. Fracture surface of as received fretting fatigue specimen 2-71 (733,590 cycles).

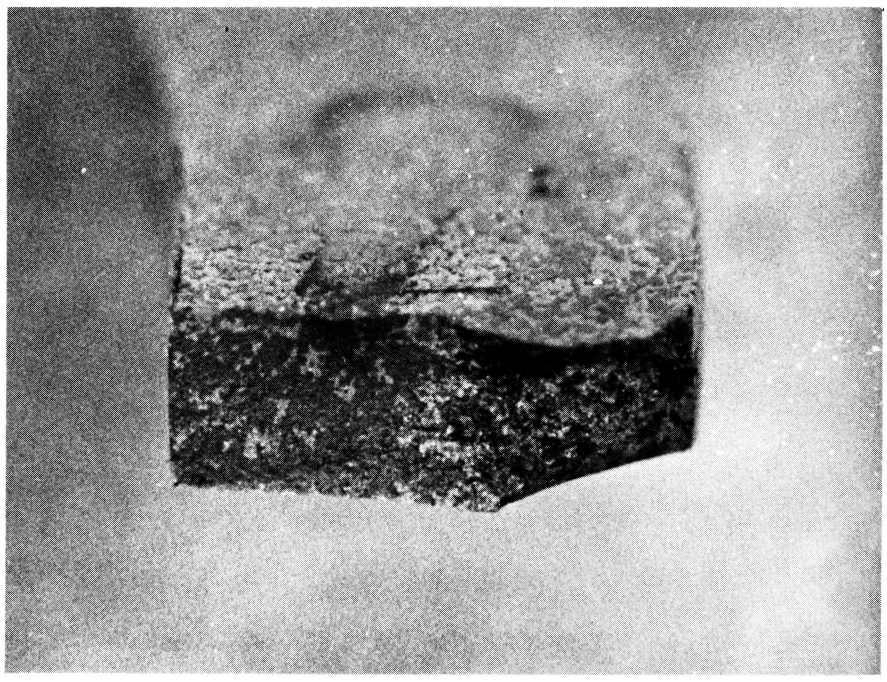

Figure 67. Fracture surface of as received vacuum fretting fatigue specimen 7-59 (2,731,090 cycles).

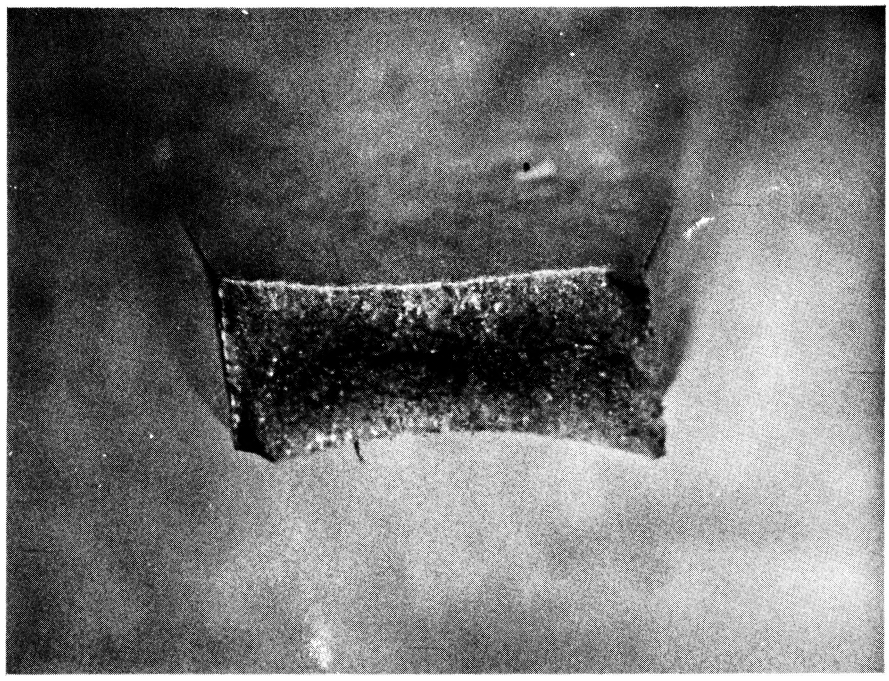

Figure 68. Fracture surface of martensite baseline fatigue specimen 3-19 (1,790 cycles).

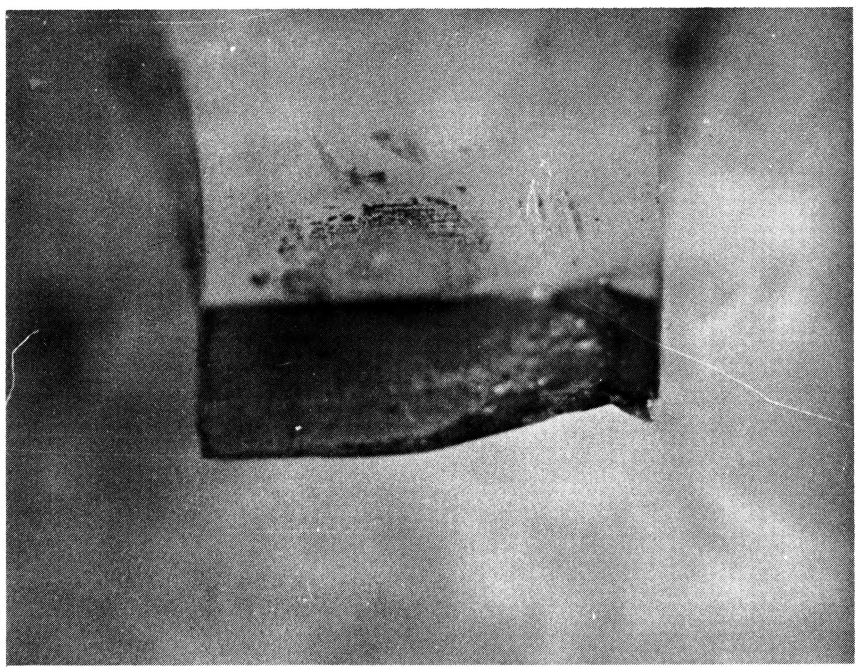

Figure 69. Fracture surface of martensite fretting fatigue specimen 4-41 (1,034,640 cycles).

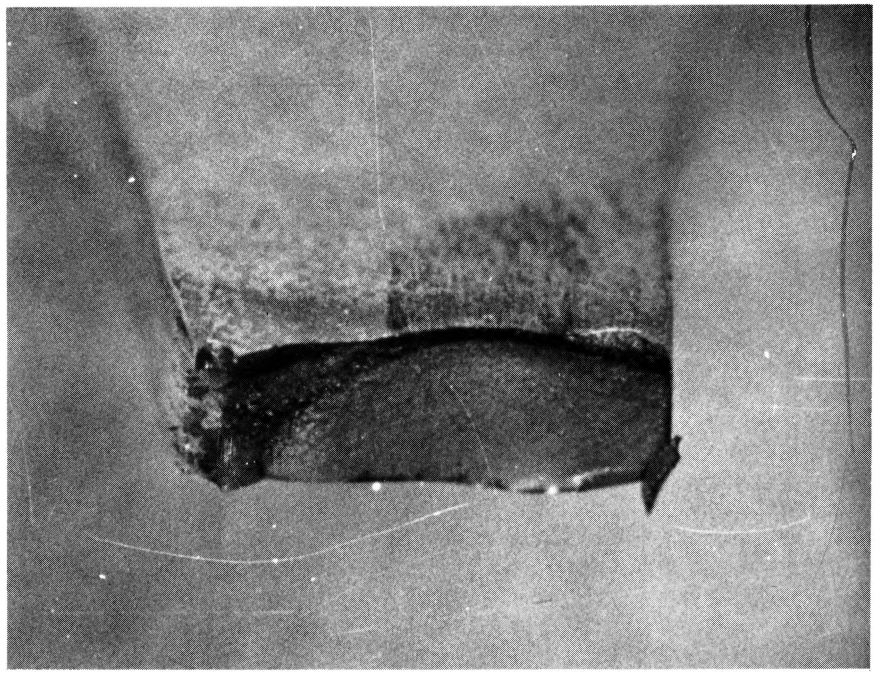

Figure 70. Fracture surface of martensite vacuum fretting fatigue specimen 8-68 (2,813,990 cycles).

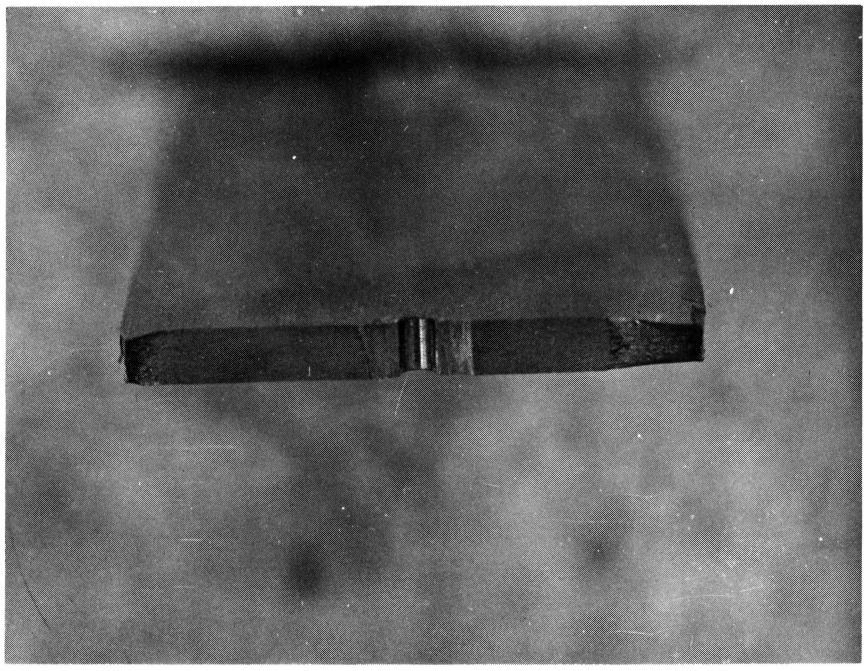

Figure 71. Fracture surface of as received crack growth specimen 5-46.

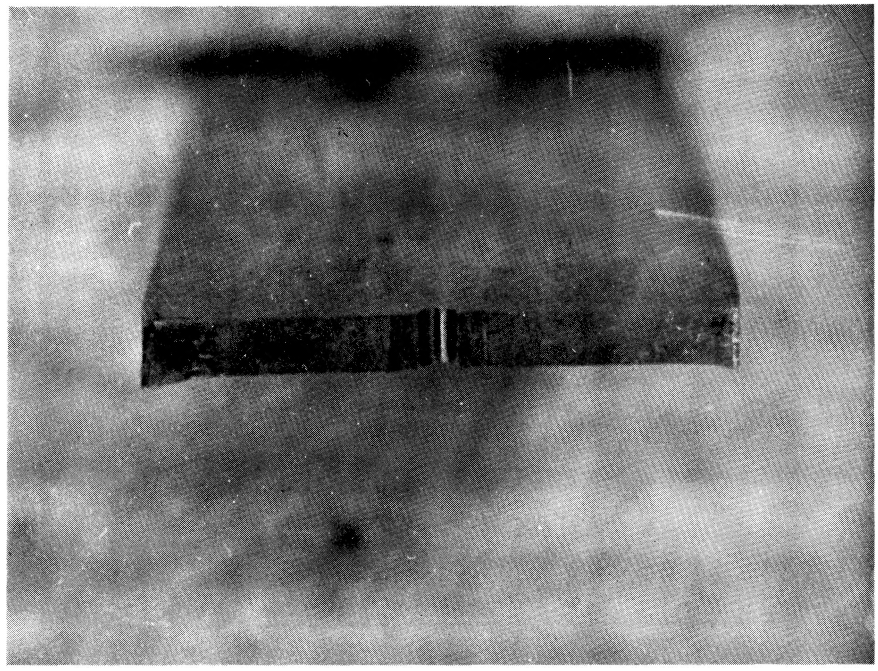

Figure 72. Fracture surface of martensite crack growth specimen 6-49.

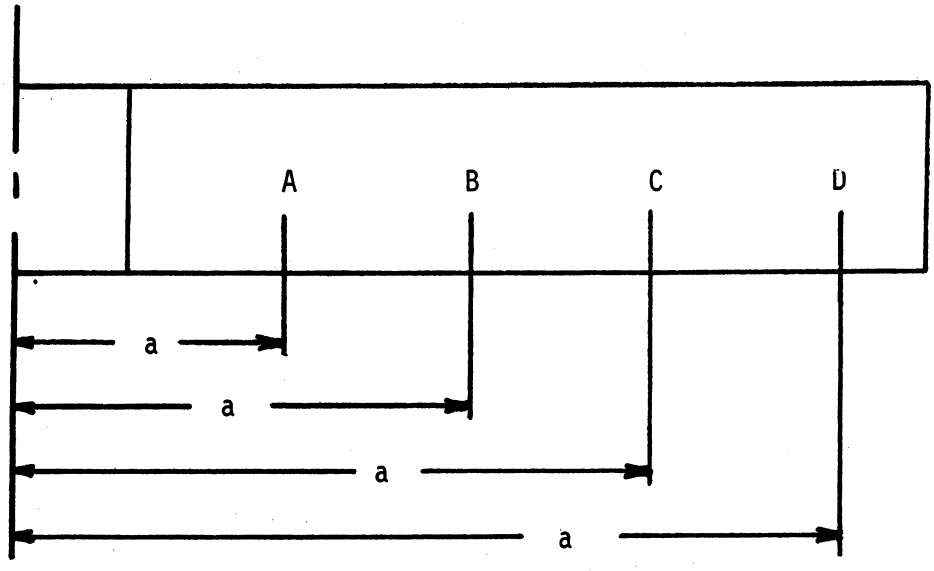

Figure 73. Schematic of scanning electron microscopic analysis of crack growth specimens.

TABLE 11

FRACTOGRAPHIC LAYOUT FOR

CRACK GROWTH SPECIMENS

Specimen	Section	Average Crack Length (2a) (in.)	Average da/dN $\times 10^{-6}$ in/cycle	Average ΔK (ksi$\sqrt{in}$)
5-46	A	.296	0.6	18.2
	B	.536	2.0	23.7
	C	.752	160	38.1
	D	unstable	-	-
6-49	A	.296	2.5	15.7
	B	.536	6.0	23.5
	C	.785	46.0	45.0
	D	unstable	-	-

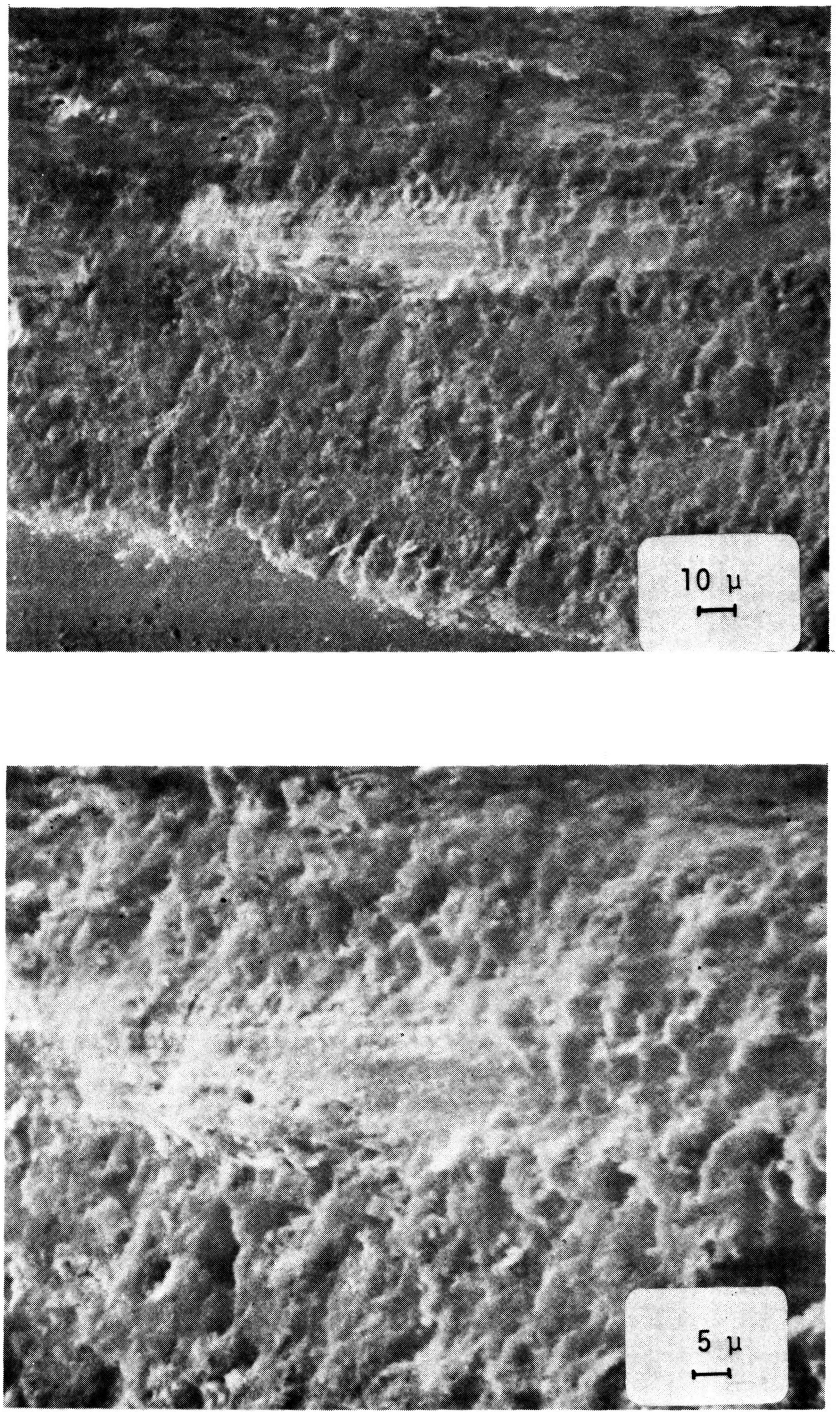

Figure 74. Wear surface of an as received specimen (2-15; 544,220 cycles) - fretting fatigue in air.

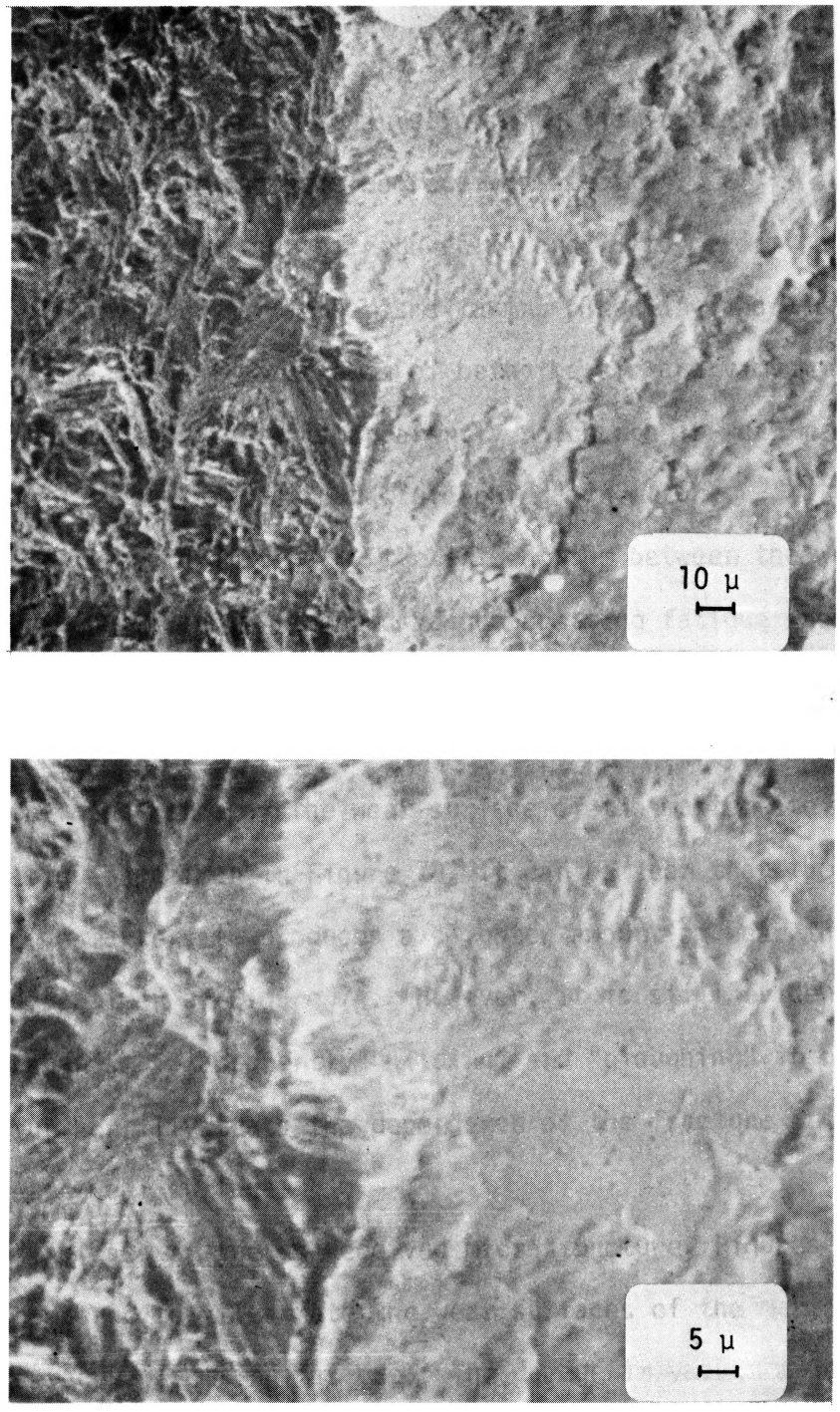

Figure 75. Intersection of wear and fracture surfaces of an as received specimen (2-15; 544,220 cycles) - fretting fatigue in air.

interaction of the process in conjunction with the initiation region of the fracture surface of the same as received specimen.

A comparison may be made of Figures 74 and 76 to determine the difference, if any, in wear mechanisms taking place in laboratory air and vacuum. The overall appearance of both the air and vacuum wear surfaces establishes that there is apparently no change in wear mechanism as both appear to be "sliding" and "ploughing" in nature.

Figure 77 shows dramatically the interaction between the wear and initiation region of an as received vacuum fretting fatigue specimen. Cracking on the wear surface in a direction perpendicular to the axial loading is particularly noted in connection with the fracture surface.

From the appearance of the wear surface of the martensite air fretting fatigue specimen in Figure 78, it can be seen that the harder surface of the martensite produces a slighter amount of wear than the as received specimen of Figure 74. However, it is still evident that the wear mechanism is apparently "sliding" and "ploughing" in nature. Figure 79 further illustrats the dependence of the fracture initiation on the damaged wear surface.

As in the case of the as received microstructure, Figures 78 and 80 may be compared to illustrate the wear surfaces of the martensite for air and vacuum fretting fatigue. The damage in vacuum appears larger in its extent than the damage in air. However, this may be due to the larger number of cycles experienced in the vacuum test. The interaction of this damage with the fracture initiation region is again apparent in Figure 81. Figure 81 also more clearly illustrates the "sliding" and "ploughing" appearance of the wear surface of a martensite

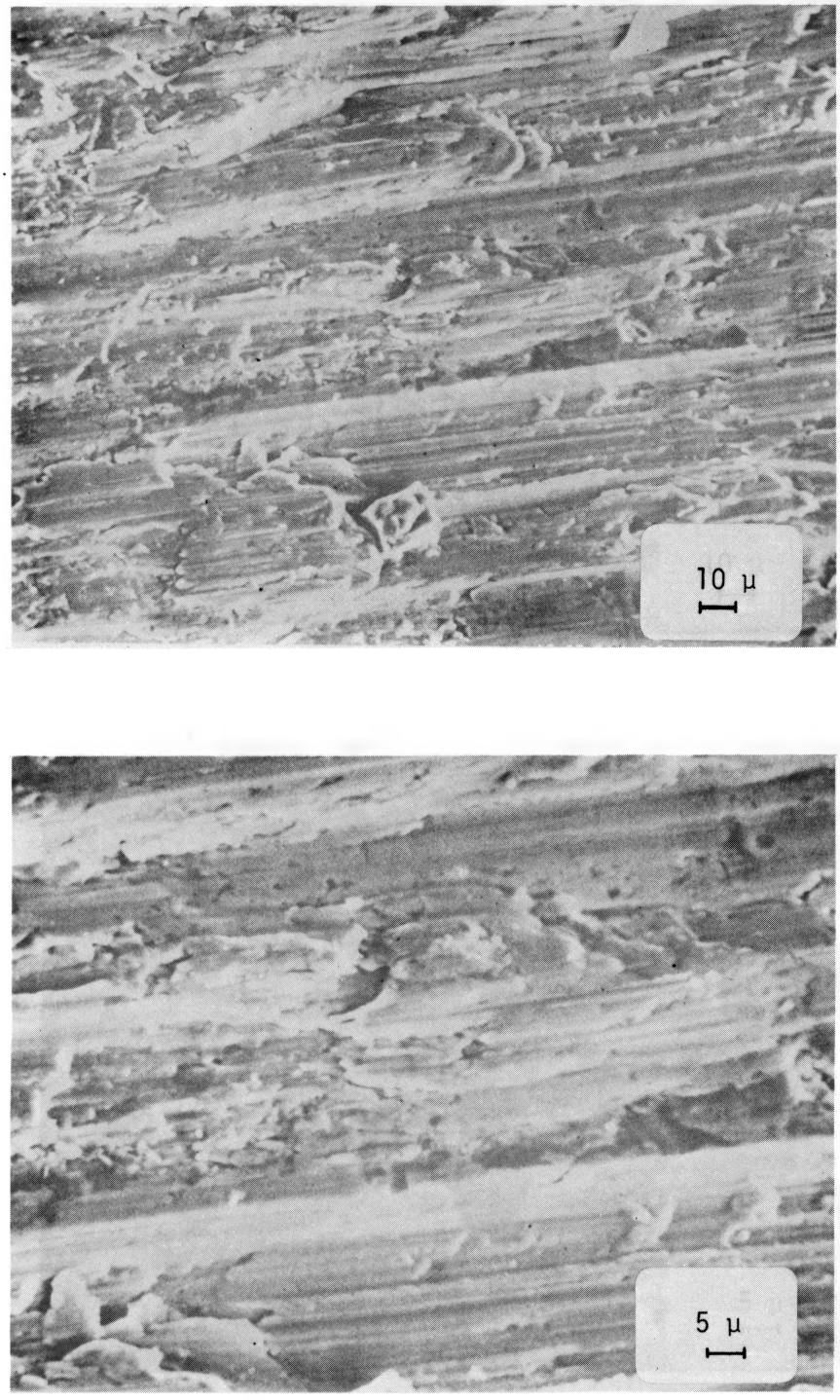

Figure 76. Wear surface of an as received specimen (7-58; 973,230 cycles) - fretting fatigue in vacuum.

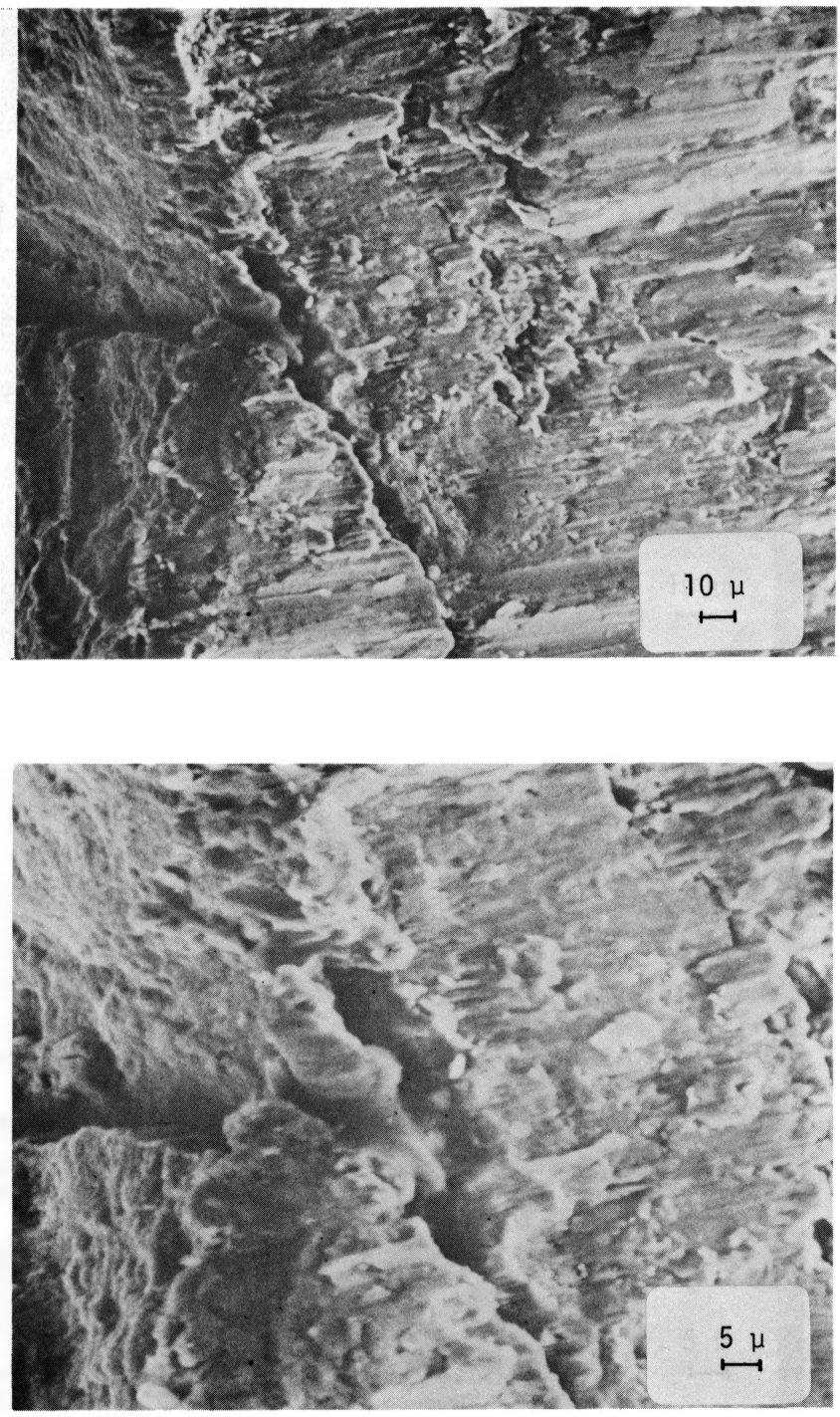

Figure 77. Intersection of wear and fracture surfaces of an as received specimen (7-58; 973,230 cycles) - fretting fatigue in vacuum.

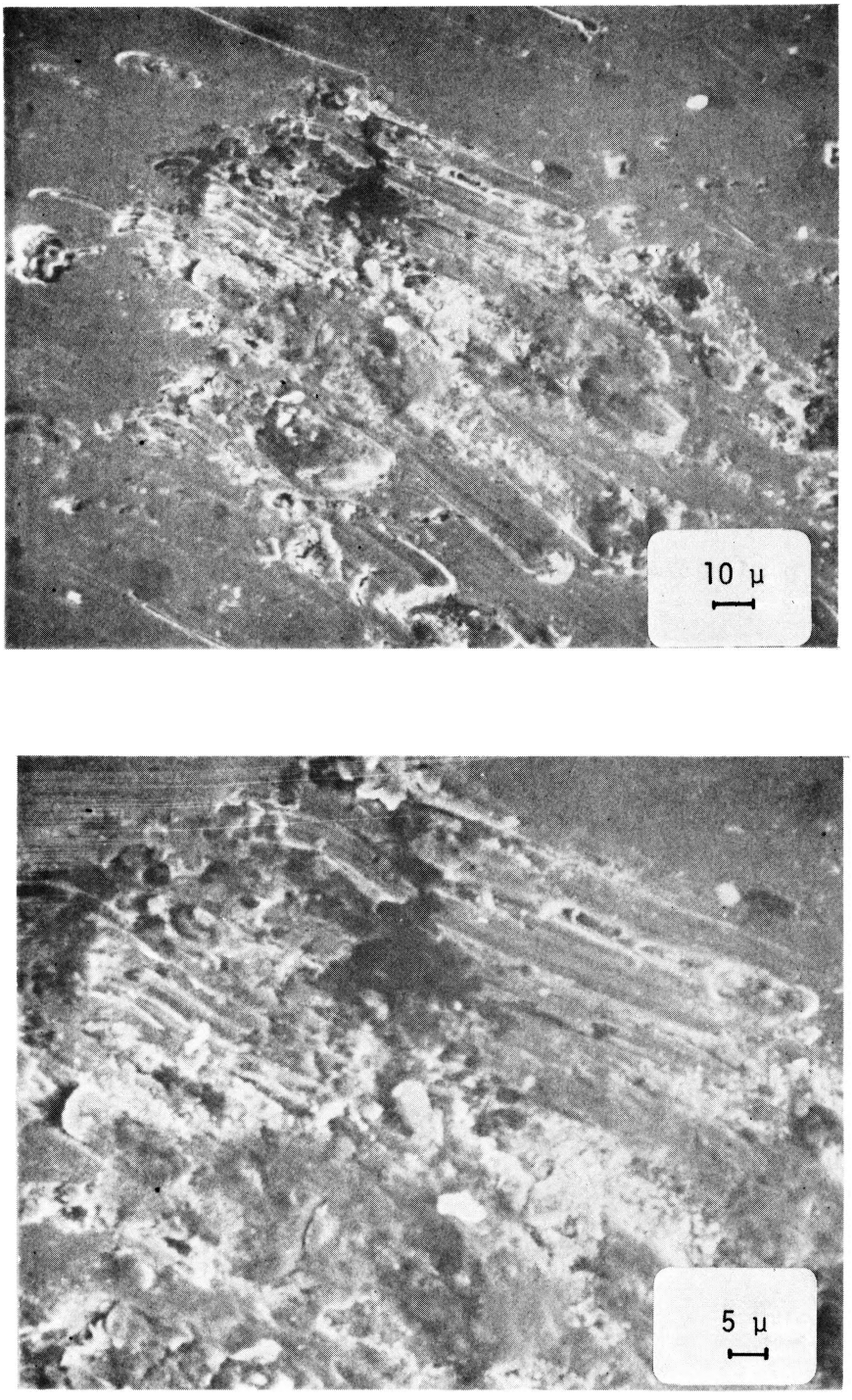

Figure 78. Wear surface of a martensite specimen (4-38; 342,250 cycles) - fretting fatigue in air.

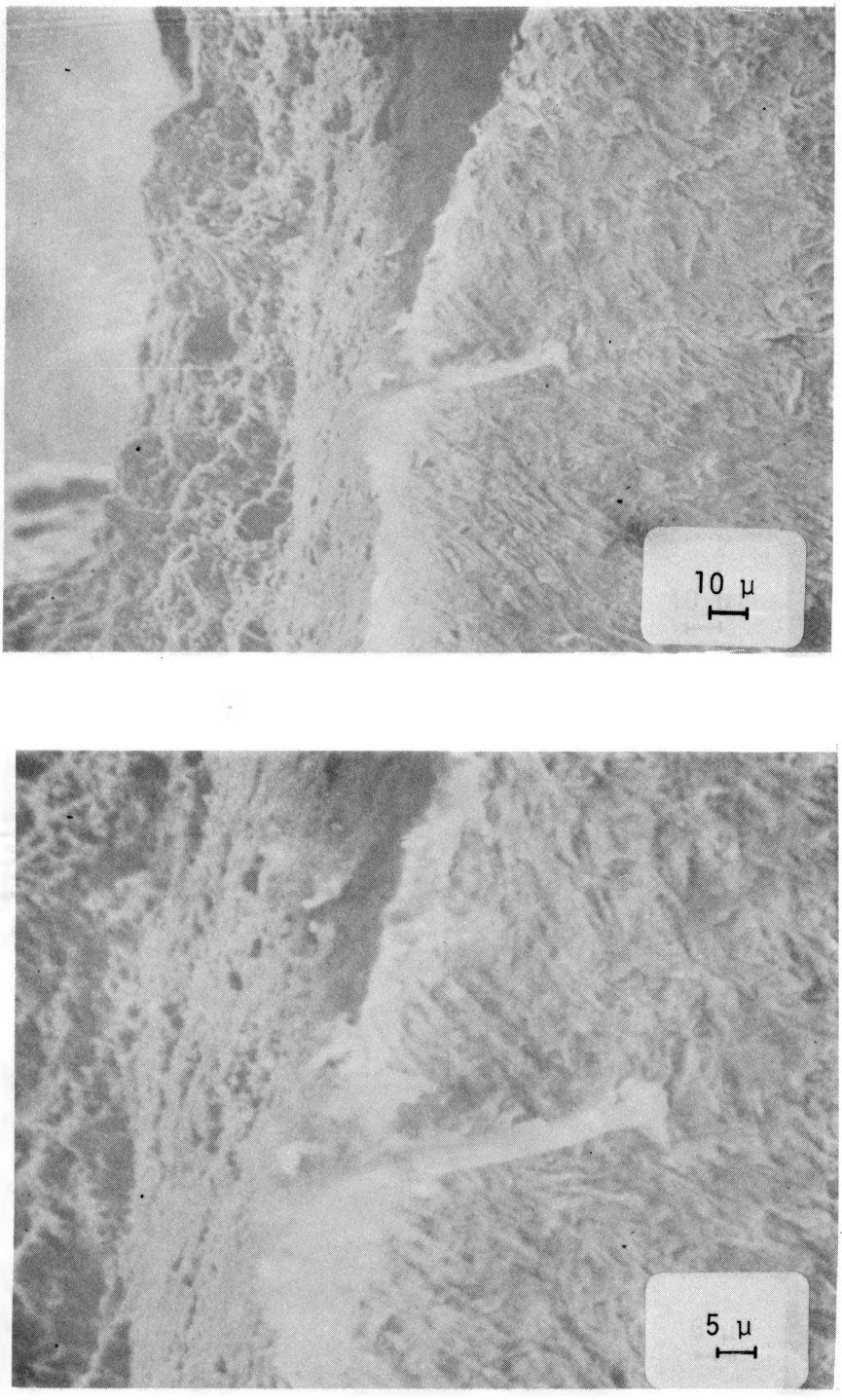

Figure 79. Intersection of wear and fracture surfaces of a martensite specimen (4-38; 342,250 cycles) - fretting fatigue in air.

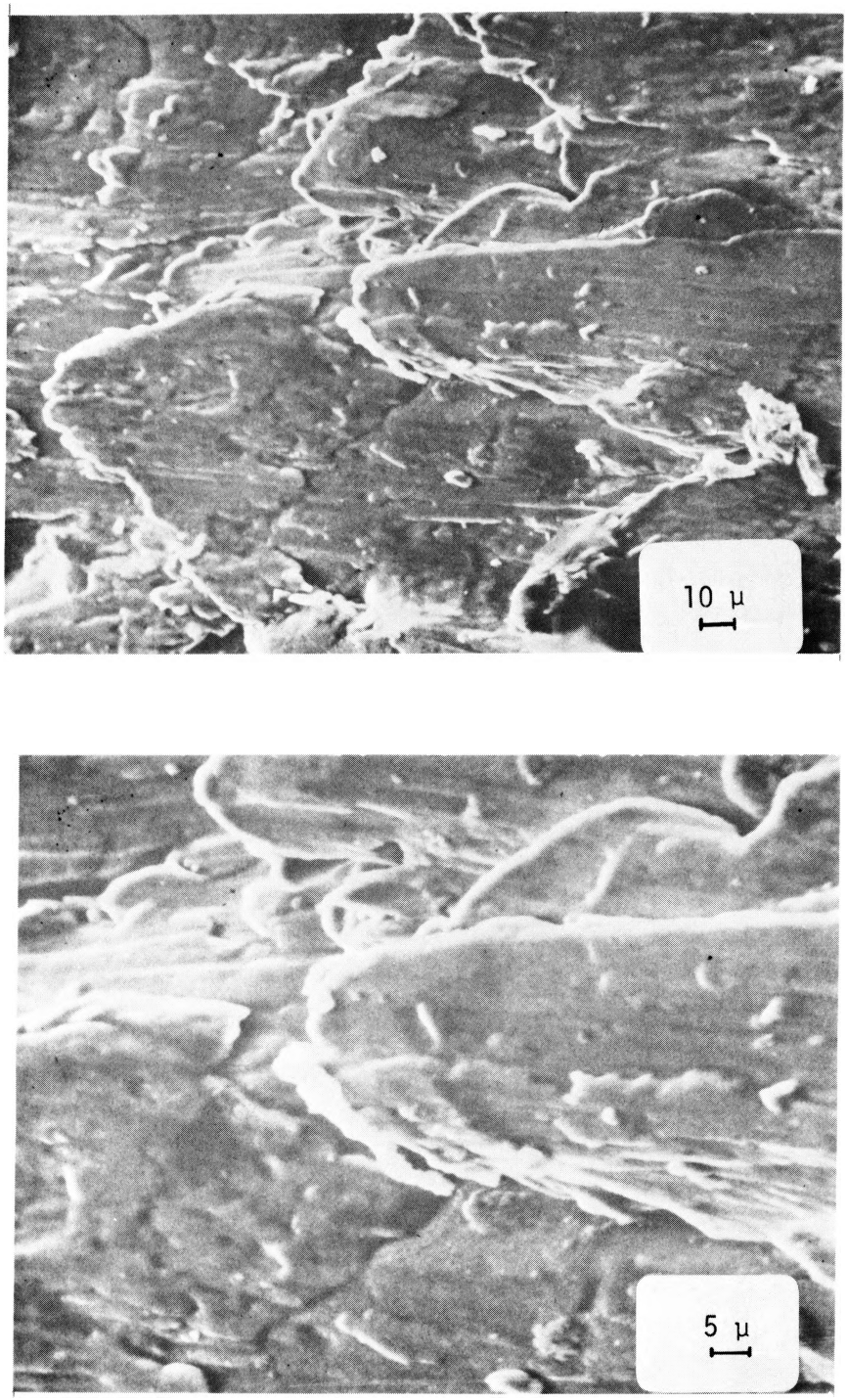

Figure 80. Wear surface of a martensite specimen (8-65; 2,128,300) - fretting fatigue in vacuum.

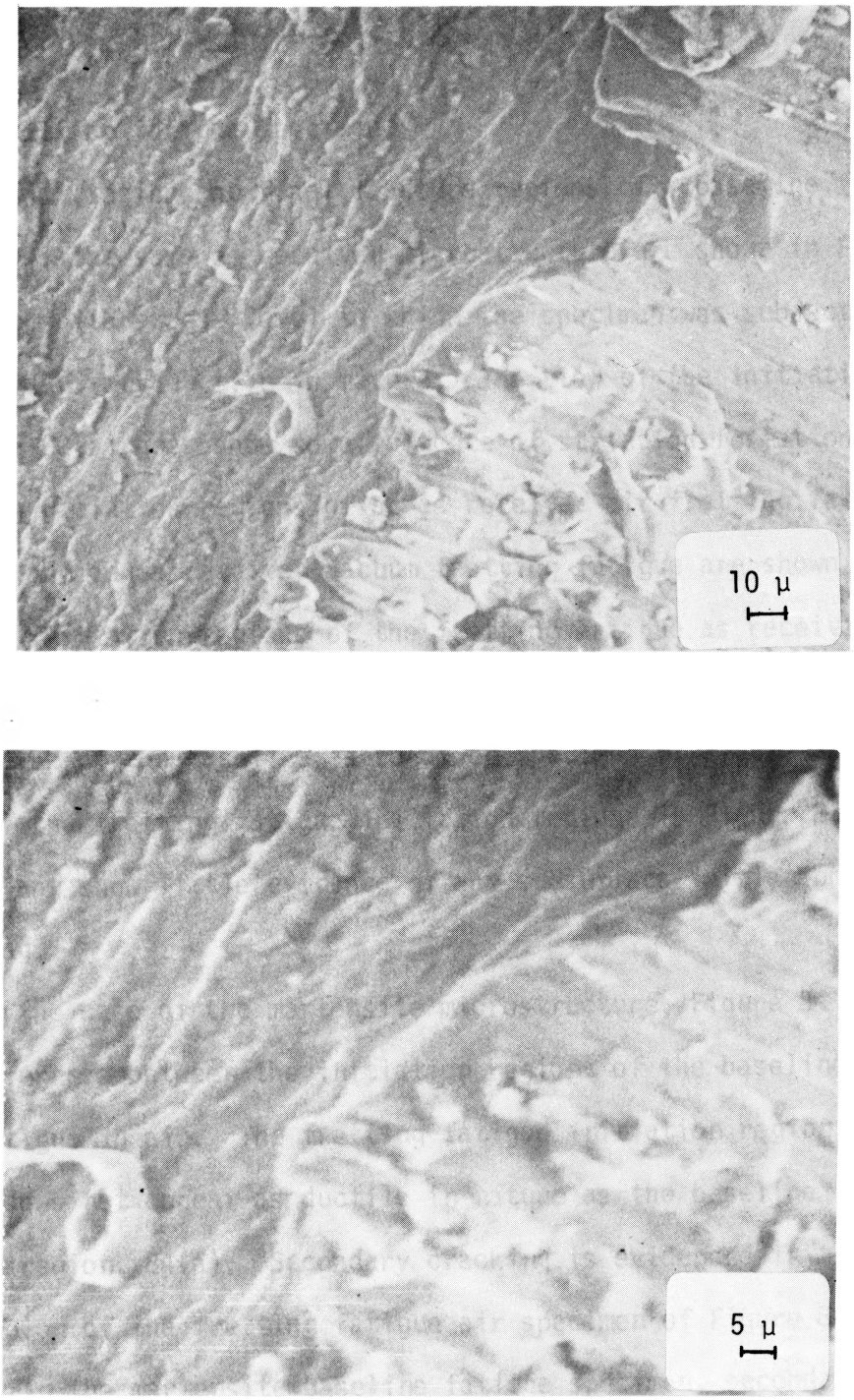

Figure 81. Intersection of wear and fracture surfaces of a martensite specimen (8-65; 2,128,300 cycles) - fretting fatigue in vacuum.

vacuum fretting fatigue specimen.

The initiation and final fracture regions of a baseline fatigue specimen of the same as received microstructure are shown in Figure 82. Due to the high stress level to which the specimen was subjected, both views appear very ductile in nature. The view of the initiation region in Figure 82(a) does show some evidence of striation formation.

The initiation regions of an as received air fretting fatigue specimen and an as received vacuum fretting fatigue are shown in Figure 83. The initiation regions of the fretting fatigue as received specimens both in air and vacuum appear slightly different than the initiation region of the baseline as received specimen of Figure 82. These views of the fretting fatigue initiation regions in Figure 83 appear similar and show little evidence of any subsurface initiation mechanism occurring.

In the case of the martensite microstructure, Figure 84 illustrates the difference between the initiation regions of the baseline and fretting fatigue in air. The fretting fatigue initiation region, Figure 84(b), does not appear as ductile in nature as the baseline fatigue initiation region, 84(a). Secondary cracking is evidenced in the initiation region of the fretting fatigue air specimen of Figure 84 (b), whereas in the martensite baseline fatigue specimen, secondary cracking is noted in both the mid and unstable regions (Figures 85 and 86).

The initiation region of the martensite vacuum fretting fatigue fracture surface of Figure 87 shows amounts of fretting debris which may have contributed to the failure process. However, comparing this

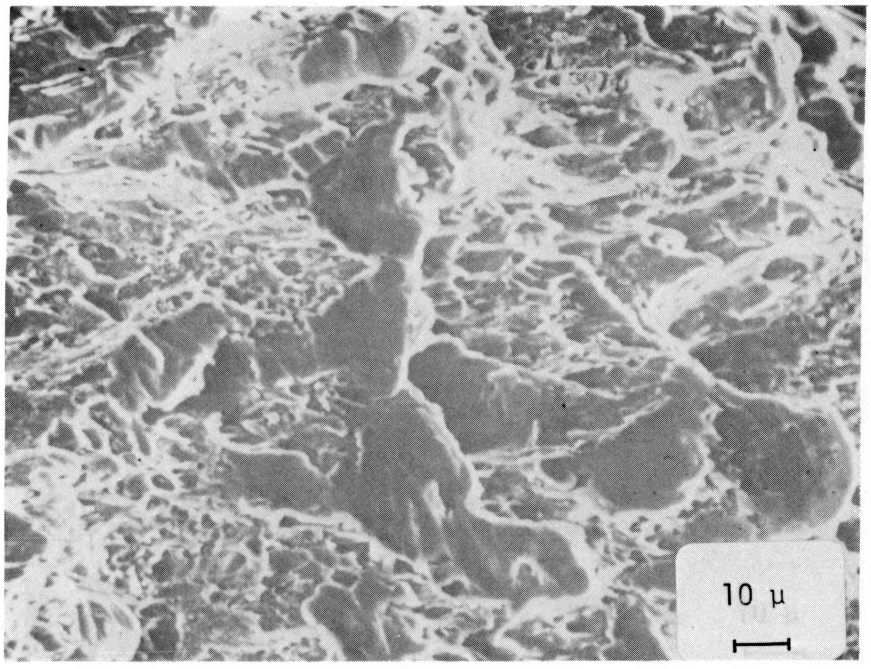

(a)

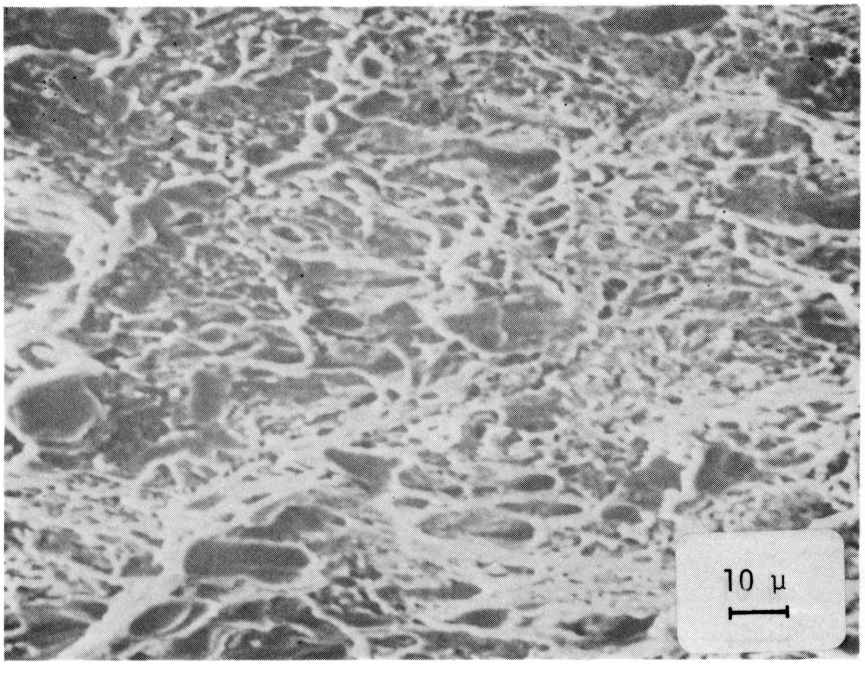

(b)

Figure 82. The (a) initiation and (b) final fracture regions of baseline fatigue specimen 1-04 (7,640 cycles).

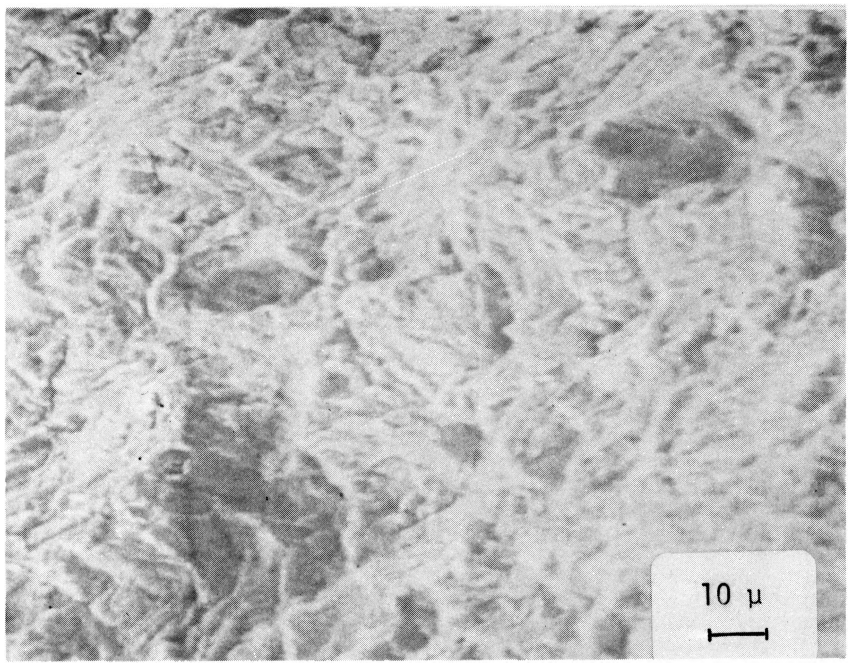

(a)

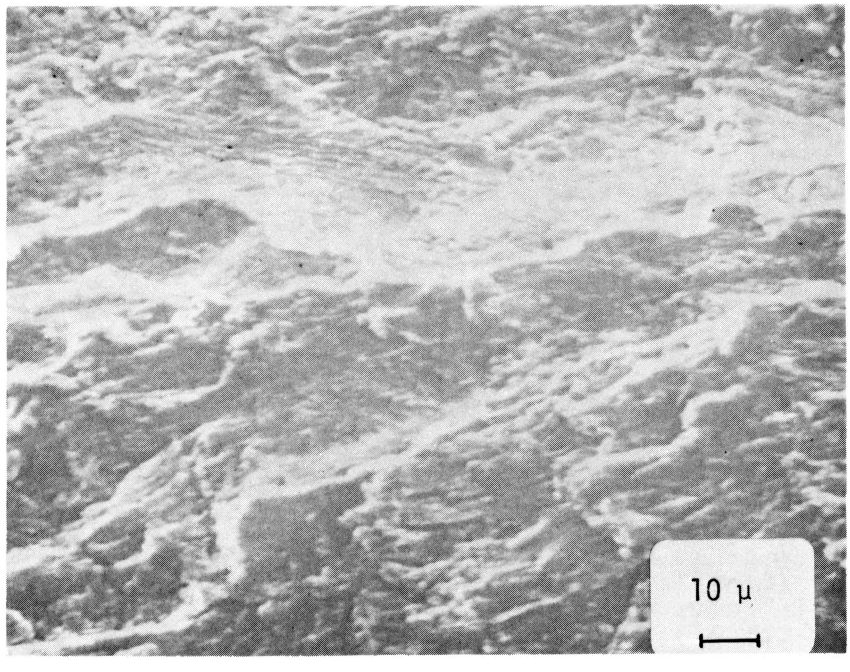

(b)

Figure 83. Initiation regions of (a) as received specimen 2-15 (544,220 cycles) - fretting fatigue in air and (b) as received specimen 7-59 (2,371,090 cycles) - fretting fatigue in vacuum.

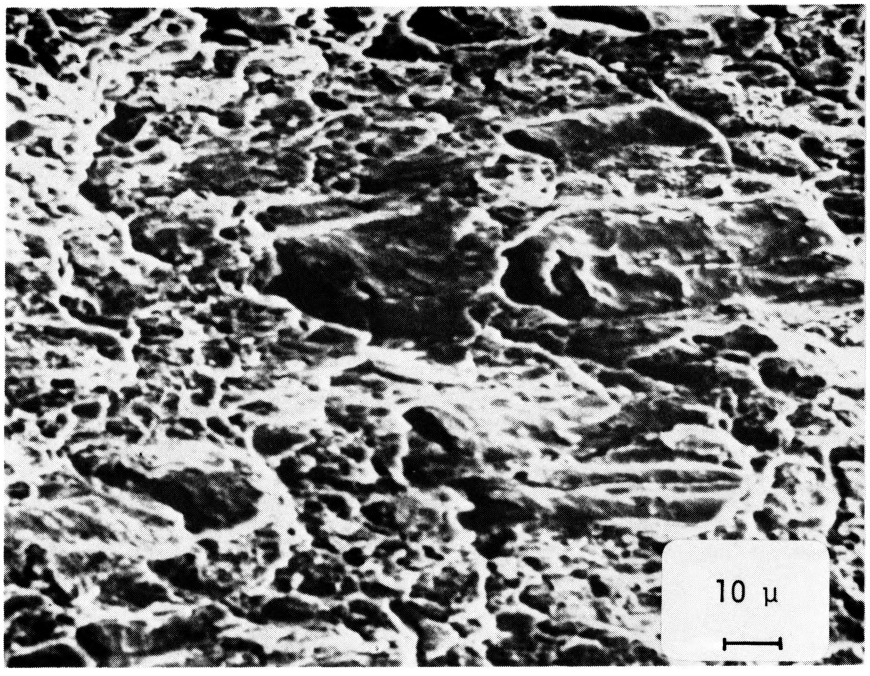

(a)

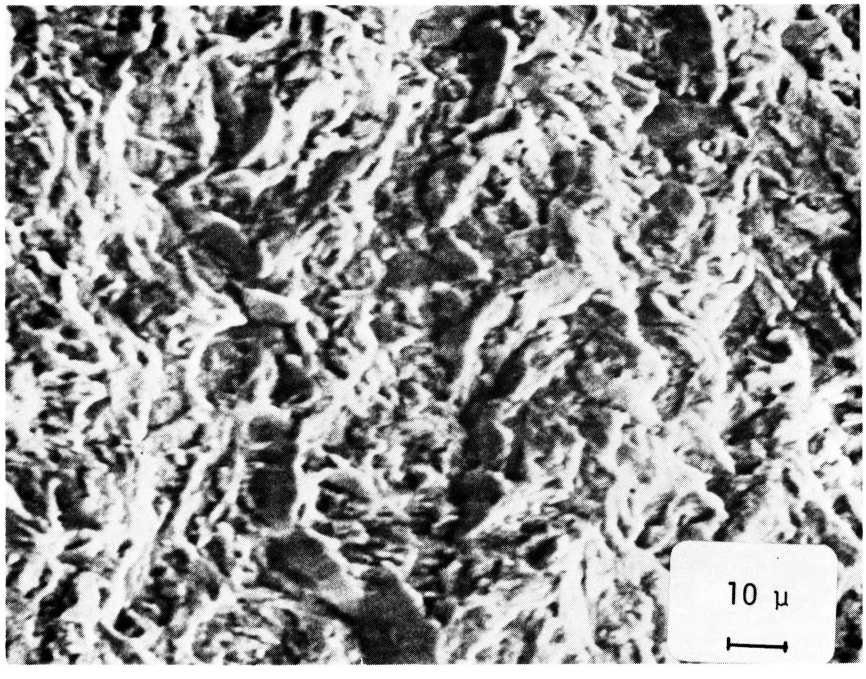

(b)

Figure 84. Initiation regions of martensite specimens (a) 3-19 (1,790 cycles) - baseline fatigue and (b) 4-41 (1,034,640 cycles) - fretting fatigue in air.

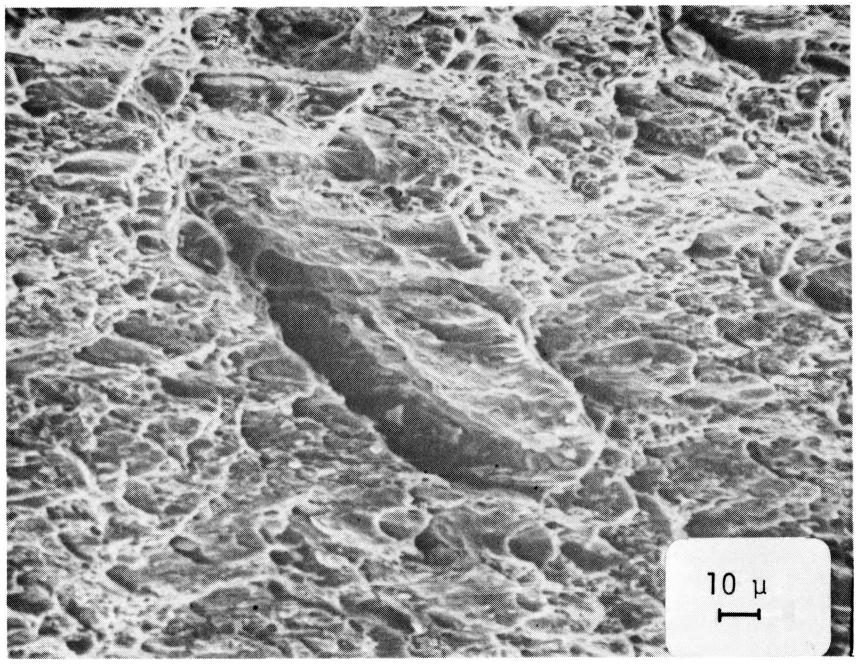

Figure 85. Secondary cracking near unstable growth region of martensite specimen 3-19 (1,790 cycles) - baseline fatigue.

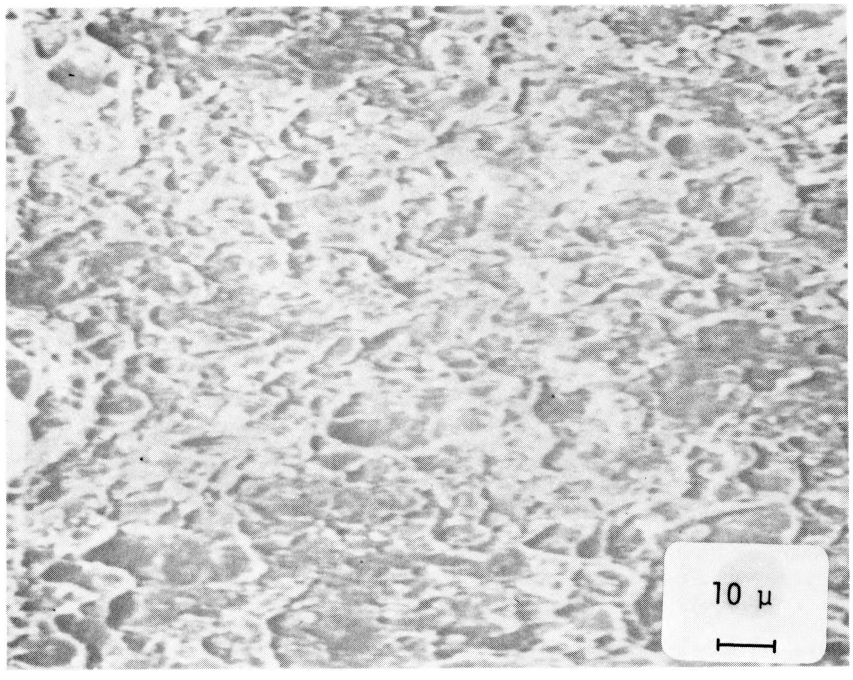

Figure 86. Final fracture region of martensite specimen 3-19 (1,790 cycles) - baseline fatigue.

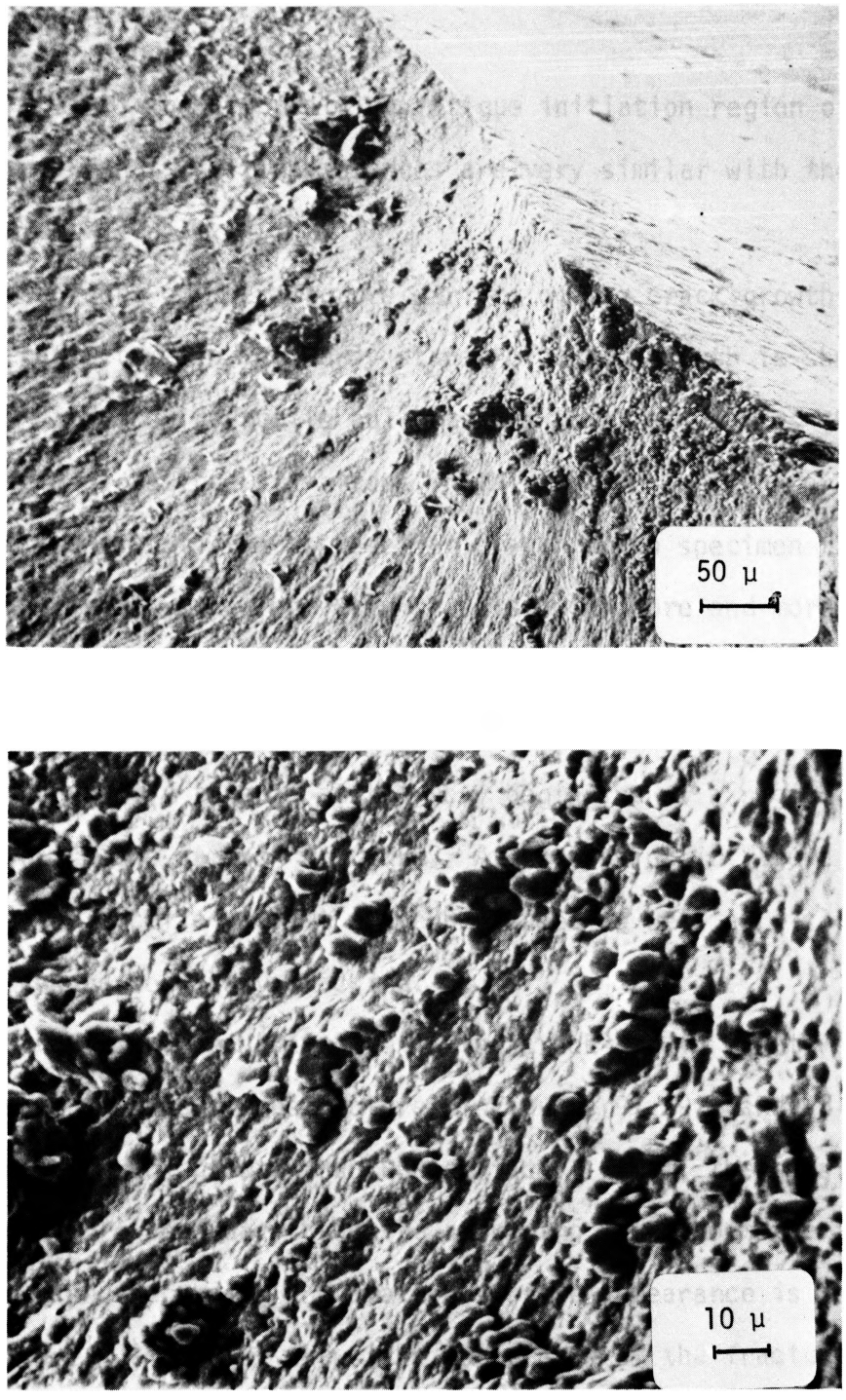

Figure 87. Initiation region of martensite specimen 8-68 (2,813,990 cycles) - fretting fatigue in vacuum.

surface to that of the air fretting fatigue initiation region of Figure 84, it is noted that their appearances are very similar with the exception of the debris.

The appearance of the fracture surface of the crack growth as received microstructure in the early stages of crack growth is shown in Figure 88. Microscopic ductile pullouts are noted as well as the random appearance of fatigue striations in this region. As the crack growth rate incrases in the as received crack growth specimen the fracture surface becomes more regularly striated with more and more evidences of ductile separation as shown in Figure 89. The surface becomes much rougher as the crack growth rate nears instability (Figure 90); macroscopically, this is at the very beginning of a region known as "slant" or "plane stress" fracture. At this point in Figure 90, larger areas or ductile pullout are experienced as well as a slight propensity toward secondary cracking.

Two main differences are noted in the crack growth fracture surface of the martensite microstructure of Figures 91, 92, and 93 from the as received crack growth fracture surface. First, there is evidence of much more secondary cracking occurring throughout the life of the specimen; and secondly, the frature surface appearance is less regular in nature. Figure 91 shows the appearance of the fracture surface during the early stages of crack growth. Secondary cracks are observed in this region along with sporadic ductile pullouts. As the crack growth rate increases, the fracture surface, as shown in Figure 92, continues to be characterized by ductile fracture including secon-

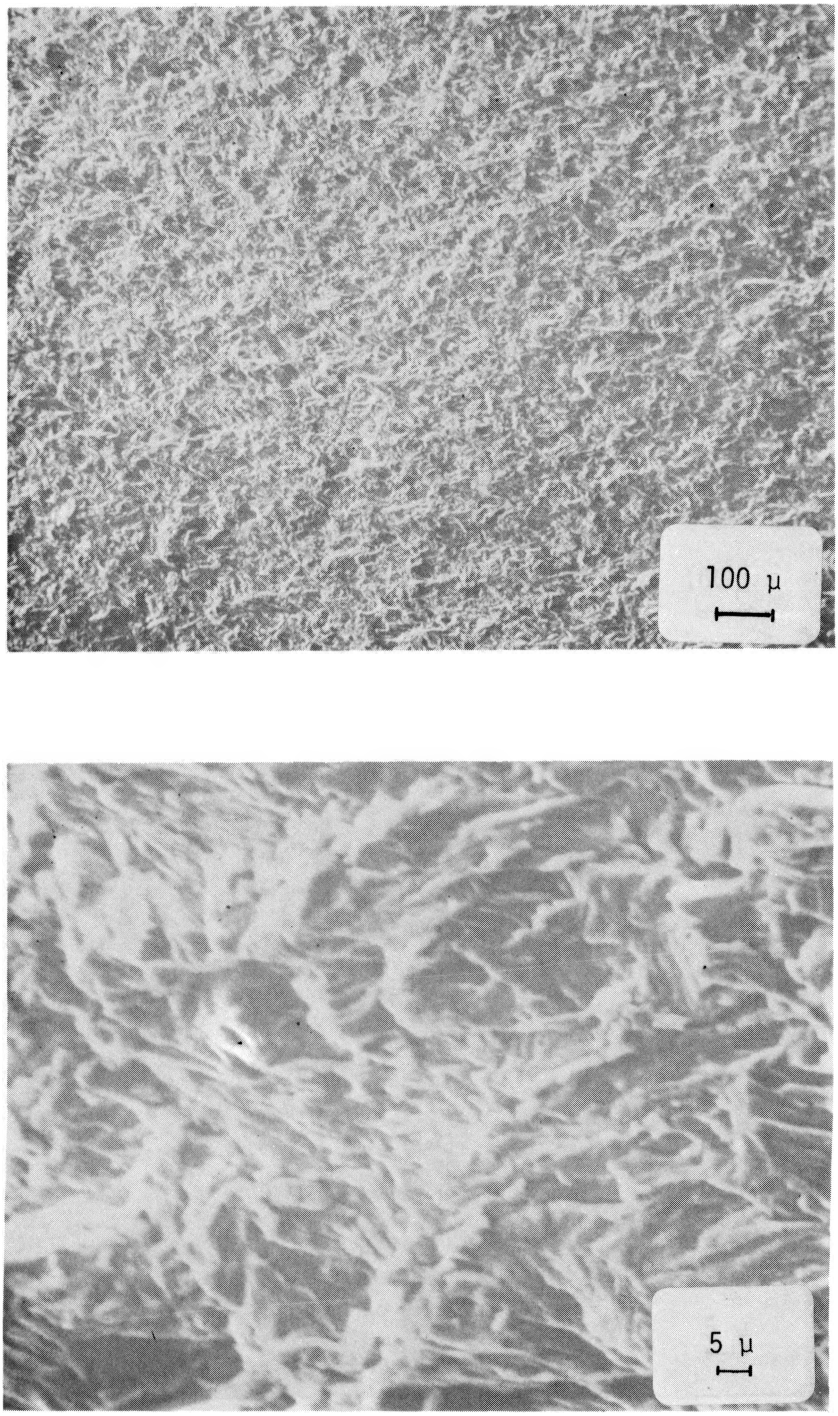

Figure 88. Slow crack growth region of as received crack growth specimen 5-46 (Position A).

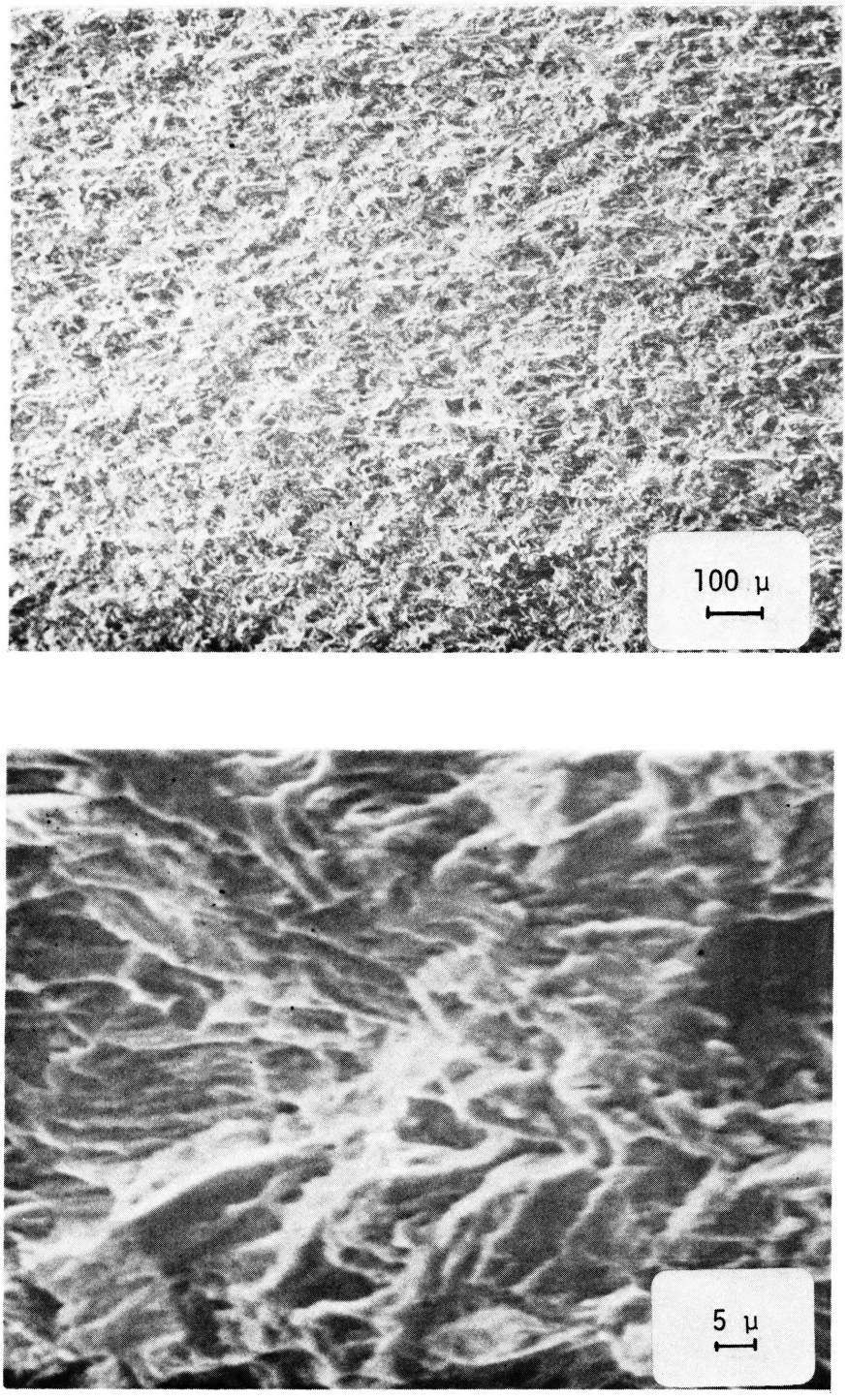

Figure 89. Mid crack growth region of as received specimen 5-46 (Position B).

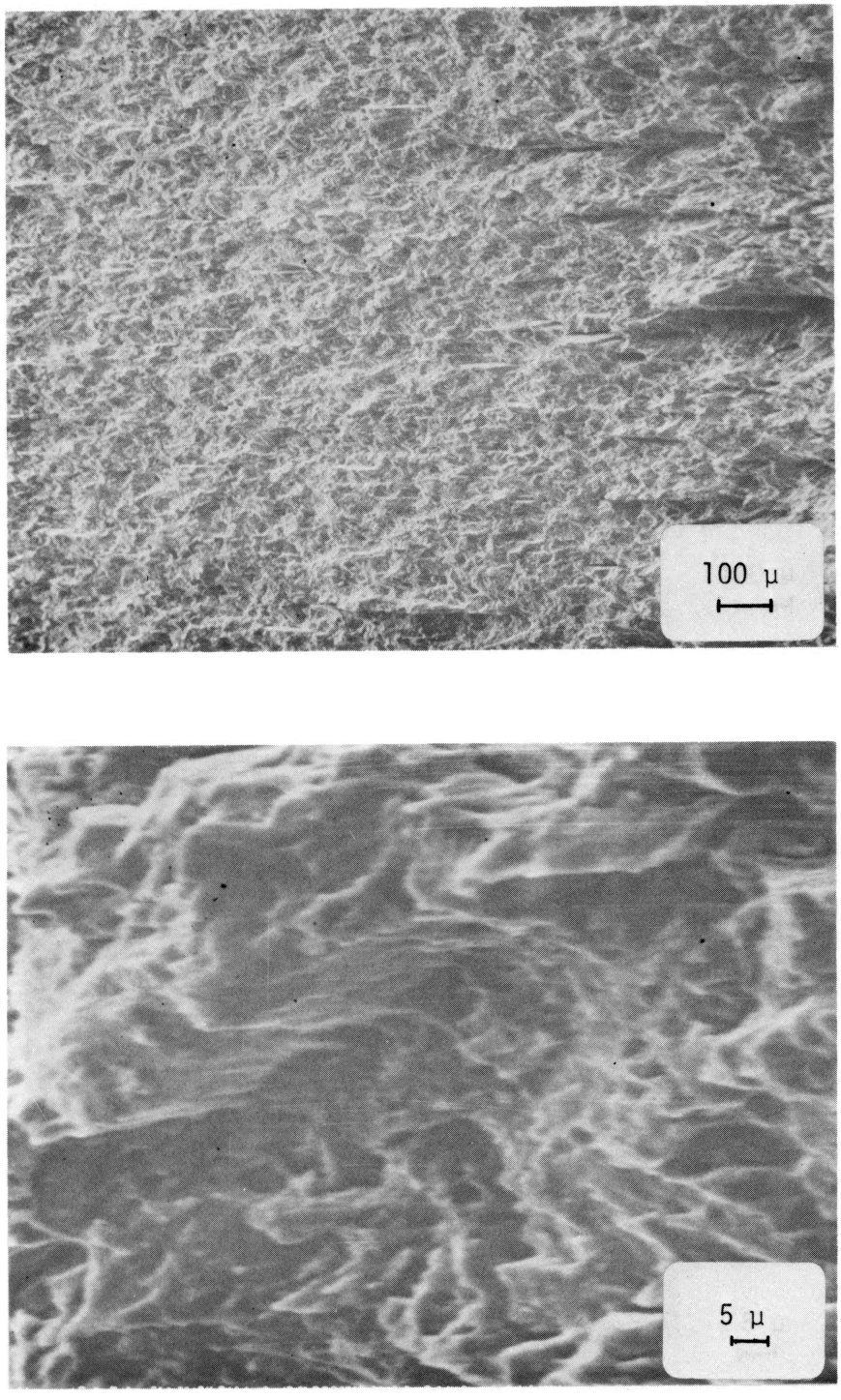

Figure 90. Crack growth nearing instability of as received specimen 5-46 (Position C).

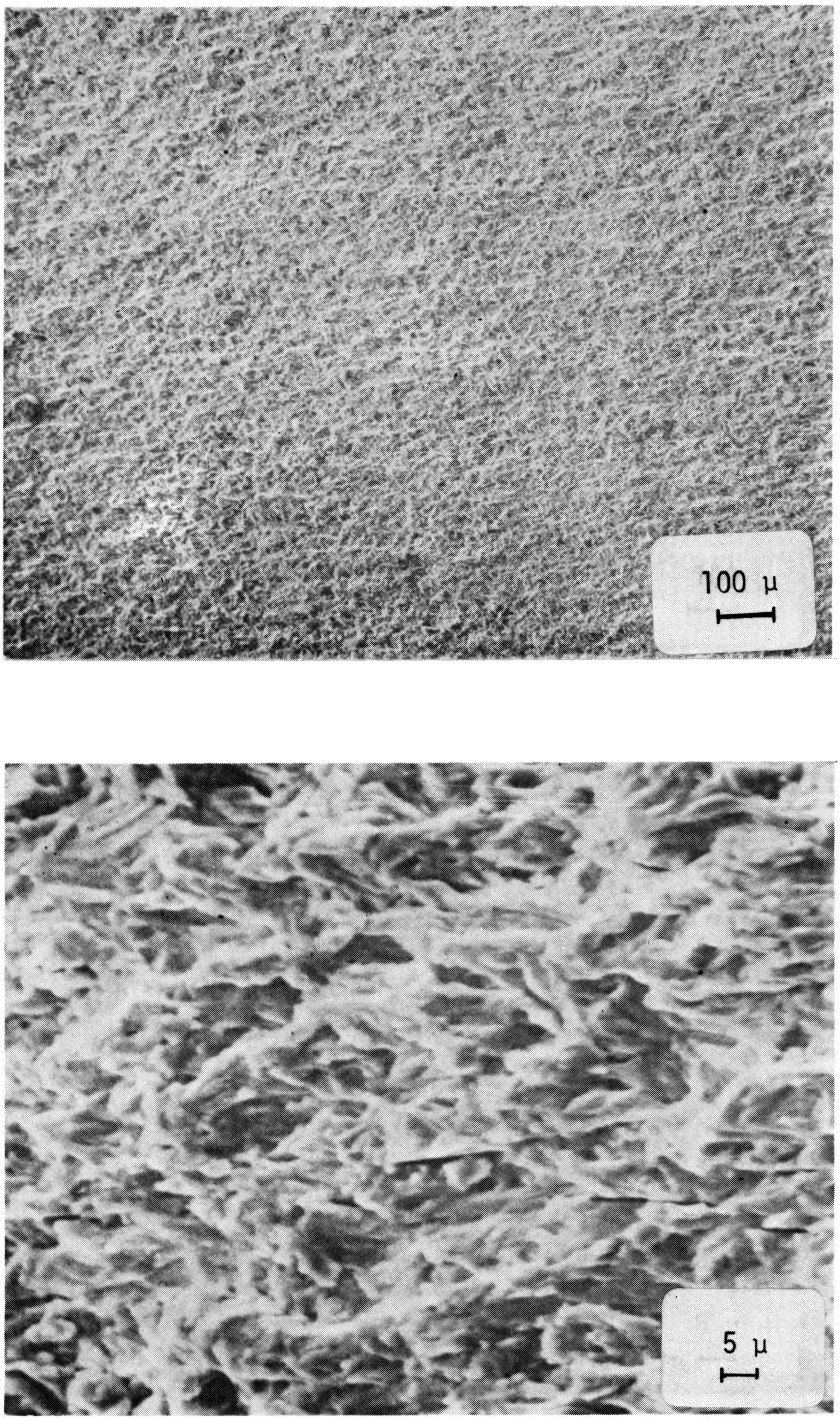

Figure 91. Slow crack growth region of martensite specimen 6-49 (Position A).

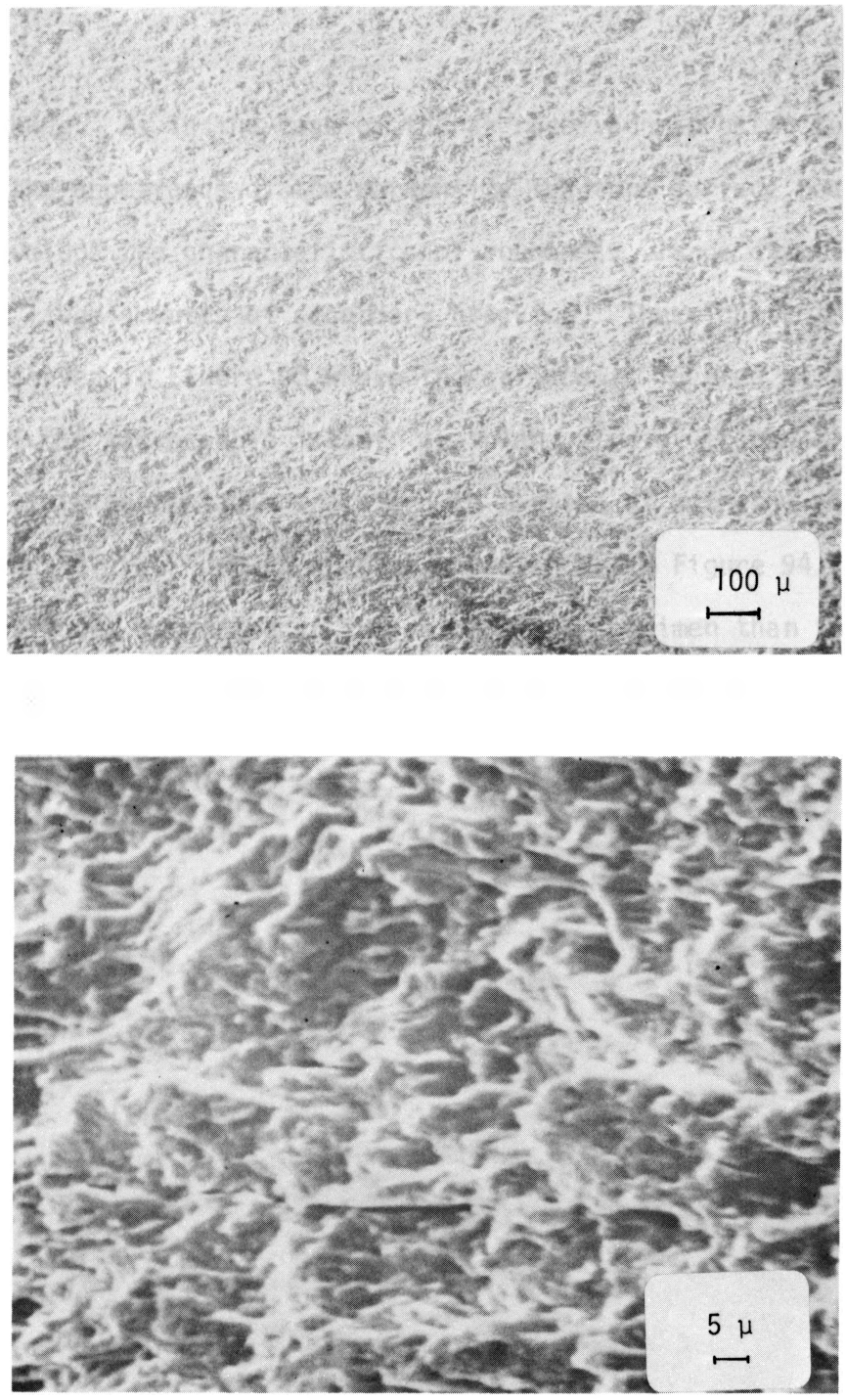

Figure 92. Mid crack growth region of martensite specimen 6-49 (Position B).

dary cracking. As in the case of the as received microstructure, Figure 90, the appearance of the martensite fracture surface near instability develops the characteristics of roughness, large ductile pullouts, and large amounts of secondary cracking. These characteristics may be observed in Figure 93 where the surface is located at the beginning of the macroscopic "slant" or "plane stress" fracture.

Finally, the unstable crack growth regions of both the as received and martensite crack growth specimens are shown in Figure 94. Larger ductile pullouts are noted in the as received specimen than in the martensite; however, again the martensite exhibits larger secondary cracks in this region.

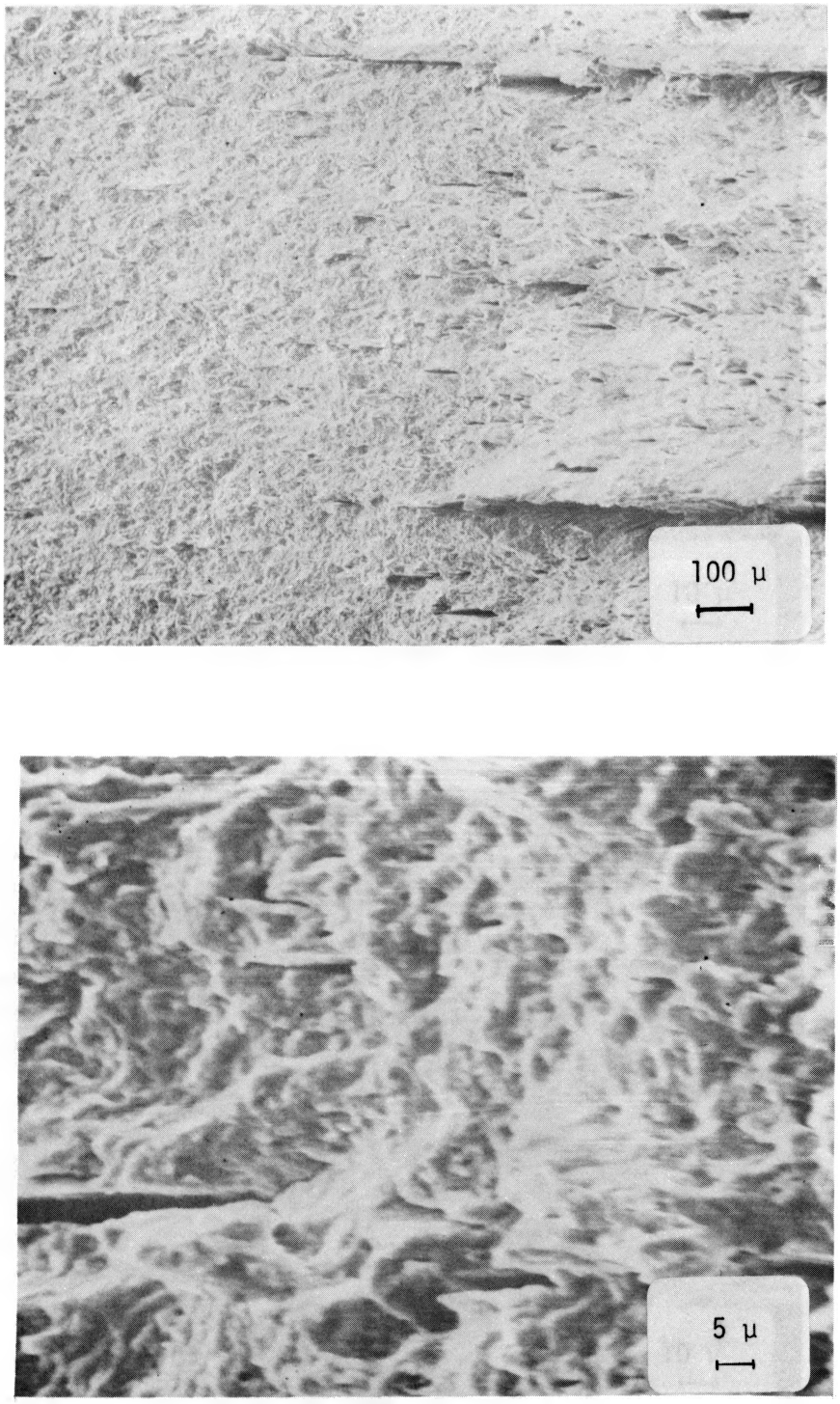

Figure 93. Crack growth nearing instability of martensite specimen 6-49 (Position C).

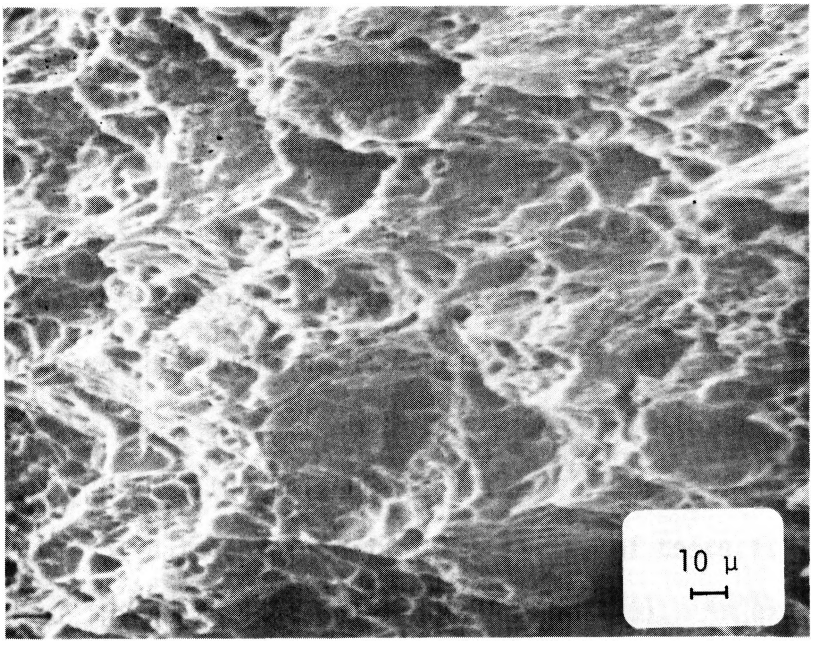

(a)

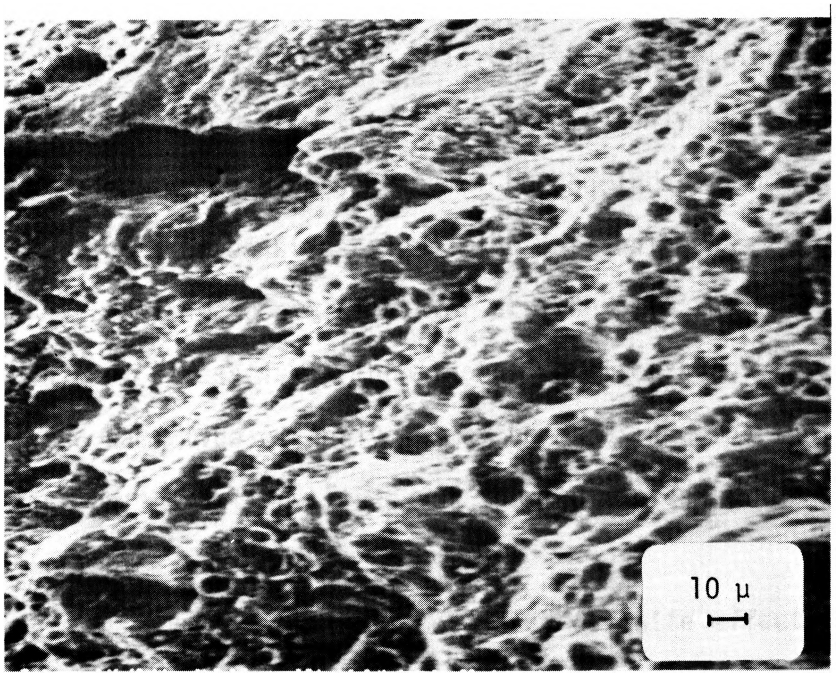

(b)

Figure 94. Unstable crack growth regions of (a) as received specimen 5-46 and (b) martensite specimen 6-49 (Position D).

6.0 EXPERIMENTAL RESULTS

As with the data analysis, the experimental results are divided into two separate sections. This provides a simple means by which each type of data can be found in the conclusions of this paper.

6.1 FATIGUE AND FRETTING FATIGUE RESULTS

The type of data obtained in these series of tests is that of stress/life (This data is tabulated in Appendix 6). An example of this type of data was presented in Figure 47 showing the comparison of the baseline fatigue characteristics of both the as received and martensite microstructures. As mentioned earlier, without sufficient repetitive data, results obtained from this type data may only be interpreted as general trends. As an example, it may be concluded from Figure 47 that, in general, for a given stress level the martensite has a longer life than the as received; conversely, for a given life the martensite will endure a higher stress level than the as received. In view of this example, the same type of analysis may be made in comparing the effects of fretting on the fatigue lives for the two microstructures in the two environments.

Figure 95 illustrates that there is a definite effect due to fretting on the fatigue lives of both the as received and martensite microstructures. This effect manifests itself in the form of reduced lives at corresponding stress levels. This effect is established in the form of trends seen from the data even though the mocrostructural differences

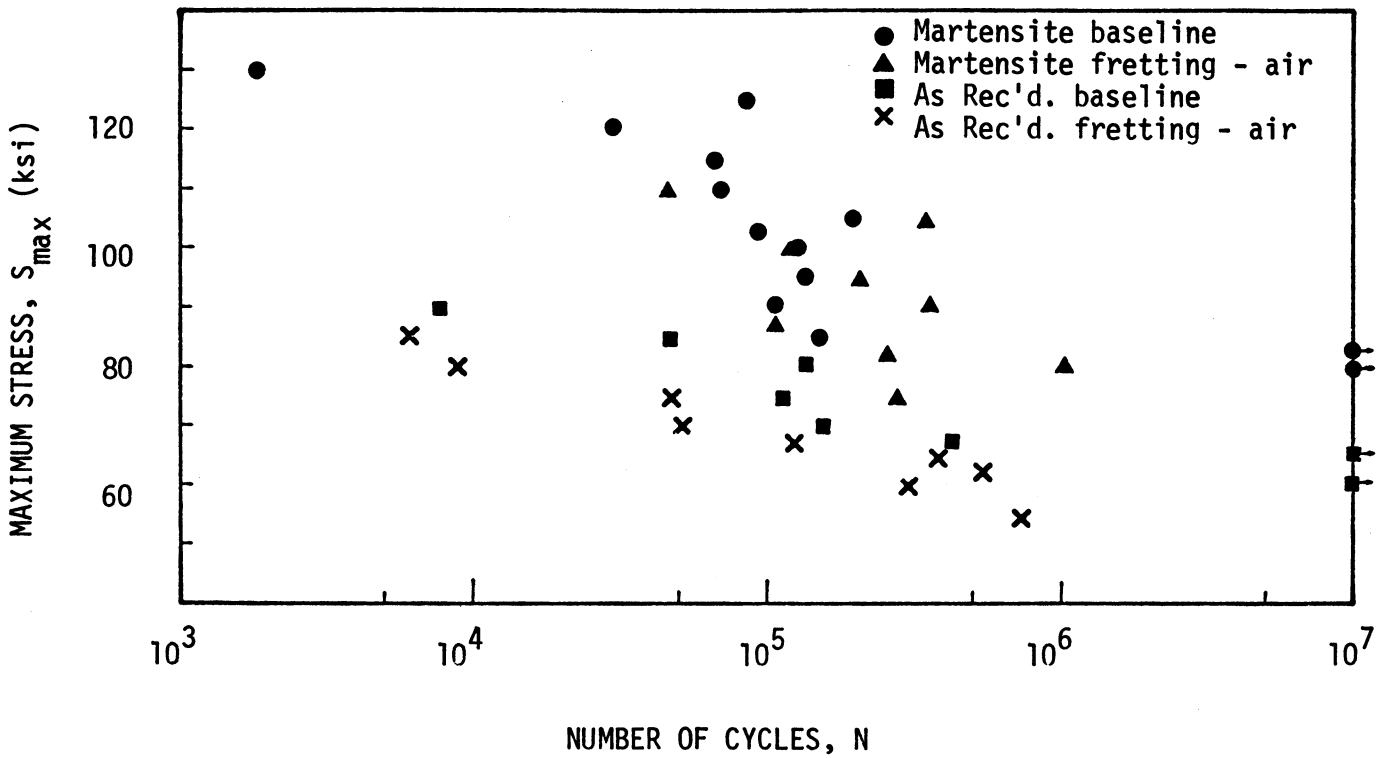

Figure 95. Comparison of the decrease in fatigue lives due to fretting of the as received and martensite microstructures.

are also apparent. The main effect to be attributed to differences in microstructure is the relative stress levels at which the fretting effect becomes predominant. As seen in Figure 97, there is little difference in lives of the baseline and fretting fatigue specimens for the martensite microstructure until the so called "fatigue limit" region; whereas, the as received microstructure exemplifies this effect throughout the range of data. In conjunction with the fractographic analysis, this difference may be explained as due to the lesser amounts of wear on the harder surface of the martensite (compare Figures 74 and 78).

As in the case of the fretting fatigue air data, the fretting fatigue vacuum data is very orderly throughout the range of data, falling between the baseline fretting fatigue air data sets. This is illustated in Figure 96. A comparison of the relative effect due to the environment (or lack of environment) can be made most readily in the region referred to as "runout" in the baseline fatigue data. In this region, it is noted that the fretting fatigue data in air and vacuum are relatively close in comparison to the baseline fatigue data. This suggests a major dependence of the fretting fatigue process on a mechanical damage theory and a lesser dependence on an environmental/chemical corrosion concept.

The fretting fatigue vacuum data for the martensite microstructure, Figure 97, is interspersed within the baseline and fretting fatigue air data throughout the range of data above the so-called baseline "runout". At the lower stress levels it may be seen in Figure 97 that the martensite data supports the conclusion with regard to environmental influ-

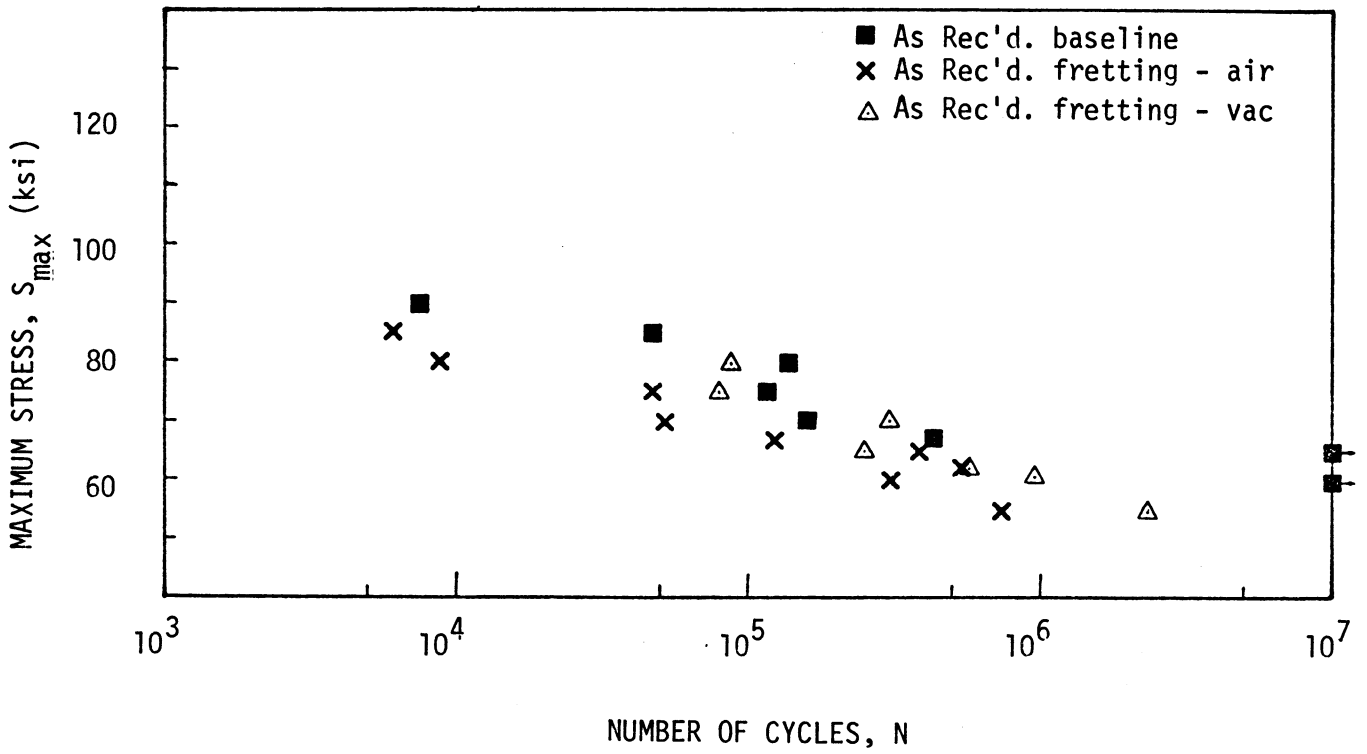

Figure 96. Comparison of air and vacuum fretting fatigue data with respect to baseline data of the as received microstructure.

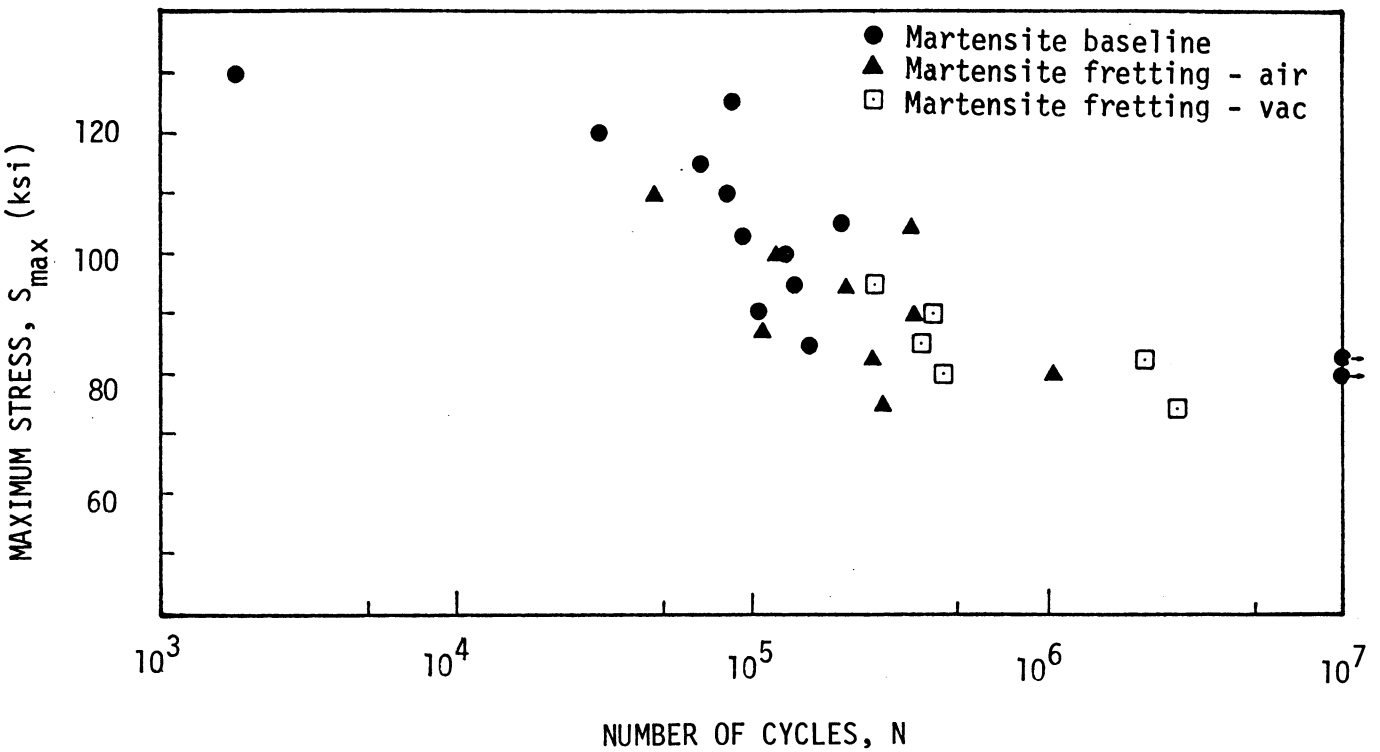

Figure 97. Comparison of air and vacuum fretting fatigue data with respect to baseline data of the martensite microstructure.

ences made from the as received data of Figure 96. Again, in the "run-out" region and below the vacuum data falls very close to the air data with respect to the baseline fatigue data.

6.2 CRACK GROWTH RESULTS

The results of the crack growth testing are in the form of crack length versus number of cycles data (This data is tabulated in Appendix 7). Two crack growth tests of each microstructure were performed for comparison.

The data from the as received crack growth tests are presented in graphical form in Figures 98 and 99. By comparing these curves, it may be seen that the behavior is dramatically different; specimen 5-44 failing in 376,300 cycles and specimen 5-46 failing in 292,110 cycles after starting from approximately the same initial crack length and operating under precisely the same loads and conditions. Poor microstructural control in the as received hot rolled sheet is cited as a principal factor in this occurrence since the same effect is not apparent in the martensite specimens prepared under controlled conditions.

Graphical presentations of the martensite crack growth data are shown in Figures 100 and 101. The comparison of these figures illustrates less scatter in the martensite data since the lives of the specimens and general shapes of their curves are very similar. These curves cannot be directly compared to those of Figures 98 and 99 since the operating loads were different. The operating loads used in the as received crack growth test were to be used in the crack growth tests of

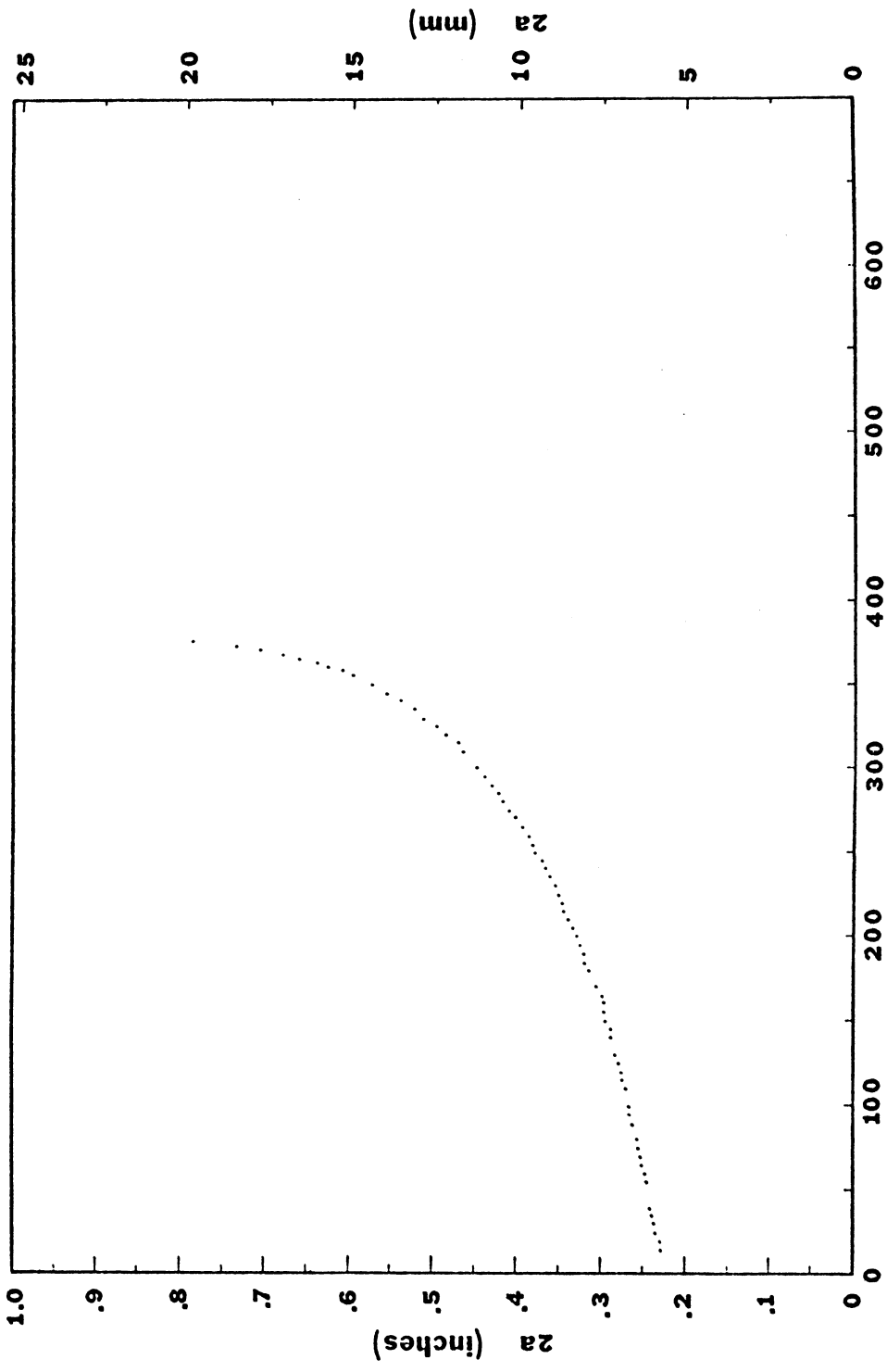

Figure 98. Crack growth curve of as received specimen 5-44.

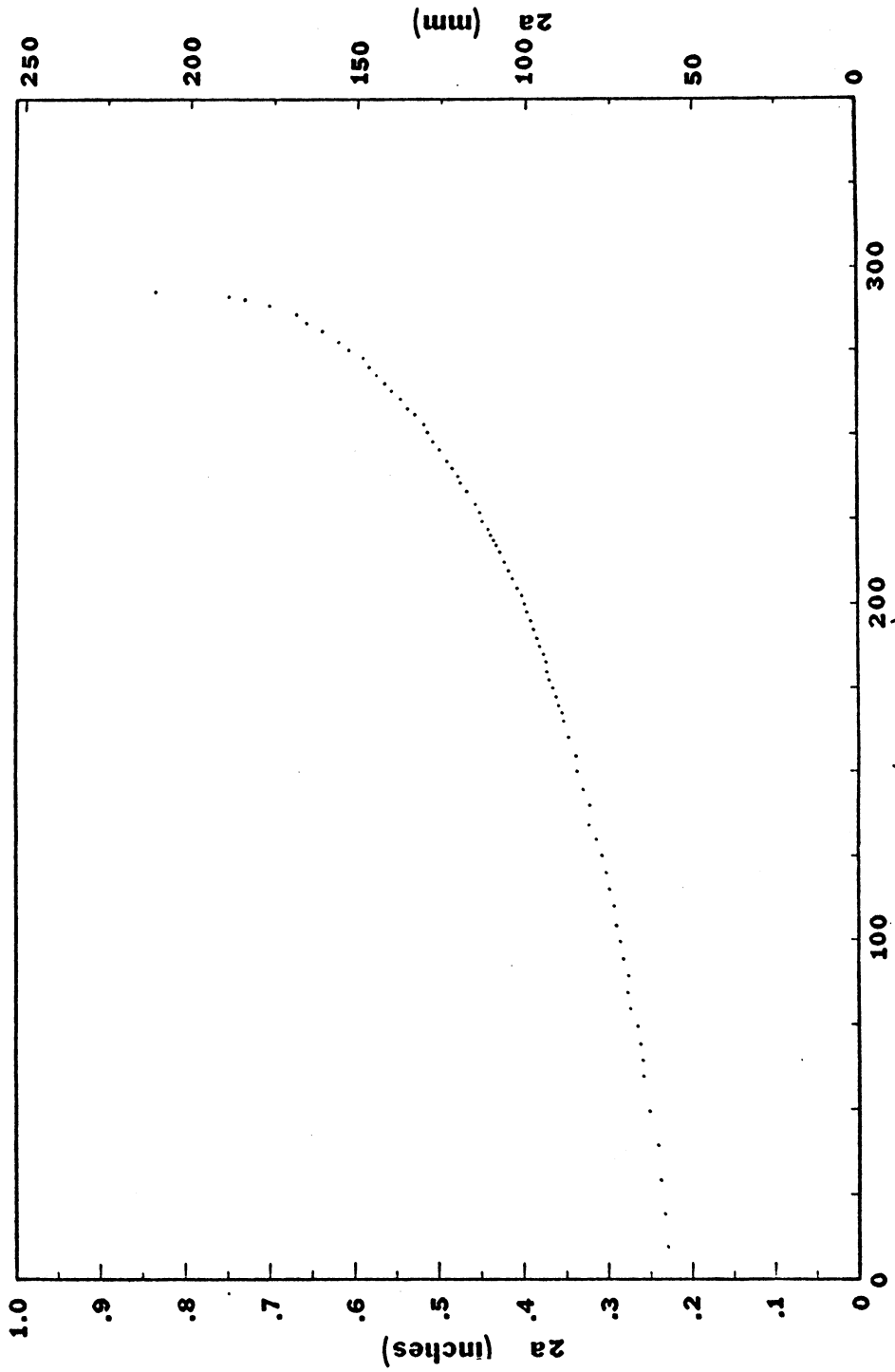

Figure 99. Crack growth curve of as received specimen 5-46.

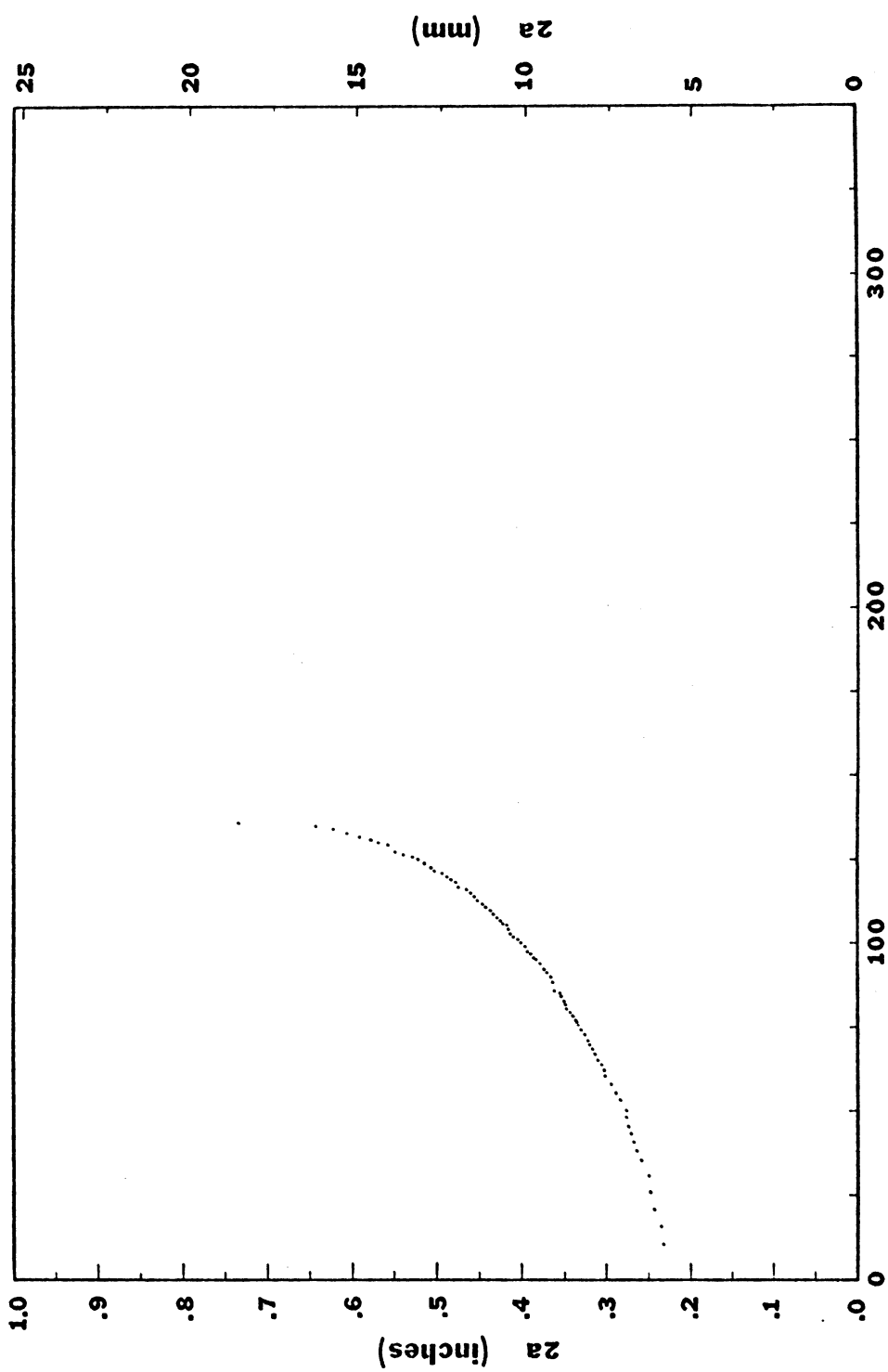

Figure 100. Crack growth curve of martensite specimen 6-48.

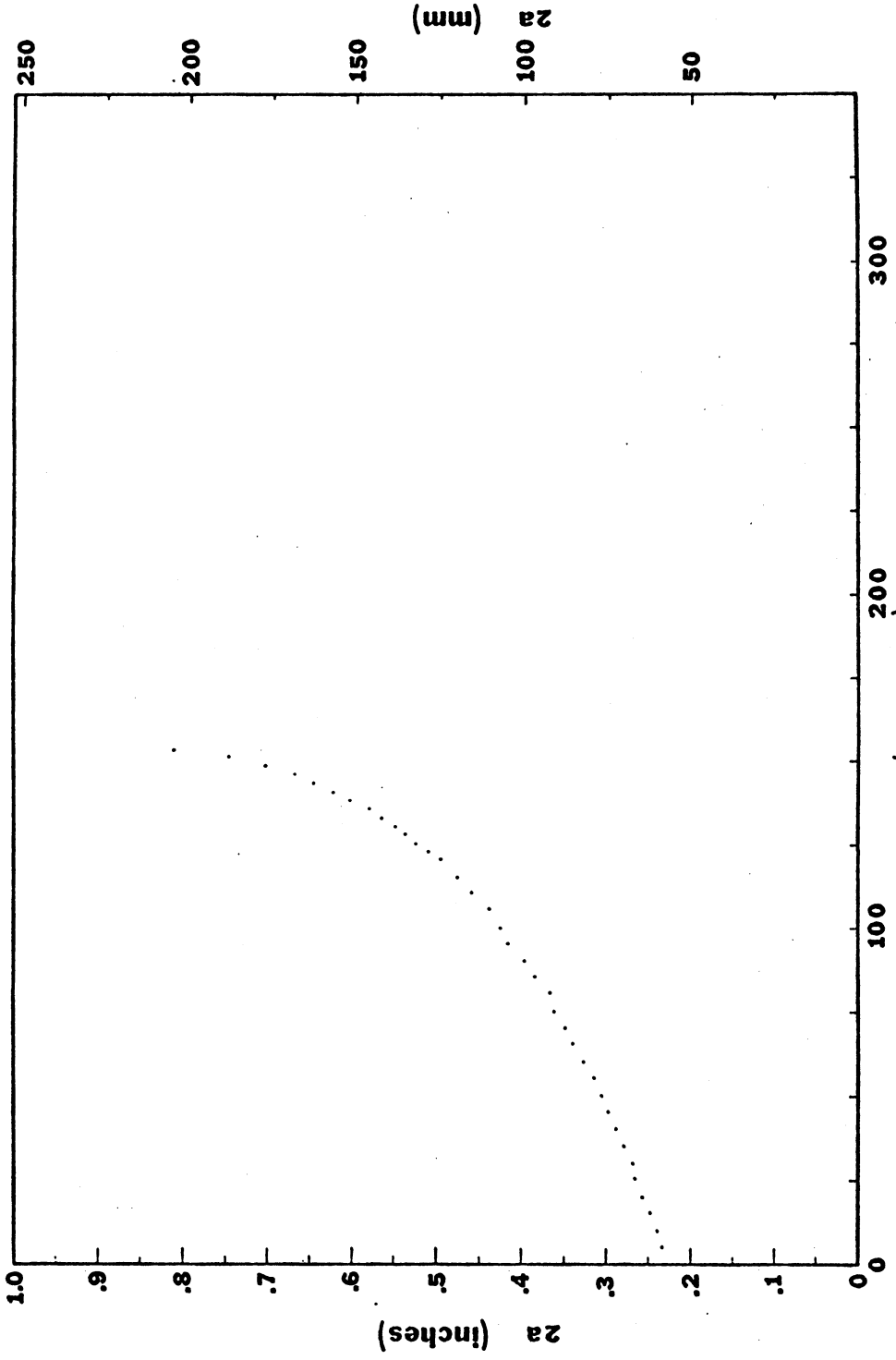

Figure 101. Crack growth curve of martensite specimen 6-49.

the martensite microstructure. However, at these loads, the fatigue cracks from precracking would not extend.

The procedures for changing the crack growth data to crack growth rate/stress intensity range data is presented in Appendix 5. By converting the data to this form it is possible to compare data sets for different materials or conditions. The fitted curves and converted data for the four crack growth tests are presented in Figures 102, 103, 104, and 105. It may be seen in these figures that the crack growth data appear to be well represented by the equations of each curve.

Figures 102 and 103 illustrate similarities in the as received data at low crack growth rates with some deviation at the higher crack growth rates. No instability data was obtained for specimen 5-44 of Figure 102. The crack growth rate steadily increased to approximately two one hundred thousandths of an inch per cycle before completely separating. In the case of as received specimen 5-46 of Figure 103. However, several data points were obtained in the unstable region (Region III of Figure 20); one point as high as two ten thousandths of an inch per cycle. The scatter of this data may be observed visually, however an example of the statistical nature of the scatter for specimen 5-46 is given in a non-dimensional form in Appendix 5.

Figures 104 and 105 represent the curve fits for the martensite crack growth specimens, 6-48 and 6-49 respectively. The method by which the parameters were picked for the fitting equations of both the as received and martensite specimens was essentially the same. However, a slight deviation from this procedure was used in the case of specimen

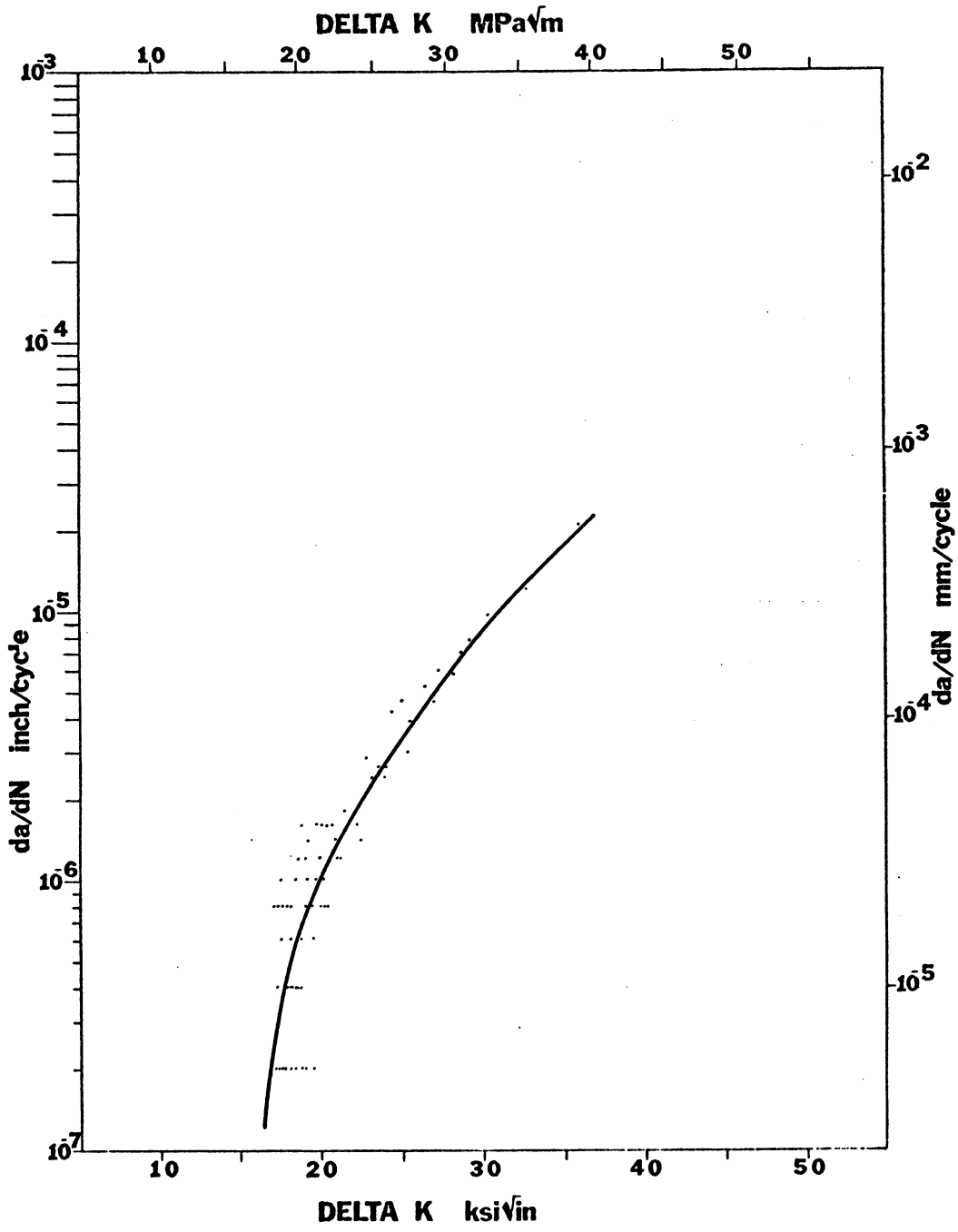

Figure 102. Curve fit to crack growth rate data of as received specimen 5-44.

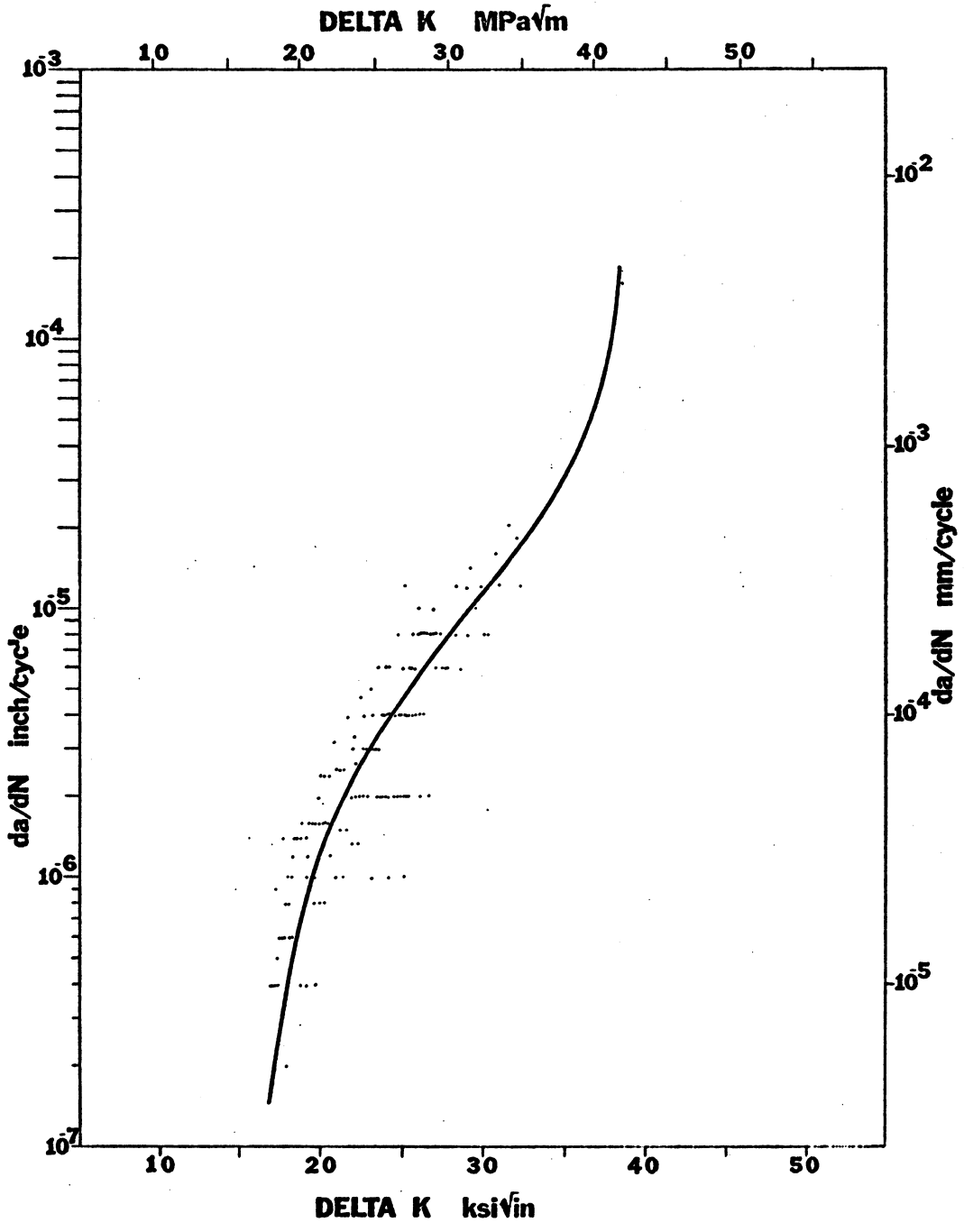

Figure 103. Curve fit to crack growth rate data of as received specimen 5-46.

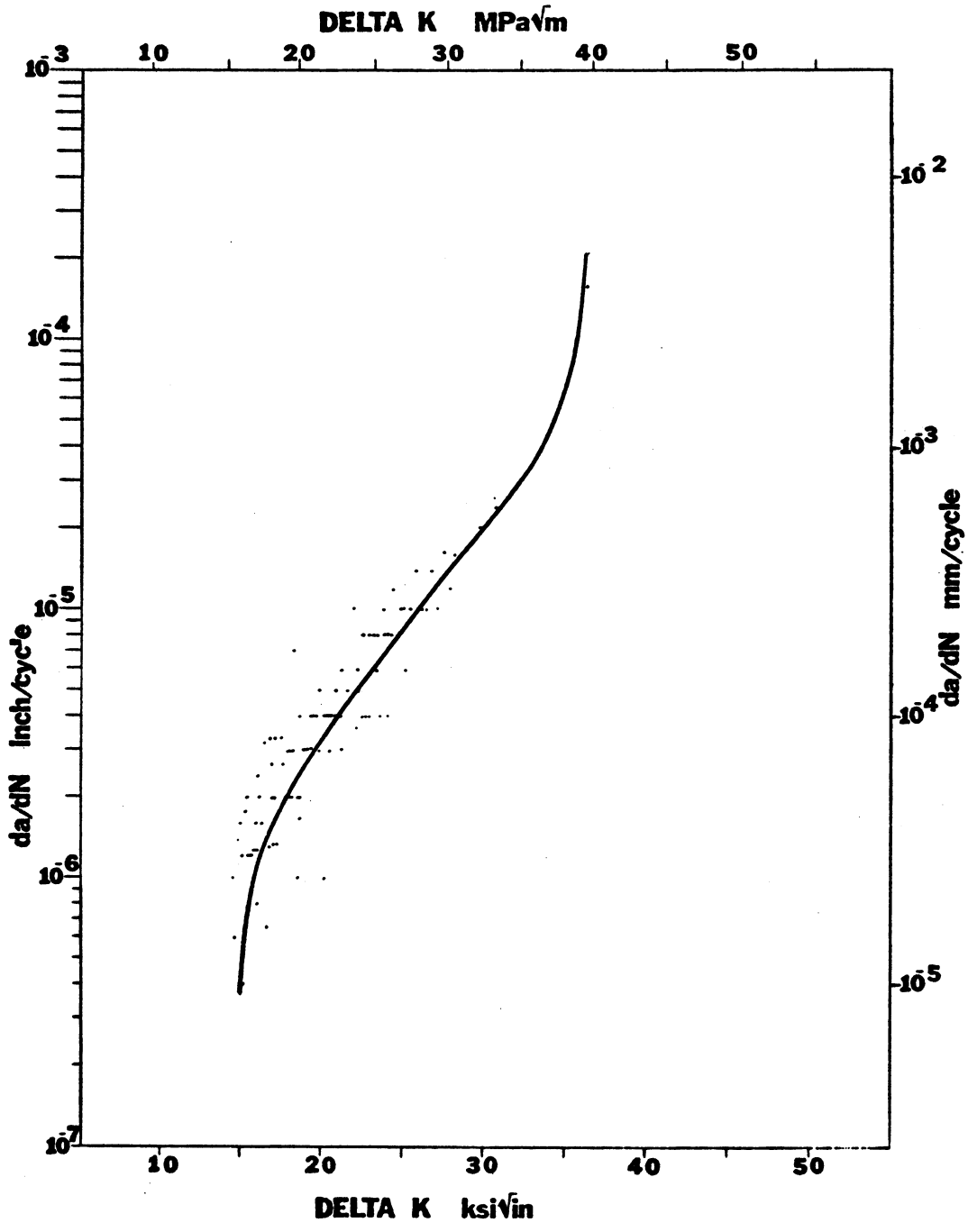

Figure 104. Curve fit to crack growth data ofmartensite specimen 6-48.

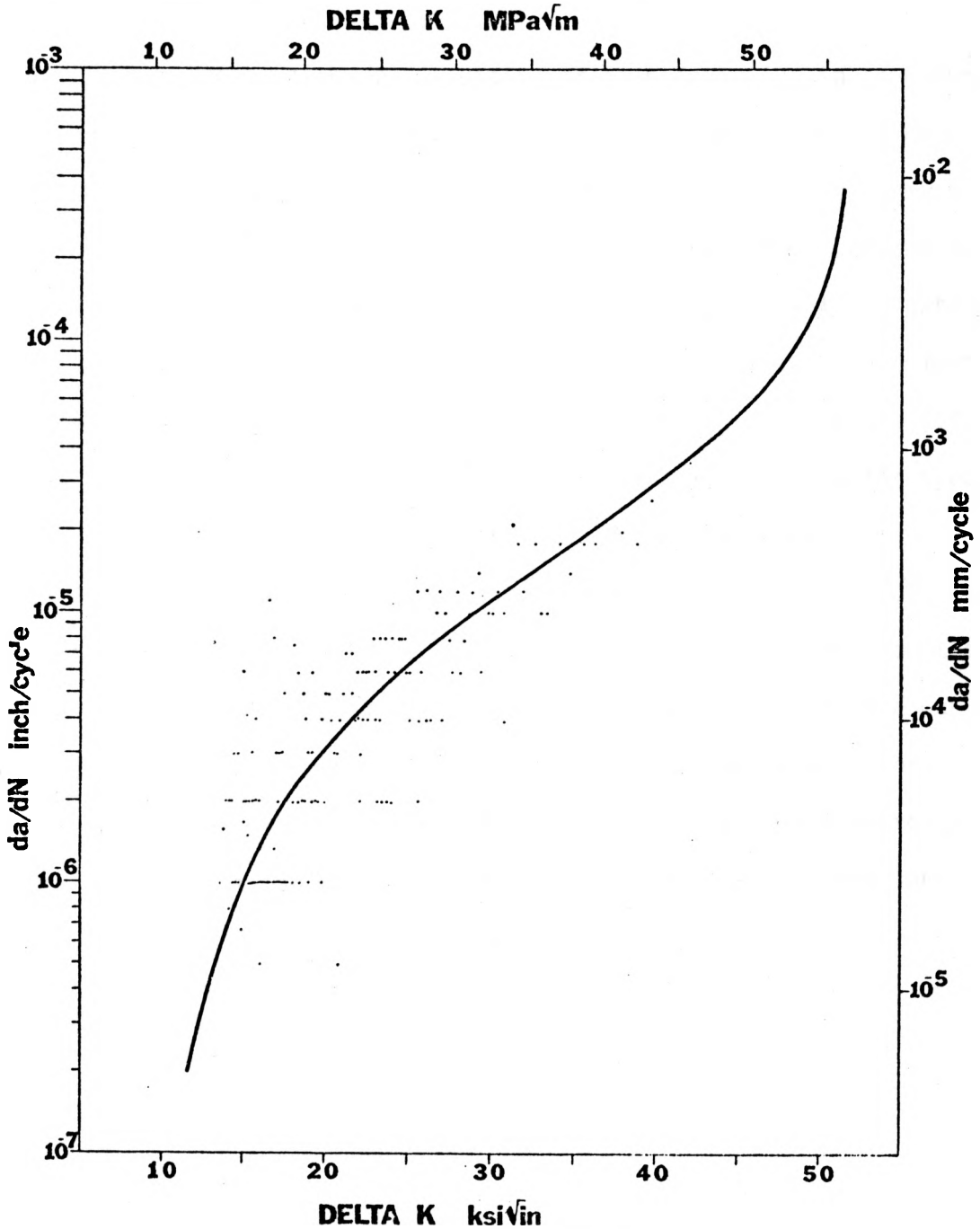

Figure 105. Curve fit to crack growth data of martensite specimen 6-49.

6-48 (Figure 104). A short discussion of this deviation in procedure is presented in the recommendations section 7.3. A comparison of Figures 104 and 105 illustrates a major difference in the crack growth rate characteristics of the two sets of martensite data. Conversely, in the threshold regions of these curves, it is noted that the data for each specimen are very repetitive. It is believed that insufficient data from specimen 6-48 were obtained, thus causing the drastic differences of data in the unstable regions. The scatter of data for specimen 6-49 is presented in a nondimensional form in Appendix 5.

A comparison of the four data sets presented in Figures 102, 103, 104, and 105 reveals that the cracking characteristics vary from the as received to the martensite microstructure. A comparison of the curves fro as received specimen 5-46 and martensite specimen 6-49 is presented in Appendix 5. This comparison illustrates a dramatic difference in crack growth behavior of two different microstructures of the same material; namely a .40/.50 carbon steel.

7.0 SYNOPSIS

7.1 CONCLUSIONS

The following conclusions are made based on the experimental and analytical results of this research effort:

1. There is a definite decrease in life due to fretting fatigue under the conditions of either air or vacuum testing.
2. The fretting fatigue process is mainly mechanical in nature.
3. The microstructural effect is evidenced in that the region of data over which the fretting process plays a predominant role is different for each microstructure.
4. The microstructural effect manifests itself in the initial stages of the fretting fatigue process.
5. The martensite microstructure has different wear and fatigue cracking characteristics than the as received microstructure, thus leading to differences in the fretting fatigue data.

The remaining conclusions are made with respect to the theories presented in section 2.2:

6. The theory of Tomlinson relies heavily on "molecular attrition" during the fretting process. The findings of this research conclude that an attrition process may be active in the surface wear process.
7. The theory of Godfrey, et al. is heavily dependent on an adhesion/oxidation principal. This is not found to be the case in the results of this study.

8. The theory of Feng and Rightmire is based on surface particles being broken away and oxidized causing abrasion of the fretting surface. While the abrasion process seems to be one of the basic mechanisms in the resulting fretting damage, the oxidation of broken surface particles does not appear to play a large role in causing the fretting damage.
9. The results of this study agree with the theory of Uhlig that the fretting process is both chemical and mechanical in nature. However, the results presented herein indicate a much larger dependence on mechanical damage than alluded to by Uhlig.
10. The findings of Halliday and Hirst that oxide formation is not a major factor in the fretting process are in agreement with those presented in this report.
11. From the results of this study, conclusions may only be made regarding the materials tested. However, a contradiction arises to the theory of Waterhouse that oxides may play an important role in the fretting fatigue process in special cases.
12. The theory of Wright regarding the complete dependence of the fretting process on oxygen is contrary to the findings of this study.

Further, this study implies that a combined wear process occurs during fretting fatigue. The principal factor in the wear process is believed to be abrasion in conjunction with adhesion of the irregular surfaces. A delamination theory apparently does not apply to the material used in this investigation, since the fractographic analysis did not reveal any

subsurface cracking phenomenon.

7.2 RECOMMENDATIONS

Based on the discoveries during the investigation of the fretting fatigue process from this study, the following recommendations are made:

1. Further vacuum and/or inert environment fretting fatigue data are needed for a variety of materials to determine the universality of the findings of this study.
2. Experimental results should be obtained far below the baseline fatigue limit of the material in question to determine oxygen/chemical effects.
3. Repetitive test at various stress levels are needed to establish scatter of fretting fatigue data. From this, the overlapping of air and vacuum data may then be determined.
4. Surface conditioning methods should be examined not only to provide basic information on the physical process of fretting fatigue, but also to provide possible methods by which designers may extend the lives of those components experiencing fretting fatigue or other wear problems.
5. A standard method by which the four parameters of the crack growth rate equation are chosen is needed. For specimens 5-44, 5-46, and 6-49, the four parameters which provided the best correlation coefficient were chosen. In the case of specimen 6-48, however, the four parameters which provided the best correlation coefficient to three significant figures combined with the best

value of standard deviation were chosen in order to provide a curve fit of physical significance.

7.3 SUMMARY

The hypothesis presented in this paper is that the microstructure plays an important role in the initial stages of fretting damage and that the mechanical damage is responsible for the largest portion of he decrease in fatigue life due to the fretting process. A verification of this hypothesis has been achieved by comparing vacuum and air fretting fatigue data for two microstructures of a .40/.50 carbon steel. For each microstructure a definite decrease in life due to fretting is experienced in the fatigue limit region of the baseline fatigue data. The decrease in life due to fretting in both vacuum and air is nearly the same, within some unknown statistical scatter, at each stress level for each microstructure.

The microstructural effect is evidenced in that the region of data over which decreases in life are experienced is different for each microstructure. The ferrite/pearlite microstructure in the as received form experiences a definite decrease in life due to fretting throughout the range of data with the decrease becoming larger at lower stress levels. The martensite microstructure experiences definite decreases in life only at stress levels near and below the baseline fatigue limit. At stress levels higher than the fatigue limit of the martensite baseline data, the effect of fretting in vacuum and air is not noticeable. Thus, the martensite microstructure is presumed to have inherent flaws

which are easily propagated at relatively high stress levels, therefore eliminating any effect due to fretting above some threshold value.

The above observations from the vacuum and air fretting fatigue results coupled with the cracking characteristics of each microstructure determined in the crack growth testing lead to the conclusions made regarding the fretting fatigue process.

REFERENCES

1. G. E. Dieter, Mechanical Metallurgy, McGraw-Hill Book Co., New York, 1961.

2. R. W. Landgraf and N. R. LaPoint, "Cyclic Stress-Strain Concepts Applied to Component Fatigue Life Prediction", Paper 740280 SAE.

3. J. A. Ewing and J. C. W. Humfrey, "The Fracture of Metals Under Repeated Alterations of Stress", Phil Trans. Roy. Soc. (London), ser. A, vol. 200, 241 (1903).

4. H. J. Gough and D. Hanson, "The Behavior of Metals Subjected to Repeated Stresses", Proc. Roy. Soc. (London), ser, A, vol. 104, (1923).

5. E. Orowan, "Theory of the Fatigue of Metals", Proc. Roy. Soc. (London), ser. A. vol. 171, (1939).

6. W. A. Wood, The Study of Metal Structures and their Mechanical Properties, Pergamon Press, New York/Toronto/Oxford/Sydney/ Braunschweig, (1971).

7. D. W. Hoeppner, The Mechanisms of Fatigue Part I - The Effect of Grain Size on Fatigue (Preliminary Results), Report No. LR 24368, Lockheed - California Company, Burbank, California, Dec. 1971.

8. D. W. Hoeppner and G. L. Goss, "A Fretting Fatigue Damage Threshold Concept", Wear, 27, pp. 61 -70 (1974).

9. R. K. Reeves, "Characterization of Fretting Fatigue Damage", A Masters thesis presented to the Graduate School of the University of Missouri - Columbia, Dec. 1974.

10. D. W. Hoeppner and G. L. Goss, "Research on the Mechanism of Fretting Fatigue", Corrosion Fatigue, NACE - 2, pp. 617 - 626, (1972).

11. R. H. Comyn and C. W. Furlani, "Fretting Corrosion - A Literature Survey", Fracture Control Program Report No. 8, College of Engineering, University of Illinois, Urbana, Illinois, May 1973.

12. J. A. Wear, "The Effect of Microstructure on the Fatigue Properties of a .40/.50 Carbon Steel", A Masters thesis presented to the Graduate School of the University of Missouri - Columbia, Dec. 1975.

13. D. A. Wilson, "The Effect of Microstructure on the Fatigue Life of Titanium", A Masters thesis presented to the Graduate School of the University of Missouri - Columbia, Dec. 1975.

14. J. E. Shigley, Mechanical Engineering Design, McGraw-Hill Book Co., New York-San Francisco-Toronto-London (1963).

15. R. E. Peterson, Stress Concentration Factors, John Wiley and Sons, New York, (1974).

16. A. A. Griffith, "The Phenomena of Rupture and Flow in Solids", Phil. Trans. Roy. Soc. (London), vol. 221A, pp. 163 - 198, (1920).

17. G. R. Irwin, "Crack Extension Force for a Part Through Crack in a Plate", ASME Transactions, Journal of Applied Mechanics, vol. 29, (1962).

18. N. E. Frost, K. J. Marsh, and L. P. Pook, Metal Fatigue, Clarendon Press - Oxford, (1974).

19. R. B. Waterhouse, Fretting Corrosion, Pergamon Press Ltd., Heading-ton Hill Hall, Oxford, (1974).

20. F. D. Bowden and D. Tabor, The Friction and Lubrication of Solids Volume II, Oxford University Press, Ely House, London W. I. (1964).

21. F. B. Seely and J. O. Smith, Advanced Mechanics of Materials, John Wiley and Sons, Inc., (1952).

22. H. Hertz, "On the Contact of Elastic Solids", Miscellaneous Papers, MacMillan and Co. (1896), (Translated by D. E. Jones).

23. N. Ohmae and T. Tsukizoe, "The Effect of Slip Amplitude on Fret-ting", Wear, 27, pp. 281 - 294 (1974).

24. D. F. Moore, Principles and Applications of Tribology, Pergamon Press, Oxford (1975).

25. N. P. Suh, "The Delamination Theory of Wear", Wear, 25, pp. 111 - 114, (1973).

26. R. B. Waterhouse and D. E. Taylor, "Fretting Debris and the Delamin-ation Theory of Wear", Wear, 29, pp. 337 - 344, (1974).

27. Vicker's Microhardness Manual.

28. Bowie, G. E.; (Personal Communication) Fall 1974.

APPENDIX 1

COMPUTER PROGRAM
FOR CALCULATING
CONTACT STRESSES

CONTACT STRESS SOLUTIONS

USING COMPUTER TECHNIQUES

An MAE 400 Project

for 3 hours credit as a

research support area

BY

Roger K. Reeves

September 1976

David W. Hoeppner Thesis Supervisor

INTRODUCTION

Contact stresses play an important role in many design situations, such as the fretting fatigue process, implying that unusual stress distributions may occur. In the example of fretting fatigue, the axial load is constantly changing, thus causing an inherent change in the normal load, which gives rise to an additional stress distribution.

Little work has been done in the area of contact stresses since the work of Hertz [1],[2],[3]*. The work of Hertz has been simplified by many sources such as the work of Seely and Smith [4]. The work of Seely and Smith in the area of contact is an extension of the earlier work of Thomas and Hoersch [5]. Seely and Smith provide procedures by which stresses may be calculated for various contact loading schemes (point contact, crossed cylinder contact, and line contact). These procedures may become useful in determining a method by which the constantly changing stress distribution may be calculated.

This paper is an initial step in developing procedures to be used in fretting fatigue distribution analyses. Herein lies the basis for future work in the form of a computer program by which contact stresses may be calculated.

PROGRAM ILLUSTRATION

The program entitled "CONTACT", developed in this investigation is given in Table 1. The general case of contact is considered with options available for such special cases as: point contact; crossed cylinder contact; and two aspects of line contact (i.e., a cylinder on a cylinder and a cylinder on a flat plate). The equations used in the program are taken from the work of Seely and Smith [4] and used with the graphs shown in Figures 1 and 2.

* Numbers in brackets indicate references

TABLE 1. Program Software - "Contact"

```
00010     CONTACT: PROC OPTIONS(MAIN);
00020     PUT LIST('ENTER 1 IF EXPLANATION OF THE PROGRAM IS ');
00030     PUT EDIT('DESIRED, 0 IF NOT')(A);
00040     GET LIST(OPTION);
00050     IF OPTION=0 THEN GO TO START;
00060     PUT SKIP;
00070     PUT LIST('THIS PROGRAM USES A METHOD OF SOLVING FOR CONTACT ');
00080     PUT SKIP;
00090     PUT LIST('STRESSES SET FORTH IN CHAPTER 11 OF "ADVANCED MECHANICS');
00100     PUT SKIP;
00110     PUT LIST('OF MATERIALS" BY SEELY AND SMITH.');
00120     PUT SKIP;
00130     PUT LIST('TO USE THIS PROGRAM YOU MUST HAVE ACCESS TO');
00140     PUT SKIP;
00150     PUT LIST('THE GRAPHS ON P.356-357 OF SEELY & SMITH.');
00160     PUT SKIP(2);
00170     PUT LIST('P=TOTAL FORCE EXERTED BY BODY 1 ON BODY 2 (POUNDS).');
00180     PUT SKIP;
00190     PUT LIST('Q=LOAD PER UNIT LENGTH FROM BODY 1 TO 2 (LBS./IN.).');
00200     PUT SKIP;
00210     PUT LIST('E1,E2=MODULI OF ELASTICITY (PSI).');
00220     PUT SKIP;
00230     PUT LIST('PO1,PO2=POISSON''S RATIO.');
00240     PUT SKIP;
00250     PUT LIST('R1,R2=MINIMUM RADII OF BODIES (INCHES).');
00260     PUT SKIP;
00270     PUT LIST('R1P,R2P=MAXIMUM RADII OF BODIES (INCHES).');
00280     PUT SKIP;
00290     PUT LIST('ALPHA=ANGLE BETWEEN PLANES CONTAINING R1 & R2 (DEGREES).');
00300     PUT SKIP(2);
00310     START: PUT LIST('ENTER 1 FOR POINT CONTACT, 2 FOR CROSSED');
00320     PUT EDIT('CYLINDERS, ALPHA=90, 3 FOR LINE CONTACT.')(A);
00330     GET LIST(TYPE);
00340     PUT SKIP;
00350     IF TYPE=1 THEN GO TO POINT;
00360     IF TYPE=2 THEN GO TO CYLIN;
00370     IF TYPE=3 THEN GO TO LINE;
00380     POINT: PUT LIST('SUPPLY R1,R1P,R2,R2P,PO1,PO2,E1,E2,P,ALPHA');
00390     GET LIST(R1,R1P,R2,R2P,PO1,PO2,E1,E2,P,ALPHA);
00400     X=(((1/R1)+(1/R1P)+(1/R2)+(1/R2P))/4);
00410     R1S=((1/R1)-(1/R1P));
00420     R2S=((1/R2)-(1/R2P));
00430     A1=((SIND(ALPHA))**2);
00440     Y=(((R1S+R2S)**2)-(4*R1S*R2S*A1));
00450     B=X+(((Y)**0.5)/4);
00460     A=X-(((Y)**0.5)/4);
00470     BA=B/A;
00480     PUT SKIP;
00490     GO TO REST;
00500     PUT SKIP;
00510     CYLIN: PUT LIST('SUPPLY R1,R2,PO1,PO2,E1,E2,P');
00520     GET LIST(R1,R2,PO1,PO2,E1,E2,P);
00530     B=(1/(2*R1));
00540     A=(1/(2*R2));
00550     BA=B/A;
00560     PUT SKIP;
00570     GO TO REST;
00580     REST: PUT EDIT('B/A=',BA)(A(5),F(8,2));
00590     PUT SKIP(2);
00600     PUT LIST('SUPPLY CB,CSN,CSS,CSSG,CZS FROM GRAPHS');
00610     GET LIST(CB,CSN,CSS,CSSG,CZS);
00620     D=(1/(A+B))*(((1-(PO1**2))/E1)+((1-(PO2**2))/E2));
```

TABLE 1. (cont.)

```
00630     B1=CB*((P*D)**(1/3));
00640     BD=B1/D;
00650     SN=-CSN*BD;
00660     SS=CSS*BD;
00670     SSG=CSSG*BD;
00680     ZS=CZS*B1;
00690     PUT SKIP(2);
00700     PUT EDIT('MAXIMUM PRINCIPAL STRESS IS',SN)(A(30),F(10,2));
00710     PUT EDIT(' PSI')(A);
00720     PUT SKIP;
00730     PUT EDIT('MAXIMUM SHEARING STRESS IS',SS)(A(30),F(10,2));
00740     PUT EDIT(' PSI')(A);
00750     PUT SKIP;
00760     PUT EDIT('MAXIMUM OCTAHEDRAL STRESS IS',SSG)(A(30),F(10,2));
00770     PUT EDIT(' PSI')(A);
00780     PUT SKIP;
00790     PUT EDIT('LOCATION OF SHEARING STRESS IS',ZS)(A(30),F(10,3));
00800     PUT EDIT(' INCHES')(A);
00810     PUT SKIP(2);
00820     GO TO STOP;
00830     LINE: PUT EDIT('ENTER 1 IF CYLINDER ON PLANE')(A);
00840     GET LIST(PLANE);
00850     PUT SKIP;
00860     IF PLANE=1 THEN GO TO CPLANE;
00870     PUT LIST('SUPPLY R1,R2,PO1,PO2,E1,E2,Q');
00880     GET LIST(R1,R2,PO1,PO2,E1,E2,Q);
00890     D=(1/((1/(2*R1))+(1/(2*R2))))*(((1-(PO1**2))/E1)+((1-(PO2**2))/E2));
00900     GO TO LAST;
00910     CPLANE: PUT LIST('SUPPLY R1,PO1,PO2,E1,E2,Q');
00920     GET LIST(R1,PO1,PO2,E1,E2,Q);
00930     D=(((1-(PO1**2))/E1)+((1-(PO2**2))/E2))*2*R1;
00940     LAST: B1=(((2*Q*D)/3.141592654)**0.5);
00950     B1D=B1/D;
00960     SX=-2*PO2*B1D;
00970     SY=-B1D;
00980     SZ=-B1D;
00990     SS=0.3*B1D;
01000     SSG=0.27*B1D;
01010     ZS=0.7861*B1;
01020     PUT SKIP;
01030     PUT LIST('MAXIMUM PRINICIPAL STRESSES ARE');
01040     PUT SKIP;
01050     PUT EDIT('          X DIRECTION',SX)(A(22),F(10,2));
01060     PUT EDIT(' PSI')(A);
01070     PUT SKIP;
01080     PUT EDIT('          Y DIRECTION',SY)(A(22),F(10,2));
01090     PUT EDIT(' PSI')(A);
01100     PUT SKIP;
01110     PUT EDIT('          Z DIRECTION',SZ)(A(22),F(10,2));
01120     PUT EDIT(' PSI')(A);
01130     PUT SKIP;
01140     PUT EDIT('MAXIMUM SHEARING STRESS IS',SS)(A(30),F(10,2));
01150     PUT EDIT(' PSI')(A);
01160     PUT SKIP;
01170     PUT EDIT('MAXIMUM OCTAHEDRAL STRESS IS',SSG)(A(30),F(10,2));
01180     PUT EDIT(' PSI')(A);
01190     PUT SKIP;
01200     PUT EDIT('LOCATION OF SHEARING STRESS IS',ZS)(A(30),F(10,3));
01210     PUT EDIT(' INCHES')(A);
01220     PUT SKIP(2);
01230     STOP: PUT SKIP;
01240     END CONTACT;
```

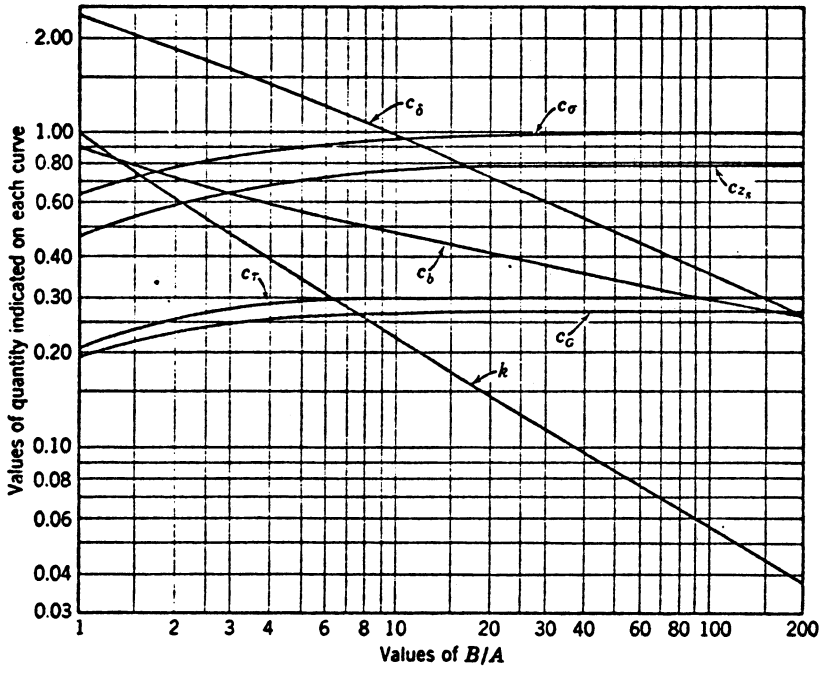

Figure 1. Values of contact coefficients for determining stresses and deflections between two bodies in contact. [4]

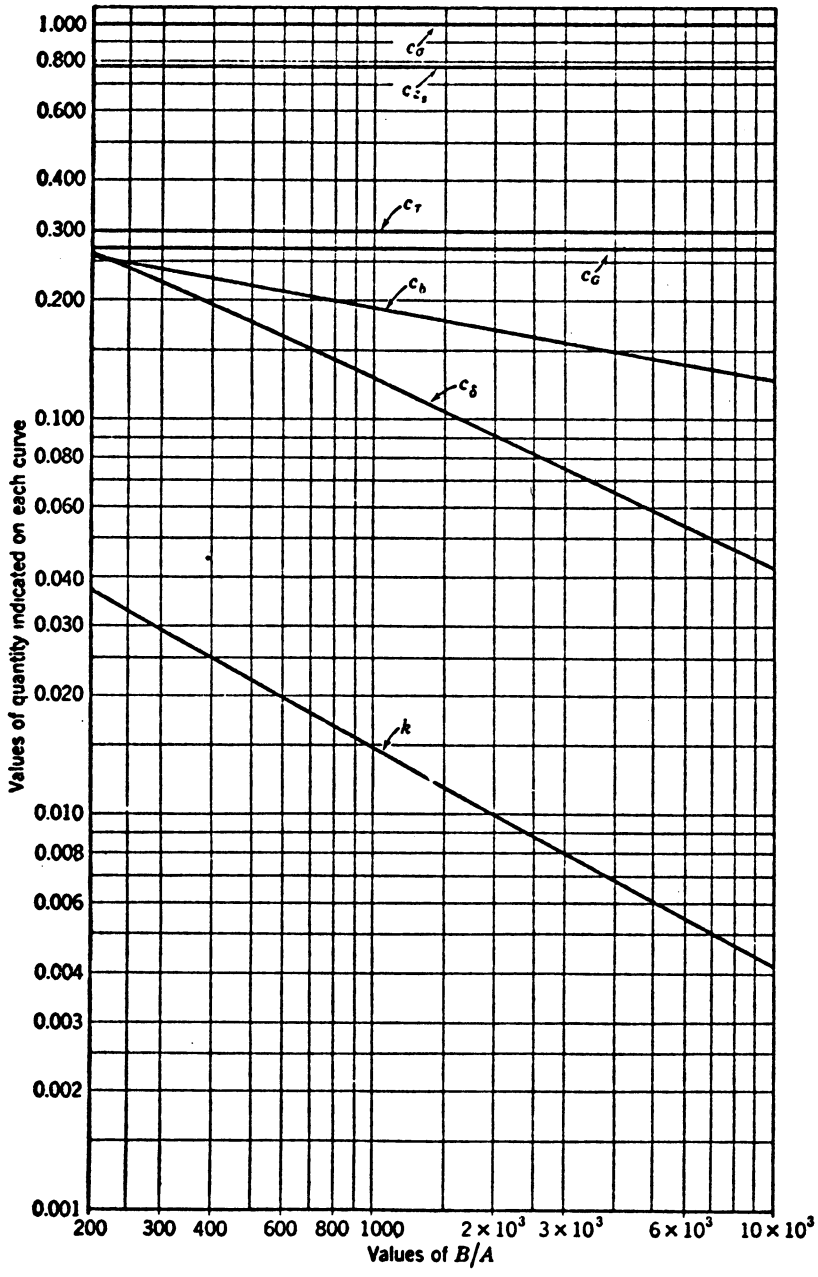

Figure 2. Values of contact coefficients for determining stresses and deflections between two bodies in contact. [4]

In order to illustrate the use of the program, various example problems are given [4]:

PROBLEM 1. Two semicircular disks of steel are brought into contact under a load P=1000 lbs. The radii of curvature of the surfaces at the point of contact are R_1=2 inches, R_1'=5 inches, R_2=3 inches, and R_2'=8 inches. The angle, α, between the planes of minimum curvature is 60 degrees. Compute the maximum principal stress, the maximum shearing stress, the maximum octahedral shearing stress, and the location of the maximum shearing stress below the surface of contact in body 2 due to the applied load.
$E_1=E_2$=30,000,000 psi; and $\mu_1=\mu_2$=.25

The solution of this problem with an explanation of the program is as follows:

```
ENTER 1 IF EXPLANATION OF THE PROGRAM IS  DESIRED, 0 IF NOT
:
1

THIS PROGRAM USES A METHOD OF SOLVING FOR CONTACT
STRESSES SET FORTH IN CHAPTER 11 OF "ADVANCED MECHANICS
OF MATERIALS" BY SEELY AND SMITH.
TO USE THIS PROGRAM YOU MUST HAVE ACCESS TO
THE GRAPHS ON P.356-357 OF SEELY & SMITH.

P=TOTAL FORCE EXERTED BY BODY 1 ON BODY 2 (POUNDS).
Q=LOAD PER UNIT LENGTH FROM BODY 1 TO 2 (LBS./IN.).
E1,E2=MODULI OF ELASTICITY (PSI).
PO1,PO2=POISSON'S RATIO.
R1,R2=MINIMUM RADII OF BODIES (INCHES).
R1P,R2P=MAXIMUM RADII OF BODIES (INCHES).
ALPHA=ANGLE BETWEEN PLANES COTAINING R1 & R2 (DEGREES).

ENTER 1 FOR POINT CONTACT, 2 FOR CROSSED CYLINDERS, ALPHA=90, 3 FOR LINE CONTACT.
:
1

SUPPLY R1,R1P,R2,R2P,PO1,PO2,E1,E2,P,ALPHA
:
2 5 3 8 .25 .25 30000000 30000000 1000 60

B/A=      1.60

SUPPLY CB,CSN,CSS,CSSG,CZS FROM GRAPHS
:
.78 .73 .24 .22 .56

MAXIMUM PRINCIPAL STRESS IS    -251207.88 PSI
MAXIMUM SHEARING STRESS IS       82568.88 PSI
MAXIMUM OCTAHEDRAL STRESS IS     75706.84 PSI
LOCATION OF SHEARING STRESS IS       0.021 INCHES
```

PROBLEM 2. A steel railway car wheel 33 inches in diameter rolls on a steel rail whose top surface has a cross radius of 12 inches. The wheel pressure on the rail head is 25,000 lbs. Calculate the maximum principal stress, the maximum shearing stress, the maximum octahedral shearing stress, and the location below the surface of the rail at which the maximum shearing stress occurs.

$E_1=E_2=30{,}000{,}000$ psi; and $\mu_1=\mu_2=.25$

The solution of this problem is as follows:

```
ENTER 1 FOR POINT CONTACT, 2 FOR CROSSED CYLINDERS, ALPHA=90, 3 FOR LINE CONTACT.
:
2

SUPPLY R1,R2,PO1,PO2,E1,E2,P
:
12 16.5 .25 .25 30000000 30000000 25000

B/A=      1.38

SUPPLY CB,CSN,CSS,CSSG,CZS FROM GRAPHS
:
.81 .70 .24 .22 .53


MAXIMUM PRINCIPAL STRESS IS    -182161.69 PSI
MAXIMUM SHEARING STRESS IS       62443.59 PSI
MAXIMUM OCTAHEDRAL STRESS IS     57244.54 PSI
LOCATION OF SHEARING STRESS IS       0.129 INCHES
```

PROBLEM 3. Two steel cylinders of radii $R_1=2$ inches and $R_2=6$ inches have their longitudinal axes parallel and are pressed against each other by a load of q=1500 lbs/inch. Compute the maximum principal stress (where the z axis is directed into cylinder 2 parallel to the contact load and where the x and y axes are in the plane of contact; x being parallel to the longitudinal axis of the cylinders and y being perpendicular to the longitudinal axis), the maximum shearing stress, the maximum octahedral shearing stress, and the location below the surface of cylinder 2 at which the maximum shearing stress occurs.

$E_1=E_2=30{,}000{,}000$ psi; and $\mu_1=\mu_2=.25$

The solution of this problem is given as follows:

```
ENTER 1 FOR POINT CONTACT, 2 FOR CROSSED CYLINDERS, ALPHA=90, 3 FOR LINE CONTACT.
:
3

ENTER 1 IF CYLINDER ON PLANE
:


SUPPLY R1,R2,PO1,PO2,E1,E2,Q
:
2 6 .25 .25 30000000 30000000 1500

MAXIMUM PRINICIPAL STRESSES ARE
          X DIRECTION  -35682.47 PSI
          Y DIRECTION  -71364.94 PSI
          Z DIRECTION  -71364.94 PSI
MAXIMUM SHEARING STRESS IS       21409.48 PSI
MAXIMUM OCTAHEDRAL STRESS IS     19268.53 PSI
LOCATION OF SHEARING STRESS IS       0.011 INCHES
```

PROBLEM 4. Assuming the top surface of the rail in PROBLEM 2 is flat and horizontal with a width of 2 inches, calculate the maximum principal stress (with axes x, y, z oriented as in PROBLEM 3), the maximum shearing stress, the maximum octahedral shearing stress, and the depth below the surface of the rail at which the maximum shearing stress occurs. P=25,000 lbs; $E_1=E_2=30{,}000{,}000$ psi; and $\mu_1=\mu_2=.25$

The solution of this problem is given as follows:

```
ENTER 1 FOR POINT CONTACT, 2 FOR CROSSED CYLINDERS, ALPHA=90, 3 FOR LINE CONTACT.
:
3

ENTER 1 IF CYLINDER ON PLANE
:
1

SUPPLY R1,PO1,PO2,E1,E2,Q
:
16.5 .25 .25 30000000 30000000 12500

MAXIMUM PRINICIPAL STRESSES ARE
          X DIRECTION  -31057.61 PSI
          Y DIRECTION  -62115.22 PSI
          Z DIRECTION  -62115.22 PSI
MAXIMUM SHEARING STRESS IS       18634.56 PSI
MAXIMUM OCTAHEDRAL STRESS IS     16771.11 PSI
LOCATION OF SHEARING STRESS IS       0.101 INCHES
```

CONCLUSIONS AND RECOMMENDATIONS

It is evident that the program, "CONTACT", is a simplified version for calculating contact stresses. However, further work in this area may be directed toward the solution of more complex contact situations which illustrate the actual contact loadings of interest. Further computerized stress analyses using the contact load plus any additional load, such as fatigue in the case of fretting fatigue, may be investigated.

This program provides a starting point at which further computer techniques may be developed to analyze contact stresses. This type of analysis of complex contact problems is the method by which unusual stress distributions must be determined.

REFERENCES

1. Hertz, Heinrich; Miscellaneous Papers, chapter V; Translation by D. E. Jones; MacMillian and Co., London, 1896.
2. Hertz, Heinrich; Miscellaneous Papers, chapter VI; Translation by D. E. Jones; MacMillian and Co., London, 1896.
3. Hertz, Heinrich; Miscellaneous Papers, chapter XV; Translation by D. E. Jones; MacMillian and Co., London, 1896.
4. Seely, F. B. and Smith, J. O.; Advanced Mechanics Of Materials, chapter 11; John Wiley and Sons, Inc., 1952.
5. Thomas, H. R. and Hoersch, V. A.; "Stresses Due To The Pressure Of One Elastic Solid Upon Another", University of Illinois Experiment Station, Bulletin No. 212; July, 1930.

APPENDIX 2

COMPOSITION ANALYSIS

BY

UMC GEOLOGY DEPT.

RESULTS OF QUALITATIVE AND SEMI-QUANTITATIVE ELECTRON MICROPROBE ANALYSIS OF A STEEL SAMPLE FROM ROGER REEVES DEPARTMENT OF MECHANICAL AND AEROSPACE ENGINEERING

October 21, 1976

Constance K. Barsky
Microprobe Service
Department of Geology
University of Missouri--Columbia
Columbia, Missouri 65201

Results

The results of qualitative electron microprobe analysis of the steel sample indicates the presence of the following elements:

iron
manganese
chromium
silicon.

Semi-quantitative analysis indicates that the last three elements listed above are present at the following levels of concentration:

manganese	8230 ± 1900 ppm
chromium	740 ± 170 ppm
silicon	1760 ± 480 ppm.

Sample Description and Preparation

An approximately 12 mm x 6 mm polished sample mounted in plastic was presented for analysis. It was not carbon coated. G-C brand Silver Print was used to provide electrical contact between the steel specimen and the sample holder. No conduction problems were observed using this method.

Analysis

Qualitative and semi-quantitative analyses were conducted using an Applied Research Laboratories Electron Microprobe X-Ray Analyzer--Scanning Microscope (ARL EMX-SM 121000).

Qualitative Analysis: Wavelength scans were collected for one 25 micron diameter area. Table 1 lists the operating parameters. Using three different analyzing crystals, the effective wavelength range extended from 1.20 Å to 23.3 Å. Copies of these scans are included with this report.

Table 1

Electron Microprobe Operating Parameters
for Wavelength Scans

Accelerating Voltage:	15 kilovolts
Emission Current:	190 microamps
Specimen Current:	0.03 microamps on brass
Beam Diameter:	25 microns
Beam Penetration:	3 microns or less
Detection Limits:	500 to 1000 ppm for most elements

Spectrometer[1]	Crystal	Effective Wavelength Ranges in Angstroms
#1	PET (pentaerythritol)	2.60 - 7.83
#2	LiF (lithium fluoride)	1.20 - 3.60
#3	RAP (rubidium acid phthalate)	7.79 - 23.3

Detector	Attenuator	Coarse Gain	Fine Gain	Baseline (volts)	Ratemeter Range (Y-axis deflection)[2]
#1	20	4	8.5	1.0	1000 cts/sec
#2	15	8	6.5	1.0	1000 cts/sec
#3	11	8	9.0	1.0	1000 cts/sec

1. Spectrometers are LiF geared; they were motor driven at 0.1 Angstroms per minute.

2. Deflection of the Y-axis of the flat-bed recorder was adjusted to maximize low intensity peaks without creating excessive background noise.

X-ray emission peaks were identified using the July, 1970, edition of X-RAY EMISSION AND ABSORPTION EDGE WAVELENGTHS AND INTERCHANGE SETTINGS FOR LIF GEARED CURVED CRYSTAL SPECTROMETER, by E. W. White and G. G. Johnson (Earth and Mineral Sciences Experiment Station Special Publication No. I-70, Pennsylvania State University). All major peaks have been identified. They have been labeled on the scans with the element symbol, electron shell and order of x-ray emission line.

Semi-quantitative Analysis: Table 2 lists the operating conditions and crystal settings utilized for the semi-quantitative analysis. Using a point source, at least nine different points on the specimen were analyzed for each of the three elements--silicon, manganese and chromium--on the peak positions. Background counts were also accummulated at positions $\pm$ 0.0500 divisions off the peak positions. For a fixed beam current of 400000, termination of counting times averaged 8.35 seconds.

Standards used for the analyses were the silicon, manganese and chromium mounts of the ARL standard.

The counting errors on the standards range from 0.4% for silicon to 2.6% for manganese. The counting errors on the steel sample average 7% for each of the three elements analyzed for. The total errors (1σ) for each element are 9.1% for silicon, 7.7% for manganese, 7.7% for chromium. These total errors include an assumed 3% error in the composition of each of the three standards in addition to the counting errors on both the appropriate standard and the sample.

Table 2

Electron Microprobe Operating Parameters
for Semi-Quantitative Analysis

Operating consitions, except for beam size, are the same at those listed at the biginning of Table 1.

Beam size: point source
Fixed Beam Current: 4000000

Crystal Settings

Detector	Element	Peak	Attenuator	Coarse Gain	Fine Gain	Baseline (volts)	Window (Volts)	STD	LLD[1] (ppm)
#1 PET	Si	3.2800	20	8	5.0	1.7	3.1	ARL-Si	200
#2 LiF	Mn	2.1050	15	4	7.75	2.0	2.5	ARL-Mn	600
#2 LiF	Cr	2.2920	15	4	8.75	2.0	2.5	ARL-Cr	400

1. Lower limit of detection calculated using a net peak determined to be 3 times the standard deviation of the background counts.

The estimated concentrations of these elements in the steel sample are reported below with an associated error of 3σ:

silicon	1760 $\pm$ 480 ppm
manganese	8230 $\pm$ 1900 ppm
chromium	740 $\pm$ 170 ppm.

These values represent a "first approximation" solution--no correction procedures were applied to the raw data.

APPENDIX 3

SAMPLE CALCULATION OF LOAD LEVELS AND MACHINE SETTINGS FOR FATIGUE TESTING

The following procedure was used to determine the control settings to obtain the desired stress levels in the fatigue specimens during each test. (Actual conditions from the test of specimen 1-06 are given.)

1. The test number, microstructure, date, type of test, frequency, and R ratio are recorded:

   Test #6 As Received 3/29/76 - 4/4/76 Baseline

   R = +0.1 f = 20 hz

2. The maximum stress level at which the specimen will be subjected is recorded:

   S_{max} = 65 ksi (448.4 MPa)

3. Corresponding minimum and mean stresses are calculated:

   $S_{min} = (S_{max})(R) = (65)(0.1) = 6.5$ ksi (44.8 MPa)

   $S_{mean} = (S_{max} + S_{min})/2 = (65 + 6.5)/2 = 35.8$ ksi (246.9 MPa)

4. The smallest cross section of the fatigue specimen is measured and calculated:

   Width = .253 in (6.43e-03 m)

   Thickness = .100 in (2.54e-03 m)

   Area = (.253)(.100) = .0253 in^2 (1.63e-05 m^2)

5. The loads required to provide the chosen stress levels are computed:

   $P_{max} = (S_{max})(Area) = 1645$ pounds (7321 N)

   $P_{mean} = (S_{mean})(Area) = 904.8$ pounds (4027 N)

   $P_{min} = (S_{min})(Area) = 164.5$ pounds (732 N)

6. Voltages are calculated corresponding to the desired loads. The load range used was 4500 pounds over a 10 volt maximum readout.

   $\text{Voltage} = \left(\frac{\text{desired load}}{\text{operating range}}\right)(10 \text{ volts})$

   thus,

   $V_{max} = (1645/4500)(10) = 3.66$ volts

   $V_{mean} = (904.8/4500)(10) = 2.01$ volts

   $V_{min} = (164.5/4500)(10) = .37$ volts

7. The span setting (for presetting the alternating voltage or load) is calculated:

   $\text{Span} = \left(\frac{P_{max} - P_{min}}{\text{operating range}}\right)(500) = [(1645 - 164.5)/4500](500) = 165$

   (This setting is approximate and usually both span and mean value settings must be adjusted during the initial stages of the test.)

8. The temperature and relative humidity are observed and recorded at the beginning and throughout the test. In the case of long tests, the range of values are recorded.

   Temperature = 70F - 84F (21C - 29C)

   Relative Humidity = 31% - 46%

9. Finally, the number of cycles to failure are recorded.

   N = 10,000,000 NF*

* In the case of this particular specimen, there was no failure after ten million cycles and therefore the test was considered a "runout".

APPENDIX 4

SAMPLE CALCULATION OF LOAD LEVELS AND MACHINE SETTINGS FOR FRETTING FATIGUE TESTING

The following procedure was used to determine the control settings to obtain the desired stress levels in the fretting fatigue specimens during each test. (Actual conditions from the test of specimen 4-35 are given.)

1. The test number, microstructure, date, type of test, frequency, and R ratio are recorded:

   Test #35 Martensite 6/1/76 Fretting-Air

   R = +0.1 f = 20hz

2. The maximum stress level at which the specimen will be subjected is recorded:

   S_{max} = 90 ksi (621 MPa)

3. Corresponding minimum and mean stresses are calculated:

   $S_{min} = (S_{max})(R) = (90)(0.1) = 9$ ksi (62.1 MPa)

   $S_{mean} = (S_{max} + S_{min})/2 = (90 + 9)/2 = 49.5$ ksi (341 MPa)

4. The smallest cross section of the fatigue specimen is measured and calculated:

   Width = .248 in (6.3e-03 m)

   Thickness = .100 in (2.54e-03 m)

   Area = (.248)(.100) = .0248 in^2 (1.6e-05 m^2)

5. The loads required to provide the chosen stress levels are computed:

   $P_{max} = (S_{max})(Area) = 2232$ pounds (9932 N)

   $P_{mean} = (S_{mean})(Area) = 1227.6$ pounds (5462 N)

   $P_{min} = (S_{min})(Area) = 223.2$ pounds (993.2 N)

6. Voltages are calculated corresponding to the desired loads. The load range used was 4500 pounds over a 10 volt maximum readout.

   Voltage = $\left(\frac{\text{desired load}}{\text{operating range}}\right)$(10 volts)

   thus,

   V_{max} = (2232/4500)(10) = 4.96 volts

   V_{mean} = (1227.6/4500)(10) = 2.73 volts

   V_{min} = (223.2/4500)(10) = .50 volts

7. The span setting (for presetting the alternating voltage or load) is calculated:

   Span = $\left(\frac{P_{max} - P_{min}}{\text{operating range}}\right)$(500) = [(2232 - 223.2)/4500](500) = 223

   (This setting is approximate and usually both span and mean value settings must be adjusted during the initial stages of the test.)

8. The cross section of the fretting pad is measured and calculated:

   Width = .250 in (6.35e-03 m)

   Length = .250 in (6.35e-03 m)

   Area = (.250)(.250) = 0.0625 in^2 (4.03e-05 m^2)

9. The load required to provide a normal stress of 6 ksi (41.1 MPa) is calculated:

   Normal Load = (Normal Stress)(Area) = (6000)(.0625) = 375 pounds (1669 N)

10. The temperature and relative humidity are observed and recorded at the beginning and throughout the test. In the case of long tests, the range of values are recorded.

    Temperature = 77F (25C)

    Relative Humidity = 50%

11. Finally, the number of cycles to failure are recorded.

    N = 358,970

APPENDIX 5

ANALYSIS OF CENTER CRACKED PANEL CRACK GROWTH DATA OF A .40/.50 CARBON STEEL

ABSTRACT

A four parameter Weibull survivorship equation is applied in the analysis of fatigue crack growth data of two microstructures of a .40/.50 Carbon steel. A new method of optimizing variables in conjunction with standard linear regression analysis is discussed in terms of fitting curves to crack growth rate data of center cracked panels. A simplier form of this method is applied in the analysis of compliance data for the same center cracked panels. It is determined that these curve fitting methods provide curves extremely representative of the data.

INTRODUCTION

Crack growth characteristics of thin sections of material are often determined using center cracked panels similar to the one shown in Figure 1. The crack growth data is taken in the form of crack length (2a) after some number of cycles (N); examples of curves from these types of data are shown in Figures 2 and 3. Various curve fitting techniques may be employed to determine a suitable equation to represent this type of data since a plot of crack growth rate (da/dN) versus stress intensity range (ΔK) is ultimately desired. However, during the data aquisition, the incremental crack length readings are small enough that the crack growth data (a-N) may be converted to crack growth rate data (da/dN-ΔK) by using a crack growth rate of the form:

$$da/dN = \Delta a/\Delta N \tag{1}$$

and a stress intensity range from the equation:

$$K = \frac{P\sqrt{c}}{BW} Y \tag{2}$$

where P is the applied load, B is the specimen thickness, W is the specimen width, c is the crack length, and Y is a geometric factor called the stress intensity coefficient.

The most widely used form of the stress intensity coefficient, Y, is given as [1]:

Figure 1. Center cracked panel for crack growth testing.

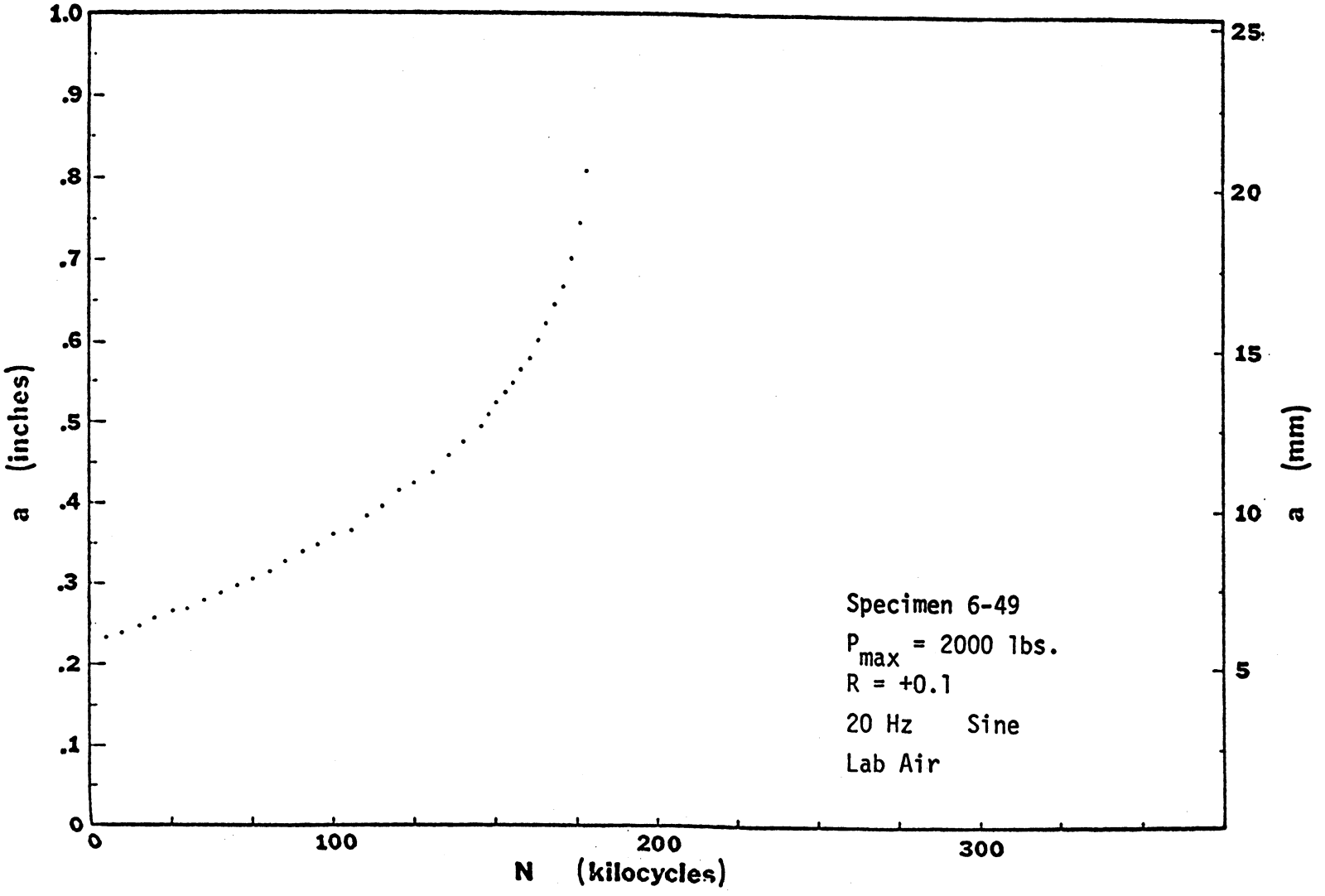

Figure 3. Crack growth curve for specimen 6-49

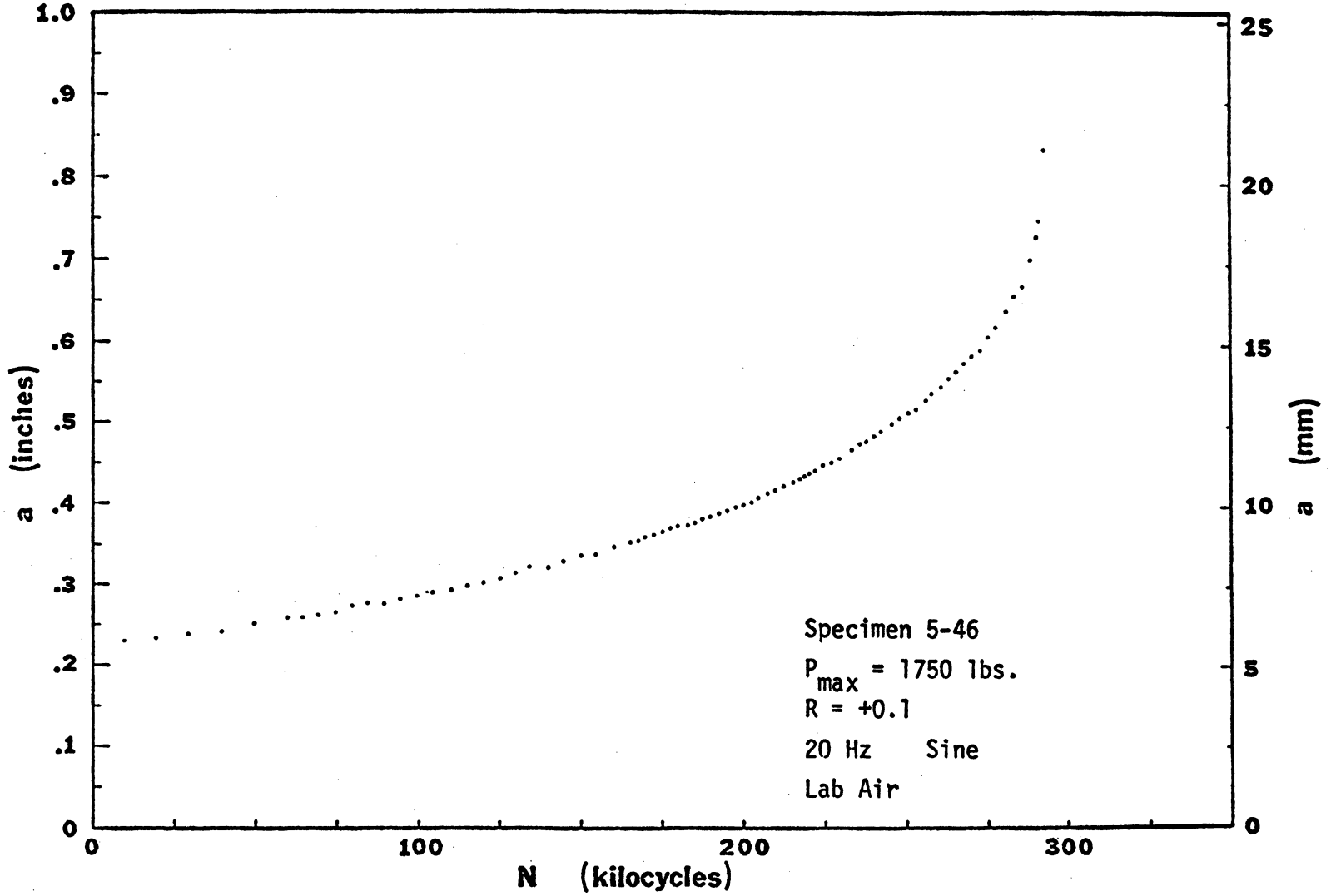

Figure 2. Crack growth curve for specimen 5-46.

$$Y = 1.77 + .227(2a/W) - .510(2a/W)^2 + 2.7(2a/W)^3 \quad (3)$$

for center cracked panels. Brown [2] indicates that:

$$KB/P = [(1/2W)\frac{d(CEB)}{d(c/W)}]^{1/2} \quad (4)$$

where CEB is the non-dimensional compliance parameter given by:

$$CEB = EB\delta/P \quad (5)$$

and E is the modulus of elasticity of the material, B is the specimen thickness, P is the applied load, and δ is the crack opening displacement for the given load. By combining equations (2) and (4) the following expression for the dimensionless stress intensity coefficient emerges:

$$Y = [.5(\frac{1}{2a/W})\frac{d(CEB)}{d(2a/W)}]^{1/2} \quad (6)$$

This equation may then be compared to the polynomial expression of equation (3) by determining an equation representing the functional dependence of the non-dimensional compliance parameter (CEB) on the normalized crack length (2a/W).

To determine the relationship between the non-dimensional compliance parameter (CEB) and the normalized crack length (2a/W), an equation* is proposed of the form:

*this equation is taken from the Weibull survivorship function

$$(1 - 2a/W) = \exp(-(\frac{CEB - e}{v - e})^k) \tag{7}$$

Equation (7) may be rearranged in the following form:

$$[-\ln(1 - 2a/W)]^{1/k} = \frac{CEB}{v-e} - \frac{e}{v-e} \tag{8}$$

or:

$$y = bx + a \tag{9}$$

where,

$$y = [-\ln(1 - 2a/W)]^{1/k}$$

$$x = CEB$$

$$b = \frac{1}{v-e}$$

and

$$a = -\frac{e}{v-e}$$

A regression analysis of y on x using compliance data may be made by systemmatically guessing values of (1/k) in the form of equation (9). From this, values of e and v are determined thus giving an equation relating the non-dimensional compliance parameter (CEB) to the normalized crack length (2a/W). Values of the stress intensity coefficient (Y) may then be determined for corresponding normalized crack lengths

(2a/W) as given in equation (6).

As shown in equation (2), the value of the stress intensity coefficient (Y) as a function of normalized crack length (2a/W) is neccessary in converting crack growth data (a-N) to the more utilized form of crack growth rate data (da/dN-ΔK). Once the raw data (2a-N) is converted to the crack growth rate data (da/dN-ΔK), it is desireable to establish, in equation form, the functional dependence of the crack growth rate (da/dN) on the stress intensity range (ΔK). Many equations have been proposed [3] with the most popular being the one proposed by Paris:

$$da/dN = C(\Delta K)^n \tag{10}$$

It is readily seen that this equation forms a straight line on the normal log-log or log-linear plots of crack growth rate (da/dN) and stress intensity range (ΔK). Therefore equation (10) provides a curve fit that may define some middle segment of the actual data but may be totally inadequate in representing the threshold (slow crack growth) region where most of the fatigue life occurs.

Another equation is proposed which will more adequately represent the actual crack growth rate (da/dN)/stress intensity range (ΔK) data. The equation is similar to the one used for compliance in that it is also of the form of the Weibull survivorship function:

$$1 - \frac{\Delta K}{K_B} = \exp\left(-\left(\frac{da/dN - e}{v - e}\right)^k\right) \tag{11}$$

In equation (11), ΔK is the stress intensity range, K_B is a parameter which takes on the value of ΔK corresponding to unstable crack growth (i.e., $da/dN \rightarrow \infty$), da/dN is the crack growth rate, v is the Weibull characteristic value parameter, e is the Weibull threshold parameter, and k is the Weibull shaping parameter.

Equation (11) may be rearranged in the following form:

$$[-\ln(1 - \frac{\Delta K}{K_B})]^{1/k} = \frac{da/dN}{v-e} - \frac{e}{v-e} \qquad (12)$$

which is the same as the form of equation (9). In this application, by incrementing and optimizing the parameter (K_B) and the shaping parameter (k), linear regression analyses may be applied to find the threshold parameter (e) and the characteristic value parameter (v).

Data Analysis Techniques

Experiments were conducted to establish data sets containing normalized crack length (2a/W) and their corresponding non-dimensional compliance values (CEB) for the as received (a ferrite/pearlite structure) and martensitic microstructures of a .40/.50 carbon steel. These data are listed in Tables 1 and 2. Each of these data sets are seperately used in a computer program entitled "WBLCEB" to determine values of the shaping parameter (k), the threshold parameter (e), and the characteristic value parameter (v), as well as the sample correlation coefficient (R) given by:

TABLE 1

COMPLIANCE DATA FOR SPECIMEN 5-43

CEB	2a/W
1.5200	0.2520
1.5900	0.2840
1.7000	0.2970
1.7500	0.3380
1.7900	0.3680
1.9000	0.4000
1.7900	0.4220
1.9800	0.4480
1.9100	0.4650
2.0900	0.5120
2.5700	0.5550
2.5300	0.5730
2.8700	0.5860
2.4600	0.6010
2.8700	0.6180
2.6700	0.6430
2.9900	0.6830

TABLE 2

COMPLIANCE DATA FOR SPECIMEN 6-47

CEB	2a/W
1.5600	0.2040
1.7200	0.2210
1.5400	0.2420
1.5600	0.2720
1.6800	0.2900
1.5400	0.3120
1.6600	0.3400
1.8100	0.3600
1.9600	0.3840
1.9400	0.4150
1.9300	0.4290
1.9000	0.4420
2.1500	0.4660
2.1200	0.4760
2.1100	0.4880
2.0700	0.5050
2.1300	0.5190
2.1500	0.5340
2.2600	0.5520
2.2700	0.5720
2.5900	0.5930
2.4100	0.6160

$$R = \frac{n\Sigma xy - \Sigma x \Sigma y}{(((n\Sigma x^2 - (\Sigma x)^2) - (n\Sigma y^2 - (\Sigma y)^2))^{1/2})} \quad (13)$$

By systemmatically iterating values of the inverse of the shape parameter (1/k), a maximum value may be established for the sample correlation coefficient (R). Illustrations of the use of the program "WBLCEB" are given in Tables 3 and 4 for the as received and martensitic microstructures respectively.

The regression analysis results of the program "WBLCEB" are shown in Figure 4 for the as received microstructure and Figure 5 for the martensitic microstructure. These figures illustrate that 99.6 percent of the data points fall within a three sigma scatter band. The scatter in the vertical (y) direction about the regression line is the standard deviation as given by:

$$S = \frac{1}{n-1} \sum_{j=1}^{n} (y_j - \bar{y})^2 \quad (14)$$

More importantly, Figures 6 and 7 illustrate the manner in which this curve fitting technique exemplifies the actual data.

The curve fitting technique for the crack growth rate (da/dN-ΔK) data is similar to the compliance curve fit. However, an additional variable (K_B) defining the stress intensity range as the crack growth becomes unstable is introduced.

Before beginning the regression analysis and curve fit, the raw

TABLE 3

PROGRAM "WBLCEB" FOR SPECIMEN 5-43

```
LLW=W LOWER LIMIT, ULW=W UPPER LIMIT
:
1.2 1.3
        W                R
   1.20000        0.96073681
   1.21000        0.96074170
   1.22000        0.96074361
   1.23000        0.96073753
   1.24000        0.96073121
   1.25000        0.96072137
   1.26000        0.96072082
   1.27000        0.96069854
   1.28000        0.96067792
   1.29000        0.96065930
   1.30000        0.96066496

ENTER FLAG=1 IF BESTW FOUND, FLAG=0 IF NOT
:
1
SUPPLY BESTW
:
1.22

     BESTW             R
   1.22000        0.96074361

THE SLOPE  OF THE REGRESSION LINE M= 0.57517029
THE VERTICAL INTERCEPT B= -0.62382746
THE SAMPLE CORRELATION COEFFICIENT R=  0.96074361

THE SCATTER IN THE VERTICAL (Y) DIRECTION
OF THE OBSERVED POINTS ABOUT THE REGRESSION
LINE IS FOUND TO BE  0.08215035
THIS IS THE STANDARD DEVIATION AND
AT THIS VERTICAL DISTANCE ABOVE AND BELOW
THE REGRESSION LINE, TWO PARALLEL LINES
WILL INCLUDE 68.3% OF THE POINTS, AT TWICE
THIS DISTANCE, 95.4% OF THE POINTS ARE INCLUDED
AND AT THREE TIMES THIS DISTANCE 99.67
OF THE POINTS ARE INCLUDED WHICH IS
KNOWN AS A THREE SIGMA BAND

IF THE WEIBULL EQUATION IS EXPRESSED
AS P(X)=EXP(-((X-E)/(V-E))**K), AND
IN OUR CASE P(X)=(1-2A/N) AND
X=EBB/P=CEB THEN THE WEIBULL CRACK
GROWTH PARAMETERS K, E, V ARE

        K                E                V
 0.81967258       1.08241272       2.81858635

ENTER DOIT=1 IF CEB IS TO BE LISTED, DOIT=1 IF NOT
:

0
ENTER 1 IF RAW DATA IS TO BE LISTED , 0 IF NOT
:
1
```

2A/N	CEB	-LN(1-2A/N)**1/K	M*CEB+B
0.2520	1.5200	2.212E-01	2.520E-01
0.2880	1.5900	2.625E-01	2.924E-01
0.2970	1.7000	2.801E-01	3.557E-01
0.3330	1.7500	3.395E-01	3.886E-01
0.3680	1.7900	3.860E-01	4.076E-01
0.4000	1.9000	4.406E-01	4.709E-01
0.4220	1.7900	4.803E-01	4.076E-01
0.4480	1.9800	5.299E-01	5.170E-01
0.4650	1.9100	5.641E-01	4.767E-01
0.5120	2.0000	6.660E-01	5.203E-01
0.5550	2.5700	7.729E-01	8.368E-01
0.5730	2.5300	8.213E-01	8.128E-01
0.5860	2.8700	8.579E-01	1.038E+00
0.6010	2.4600	9.013E-01	7.935E-01
0.6130	2.8700	9.582E-01	1.038E+00
0.6430	2.6700	1.037E+00	9.148E-01
0.6630	2.9900	1.184E+00	1.099E+00

TABLE 4

PROGRAM "WBLCEB" FOR SPECIMEN 6-47

```
LLW=W LOWER LIMIT, ULW=W UPPER LIMIT
:
1.4 1.8
      W                R
  1.40000        0.97097647
  1.44000        0.97117788
  1.48000        0.97132638
  1.52000        0.97140311
  1.56000        0.97140956
  1.60000        0.97136439
  1.64000        0.97125119
  1.68000        0.97108442
  1.72000        0.97085029
  1.76000        0.97056657
  1.80000        0.97022563

ENTER FLAG=1 IF BESTW FOUND, FLAG=0 IF NOT
:
1
SUPPLY BESTW
:
1.56

    BESTW            R
  1.56000        0.97140956

THE SLOPE  OF THE REGRESSION LINE M= 0.80506569
THE VERTICAL INTERCEPT B= -1.13520432
THE SAMPLE CORRELATION COEFFICIENT R=  0.97140956

THE SCATTER IN THE VERTICAL (Y) DIRECTION
OF THE OBSERVED POINTS ABOUT THE REGRESSION
LINE IS FOUND TO BE:  0.07365801
THIS IS THE STANDARD DEVIATION AND
AT THIS VERTICAL DISTANCE ABOVE AND BELOW
THE REGRESSION LINE, TWO PARALLEL LINES
WILL INCLUDE 68.3% OF THE POINTS. AT THIS
THIS DISTANCE, 95.4% OF THE POINTS ARE INCLUDED
AND AT THREE TIMES THIS DISTANCE 99.6%
OF THE POINTS ARE INCLUDED WHICH IS
KNOWN AS A THREE SIGMA BAND

IF THE WEIBULL EQUATION IS EXPRESSED
AS P(X)=EXP(-((X-E)/(V-E))**K), AND
IN OUR CASE P(X)=(1-2A/W) AND
X=BBD/P=CEB THEN THE WEIBULL CRACK
GROWTH PARAMETERS K, E, V ARE

       K                E                V
 0.64102584       1.41007614       2.65221119


ENTER DOIT=1 IF CEB IS TO BE LISTED, DOIT=0 IF NOT
:
0
ENTER 1 IF RAW DATA IS TO BE LISTED , 0 IF NOT
:
1
```

2A/W	CEB	-LN(1-2A/W)**1/K	M*CEB+B
0.2040	1.5600	9.973E-02	1.207E-01
0.2210	1.7200	1.148E-01	2.485E-01
0.2420	1.5400	1.350E-01	1.006E-01
0.2720	1.5600	1.670E-01	1.207E-01
0.2900	1.6800	1.880E-01	2.173E-01
0.3120	1.5400	2.156E-01	1.006E-01
0.3400	1.6600	2.541E-01	2.012E-01
0.3600	1.8100	2.881E-01	3.220E-01
0.3840	1.9600	3.229E-01	4.827E-01
0.4150	1.9400	3.782E-01	4.266E-01
0.4290	1.9300	4.052E-01	4.186E-01
0.4420	1.9000	4.314E-01	3.944E-01
0.4660	2.1500	4.832E-01	5.957E-01
0.4760	2.1200	5.061E-01	5.715E-01
0.4880	2.1100	5.347E-01	5.635E-01
0.5050	2.0700	5.778E-01	5.313E-01
0.5100	2.1300	6.145E-01	5.796E-01
0.5340	2.1500	6.565E-01	5.957E-01
0.5520	2.2600	7.101E-01	6.842E-01
0.5720	2.2700	7.741E-01	6.923E-01
0.5930	2.5900	8.469E-01	9.499E-01
0.6160	2.8100	9.339E-01	8.059E-01
0.6440	2.6100	1.052E+00	9.660E-01

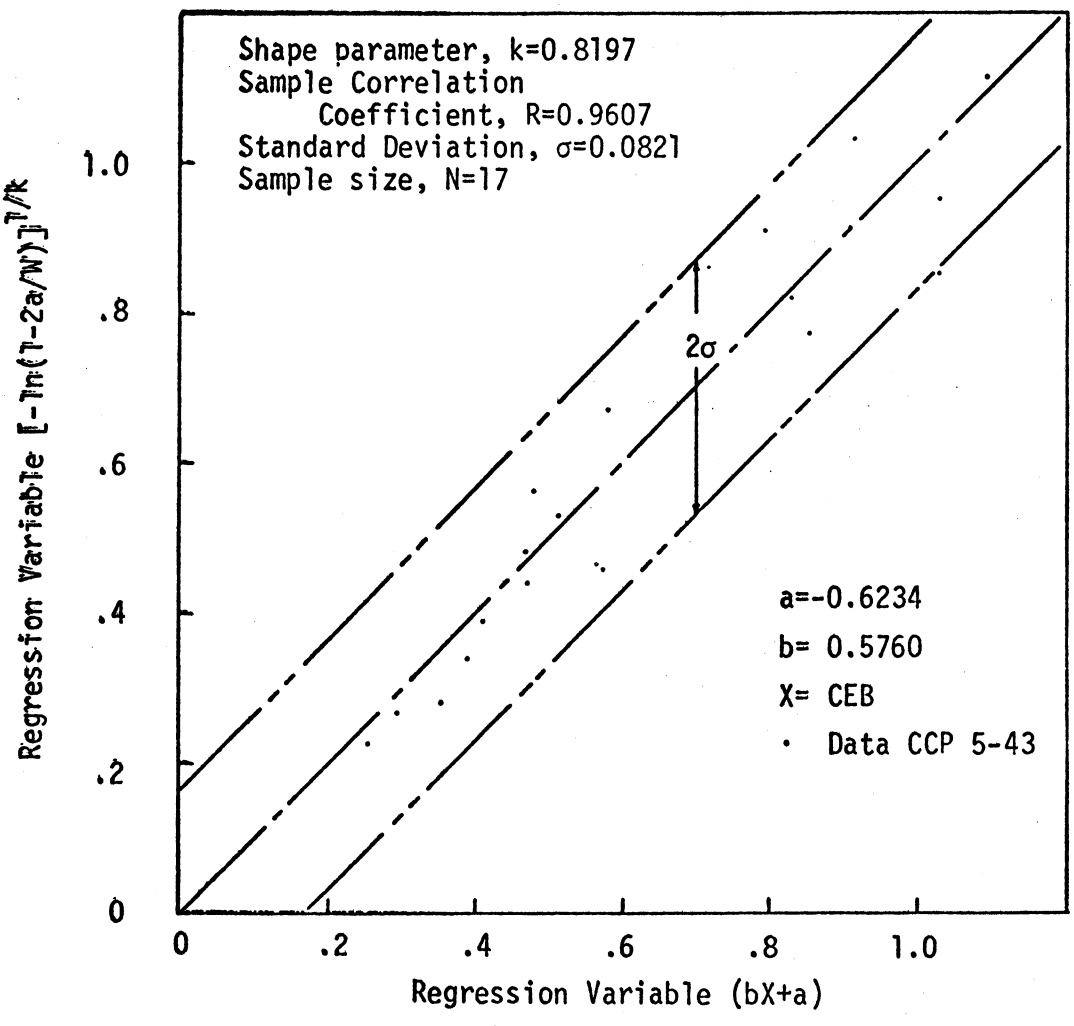

Figure 4. Linear regression of compliance data for specimen 5-43.

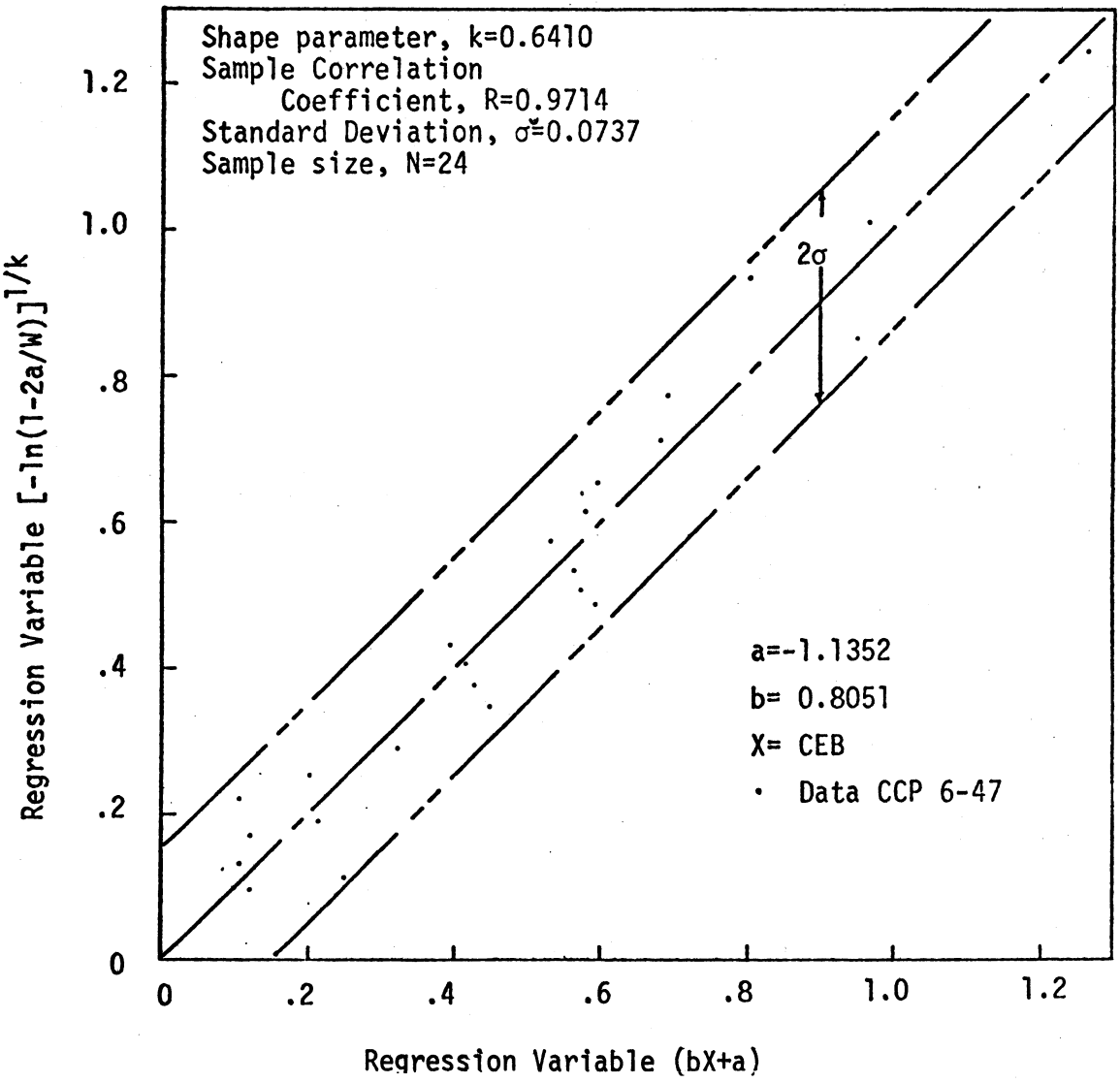

Figure 5. Linear regression of compliance data for specimen 6-47.

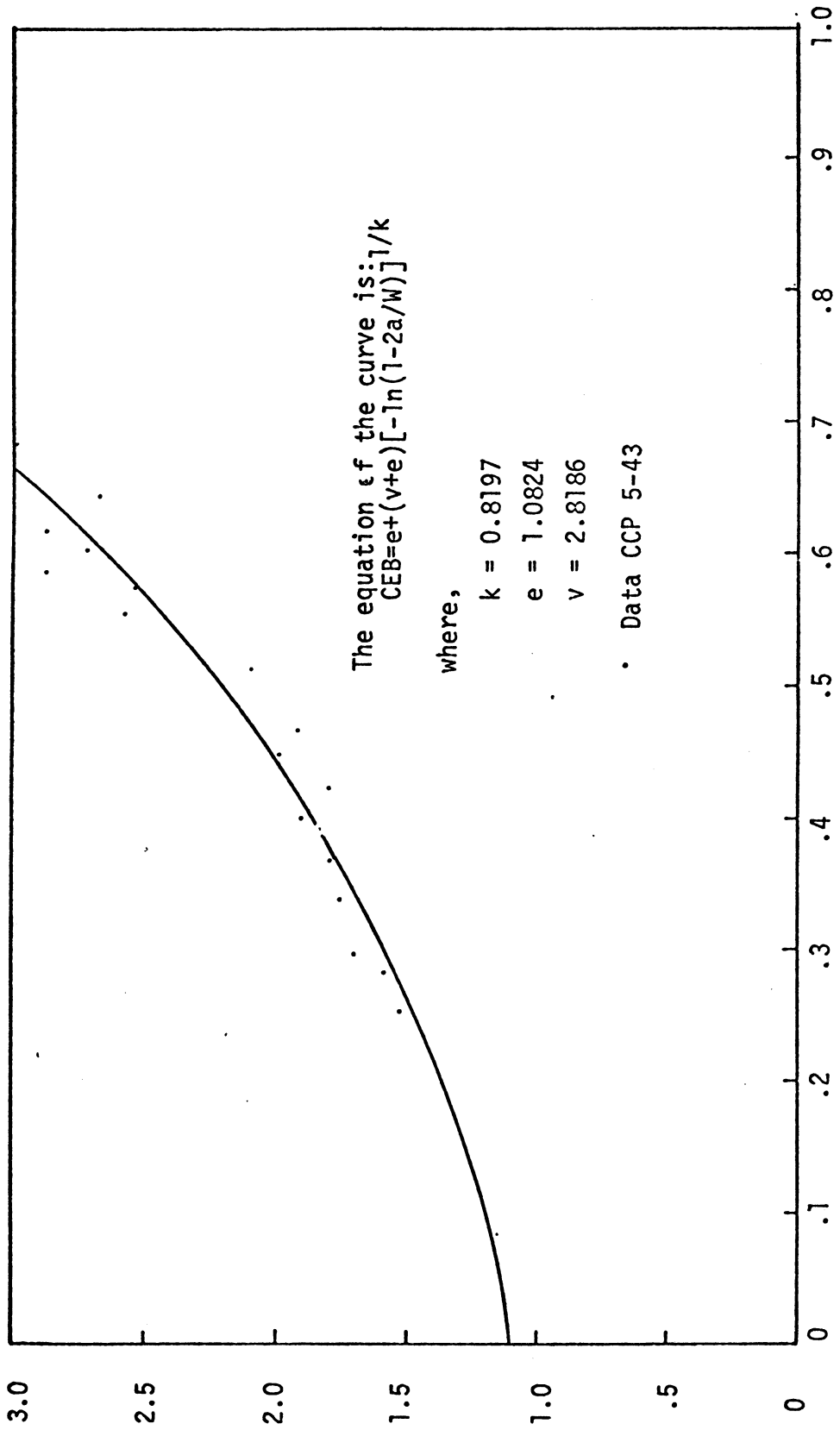

Figure 6. Relationship of data points to the proposed equation relating non-dimensional compliance to normalized crack length for specimen 5-43.

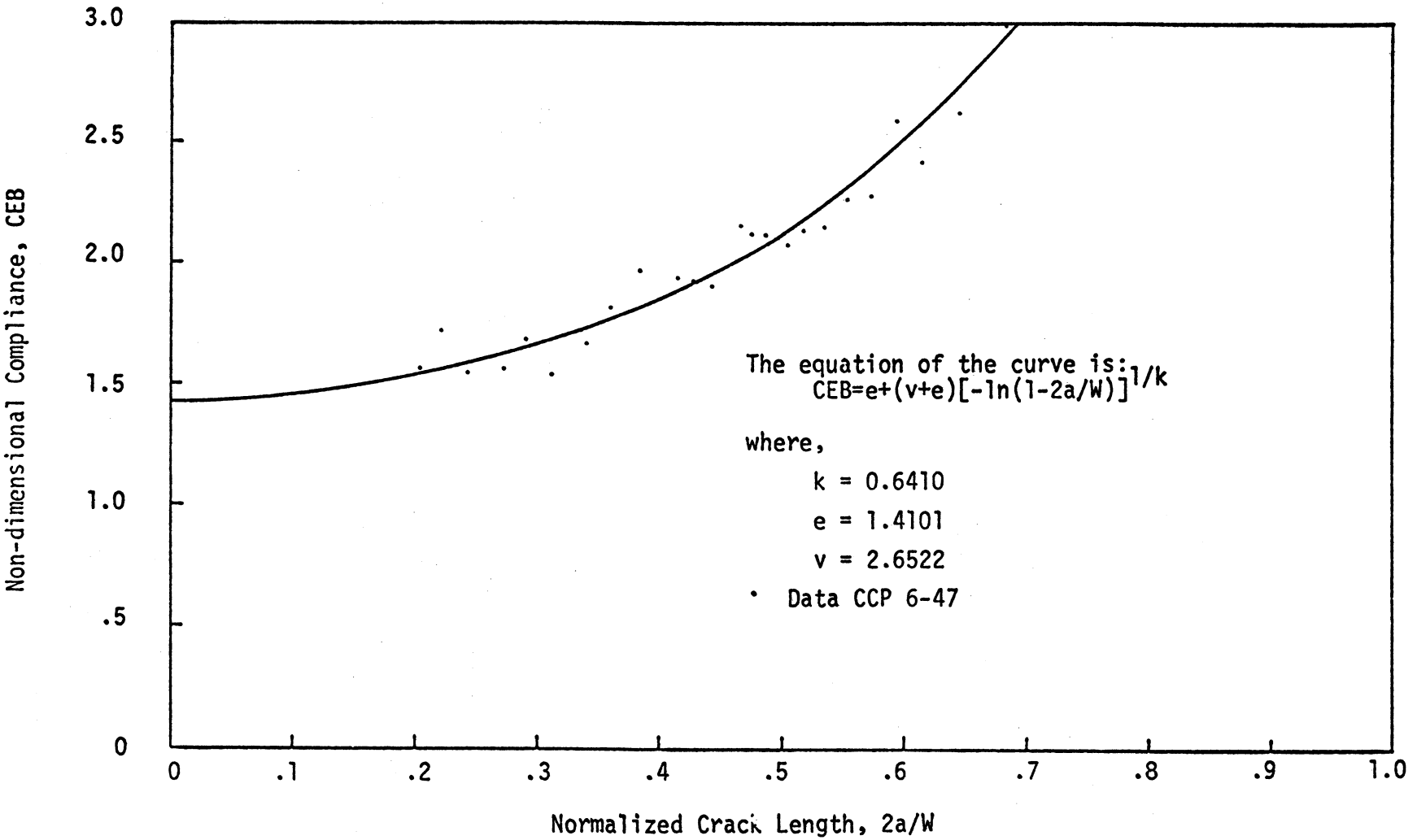

Figure 7. Relationship of data points to the proposed equation relating non-dimensional compliance to normalized crack length for specimen 6-47.

data (2a-N) must be converted to data consisting of crack growth rate (da/dN) and stress intensity range (ΔK). The values of stress intensity range are calculated using equation (2), where the values of the stress intensity coefficient (Y) are determined from the compliance data for the given material and microstructure. The raw data (2a-N) is given in Tables 5 and 6 for the as received and martensitic microstructures respectively. The corresponding graphs of these data are given in Figures 2 and 3. Illustrations of the conversion of the raw data to the crack growth rate data as performed in the program "CCPANK" are given in Tables 7 and 8.

The regression analysis results of the program "WANKHS" are shown in Figure 8 for the as received microstructure and Figure 9 for the martensitic microstructure. This analysis not only iterates on the inverse of the shaping parameter (1/k) to find the maximum value of the sample correlation coefficient, R, as given in equation (13), but also includes an optimization process by which the best value of the stress intensity range at unstable crack growth (K_B) may be found. After this point is reached, the regression analysis is carried out exactly as it was for the compliance data.

The crack growth rate data obtained from the program "CCPANK", and the values of the four Weibull parameters, obtained from the regression analysis, are used to determine the equation of a curve which will fit the crack growth rate data as given in equation (12). This

TABLE 5

CRACK GROWTH DATA FOR SPECIMEN 5-46

N*	2a**	N	2a	N	2a	N	2a
0	226	197.5	395	258.5	537	279.5	631
10	230	200	399	259	540	280	636
20	234	202.5	405	259.5	541	280.5	639
30	238	205	409	260	543	281	643
40	242	207.5	412	260.5	546	281.5	647
50	251	210	418	261	548	282	650
60	256	212.5	421	261.5	551	282.5	653
65	259	215	429	262.5	552	283	656
70	262	217	431	263	553	283.5	660
75	265	219	436	263.5	555	284	664
80	272	221	439	264	557	284.5	668
85	276	223	444	264.5	559	285	674
90	277	225	449	265	561	285.5	677
95	281	227	451	265.5	563	286	683
100	285	229	459	266	564	286.5	687
105	290	231	462	266.5	568	287	694
110	293	233	468	267	569	287.5	699
115	298	234	471	267.5	571	288	705
120	301	236	473	268	573	288.5	709
125	307	237.5	477	268.5	575	289	713
130	314	239	482	269	576	289.5	721
135	321	240.5	484	269.5	579	290	727
140	323	242	487	270	581	290.5	737
145	330	243.5	494	270.5	582	291	746
150	338	244.5	496	271.5	583	291.5	752
155	340	245.5	499	272	589	292	832
160	347	246.5	501	272.5	590		
165	352	247.5	505	273	593		
167.5	355	248.5	507	273.5	595		
170	359	249.5	510	274	599		
172.5	361	250.5	511	274.5	602		
175	365	251.5	516	275	604		
177.5	369	252.5	517	275.5	606		
180	370	253.5	521	276	611		
182.5	373	254.5	524	276.5	615		
185	376	255.5	527	277	616		
187.5	381	256.5	533	277.5	618		
190	383	257	534	278	622		
192.5	389	257.5	535	278.5	626		
195	393	258	536	279	627		

*Number of kilocycles.
**Crack length in milli inches.

TABLE 6

CRACK GROWTH DATA FOR SPECIMEN 6-49

N*	2a**	N	2a	N	2a	N	2a
0	226	65	340	111	462	136	588
5	231	66	341	113	463	136.5	590
10	239	69	345	114	470	137	595
12.5	244	70	348	115	475	137.5	601
15	246	71	350	116	482	138	603
17.5	251	72	351	117	487	138.5	608
20	256	73	354	117.5	489	139	612
21	259	75	360	118	492	139.5	615
23	261	77	361	119	495	140	621
24	264	78	362	119.5	497	140.5	624
26	266	79	363	120.5	499	141	628
27	267	80	364	121	501	141.5	634
28	268	81	365	121.5	504	142	641
31	270	82	367	122	507	142.5	644
32	276	84	382	122.5	510	143	649
33	278	85	384	123	512	143.5	654
36	283	86	385	123.5	516	144	660
37	284	87	391	124	519	144.5	665
38	286	88	393	124.5	521	145	667
39	287	89	394	125	522	145.5	676
41	290	90	396	125.5	524	146	682
42	292	91	401	126	528	146.5	691
44	294	92	405	126.5	529	147	696
45	295	93	407	127	533	147.5	701
46	297	94	410	127.5	536	148	710
47	300	95	413	128	537	148.5	717
48	302	96	414	128.5	541	149	726
50	304	97	420	129	542	149.5	735
51	308	98	422	130	548	150	745
52	309	99	424	130.5	552	150.5	754
54	313	101	428	131	556	151	767
55	314	102	431	131.5	560	151.5	785
56	315	103	435	132	563	152	808
58	316	104	436	132.5	565		
59	317	105	438	133	568		
60	328	106	443	133.5	574		
61	329	107	448	134	576		
62	330	108	452	134.5	577		
63	331	109	455	135	580		
64	332	110	458	135.5	586		

*Number of kilocycles.
**Crack length in milli inches.

TABLE 7

PROGRAM "CCPANK" FOR SPECIMEN 5-46

```
SUPPLY WEIBULL PARAMETERS K, E, V FROM CEB VS. 2A/W
?
.81967256 1.08241372 2.81658635
SUPPLY SUB-INITIAL CRACK LENGTH, 2A IN INCHES
?
.226

Y1 IS CALCULATED FROM POLYNOMIAL PARAMETERS
DK1 IS CALCULATED WITH Y1
Y2 IS CALCULATED FROM WEIBULL PARAMETERS
DK2 IS CALCULATED WITH Y2
```

I	2A (MILS)	DA	N (KILOCYCLES)	DN (KILOCYCLES)	DA/DN (IN/CYCLE)	DK1 (PSI $\sqrt{IN.}$)	Y1	DK2 (PSI $\sqrt{IN.}$)	Y2
1	226	4	0.00	10.00	4.00E-07	14266.190	1.821	16080.695	2.180
2	230	4	10.00	10.00	4.00E-07	14421.960	1.823	16234.759	2.139
3	234	4	20.00	10.00	4.00E-07	14555.250	1.824	17300.916	2.131
4	238	4	30.00	10.00	4.00E-07	14680.088	1.826	17076.891	2.122
5	242	9	40.00	10.00	9.00E-07	14800.955	1.829	17209.338	2.105
6	251	5	50.00	10.00	5.00E-07	15153.227	1.831	17383.582	2.096
7	256	3	60.00	5.00	6.00E-07	15252.027	1.832	17490.852	2.090
8	259	3	65.00	5.00	6.00E-07	15351.621	1.834	17458.191	2.085
9	262	3	70.00	5.01	6.00E-07	15449.023	1.835	17515.570	2.080
10	265	7	75.00	5.00	1.40E-06	15677.938	1.838	17689.709	2.069
11	272	4	80.00	5.00	8.00E-07	15888.371	1.840	17726.672	2.063
12	276	1	85.00	5.00	2.00E-07	15980.961	1.840	17705.910	2.062
13	277	4	90.00	5.00	8.00E-07	15971.102	1.842	17823.008	2.056
14	281	4	95.00	5.00	8.00E-07	16161.055	1.844	17900.281	2.050
15	285	5	100.00	5.00	1.00E-06	16263.262	1.846	17997.152	2.043
16	290	3	105.00	5.00	6.00E-07	16361.492	1.848	18055.418	2.039
17	293	5	110.00	5.00	1.00E-06	16522.418	1.851	18152.828	2.033
18	298	3	115.00	5.00	6.00E-07	16619.896	1.852	18211.820	2.030
19	301	6	120.00	5.00	1.20E-06	16813.617	1.855	18320.074	2.023
20	307	7	125.00	5.00	1.40E-06	17040.067	1.859	18467.070	2.015
21	314	7	130.00	5.00	1.40E-06	17266.699	1.863	18605.938	2.008
22	321	2	135.00	5.00	4.00E-07	17321.391	1.864	18665.766	2.006
23	323	7	140.00	5.00	1.40E-06	17550.320	1.868	18785.832	1.999
24	330	8	145.00	5.00	1.60E-06	17818.203	1.872	18987.137	1.993
25	338	2	150.00	5.00	4.00E-07	17803.293	1.873	18987.691	1.991
26	340	7	155.00	5.00	1.40E-06	18111.527	1.878	19130.320	1.986
27	347	5	160.00	5.00	1.00E-06	18275.027	1.881	19232.992	1.982
28	352	3	165.00	2.50	1.20E-06	18373.352	1.885	19298.782	1.980
29	355	8	167.50	2.50	1.60E-06	18508.691	1.888	19377.562	1.977
30	359	2	170.00	2.50	8.00E-07	18579.809	1.890	19410.199	1.976
31	361	8	172.50	2.50	1.60E-06	18702.332	1.893	19502.793	1.974
32	365	8	175.00	2.50	1.60E-06	18834.551	1.896	19586.422	1.971
33	369	1	177.50	2.50	4.00E-07	18867.656	1.896	19607.889	1.971
34	370	3	180.00	2.50	1.20E-06	18962.160	1.899	19674.738	1.969
35	373	3	182.50	2.50	1.20E-06	19056.879	1.901	19738.262	1.968
36	376	5	185.00	2.50	2.00E-06	19233.633	1.905	19849.738	1.965
37	381	2	187.50	2.50	8.00E-07	19309.582	1.907	19883.523	1.964
38	383	6	190.00	2.50	2.40E-06	19511.965	1.912	20012.652	1.962
39	389	4	192.50	2.50	1.60E-06	19636.895	1.915	20099.371	1.960
40	393	2	195.00	2.50	8.00E-07	19708.551	1.917	20142.926	1.960
41	395	4	197.50	2.50	1.60E-06	19840.359	1.920	20230.813	1.958
42	399	6	200.00	2.50	2.40E-06	20048.477	1.926	20362.668	1.956
43	405	4	202.50	2.50	1.60E-06	20182.188	1.929	20451.520	1.955
44	409	3	205.00	2.50	1.20E-06	20285.709	1.932	20518.516	1.954
45	412	6	207.50	2.50	2.40E-06	20493.258	1.938	20653.527	1.952
46	418	3	210.00	2.50	1.20E-06	20597.699	1.941	20721.527	1.951
47	421	8	212.50	2.50	3.20E-06	20878.148	1.949	20904.543	1.951
48	429	2	215.00	2.00	1.00E-06	20982.762	1.951	21050.688	1.951
49	431	5	217.00	2.00	2.50E-06	21126.059	1.956	21067.762	1.951

TABLE 7 (cont.)

50	436	3	219.00	2.00	1.50E-06	21233.027	1.959	21136.805	1.950
51	439	5	221.00	2.00	2.50E-06	21412.313	1.965	21258.625	1.950
52	444	5	223.00	2.00	2.50E-06	21592.918	1.971	21373.830	1.950
53	449	2	225.00	2.00	1.00E-06	21665.516	1.972	21421.282	1.950
54	451	8	227.00	2.00	4.00E-06	21958.191	1.982	21618.348	1.951
55	459	3	229.00	2.00	1.50E-06	22068.902	1.985	21687.523	1.951
56	462	6	231.00	2.00	3.00E-06	22291.691	1.992	21835.152	1.951
57	468	3	233.00	1.50	2.00E-06	22404.191	1.996	21909.617	1.952
58	471	2	234.50	1.50	1.33E-06	22479.395	1.999	21959.508	1.952
59	473	4	236.00	1.50	2.67E-06	22630.512	2.003	22059.883	1.953
60	477	5	237.50	1.50	3.33E-06	22830.883	2.010	22186.512	1.954
61	482	2	239.00	1.50	1.33E-06	22907.873	2.012	22237.527	1.954
62	484	3	240.50	1.50	2.00E-06	23012.301	2.016	22318.438	1.955
63	487	7	242.00	1.50	4.67E-06	23228.578	2.020	22405.801	1.957
64	494	2	243.50	1.00	2.00E-06	23362.336	2.029	22582.121	1.957
65	496	3	244.50	1.00	3.00E-06	23581.738	2.032	22627.000	1.958
66	499	2	245.50	1.00	2.00E-06	23650.719	2.035	22670.879	1.959
67	501	4	246.50	1.00	4.00E-06	23718.535	2.041	22786.328	1.960
68	505	2	247.50	1.00	2.00E-06	23798.375	2.043	22839.914	1.961
69	507	3	248.50	1.00	3.00E-06	23917.782	2.048	22920.727	1.962
70	510	1	249.50	1.00	1.00E-06	23950.309	2.049	22987.777	1.963
71	511	5	250.50	1.00	5.00E-06	24161.508	2.057	23083.077	1.965
72	516	1	251.50	1.00	1.00E-06	24202.223	2.059	23111.818	1.965
73	517	4	252.50	1.00	4.00E-06	24365.973	2.068	23221.738	1.967
74	521	3	253.50	1.00	3.00E-06	24484.598	2.068	23305.152	1.968
75	524	3	254.50	1.00	3.00E-06	24613.961	2.073	23380.148	1.970
76	527	6	255.50	1.00	6.00E-06	24866.949	2.082	23558.934	1.973
77	533	1	256.50	0.50	2.00E-06	24907.978	2.084	23587.465	1.973
78	534	1	257.00	0.50	2.00E-06	24940.277	2.086	23616.079	1.974
79	535	1	257.50	0.50	2.00E-06	24991.582	2.087	23654.738	1.975
80	536	1	258.00	0.50	2.00E-06	25033.953	2.089	23673.473	1.975
81	537	3	258.50	0.50	6.00E-06	25161.699	2.093	23760.105	1.977
82	540	1	259.00	0.50	2.00E-06	25208.340	2.095	23780.125	1.977
83	541	2	259.50	0.50	4.00E-06	25290.059	2.098	23847.379	1.979
84	543	3	260.00	0.50	6.00E-06	25410.305	2.103	23935.285	1.980
85	546	2	260.50	0.50	4.00E-06	25505.895	2.107	23994.250	1.982
86	548	3	261.00	0.50	6.00E-06	25636.496	2.112	24083.258	1.984
87	551	1	261.50	1.00	1.00E-06	25660.207	2.113	24112.986	1.984
88	552	1	262.50	0.50	2.00E-06	25728.304	2.115	24142.961	1.985
89	553	2	263.00	0.50	4.00E-06	25811.887	2.118	24202.960	1.986
90	555	2	263.50	0.50	4.00E-06	25900.185	2.122	24263.259	1.988
91	557	2	264.00	0.50	4.00E-06	25985.770	2.125	24323.902	1.989
92	559	2	264.50	0.50	4.00E-06	26077.781	2.129	24384.848	1.991
93	561	2	265.00	0.50	4.00E-06	26167.152	2.132	24445.082	1.992
94	563	1	265.50	0.50	2.00E-06	26212.504	2.134	24476.828	1.993
95	564	4	266.00	0.50	8.00E-06	26302.301	2.141	24600.609	1.996
96	568	1	266.50	0.50	2.00E-06	26437.633	2.143	24631.738	1.996
97	569	2	267.00	0.50	4.00E-06	26528.559	2.146	24694.285	1.998
98	571	2	267.50	0.50	4.00E-06	26619.895	2.150	24757.152	2.000
99	573	2	268.00	0.50	4.00E-06	26711.695	2.154	24820.355	2.001
100	575	1	268.50	0.50	2.00E-06	26757.695	2.156	24852.086	2.002
101	576	3	269.00	0.50	6.00E-06	26896.281	2.161	24947.781	2.005
102	579	2	269.50	0.50	4.00E-06	26989.207	2.165	25012.008	2.006
103	581	1	270.00	0.50	2.00E-06	27035.699	2.167	25044.250	2.007
104	582	1	270.50	1.00	1.00E-06	27082.270	2.169	25076.602	2.008
105	583	6	271.50	0.50	1.20E-05	27365.117	2.180	25272.977	2.013
106	589	1	272.00	0.50	2.00E-06	27412.578	2.182	25305.438	2.014
107	590	3	272.50	0.50	6.00E-06	27555.535	2.188	25405.883	2.017
108	593	2	273.00	0.50	4.00E-06	27651.938	2.192	25471.641	2.019
109	595	4	273.50	0.50	8.00E-06	27848.461	2.200	25606.313	2.023
110	599	3	274.00	0.50	6.00E-06	27990.496	2.206	25705.328	2.025
111	602	2	274.50	0.50	4.00E-06	28088.223	2.210	25773.809	2.028
112	604	2	275.00	0.50	4.00E-06	28186.559	2.214	25842.703	2.030
113	606	5	275.50	0.50	1.00E-05	28536.188	2.228	26081.691	2.035
114	611	4	276.00	0.50	8.00E-06	28634.328	2.232	26150.762	2.040

TABLE 7 (cont.)

115	615	1	276.50	0.50	2.00E-06	28698.688	2.235	26196.270	2.041
116	616	2	277.00	0.50	4.00E-06	28795.656	2.239	26267.668	2.043
117	618	4	277.50	0.50	8.00E-06	28980.078	2.247	26411.691	2.048
118	622	4	278.00	0.50	8.00E-06	29178.359	2.256	26557.484	2.052
119	626	1	278.50	0.50	2.00E-06	29285.973	2.258	26594.215	2.053
120	627	4	279.00	0.50	8.00E-06	29853.656	2.267	26742.270	2.058
121	631	5	279.50	0.50	1.00E-05	29715.000	2.279	26920.953	2.065
122	636	3	280.00	0.50	6.00E-06	29974.875	2.285	27043.988	2.068
123	639	4	280.50	0.50	8.00E-06	30068.461	2.294	27107.746	2.070
124	643	4	281.00	0.50	8.00E-06	30308.047	2.303	27353.873	2.079
125	647	3	281.50	0.50	6.00E-06	30467.078	2.310	27471.617	2.083
126	650	3	282.00	0.50	6.00E-06	30631.250	2.316	27590.938	2.088
127	653	3	282.50	0.50	6.00E-06	30796.605	2.325	27711.441	2.092
128	656	4	283.00	0.50	8.00E-06	31018.898	2.338	27873.094	2.098
129	660	4	283.50	0.50	8.00E-06	31243.328	2.348	28032.750	2.105
130	664	4	284.00	0.50	8.00E-06	31469.902	2.358	28205.781	2.110
131	668	6	284.50	0.50	1.20E-05	31813.516	2.369	28460.672	2.120
132	674	3	285.00	0.50	6.00E-06	31987.613	2.377	28589.156	2.124
133	677	6	285.50	0.50	1.20E-05	32338.996	2.392	28853.273	2.135
134	683	4	286.00	0.50	8.00E-06	32576.098	2.403	29031.871	2.142
135	687	7	286.50	0.50	1.40E-05	32896.492	2.422	29359.758	2.158
136	694	5	287.00	0.50	1.00E-05	33301.133	2.435	29583.684	2.163
137	699	6	287.50	0.50	1.20E-05	33671.582	2.452	29869.035	2.175
138	705	4	288.00	0.50	8.00E-06	33921.543	2.463	30062.965	2.183
139	709	4	288.50	0.50	8.00E-06	34173.918	2.474	30259.918	2.191
140	713	8	289.00	0.50	1.60E-05	34686.059	2.498	30663.332	2.208
141	721	6	289.50	0.50	1.20E-05	35071.711	2.515	30974.500	2.221
142	727	10	290.00	0.50	2.00E-05	35780.535	2.545	31519.625	2.244
143	737	9	290.50	0.50	1.80E-05	36351.063	2.573	32012.938	2.266
144	746	6	291.00	0.50	1.20E-05	36766.887	2.592	32368.902	2.281
145	752	80	291.50	0.50	1.60E-04	42915.199	2.877	38086.598	2.553

TABLE 8

PROGRAM "CCPANK" FOR SPECIMEN 6-49

```
SUPPLY WEIBULL PARAMETERS K, E, V FROM CID VS. 2A/W
?
.68102584 1.41007614 2.65221119
SUPPLY SUB-INITIAL CRACK LENGTH, 2A I' INCHES
?
.226

Y1 IS CALCULATED FROM POLYNOMIAL PARAMETERS
DK1 IS CALCULATED WITH Y1
Y2 IS CALCULATED FROM WEIBULL PARAMETERS
DK2 IS CALCULATED WITH Y2
```

I	2A (MILS)	DA	N (KILOCYCLES)	DN	DA/DN (IN/CYCLE)	DK1 (PSI RT.IN.)	Y1	DK2 (PSI RT.IN.)	Y2
1	226	5	0.00	5.00	1.00E-06	15656.873	1.830	13763.880	1.607
2	231	8	5.00	5.00	1.60E-06	15852.829	1.831	13936.806	1.605
3	239	5	10.00	2.50	2.00E-06	16130.281	1.833	14135.922	1.604
4	244	2	12.50	2.50	8.00E-07	16213.270	1.834	14151.719	1.604
5	246	5	15.00	2.50	2.00E-06	16307.936	1.836	14331.295	1.604
6	251	5	17.50	2.50	2.00E-06	16591.828	1.839	14860.992	1.604
7	256	3	20.00	1.00	3.00E-06	16692.908	1.840	14858.910	1.603
8	259	2	21.00	2.00	1.00E-06	16765.367	1.841	14999.906	1.603
9	261	3	23.00	1.00	3.00E-06	16875.277	1.842	14998.959	1.604
10	264	2	24.00	2.00	1.00E-06	16982.508	1.844	15191.051	1.604
11	266	1	26.00	1.00	1.00E-06	16985.062	1.844	15209.195	1.604
12	267	1	27.00	1.00	1.00E-06	17021.660	1.845	15207.195	1.604
13	268	2	28.00	3.00	6.67E-07	17008.773	1.846	15053.367	1.604
14	270	6	31.00	1.00	6.00E-06	17313.875	1.849	15422.238	1.604
15	276	2	32.00	1.00	2.00E-06	17366.963	1.850	15478.625	1.605
16	278	5	33.00	3.00	1.67E-06	17560.199	1.853	15210.996	1.605
17	283	1	36.00	1.00	1.00E-06	17685.656	1.854	15282.219	1.605
18	284	2	37.00	1.00	2.00E-06	17672.566	1.855	15308.883	1.606
19	286	1	38.00	1.00	1.00E-06	17713.923	1.855	15303.236	1.606
20	287	3	39.00	2.00	1.50E-06	17824.371	1.857	15410.812	1.606
21	290	2	41.00	1.00	2.00E-06	17897.270	1.858	15475.301	1.607
22	292	2	42.00	2.00	1.00E-06	17970.188	1.859	15532.279	1.607
23	294	1	44.00	1.00	1.00E-06	18000.648	1.860	15560.755	1.607
24	295	2	45.00	1.00	2.00E-06	18079.582	1.861	15617.875	1.608
25	297	3	46.00	1.00	3.00E-06	18180.908	1.863	15703.660	1.608
26	300	2	47.00	1.00	2.00E-06	18262.912	1.864	15760.965	1.609
27	302	2	48.00	2.00	1.00E-06	18335.031	1.866	15818.367	1.610
28	304	4	50.00	1.00	4.00E-06	18481.176	1.868	15933.445	1.611
29	308	1	51.00	1.00	1.00E-06	18517.727	1.869	15962.270	1.611
30	309	4	52.00	2.00	2.00E-06	18664.996	1.872	16077.988	1.612
31	313	1	54.00	1.00	1.00E-06	18700.797	1.872	16106.809	1.613
32	314	1	55.00	1.00	1.00E-06	18737.348	1.873	16135.793	1.613
33	315	1	56.00	2.00	5.00E-07	18778.004	1.874	16148.813	1.613
34	316	1	58.00	1.00	1.00E-06	18818.660	1.874	16133.883	1.610
35	317	11	59.00	1.00	1.10E-05	19215.996	1.882	16515.176	1.613
36	328	1	60.00	1.00	1.00E-06	19251.977	1.883	16548.555	1.613
37	329	1	61.00	1.00	1.00E-06	19288.879	1.884	16573.992	1.613
38	330	1	62.00	1.00	1.00E-06	19325.301	1.885	16603.883	1.613
39	331	1	63.00	1.00	1.00E-06	19362.785	1.885	16632.918	1.613
40	332	8	64.00	1.00	8.00E-06	19650.199	1.892	16868.988	1.623
41	340	1	65.00	1.00	1.00E-06	19686.375	1.892	16899.762	1.624
42	341	4	66.00	3.00	1.33E-06	19885.332	1.896	17010.258	1.626
43	345	3	69.00	1.00	3.00E-06	19957.359	1.898	17159.246	1.627
44	348	2	70.00	1.00	2.00E-06	20032.297	1.900	17162.922	1.628
45	350	1	71.00	1.00	1.00E-06	20068.672	1.901	17199.566	1.629
46	351	3	72.00	1.00	3.00E-06	20182.273	1.903	17299.238	1.630
47	354	6	73.00	2.00	3.00E-06	20402.992	1.908	17472.621	1.634
48	360	1	75.00	2.00	5.00E-07	20446.215	1.909	17503.172	1.634
49	361	1	77.00	1.00	1.00E-06	20658.363	1.910	17533.738	1.635
50	362	1	78.00	1.00	1.00E-06	20521.961	1.911	17564.363	1.636

TABLE 8 (cont.)

51	363	1	79.00	1.00	1.00E-06	20550.879	1.912	17505.021	1.636
52	364	1	80.00	1.00	1.00E-06	20597.898	1.913	17625.719	1.637
53	365	2	81.00	1.00	2.00E-06	20673.287	1.915	17607.252	1.638
54	367	15	82.00	2.00	7.50E-06	21280.635	1.929	18158.806	1.689
55	382	2	84.00	1.00	2.00E-06	21327.169	1.931	18217.899	1.689
56	384	1	85.00	1.00	1.00E-06	21355.930	1.932	18250.986	1.690
57	385	6	86.00	1.00	6.00E-06	21600.966	1.938	18539.777	1.695
58	391	2	87.00	1.00	2.00E-06	21670.512	1.940	18503.739	1.696
59	393	1	88.00	1.00	1.00E-06	21717.791	1.941	18535.797	1.697
60	394	2	89.00	1.00	2.00E-06	21796.555	1.943	18600.066	1.698
61	396	5	90.00	1.00	5.00E-06	21988.375	1.948	18761.676	1.662
62	401	4	91.00	1.00	4.00E-06	22153.656	1.953	18901.930	1.666
63	405	2	92.00	1.00	2.00E-06	22233.633	1.955	18967.383	1.667
64	407	3	93.00	1.00	3.00E-06	22358.961	1.958	19065.996	1.670
65	410	3	94.00	1.00	3.00E-06	22475.016	1.962	19175.125	1.672
66	413	1	95.00	1.00	1.00E-06	22515.453	1.963	19199.285	1.673
67	414	6	96.00	1.00	6.00E-06	22759.453	1.970	19398.408	1.679
68	420	2	97.00	1.00	2.00E-06	22841.203	1.973	19455.793	1.680
69	422	2	98.00	1.00	2.00E-06	22923.410	1.975	19523.160	1.682
70	424	4	99.00	2.00	2.00E-06	23038.645	1.980	19658.836	1.686
71	428	3	101.00	1.00	3.00E-06	23212.961	1.984	19761.273	1.689
72	431	4	102.00	1.00	4.00E-06	23378.938	1.989	19899.750	1.693
73	435	1	103.00	1.00	1.00E-06	23421.363	1.990	19933.289	1.694
74	436	2	104.00	1.00	2.00E-06	23505.938	1.993	20002.551	1.696
75	438	5	105.00	1.00	5.00E-06	23717.398	1.998	20176.949	1.701
76	443	5	106.00	1.00	5.00E-06	23930.785	2.006	20353.094	1.706
77	448	4	107.00	1.00	4.00E-06	24112.035	2.011	20505.293	1.710
78	452	3	108.00	1.00	3.00E-06	24232.691	2.014	20602.711	1.714
79	455	3	109.00	1.00	3.00E-06	24353.965	2.020	20710.820	1.717
80	458	4	110.00	1.00	4.00E-06	24530.738	2.026	20856.027	1.722
81	462	1	111.00	2.00	5.00E-07	24562.090	2.027	20882.535	1.723
82	463	7	113.00	1.00	7.00E-06	24893.711	2.037	21153.242	1.731
83	470	5	114.00	1.00	5.00E-06	25110.356	2.045	21336.770	1.737
84	475	7	115.00	1.00	7.00E-06	25436.629	2.056	21601.461	1.746
85	482	5	116.00	1.00	5.00E-06	25666.918	2.064	21793.168	1.752
86	487	2	117.00	0.50	4.00E-06	25750.672	2.067	21870.973	1.755
87	489	3	117.50	0.50	6.00E-06	25899.547	2.072	21992.195	1.759
88	492	3	118.00	1.00	3.00E-06	26080.301	2.077	22138.695	1.763
89	495	2	119.00	0.50	4.00E-06	26138.637	2.080	22183.379	1.765
90	497	2	119.50	1.00	2.00E-06	26220.391	2.083	22262.574	1.768
91	499	2	120.50	0.50	4.00E-06	26328.559	2.087	22382.137	1.771
92	501	3	121.00	0.50	6.00E-06	26460.973	2.092	22462.219	1.775
93	504	3	121.50	0.50	6.00E-06	26612.520	2.097	22583.230	1.779
94	507	3	122.00	0.50	6.00E-06	26757.945	2.102	22705.133	1.784
95	510	2	122.50	0.50	4.00E-06	26855.910	2.106	22786.910	1.787
96	512	4	123.00	0.50	8.00E-06	27031.668	2.113	22951.782	1.793
97	516	3	123.50	0.50	6.00E-06	27200.016	2.118	23076.488	1.797
98	519	2	124.00	0.50	4.00E-06	27298.961	2.122	23166.199	1.800
99	521	1	124.50	0.50	2.00E-06	27359.379	2.124	23202.215	1.802
100	522	2	125.00	0.50	4.00E-06	27480.512	2.128	23286.586	1.805
101	524	4	125.50	0.50	8.00E-06	27651.160	2.135	23456.676	1.811
102	528	1	126.00	0.50	2.00E-06	27701.059	2.137	23499.488	1.813
103	529	4	126.50	0.50	8.00E-06	27995.828	2.145	23671.891	1.819
104	533	3	127.00	0.50	6.00E-06	28068.055	2.150	23802.430	1.824
105	536	1	127.50	0.50	2.00E-06	28111.793	2.152	23846.199	1.826
106	537	4	128.00	0.50	8.00E-06	28310.559	2.160	24022.826	1.832
107	541	1	128.50	0.50	2.00E-06	28371.758	2.162	24066.789	1.834
108	542	6	129.00	1.00	6.00E-06	28607.937	2.170	24335.656	1.844
109	548	4	130.00	0.50	8.00E-06	28901.133	2.182	24517.461	1.851
110	552	4	130.50	0.50	8.00E-06	29110.918	2.191	24701.832	1.858
111	556	4	131.00	0.50	8.00E-06	29333.773	2.199	24887.531	1.866
112	560	3	131.50	0.50	6.00E-06	29489.191	2.205	25020.578	1.872
113	563	2	132.00	0.50	4.00E-06	29600.953	2.210	25123.320	1.876
114	565	3	132.50	0.50	6.00E-06	29774.953	2.217	25286.512	1.881
115	568	6	133.00	0.50	1.20E-05	30111.309	2.230	25556.805	1.893

TABLE 8 (cont.)

116	574	2	133.50	0.50	8.00E-06	30228.508	2.238	25658.887	1.897
117	576	1	134.00	0.50	2.00E-06	30291.681	2.237	25704.121	1.899
118	577	3	134.50	0.50	6.00E-06	30353.785	2.243	25752.738	1.905
119	580	6	135.00	0.50	1.20E-05	30720.236	2.267	26158.266	1.917
120	586	2	135.50	0.50	4.00E-06	30910.000	2.282	26256.078	1.921
121	588	2	136.00	0.50	4.00E-06	31033.282	2.287	26359.583	1.925
122	590	5	136.50	0.50	1.00E-05	31328.591	2.279	26617.707	1.936
123	595	6	137.00	0.50	1.20E-05	31606.609	2.293	26838.436	1.944
124	601	2	137.50	0.50	4.00E-06	31909.703	2.298	27081.881	1.953
125	603	5	138.00	0.50	1.00E-05	32115.152	2.311	27312.219	1.965
126	608	5	138.50	0.50	1.00E-05	32362.305	2.321	27530.211	1.975
127	612	3	139.00	0.50	6.00E-06	32549.297	2.329	27690.246	1.982
128	615	6	139.50	0.50	1.20E-05	32927.602	2.344	28030.738	1.996
129	621	3	140.00	0.50	6.00E-06	33119.906	2.352	28211.238	2.004
130	624	4	140.50	0.50	8.00E-06	33370.293	2.363	28444.215	2.014
131	628	6	141.00	0.50	1.20E-05	33767.313	2.379	28800.223	2.029
132	634	7	141.50	0.50	1.40E-05	34231.129	2.399	29235.867	2.048
133	641	3	142.00	0.50	6.00E-06	34432.477	2.407	29411.613	2.056
134	644	5	142.50	0.50	1.00E-05	34771.531	2.422	29726.641	2.071
135	649	5	143.00	0.50	1.00E-05	35114.941	2.436	30047.727	2.085
136	654	6	143.50	0.50	1.20E-05	35533.926	2.454	30441.676	2.102
137	660	5	144.00	0.50	1.00E-05	35866.223	2.469	30777.469	2.118
138	665	2	144.50	0.50	4.00E-06	36028.836	2.475	30913.754	2.124
139	667	9	145.00	0.50	1.80E-05	36679.711	2.503	31541.579	2.152
140	676	6	145.50	0.50	1.20E-05	37122.129	2.522	31973.898	2.172
141	682	9	146.00	0.50	1.80E-05	37720.762	2.551	32544.383	2.203
142	691	5	146.50	0.50	1.00E-05	38181.539	2.568	33029.918	2.221
143	696	5	147.00	0.50	1.00E-05	38569.293	2.595	33422.539	2.240
144	701	9	147.50	0.50	1.80E-05	39269.023	2.615	34155.102	2.274
145	710	7	148.00	0.50	1.40E-05	39884.387	2.640	34787.578	2.302
146	717	9	148.50	0.50	1.80E-05	40585.125	2.672	35580.742	2.340
147	726	9	149.00	0.50	1.80E-05	41363.359	2.706	36372.008	2.380
148	735	10	149.50	0.50	2.00E-05	42206.680	2.748	37244.336	2.427
149	745	8	150.00	0.50	1.60E-05	43002.941	2.779	38067.305	2.473
150	754	13	150.50	0.50	2.60E-05	44186.074	2.831	39680.566	2.543
151	767	18	151.00	0.50	3.60E-05	45899.602	2.906	41858.688	2.651
152	785	23	151.50	0.50	4.60E-05	48185.340	3.008	45083.672	2.811

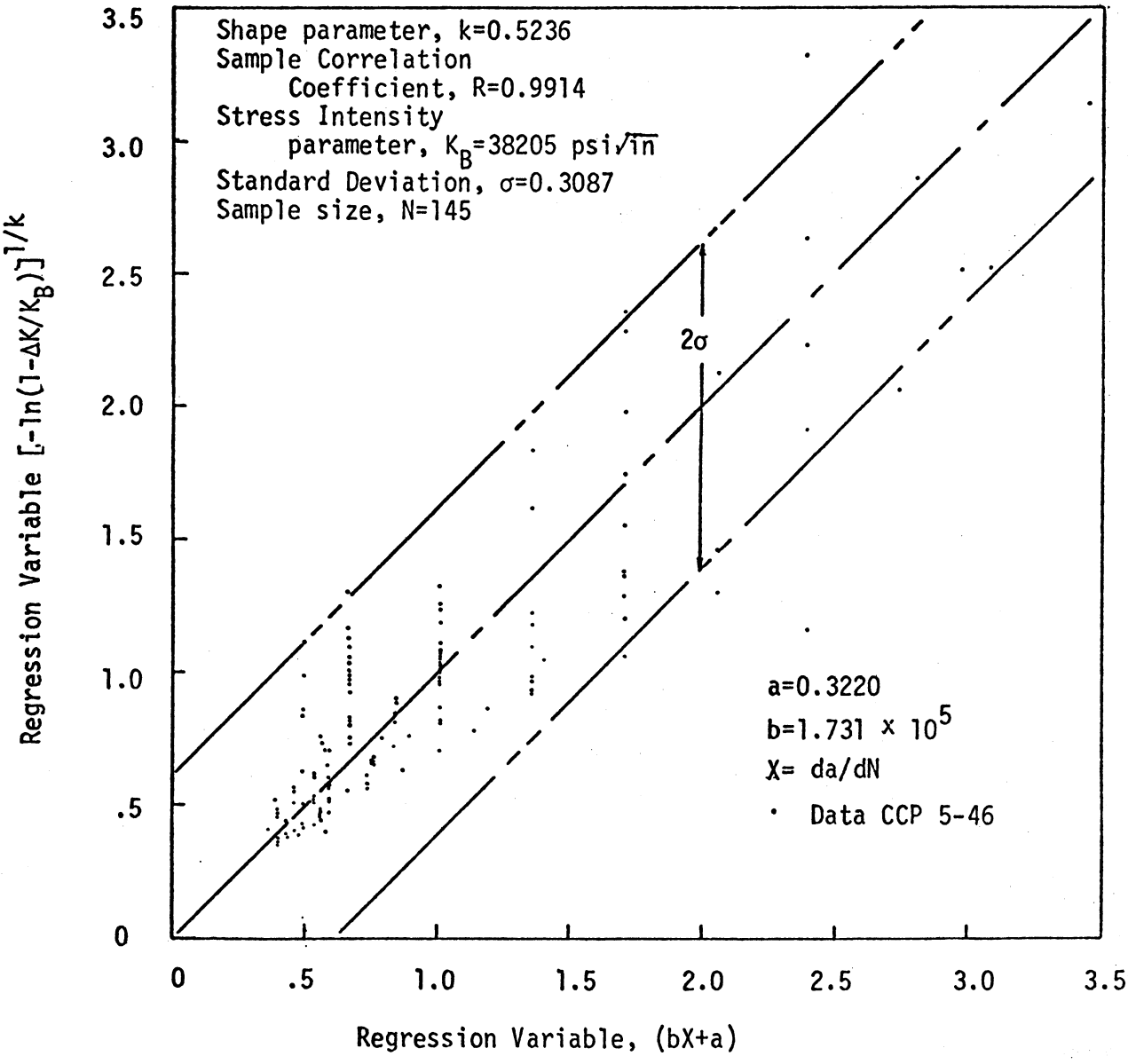

Figure 8. Linear regression of crack growth data for specimen 5-46.

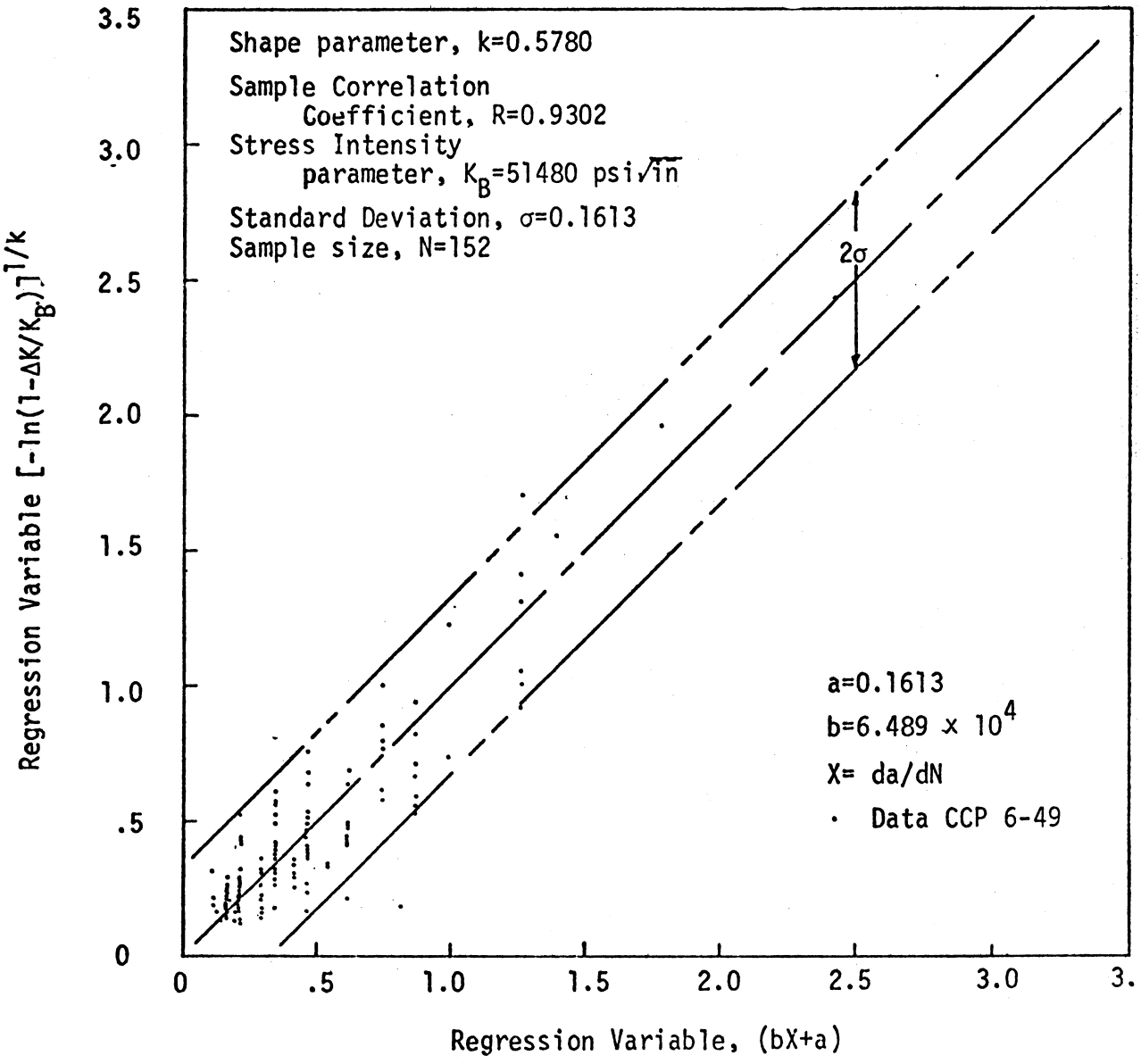

Figure 9. Linear regression of crack growth data for specimen 6-49

is performed in the program "WANKHS" as given in Tables 9 and 10. These curves are shown in Figure 10 comparing the as received and martensitic microstructures.

Conclusions

The preceding method of crack growth data analyses is a relatively simple means by which the compliance and crack growth characteristics may be exemplified and combined to establish a curve fitting procedure for crack growth rate data. It has been established [4] that this analysis for compliance data provides a better fit to actual data than the polynomial as given in equation (3). In addition, this technique provides a much more adequate curve fit for crack growth rate data than other proposed equations such as the one in equation (10).

TABLE 9

PROGRAM "WANKHS" FOR SPECIMEN 5-46

```
ENTER 1 IF AN EXPLANATION OF THE PROGRAM IS DESIRED, 0 IF NOT
:
1
WEIBULL'S 4 PARAMETER FIT FOR THIS APPLICATION IS
1-(DK/KB)=EXP(-((DX/X-E)/(V-E))**K).
IT WILL BE USED IN THE FORM Y=MX+B,
(-LN(1-(DK/KB)))**1/K=(DX/X)/(V-E)-E/(V-E).
THIS IS SO THAT BY INCREMENTING AND OPTIMIZING KB AND K
LINEAR REGRESSION STATISTICS CAN BE UTILIZED TO FIND E AND V.

SUPPLY THE INITIALIZED KB IN PSI RT.IN.
FOR THIS SET OF DATA THE MINIMUM KB= 38087
:
38195

SUPPLY THE INCREMENTS BY WHICH KB WILL BE INCREASED IN PSI RT.IN.
:
5

SUPPLY THE NUMBER OF TIMES THIS IS TO BE DONE
:
5

W=1/K IS ANOTHER INCREMENTED WEIBULL PARAMETER,
SUPPLY THE MINIMUM W FROM WHICH THE PROGRAM WILL START
:
1

SUPPLY THE NUMBER OF TIMES TO INCREASE W BY .01
:
100

 J     KB     I   BEST R  BEST W      K           E           V           M           B          STD
 1   38200   90  0.99138   1.90   5.263E-01  -1.880E-06  3.917E-06  1.725E+05  3.203E-01  3.176E-
 2   38205   91  0.99139   1.91   5.236E-01  -1.860E-06  3.910E-06  1.731E+05  3.220E-01  3.087E-
 3   38210   92  0.99139   1.92   5.208E-01  -1.838E-06  3.913E-06  1.737E+05  3.196E-01  3.099E-
 4   38215   93  0.99139   1.93   5.181E-01  -1.815E-06  3.913E-06  1.746E+05  3.169E-01  3.112E-
 5   38220   94  0.99139   1.94   5.155E-01  -1.790E-06  3.911E-06  1.756E+05  3.140E-01  3.127E-

ENTER 1 FOR NEW VALUES AND RANGES OF KB AND W, 0 TO CONTINUE
:
0
ENTER 1 IF A DEFINITION OF THE VARIABLES IS DESIRED, 0 IF NOT
:
1
J IS A COUNTER FOR KB
KB IS AN INCREMENTED WEIBULL PARAMETER
I IS THE NUMBER OF THE BEST R
BEST R IS THE BEST CORRELATION COEFFICIENT
THAT HAS BEEN CALCULATED FOR INCREMENTED W
BEST W IS AN INCREMENTED WEIBULL PARAMETER=1/K
IT HAS THE BEST CORRELATION COEFFICIENT OF ALL THOSE CHECKED
K,E,V ARE THE CALCULATED WEIBULL PARAMETERS
M IS THE SLOPE OF THE REGRESSION LINE
B IS THE VERTICAL INTERCEPT OF THE REGRESSION LINE
STD IS THE STANDARD DEVIATION OF THE REGRESSION LINE
AND AT THIS VERTICAL DISTANCE ABOVE AND BELOW
THE REGRESSION LINE, TWO PARALLEL LINES
WILL INCLUDE 68.3% OF THE POINTS.  AT THICK
THIS DISTANCE, 95.4% OF THE POINTS ARE INCLUDED
AND AT THREE TIMES THIS DISTANCE 99.7%
OF THE POINTS ARE INCLUDED WHICH IS
KNOWN AS A THREE SIGMA BAND
```

TABLE 9 (cont.)

```
ENTER 1 IF DA/DI AND THE REGRESSION VARIABLES ARE
TO BE INCREMENTALLY CALCULATED AND LISTED,  0 IF NOT
:
0
ENTER 1 IF THE REDUCED WEIBULL VARIATE Z AND THE REGRESSION VARIABLES,
ARE TO BE LISTED OUT, 0 IF NOT
:
1
Z IS CALCULATED AS, Z=(Y-E)/(V-E),
WHERE  Y=DA/DI.
THE PROBABILITY OF SURVIVAL FUNCTION IS EXPRESSED
AS P1(I)=EXP((-Z(I))**K), AND
P2(I)=(1-DK(I)/KB).

THE REGRESSION VARIABLES ARE
Y=-LN(1-DK/KB)**1/K
YY=LN*(DA/DI)+B

SUPPLY KB,K,E,V,M,B TO BE USED IN THE EQUATIONS
:
38205 5.236e-01 -1.860e-06 3.916e-06 1.731e+05 3.220e-01

ENTER 1 IF EVERY DA/DI POINT FROM THE DATA IS TO BE USED
ENTER 2 IF EVERY OTHER DA/DI IS TO BE USED
ENTER 3 FOR EVERY THIRD, ETC.
:
1
```

DA/DI (IN./CYCLE)	DK (PSI.SQ.IN.)	Z VARIATE	P1	P2	Y	YY
4.000E-07	16943.691	3.913E-01	0.5428	0.5509	3.552E-01	3.912E-01
4.000E-07	16934.759	3.913E-01	0.5428	0.5509	3.548E-01	3.912E-01
4.000E-07	17000.813	3.913E-01	0.5428	0.5559	3.636E-01	3.912E-01
4.000E-07	17076.391	3.913E-01	0.5428	0.5559	3.677E-01	3.912E-01
9.000E-07	17248.238	4.777E-01	0.5078	0.5405	3.776E-01	4.777E-01
5.000E-07	17343.578	4.006E-01	0.5343	0.5460	3.831E-01	4.006E-01
6.000E-07	17400.852	4.259E-01	0.5275	0.5445	3.864E-01	4.259E-01
6.000E-07	17458.188	4.259E-01	0.5275	0.5430	3.898E-01	4.259E-01
5.000E-07	17515.566	4.259E-01	0.5275	0.5415	3.931E-01	4.259E-01
1.400E-06	17669.785	5.643E-01	0.4765	0.5300	4.011E-01	5.643E-01
8.000E-07	17726.672	4.605E-01	0.5136	0.5360	4.058E-01	4.605E-01
2.000E-07	17745.906	3.566E-01	0.5503	0.5355	4.070E-01	3.566E-01
8.000E-07	17823.008	4.605E-01	0.5136	0.5335	4.117E-01	4.605E-01
8.000E-07	17900.277	4.605E-01	0.5136	0.5315	4.164E-01	4.605E-01
1.000E-06	17997.148	4.952E-01	0.5005	0.5280	4.225E-01	4.951E-01
6.000E-07	18055.418	4.259E-01	0.5275	0.5270	4.261E-01	4.259E-01
1.000E-06	18152.828	4.952E-01	0.5005	0.5240	4.323E-01	4.951E-01
6.000E-07	18211.830	4.259E-01	0.5275	0.5233	4.361E-01	4.259E-01
1.200E-06	18329.070	5.299E-01	0.4882	0.5202	4.437E-01	5.297E-01
1.800E-06	18467.066	5.643E-01	0.4765	0.5165	4.528E-01	5.643E-01
1.400E-06	18605.938	5.643E-01	0.4765	0.5130	4.621E-01	5.643E-01
4.000E-07	18685.766	3.913E-01	0.5428	0.5120	4.668E-01	3.912E-01
1.400E-06	18785.625	5.643E-01	0.4765	0.5083	4.767E-01	5.643E-01
1.600E-06	18967.137	5.999E-01	0.4655	0.5031	4.859E-01	5.999E-01
4.000E-07	18987.688	3.913E-01	0.5428	0.5030	4.868E-01	3.912E-01
1.400E-06	19130.316	5.643E-01	0.4765	0.4993	4.966E-01	5.643E-01
1.000E-06	19232.508	4.952E-01	0.5005	0.4966	5.060E-01	4.951E-01
1.200E-06	19294.738	5.297E-01	0.4882	0.4950	5.105E-01	5.297E-01
1.600E-06	19377.563	5.999E-01	0.4655	0.4928	5.166E-01	5.999E-01
8.000E-07	19419.105	4.605E-01	0.5136	0.4917	5.197E-01	4.605E-01
1.600E-06	19502.563	5.999E-01	0.4655	0.4895	5.260E-01	5.999E-01
1.600E-06	19586.832	5.999E-01	0.4655	0.4873	5.323E-01	5.999E-01
4.000E-07	19607.855	3.913E-01	0.5428	0.4868	5.339E-01	3.912E-01
1.200E-06	19679.730	5.297E-01	0.4882	0.4851	5.397E-01	5.297E-01
1.200E-06	19734.262	5.299E-01	0.4882	0.4835	5.436E-01	5.297E-01

TABLE 9 (cont.)

2.000E-06	19840.730	6.683E-01	0.4459	0.4607	5.519E-01	6.683E-01
8.000E-07	19883.520	4.695E-01	0.5136	0.4796	5.553E-01	4.695E-01
2.400E-06	20012.698	7.375E-01	0.4263	0.4762	5.655E-01	7.375E-01
1.600E-06	20099.367	5.990E-01	0.4655	0.4739	5.725E-01	5.990E-01
8.000E-07	20142.926	4.695E-01	0.5136	0.4728	5.760E-01	4.695E-01
1.600E-06	20230.406	5.990E-01	0.4655	0.4705	5.832E-01	5.990E-01
2.400E-06	20362.656	7.375E-01	0.4263	0.4670	5.941E-01	7.375E-01
1.600E-06	20451.520	5.990E-01	0.4655	0.4647	6.016E-01	5.990E-01
1.200E-06	20518.516	5.297E-01	0.4882	0.4629	6.073E-01	5.297E-01
2.400E-06	20653.523	7.375E-01	0.4263	0.4594	6.189E-01	7.374E-01
1.200E-06	20721.523	5.297E-01	0.4882	0.4576	6.248E-01	5.297E-01
3.200E-06	20904.543	8.760E-01	0.3938	0.4529	6.410E-01	8.759E-01
1.000E-06	20950.684	4.952E-01	0.5005	0.4516	6.451E-01	4.951E-01
2.500E-06	21066.762	7.584E-01	0.4219	0.4486	6.556E-01	7.587E-01
1.500E-06	21136.895	5.817E-01	0.4729	0.4463	6.620E-01	5.816E-01
2.500E-06	21254.625	7.584E-01	0.4219	0.4437	6.729E-01	7.587E-01
2.500E-06	21373.430	7.584E-01	0.4219	0.4406	6.841E-01	7.587E-01
1.000E-06	21421.238	4.952E-01	0.5005	0.4393	6.886E-01	4.951E-01
4.000E-06	21614.348	1.015E+00	0.3651	0.4383	7.072E-01	1.015E+00
1.500E-06	21687.520	5.817E-01	0.4729	0.4323	7.188E-01	5.816E-01
3.000E-06	21835.195	8.814E-01	0.4011	0.4305	7.261E-01	8.813E-01
2.000E-06	21909.613	6.683E-01	0.4459	0.4295	7.366E-01	6.682E-01
1.330E-06	21959.504	5.523E-01	0.4806	0.4282	7.417E-01	5.522E-01
2.670E-06	22059.883	7.843E-01	0.4186	0.4256	7.520E-01	7.842E-01
3.330E-06	22186.512	8.805E-01	0.3865	0.4193	7.655E-01	8.804E-01
1.330E-06	22237.523	5.522E-01	0.4806	0.4179	7.705E-01	5.522E-01
2.000E-06	22314.434	6.683E-01	0.4459	0.4159	7.787E-01	6.682E-01
4.670E-06	22495.801	1.131E+00	0.3483	0.4112	7.993E-01	1.130E+00
2.000E-06	22568.117	6.683E-01	0.4459	0.4099	8.040E-01	6.682E-01
3.000E-06	22687.906	8.814E-01	0.4011	0.4077	8.127E-01	8.813E-01
2.000E-06	22679.879	6.683E-01	0.4459	0.4066	8.186E-01	6.682E-01
4.000E-06	22786.324	1.015E+00	0.3651	0.4035	8.305E-01	1.015E+00
2.000E-06	22839.910	6.683E-01	0.4459	0.4022	8.367E-01	6.682E-01
3.000E-06	22920.727	8.814E-01	0.4011	0.4001	8.460E-01	8.813E-01
1.000E-06	22947.773	4.952E-01	0.5005	0.3994	8.491E-01	4.951E-01
5.000E-06	23083.977	1.186E+00	0.3383	0.3958	8.650E-01	1.185E+00
1.000E-06	23111.410	4.952E-01	0.5005	0.3951	8.682E-01	4.951E-01
4.000E-06	23221.738	1.015E+00	0.3651	0.3922	8.814E-01	1.015E+00
3.000E-06	23305.148	8.814E-01	0.4011	0.3900	8.915E-01	8.813E-01
3.000E-06	23380.145	8.814E-01	0.4011	0.3878	9.017E-01	8.813E-01
6.000E-06	23558.934	1.361E+00	0.3068	0.3834	9.228E-01	1.361E+00
2.000E-06	23587.465	6.683E-01	0.4459	0.3826	9.264E-01	6.682E-01
2.000E-06	23616.066	6.683E-01	0.4459	0.3819	9.300E-01	6.682E-01
2.000E-06	23644.730	6.683E-01	0.4459	0.3811	9.336E-01	6.682E-01
2.000E-06	23673.473	6.683E-01	0.4459	0.3804	9.373E-01	6.682E-01
6.000E-06	23760.102	1.361E+00	0.3068	0.3781	9.484E-01	1.361E+00
2.000E-06	23789.125	6.683E-01	0.4459	0.3773	9.521E-01	6.682E-01
4.000E-06	23847.379	1.015E+00	0.3651	0.3758	9.597E-01	1.015E+00
6.000E-06	23935.281	1.361E+00	0.3068	0.3735	9.712E-01	1.361E+00
4.000E-06	23994.256	1.015E+00	0.3651	0.3720	9.790E-01	1.015E+00
6.000E-06	24083.254	1.361E+00	0.3068	0.3696	9.909E-01	1.361E+00
1.000E-06	24113.086	4.952E-01	0.5005	0.3689	9.950E-01	4.951E-01
2.000E-06	24142.961	6.683E-01	0.4459	0.3681	9.990E-01	6.682E-01
4.000E-06	24202.969	1.015E+00	0.3651	0.3665	1.007E+00	1.015E+00
4.000E-06	24263.285	1.015E+00	0.3651	0.3649	1.015E+00	1.015E+00
4.000E-06	24323.898	1.015E+00	0.3651	0.3633	1.023E+00	1.015E+00
4.000E-06	24384.804	1.015E+00	0.3651	0.3617	1.032E+00	1.015E+00
4.000E-06	24446.075	1.015E+00	0.3651	0.3601	1.041E+00	1.015E+00
2.000E-06	24476.826	6.683E-01	0.4459	0.3593	1.045E+00	6.682E-01
8.000E-06	24600.605	1.727E+00	0.2663	0.3561	1.063E+00	1.707E+00
2.000E-06	24631.738	6.683E-01	0.4459	0.3553	1.068E+00	6.682E-01
4.000E-06	24694.281	1.015E+00	0.3651	0.3537	1.077E+00	1.014E+00
4.000E-06	24757.195	1.015E+00	0.3651	0.3521	1.086E+00	1.014E+00
4.000E-06	24820.352	1.015E+00	0.3651	0.3505	1.095E+00	1.014E+00
2.000E-06	24852.086	6.683E-01	0.4459	0.3497	1.100E+00	6.682E-01

TABLE 9 (cont.)

6.000E-06	24947.777	1.361E+00	0.3388	0.3470	1.115E+00	1.361E+00
4.000E-06	25012.008	1.015E+00	0.3651	0.3753	1.139E+00	1.015E+00
2.000E-06	25048.250	6.682E-01	0.4459	0.3885	1.139E+00	6.682E-01
1.000E-06	25076.602	4.951E-01	0.5005	0.3836	1.138E+00	4.951E-01
1.200E-05	25272.477	2.809E+00	0.2057	0.3365	1.165E+00	2.309E+00
2.000E-06	25305.434	6.682E-01	0.4459	0.3370	1.170E+00	6.682E-01
6.000E-06	25404.883	1.361E+00	0.3388	0.3359	1.186E+00	1.361E+00
4.000E-06	25471.691	1.015E+00	0.3651	0.3333	1.197E+00	1.015E+00
8.000E-06	25606.313	1.707E+00	0.2663	0.3298	1.219E+00	1.707E+00
6.000E-06	25710.320	1.361E+00	0.3388	0.3271	1.236E+00	1.361E+00
4.000E-06	25776.809	1.015E+00	0.3651	0.3253	1.248E+00	1.015E+00
4.000E-06	25845.699	1.015E+00	0.3651	0.3235	1.260E+00	1.015E+00
1.000E-05	26019.688	2.053E+00	0.2339	0.3189	1.290E+00	2.053E+00
8.000E-06	26160.762	1.707E+00	0.2663	0.3153	1.315E+00	1.707E+00
2.000E-06	26196.270	6.682E-01	0.4459	0.3143	1.322E+00	6.682E-01
4.000E-06	26267.660	1.015E+00	0.3651	0.3125	1.335E+00	1.015E+00
8.000E-06	26411.638	1.707E+00	0.2663	0.3097	1.362E+00	1.707E+00
8.000E-06	26557.469	1.707E+00	0.2663	0.3062	1.389E+00	1.707E+00
2.000E-06	26594.215	6.682E-01	0.4459	0.3053	1.396E+00	6.682E-01
8.000E-06	26742.270	1.707E+00	0.2663	0.3029	1.425E+00	1.707E+00
1.000E-05	26929.840	2.053E+00	0.2339	0.2991	1.463E+00	2.053E+00
6.000E-06	27043.926	1.361E+00	0.3388	0.2981	1.496E+00	1.361E+00
8.000E-06	27197.742	1.707E+00	0.2663	0.2981	1.518E+00	1.707E+00
8.000E-06	27353.473	1.707E+00	0.2663	0.2989	1.552E+00	1.707E+00
6.000E-06	27471.613	1.361E+00	0.3388	0.2989	1.578E+00	1.361E+00
6.000E-06	27599.934	1.361E+00	0.3388	0.2770	1.608E+00	1.361E+00
6.000E-06	27711.438	1.361E+00	0.3388	0.2747	1.632E+00	1.361E+00
8.000E-06	27873.930	1.707E+00	0.2663	0.2738	1.669E+00	1.707E+00
8.000E-06	28032.758	1.707E+00	0.2663	0.2681	1.700E+00	1.707E+00
8.000E-06	28205.777	1.707E+00	0.2663	0.2617	1.739E+00	1.707E+00
1.200E-05	28469.672	2.809E+00	0.2057	0.2551	1.815E+00	2.309E+00
6.000E-06	28599.152	1.361E+00	0.3388	0.2517	1.849E+00	1.361E+00
1.200E-05	28853.270	2.809E+00	0.2057	0.2448	1.921E+00	2.309E+00
8.000E-06	29031.867	1.707E+00	0.2663	0.2401	1.971E+00	1.707E+00
1.400E-05	29351.758	2.746E+00	0.1932	0.2319	2.066E+00	2.746E+00
1.000E-05	29543.684	2.053E+00	0.2339	0.2257	2.130E+00	2.053E+00
1.200E-05	29960.031	2.809E+00	0.2057	0.2152	2.231E+00	2.309E+00
8.000E-06	30062.965	1.707E+00	0.2663	0.2131	2.298E+00	1.707E+00
8.000E-06	30259.918	1.707E+00	0.2663	0.2080	2.368E+00	1.707E+00
1.600E-05	30663.328	3.092E+00	0.1643	0.1974	2.520E+00	3.092E+00
1.200E-05	30974.500	2.809E+00	0.2057	0.1903	2.647E+00	2.309E+00
2.000E-05	31510.625	3.785E+00	0.1383	0.1752	2.896E+00	3.788E+00
1.800E-05	32012.934	3.438E+00	0.1522	0.1621	3.137E+00	3.438E+00
1.200E-05	32353.898	2.809E+00	0.2057	0.1539	3.329E+00	2.309E+00
1.600E-04	38086.598	2.802E+01	0.0033	0.0031	2.949E+01	2.802E+01

TABLE 10

PROGRAM "WANKHS" FOR SPECIMEN 6-49

```
ENTER 1 IF AN EXPLANATION OF THE PROGRAM IS DESIRED, 0 IF NOT
:
1
WEIBULL'S 4 PARAMETER FIT FOR THIS APPLICATION IS
1-(DK/DB)=EXP(-((DA/DC-F)/(V-E)))**(1/K).
IT WILL BE USED IN THE FORM Y=C+B,
(-LN(1-(DK/DB)))**1/K=(DA/DC)/(V-E)-F/(V-E).
THIS IS SO THAT BY INCREMENTING AND OPTIMIZING K AND K
LINEAR REGRESSION STATISTICS CAN BE UTILIZED TO FIND E AND V.

SUPPLY THE INITIALIZED KB IN PSI PT.X,
FOR THIS SET OF DATA THE MINIMUM KB= 51380
:
51450

SUPPLY THE INCREMENTS BY WHICH KB WILL BE INCREASED IN PSI PT.X.
:
10

SUPPLY THE NUMBER OF TIMES THIS IS TO BE DONE
:
6

K=1/K IS ANOTHER INCREMENTED WEIBULL PARAMETER,
SUPPLY THE MINIMUM W FROM WHICH THE PROGRAM WILL START
:
1

SUPPLY THE NUMBER OF TIMES TO INCREASE W BY .01
:
100

 J     KB     I   BEST R  BEST W       K          E          V          M          B          STD
 1   51460   73  0.93022   1.73   5.780E-01  -1.385E-06  1.808E-05  6.501E+08  8.721E-02  1.615E-01
 2   51470   73  0.93022   1.73   5.780E-01  -1.384E-06  1.805E-05  6.805E+08  8.730E-02  1.615E-01
 3   51480   73  0.93023   1.73   5.780E-01  -1.384E-06  1.806E-05  6.809E+08  8.726E-02  1.613E-01
 4   51490   73  0.93022   1.73   5.780E-01  -1.383E-06  1.807E-05  6.803E+08  8.768E-02  1.613E-01


ENTER 1 FOR NEW VALUES AND RANGES OF KB AND W, 0 TO CONTINUE
:
0
ENTER 1 IF A DEFINITION OF THE VARIABLES IS DESIRED, 0 IF NOT
:
1
J IS A COUNTER FOR KB
KB IS AN INCREMENTED WEIBULL PARAMETER
I IS THE NUMBER OF THE BEST R
BEST R IS THE BEST CORRELATION COEFFICIENT
THAT HAS BEEN CALCULATED FROM INCREMENTED W
BEST W IS AN INCREMENTED WEIBULL PARAMETER=1/K
IT HAS THE BEST CORRELATION COEFFICIENT OF ALL THOSE CHECKED
K,E,V ARE THE CALCULATED WEIBULL PARAMETERS
F IS THE SLOPE OF THE REGRESSION LINE
B IS THE VERTICAL INTERCEPT OF THE REGRESSION LINE
STD IS THE STANDARD DEVIATION OF THE REGRESSION LINE
AND AT THIS VERTICAL DISTANCE ABOVE AND BELOW
THE REGRESSION LINE, TWO PARALLEL LINES
WILL INCLUDE 68.3% OF THE POINTS.  AT THIS
THIS DISTANCE, 95.4% OF THE POINTS ARE INCLUDED
AND AT THREE TIMES THIS DISTANCE 99.6%
OF THE POINTS ARE INCLUDED WHICH IS
KNOWN AS A THREE SIGMA BAND

ENTER 1 IF DA/DN AND THE REGRESSION VARIABLES ARE
```

TABLE 10 (cont.)

```
TO BE INCREMENTALLY CALCULATED AND LISTED,  0 IF NOT
:
0
ENTER 1 IF THE REDUCED WEIBULL VARIATE Z AND THE REGRESSION VARIABLES,
ARE TO BE LISTED OUT, 0 IF NOT
:
1
Z IS CALCULATED AS, Z=(X-B)/(V-B),
WHERE  X=DK/DI.
THE PROBABILITY OF SURVIVAL FUNCTION IS EXPRESSED
AS P1(I)=EXP((-Z(I))**K), BUT
P2(I)=(1-DK(I)/KB).

THE REGRESSION VARIABLES ARE
Y=-LN(1-DK/KB)**1/K
YY=M*(DA/DI)+B

SUPPLY KB,K,B,V,M,B TO BE USED IN THE EQUATIONS
:
51830 5.780e-01 -1.389e-06 1.406e-05 6.469e+04 8.750e-02

ENTER 1 IF EVERY DA/DI POINT FROM THE DATA IS TO BE USED
ENTER 2 IF EVERY OTHER DA/DI IS TO BE USED
ENTER 3 FOR EVERY THIRD, ETC.
:
1
```

DA/DI (IN./CYCLE)	DK (PSI.SQ.IN.)	Z VARIATE	P1	P2	Y	YY
1.000E-06	13763.885	1.523E-01	0.7138	0.7326	1.332E-01	1.523E-01
1.500E-06	13906.892	1.618E-01	0.6688	0.7303	1.378E-01	1.618E-01
2.000E-06	14125.932	2.173E-01	0.6611	0.7256	1.398E-01	2.173E-01
8.000E-07	14181.719	1.285E-01	0.7269	0.7245	1.410E-01	1.285E-01
2.000E-06	14321.291	2.173E-01	0.6611	0.7218	1.438E-01	2.173E-01
2.000E-06	14460.969	2.173E-01	0.6611	0.7191	1.467E-01	2.173E-01
3.000E-06	14584.906	2.333E-01	0.6158	0.7175	1.485E-01	2.333E-01
1.000E-06	14600.302	1.523E-01	0.7138	0.7168	1.490E-01	1.523E-01
3.000E-06	14684.905	2.333E-01	0.6188	0.7147	1.514E-01	2.333E-01
1.000E-06	14741.051	1.523E-01	0.7138	0.7137	1.526E-01	1.523E-01
1.000E-06	14769.102	1.523E-01	0.7138	0.7131	1.532E-01	1.523E-01
1.000E-06	14797.152	1.523E-01	0.7138	0.7126	1.538E-01	1.523E-01
6.670E-07	14853.363	1.305E-01	0.7288	0.7115	1.550E-01	1.305E-01
6.000E-06	15022.230	8.769E-01	0.5211	0.7082	1.587E-01	8.769E-01
2.000E-06	15078.635	2.173E-01	0.6611	0.7071	1.599E-01	2.173E-01
1.670E-06	15219.902	1.950E-01	0.6772	0.7044	1.630E-01	1.950E-01
1.000E-06	15248.219	1.523E-01	0.7138	0.7038	1.636E-01	1.523E-01
2.000E-06	15304.683	2.173E-01	0.6611	0.7027	1.648E-01	2.173E-01
1.000E-06	15333.238	1.523E-01	0.7138	0.7022	1.655E-01	1.523E-01
1.500E-06	15418.413	1.808E-01	0.6669	0.7005	1.675E-01	1.808E-01
2.000E-06	15475.301	2.173E-01	0.6611	0.6994	1.687E-01	2.173E-01
1.000E-06	15532.273	1.523E-01	0.7138	0.6983	1.700E-01	1.523E-01
1.000E-06	15560.781	1.523E-01	0.7138	0.6977	1.707E-01	1.523E-01
2.000E-06	15617.875	2.173E-01	0.6611	0.6966	1.720E-01	2.173E-01
3.000E-06	15703.656	2.333E-01	0.6188	0.6950	1.740E-01	2.333E-01
2.000E-06	15760.965	2.173E-01	0.6611	0.6938	1.753E-01	2.173E-01
1.000E-06	15818.363	1.523E-01	0.7138	0.6927	1.766E-01	1.523E-01
8.000E-06	15933.891	3.471E-01	0.5813	0.6905	1.793E-01	3.471E-01
1.000E-06	15962.270	1.523E-01	0.7138	0.6899	1.800E-01	1.523E-01
2.000E-06	16077.285	2.173E-01	0.6611	0.6877	1.826E-01	2.173E-01
1.000E-06	16106.109	1.523E-01	0.7138	0.6871	1.833E-01	1.523E-01
1.000E-06	16135.793	1.523E-01	0.7138	0.6866	1.841E-01	1.523E-01
5.000E-07	16148.813	1.206E-01	0.7456	0.6860	1.848E-01	1.206E-01
1.000E-06	16193.343	1.523E-01	0.7138	0.6850	1.859E-01	1.523E-01
1.100E-05	16515.176	5.018E-01	0.4180	0.6792	1.938E-01	5.018E-01
1.000E-06	16544.555	1.523E-01	0.7138	0.6786	1.951E-01	1.523E-01

TABLE 10 (cont.)

1.000E-06	16573.939	1.528E-01	0.7139	0.6789	1.948E-01	1.528E-01
1.000E-06	16603.439	1.528E-01	0.7139	0.6775	1.956E-01	1.528E-01
1.000E-06	16632.918	1.528E-01	0.7139	0.6760	1.963E-01	1.528E-01
8.000E-06	16660.977	6.067E-01	0.4728	0.6723	2.023E-01	6.067E-01
1.000E-06	16899.762	1.528E-01	0.7139	0.6717	2.030E-01	1.528E-01
1.330E-06	17019.258	1.739E-01	0.6650	0.6694	2.061E-01	1.739E-01
3.000E-06	17139.202	2.822E-01	0.6189	0.6677	2.088E-01	2.822E-01
2.000E-06	17160.822	2.173E-01	0.6611	0.6665	2.100E-01	2.173E-01
1.000E-06	17199.563	1.528E-01	0.7139	0.6659	2.109E-01	1.528E-01
3.000E-06	17290.230	2.822E-01	0.6189	0.6641	2.132E-01	2.822E-01
3.000E-06	17472.617	2.822E-01	0.6189	0.6606	2.180E-01	2.822E-01
5.000E-07	17503.172	1.200E-01	0.7456	0.6600	2.189E-01	1.200E-01
1.000E-06	17533.730	1.528E-01	0.7139	0.6594	2.197E-01	1.528E-01
1.000E-06	17568.359	1.528E-01	0.7139	0.6588	2.205E-01	1.528E-01
1.000E-06	17595.020	1.528E-01	0.7139	0.6582	2.213E-01	1.528E-01
1.000E-06	17625.719	1.528E-01	0.7139	0.6576	2.221E-01	1.528E-01
2.000E-06	17687.262	2.173E-01	0.6611	0.6564	2.238E-01	2.173E-01
7.500E-06	18154.802	5.783E-01	0.4884	0.6474	2.360E-01	5.783E-01
2.000E-06	18217.477	2.173E-01	0.6611	0.6461	2.376E-01	2.173E-01
1.000E-06	18240.316	1.528E-01	0.7139	0.6455	2.385E-01	1.528E-01
6.000E-06	18439.773	4.760E-01	0.5211	0.6410	2.440E-01	4.760E-01
2.000E-06	18503.738	2.173E-01	0.6611	0.6406	2.448E-01	2.173E-01
1.000E-06	18535.797	1.528E-01	0.7139	0.6399	2.457E-01	1.528E-01
2.000E-06	18600.063	2.173E-01	0.6611	0.6387	2.474E-01	2.173E-01
5.000E-06	18751.676	4.120E-01	0.5408	0.6356	2.518E-01	4.120E-01
4.000E-06	18891.930	3.471E-01	0.5813	0.6330	2.555E-01	3.471E-01
2.000E-06	18957.383	2.173E-01	0.6611	0.6318	2.602E-01	2.173E-01
3.000E-06	19055.992	2.822E-01	0.6189	0.6298	2.632E-01	2.822E-01
3.000E-06	19155.125	2.822E-01	0.6189	0.6279	2.662E-01	2.822E-01
1.000E-06	19138.281	1.528E-01	0.7139	0.6273	2.672E-01	1.528E-01
6.000E-06	19388.800	4.760E-01	0.5211	0.6228	2.738E-01	4.760E-01
2.000E-06	19455.699	2.173E-01	0.6611	0.6221	2.755E-01	2.173E-01
2.000E-06	19523.156	2.173E-01	0.6611	0.6208	2.777E-01	2.173E-01
2.000E-06	19659.836	2.173E-01	0.6611	0.6181	2.820E-01	2.173E-01
3.000E-06	19761.270	2.822E-01	0.6189	0.6161	2.852E-01	2.822E-01
4.000E-06	19898.750	3.471E-01	0.5813	0.6135	2.897E-01	3.471E-01
1.000E-06	19933.285	1.528E-01	0.7139	0.6128	2.908E-01	1.528E-01
2.000E-06	20002.551	2.173E-01	0.6611	0.6115	2.931E-01	2.173E-01
5.000E-06	20176.985	4.120E-01	0.5408	0.6081	2.989E-01	4.120E-01
5.000E-06	20353.094	4.120E-01	0.5408	0.6046	3.047E-01	4.120E-01
4.000E-06	20495.293	3.471E-01	0.5813	0.6019	3.095E-01	3.471E-01
3.000E-06	20602.711	2.822E-01	0.6189	0.5998	3.132E-01	2.822E-01
3.000E-06	20710.516	2.822E-01	0.6189	0.5977	3.169E-01	2.822E-01
4.000E-06	20856.023	3.471E-01	0.5813	0.5950	3.220E-01	3.471E-01
5.000E-07	20892.531	1.200E-01	0.7456	0.5942	3.232E-01	1.200E-01
7.000E-06	21150.238	5.815E-01	0.4957	0.5902	3.304E-01	5.815E-01
5.000E-06	21336.770	4.120E-01	0.5408	0.5865	3.381E-01	4.120E-01
7.000E-06	21601.461	5.815E-01	0.4957	0.5828	3.458E-01	5.815E-01
5.000E-06	21793.109	4.120E-01	0.5408	0.5787	3.560E-01	4.120E-01
4.000E-06	21970.873	3.471E-01	0.5813	0.5759	3.569E-01	3.471E-01
6.000E-06	21987.102	4.760E-01	0.5211	0.5739	3.638E-01	4.760E-01
3.000E-06	22109.602	2.822E-01	0.6189	0.5726	3.679E-01	2.822E-01
4.000E-06	22183.379	3.471E-01	0.5813	0.5701	3.715E-01	3.471E-01
2.000E-06	22262.570	2.173E-01	0.6611	0.5675	3.780E-01	2.173E-01
4.000E-06	22342.137	3.471E-01	0.5813	0.5649	3.772E-01	3.471E-01
6.000E-06	22462.219	4.760E-01	0.5211	0.5637	3.810E-01	4.760E-01
6.000E-06	22583.227	4.760E-01	0.5211	0.5613	3.867E-01	4.760E-01
6.000E-06	22705.133	4.760E-01	0.5211	0.5590	3.910E-01	4.760E-01
4.000E-06	22776.906	3.471E-01	0.5813	0.5578	3.950E-01	3.471E-01
8.000E-06	22951.738	6.067E-01	0.4728	0.5582	4.017E-01	6.067E-01
6.000E-06	23076.477	4.760E-01	0.5211	0.5517	4.060E-01	4.760E-01
4.000E-06	23160.195	3.471E-01	0.5813	0.5501	4.108E-01	3.471E-01
2.000E-06	23202.215	2.173E-01	0.6611	0.5493	4.122E-01	2.173E-01
4.000E-06	23286.566	3.471E-01	0.5813	0.5477	4.150E-01	3.471E-01
8.000E-06	23456.676	6.067E-01	0.4728	0.5448	4.230E-01	6.067E-01

TABLE 10 (cont.)

2.000E-06	23899.488	2.173E-01	0.6611	0.5535	8.249E-01	2.173E-01
8.000E-06	23671.991	6.067E-01	0.8729	0.5902	8.323E-01	6.067E-01
6.000E-06	23502.830	8.769E-01	0.5211	0.5376	8.380E-01	8.769E-01
2.000E-06	23846.198	2.173E-01	0.6611	0.5369	8.400E-01	2.173E-01
8.000E-06	24022.826	6.067E-01	0.8729	0.5338	8.479E-01	6.067E-01
2.000E-06	24066.705	2.173E-01	0.6611	0.5325	8.497E-01	2.173E-01
6.000E-06	24335.652	8.769E-01	0.5211	0.5273	8.631E-01	8.769E-01
8.000E-06	24517.861	6.067E-01	0.8729	0.5237	8.705E-01	6.067E-01
8.000E-06	24701.822	6.067E-01	0.8729	0.5202	8.781E-01	6.067E-01
8.000E-06	24887.527	6.067E-01	0.8729	0.5166	8.858E-01	6.067E-01
6.000E-06	25028.574	8.769E-01	0.5211	0.5139	8.917E-01	8.769E-01
8.000E-06	25133.316	3.871E-01	0.5813	0.5120	8.965E-01	3.871E-01
6.000E-06	25266.512	8.769E-01	0.5211	0.5092	9.065E-01	8.769E-01
1.200E-05	25556.095	9.663E-01	0.3088	0.5036	9.211E-01	9.663E-01
4.000E-06	25654.887	3.871E-01	0.5813	0.5017	9.260E-01	3.871E-01
2.000E-06	25708.117	2.173E-01	0.6611	0.5007	9.286E-01	2.173E-01
6.000E-06	25852.739	8.769E-01	0.5211	0.4979	9.362E-01	8.769E-01
1.200E-05	26158.266	9.663E-01	0.3088	0.4929	9.521E-01	9.663E-01
4.000E-06	26256.974	3.871E-01	0.5813	0.4900	9.575E-01	3.871E-01
4.000E-06	26358.583	3.871E-01	0.5813	0.4880	9.639E-01	3.871E-01
1.000E-05	26617.703	7.367E-01	0.8326	0.4839	9.772E-01	7.367E-01
1.200E-05	26934.438	9.663E-01	0.3088	0.4788	9.988E-01	9.663E-01
4.000E-06	27081.838	3.871E-01	0.5813	0.4787	9.991E-01	3.871E-01
1.000E-05	27312.219	7.367E-01	0.8326	0.4695	1.016E+00	7.367E-01
8.000E-06	27532.211	6.067E-01	0.8729	0.4652	1.029E+00	6.067E-01
6.000E-06	27709.282	8.769E-01	0.5211	0.4619	1.039E+00	8.769E-01
1.200E-05	28030.734	9.663E-01	0.3088	0.4553	1.059E+00	9.663E-01
6.000E-06	28211.239	8.769E-01	0.5211	0.4520	1.071E+00	8.769E-01
8.000E-06	28444.215	6.067E-01	0.8729	0.4475	1.085E+00	6.067E-01
1.200E-05	28690.323	9.663E-01	0.3088	0.4406	1.109E+00	9.663E-01
1.400E-05	29225.063	9.951E-01	0.3087	0.4323	1.137E+00	9.960E-01
6.000E-06	29411.813	8.769E-01	0.5211	0.4287	1.150E+00	8.769E-01
1.000E-05	29726.641	7.367E-01	0.8326	0.4220	1.172E+00	7.367E-01
1.000E-05	30087.727	7.367E-01	0.8326	0.4163	1.192E+00	7.367E-01
1.200E-05	30441.676	8.663E-01	0.3988	0.4087	1.221E+00	9.663E-01
1.000E-05	30777.469	7.367E-01	0.8326	0.4021	1.245E+00	7.367E-01
4.000E-06	30917.758	3.871E-01	0.5813	0.3995	1.257E+00	3.871E-01
1.800E-05	31581.566	1.256E+00	0.3106	0.3873	1.312E+00	1.256E+00
1.200E-05	31973.095	9.663E-01	0.3088	0.3739	1.385E+00	9.663E-01
1.800E-05	32684.383	1.256E+00	0.3106	0.3653	1.409E+00	1.256E+00
1.000E-05	33028.910	7.367E-01	0.8326	0.3588	1.445E+00	7.367E-01
1.000E-05	33422.535	7.367E-01	0.8326	0.3508	1.488E+00	7.367E-01
1.800E-05	34156.102	1.256E+00	0.3106	0.3365	1.559E+00	1.256E+00
1.800E-05	34787.570	9.961E-01	0.3087	0.3250	1.620E+00	9.960E-01
1.800E-05	35540.730	1.256E+00	0.3106	0.3096	1.717E+00	1.256E+00
1.800E-05	36372.000	1.256E+00	0.3106	0.2935	1.823E+00	1.256E+00
2.000E-05	37208.336	1.367E+00	0.3090	0.2786	1.930E+00	1.385E+00
1.800E-05	38267.305	1.256E+00	0.3106	0.2567	1.792E+00	1.256E+00
2.600E-05	39689.563	1.775E+00	0.2882	0.2290	1.956E+00	1.775E+00
3.600E-05	41853.688	2.438E+00	0.1886	0.1963	2.877E+00	2.438E+00
4.600E-05	45043.672	3.072E+00	0.1876	0.1252	3.580E+00	3.072E+00

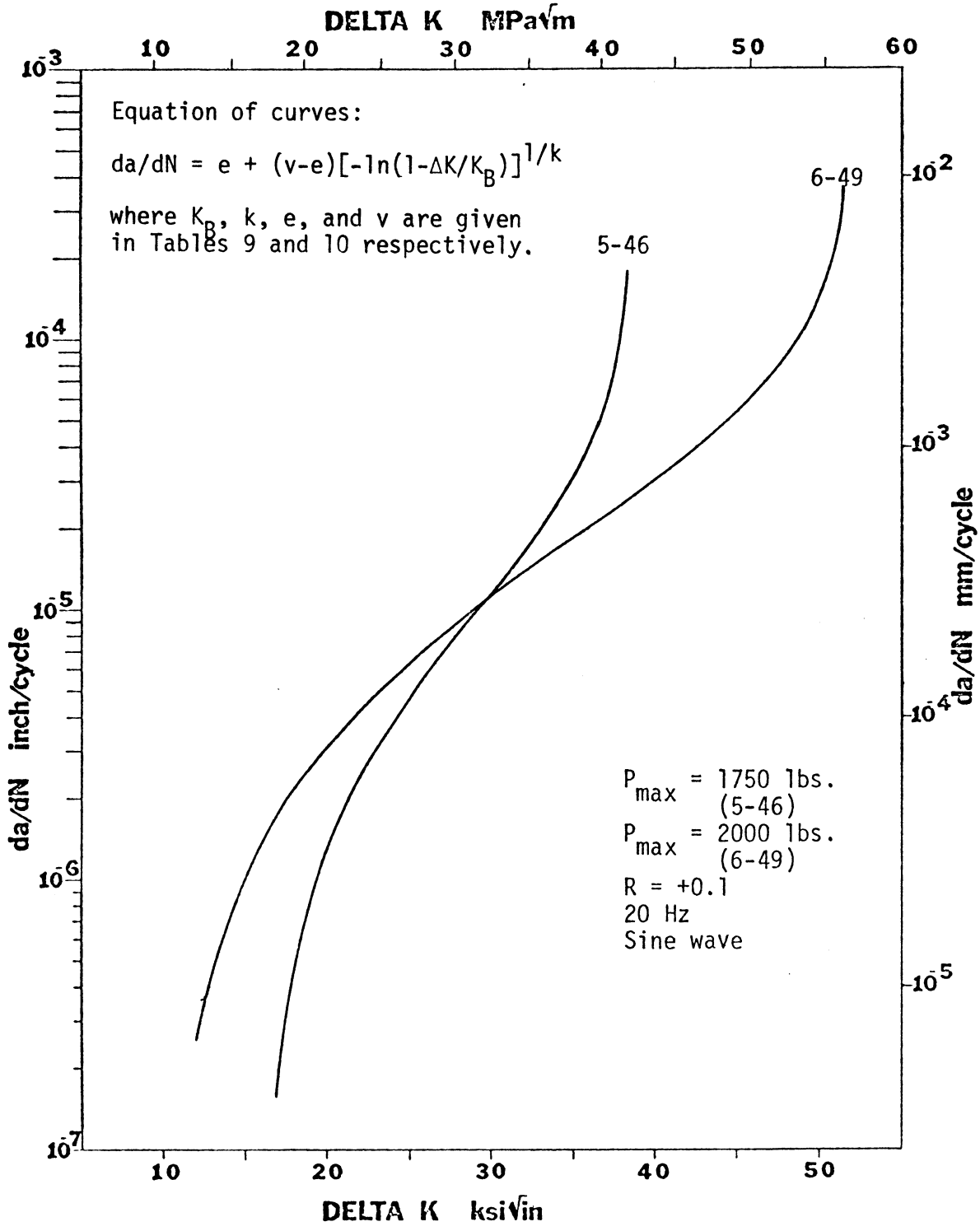

Figure 10. Comparison of crack growth rate characteristics of specimens 5-46 and 6-49.

REFERENCES

1. Brown, W. F. Jr. and Srawley, J. E.; "Plane Strain Crack Toughness Testing of High Stength Metallic Materials", ASTM-STP 410, American Society For Testing Materials, 1966.

2. Brown, W. F.;"Stress Corrosion Cracking in High Strength Steels and in Titanium and Aluminum Alloys", Advanced Research Projects Agency, Naval Research Laboratory, p. 24.

3. Hoeppner, D. W. and Krupp, W. E.; "Prediction of Component Life By Application of Fatigue Crack Growth Knowledge," Engineering Fracture Mechanics, Vol. 6, 1974.

4. Reeves, R. K.; Qualifying examination project, University of Missouri - Columbia, Fall 1974.

APPENDIX 6

STRESS/LIFE DATA FOR
THE .40/.50 CARBON STEEL

AS RECEIVED BASELINE

FATIGUE DATA

Specimen #	Max. Stress (ksi)	Max. Stress (MPa)	N (cycles)
1-04	90	620.8	7,640
1-13	85	586.3	47.520
1-03	80	551.8	138,880
1-05	75	517.4	114,910
1-01	70	482.9	157,150
1-07	67.5	465.6	427,910
1-06	65	448.4	10,006,080NF
1-02	60	413.9	10,000,000NF

AS RECEIVED FRETTING

FATIGUE DATA - AIR

Specimen #	Max. Stress (ksi)	Max. Stress (MPa)	N (cycles)
2-14	85	586.3	6,120
2-12	80	551.8	8,880
2-11	75	517.4	47,370
2-08	70	482.9	52,190
2-10	67.5	465.6	123,230
2-09	65	448.4	387,580
2-15	62.5	431.1	544,220
2-70	60	413.9	304,440
2-71	55	379.4	733,590

AS RECEIVED FRETTING

FATIGUE DATA - VACUUM

Specimen #	Max. Stress (ksi)	Max. Stress (MPa)	N (cycles)
7-56	80	551.8	87,360
7-51	75	517.4	80,010
7-53	70	482.9	309,860
7-52	65	448.4	255,820
7-55	62.5	431.1	554,500
7-58	60	413.9	973,230
7-59	55	379.4	2,371,090

MARTENSITE BASELINE

FATIGUE DATA

Specimen #	Max. Stress (ksi)	Max. Stress (MPa)	N (cycles)
3-19	130	896.7	1,790
3-20	125	862.3	84,290
3-21	120	827.8	29,580
3-22	115	793.3	66,510
3-23	110	758.8	70,050
3-24	105	724.3	198,290
3-26	102.5	707.0	92,980
3-28	100	689.8	127,520
3-29	95	655.3	138,790
3-30	90	620.8	107,130
3-31	85	586.3	150,570
3-33	82.5	569.1	10,248,830NF
3-32	80	551.8	10,012,000NF

MARTENSITE FRETTING

FATIGUE DATA - AIR

Specimen #	Max. Stress (ksi)	Max. Stress (MPa)	N (cycles)
4-37	110	758.8	45,510
4-38	105	724.3	342,250
4-36	100	689.8	121,030
4-39	95	655.3	209,380
4-35	90	620.8	358,970
4-42	87	600.1	109,920
4-40	82.5	569.1	256,770
4-41	80	551.8	1,034,640
4-69	75	517.4	276,590

MARTENSITE FRETTING

FATIGUE DATA - VACUUM

Specimen #	Max. Stress (ksi)	Max. Stress (MPa)	N (cycles)
8-60	95	655.3	260,570
8-61	90	620.8	406,240
8-64	85	586.3	374,770
8-65	82.5	569.1	128,300
8-66	80	551.8	437,260
8-68	75	517.4	2,813,990

APPENDIX 7

CRACK GROWTH DATA FOR THE .40/.50 CARBON STEEL

SPECIMEN # 5-44

Crack Length 2a (in)	Crack Length 2a (mm)	Number of kilocycles
.229	5.82	15
.230	5.84	20
.234	5.94	25
.236	5.99	30
.240	6.10	35
.241	6.12	40
.243	6.17	55
.248	6.30	60
.251	6.38	65
.252	6.40	70
.256	6.50	75
.257	6.53	80
.261	6.63	90
.265	6.73	95
.267	6.78	100
.271	6.88	110
.273	6.93	115
.276	7.01	120
.280	7.11	125
.283	7.19	130
.288	7.32	140
.289	7.34	145

SPECIMEN # 5-44 (cont.)

Crack Length 2a (in)	Crack Length 2a (mm)	Number of kilocycles
.294	7.47	150
.296	7.52	155
.297	7.54	160
.299	7.59	165
.305	7.75	170
.313	7.95	175
.314	7.98	180
.320	8.13	185
.321	8.15	190
.326	8.28	195
.330	8.38	200
.333	8.46	205
.340	8.64	210
.344	8.74	215
.347	8.81	220
.352	8.94	225
.353	8.97	230
.361	9.17	235
.367	9.32	240
.371	9.42	245
.379	9.63	250
.383	9.73	255

SPECIMEN # 5-44 (cont.)

Crack Length 2a (in)	Crack Length 2a (mm)	Number of kilocycles
.387	9.83	260
.395	10.03	265
.403	10.24	270
.410	10.41	275
.416	10.57	280
.422	10.72	285
.431	10.95	290
.439	11.15	295
.448	11.38	300
.457	11.61	305
.465	11.81	310
.472	11.99	315
.486	12.34	320
.498	12.65	325
.511	12.98	330
.523	13.28	335
.539	13.69	340
.557	14.15	345
.572	14.53	350
.598	15.19	355
.610	15.49	357.5
.625	15.88	360

SPECIMEN # 5-44 (cont.)

Crack Length 2a (in)	Crack Length 2a (mm)	Number of kilocycles
.640	16.26	362.5
.658	16.71	365
.678	17.22	367.5
.702	17.83	370
.733	18.62	372.5
.785	19.94	375

SPECIMEN # 5-46

Crack Length 2a (in)	Crack Length 2a (mm)	Number of kilocycles
.230	5.84	10
.234	5.94	20
.238	6.05	30
.242	6.15	40
.251	6.38	50
.256	6.50	60
.259	6.58	65
.262	6.65	70
.265	6.73	75
.272	6.91	80
.276	7.01	85
.277	7.04	90
.281	7.14	95
.285	7.24	100
.290	7.37	105
.293	7.44	110
.298	7.57	115
.301	7.65	120
.307	7.80	125
.314	7.98	130
.321	8.15	135
.323	8.20	140

SPECIMEN # 5-46 (cont.)

Crack Length 2a (in)	Crack Length 2a (mm)	Number of kilocycles
.330	8.38	145
.338	8.59	150
.340	8.64	155
.347	8.81	160
.347	8.81	162.5
.352	8.94	165
.355	9.02	167.5
.359	9.12	170
.361	9.17	172.5
.365	9.27	175
.369	9.37	177.5
.370	9.40	180
.373	9.47	182.5
.376	9.55	185
.381	9.68	187.5
.383	9.73	190
.389	9.88	192.5
.393	9.98	195
.395	10.03	197.5
.399	10.13	200.
.405	10.29	202.5
.409	10.39	205

SPECIMEN # 5-46 (cont.)

Crack Length 2a (in)	Crack Length 2a (mm)	Number of kilocycles
.412	10.46	207.5
.418	10.62	210
.421	10.69	212.5
.429	10.90	215
.431	10.95	217
.436	11.07	219
.439	11.15	221
.444	11.28	223
.449	11.40	225
.451	11.46	227
.459	11.66	230
.462	11.73	231
.468	11.89	233
.471	11.96	234.5
.473	12.01	236
.477	12.12	237.5
.482	12.24	239
.484	12.29	240.5
.487	12.37	242
.494	12.55	243.5
.496	12.60	244.5
.499	12.67	245.5

SPECIMEN # 5-46 (cont.)

Crack Length 2a (in)	Crack Length 2a (mm)	Number of kilocycles
.501	12.73	246.5
.505	12.83	247.5
.507	12.88	248.5
.510	12.95	249.5
.511	12.98	250.5
.516	13.11	251.5
.517	13.13	252.5
.521	13.23	253.5
.524	13.31	254.5
.524	13.31	255
.527	13.39	255.5
.527	13.39	256
.533	13.54	256.5
.534	13.56	257
.535	13.59	257.5
.536	13.61	258
.537	13.64	258.5
.540	13.72	259
.541	13.74	259.5
.543	13.79	260
.546	13.87	260.5
.548	13.92	261

SPECIMEN # 5-46 (cont.)

Crack Length 2a (in)	Crack Length 2a (mm)	Number of kilocycles
.551	14.00	261.5
.551	14.00	262
.552	14.02	262.5
.553	14.05	263
.555	14.10	263.5
.557	14.15	264
.559	14.20	264.5
.561	14.25	265
.563	14.30	265.5
.564	14.33	266
.568	14.43	266.5
.569	14.45	267
.571	14.50	267.5
.573	14.55	268
.575	14.60	268.5
.576	14.63	269
.579	14.71	269.5
.581	14.76	270
.582	14.78	270.5
.582	14.78	271
.583	14.81	271.5
.589	14.96	272

SPECIMEN # 5-46

Crack Length 2a (in)	Crack Length 2a (mm)	Number of kilocycles
.590	14.99	272.5
.593	15.06	273
.595	15.11	273.5
.599	15.21	274
.602	15.29	274.5
.604	15.34	275
.606	15.39	275.5
.611	15.52	276
.615	15.62	276.5
.616	15.65	277
.618	15.70	277.5
.622	15.80	278
.626	15.90	278.5
.627	15.93	279
.631	16.03	279.5
.636	16.15	280
.639	16.23	280.5
.643	16.33	281
.647	16.43	281.5
.650	16.51	282
.653	16.59	282.5
.656	16.66	283

SPECIMEN # 5-46 (cont.)

Crack Length 2a (in)	Crack Length 2a (mm)	Number of kilocycles
.660	16.76	283.5
.664	16.87	284
.668	16.97	284.5
.674	17.12	285
.677	17.20	285.5
.683	17.35	286
.687	17.45	286.5
.694	17.63	287
.699	17.75	287.5
.705	17.91	288
.709	18.01	288.5
.713	18.11	289
.721	18.31	289.5
.727	18.47	290
.737	18.72	290.5
.746	18.95	291
.752	19.10	291.5
.832	21.13	292

SPECIMEN # 6-48

Crack Length 2a (in)	Crack Length 2a (mm)	Number of kilocycles
.233	5.92	10
.236	5.99	15
.244	6.20	20
.250	6.35	25
.252	6.40	30
.261	6.63	35
.266	6.76	37.5
.269	6.83	40
.272	6.91	42.5
.274	6.96	45
.278	7.06	47.5
.280	7.11	50
.286	7.26	52.5
.291	7.39	55
.295	7.49	57.5
.303	7.70	60
.304	7.72	61.5
.309	7.85	63
.311	7.90	64.5
.314	7.98	66
.318	8.08	67.5
.321	8.15	69

SPECIMEN # 6-48

Crack Length 2a (in)	Crack Length 2a (mm)	Number of kilocycles
.323	8.20	70.5
.328	8.33	72
.330	8.38	73.5
.335	8.51	75
.339	8.61	76.5
.342	8.69	78
.345	8.76	79
.348	8.84	80
.350	8.89	81
.352	8.94	82
.355	9.02	83
.357	9.07	84
.364	9.25	85
.369	9.37	88
.370	9.40	89
.372	9.45	90
.376	9.55	91
.379	9.63	92
.382	9.70	93
.385	9.78	94
.388	9.86	95
.391	9.93	96

SPECIMEN # 6-48 (cont.)

Crack Length 2a (in)	Crack Length 2a (mm)	Number of kilocycles
.394	10.01	97
.398	10.11	98
.402	10.21	99
.406	10.31	100
.409	10.39	101
.414	10.52	102
.418	10.62	103
.419	10.64	104
.423	10.74	105
.427	10.85	106
.430	10.92	107
.434	11.02	108
.439	11.15	109
.443	11.25	110
.447	11.35	111
.453	11.51	112
.456	11.58	113
.461	11.71	114
.467	11.86	115
.472	11.99	115.5
.476	12.09	116.5
.478	12.14	117

SPECIMEN # 6-48 (cont.)

Crack Length 2a (in)	Crack Length 2a (mm)	Number of kilocycles
.481	12.22	117.5
.485	12.32	118
.487	12.37	118.5
.489	12.42	119
.493	12.52	119.5
.495	12.57	120
.499	12.67	120.5
.503	12.78	121
.506	12.85	121.5
.509	12.93	122
.513	13.03	122.5
.515	13.08	123
.520	13.21	123.5
.524	13.31	124
.526	13.36	124.5
.530	13.46	125
.536	13.61	125.5
.540	13.72	126
.545	13.84	126.5
.550	13.97	127
.553	14.05	127.5
.558	14.17	128

SPECIMEN # 6-48 (cont.)

Crack Length 2a (in)	Crack Length 2a (mm)	Number of kilocycles
.565	14.35	128.5
.570	14.48	129
.575	14.61	129.5
.580	14.73	130
.587	14.91	130.5
.592	15.04	131
.600	15.24	131.5
.606	15.39	132
.614	15.60	132.5
.622	15.80	133
.631	16.03	133.5
.641	16.28	134
.658	16.71	134.5
.734	18.64	135

SPECIMEN # 6-49

Crack Length 2a (in)	Crack Length 2a (mm)	Number of kilocycles
.231	5.87	5
.239	6.07	10
.244	6.20	12.5
.246	6.25	15
.251	6.38	17.5
.256	6.50	20
.259	6.58	21
.261	6.63	23
.264	6.71	24
.266	6.76	26
.267	6.78	27
.268	6.81	28
.270	6.86	31
.276	7.01	32
.278	7.06	33
.283	7.19	36
.284	7.21	37
.286	7.26	38
.287	7.29	39
.290	7.37	41
.292	7.42	42
.294	7.47	44

SPECIMEN # 6-49 (cont.)

Crack Length 2a (in)	Crack Length 2a (mm)	Number of kilocycles
.295	7.49	45
.297	7.54	46
.300	7.62	47
.302	7.67	48
.304	7.72	50
.308	7.82	51
.309	7.85	52
.313	7.95	54
.314	7.98	55
.315	8.00	56
.316	8.03	58
.317	8.05	59
.328	8.33	60
.329	8.36	61
.330	8.38	62
.331	8.41	63
.332	8.43	64
.340	8.64	65
.341	8.66	66
.345	8.76	69
.348	8.84	70
.350	8.89	71

SPECIMEN # 6-49 (cont.)

Crack Length 2a (in)	Crack Length 2a (mm)	Number of kilocycles
.351	8.92	72
.354	8.99	73
.360	9.14	75
.361	9.17	77
.362	9.19	78
.363	9.22	79
.364	9.25	80
.365	9.27	81
.367	9.32	82
.382	9.70	84
.384	9.75	85
.385	9.78	86
.391	9.93	87
.393	9.98	88
.394	10.01	89
.396	10.06	90
.401	10.19	91
.405	10.29	92
.407	10.34	93
.410	10.41	94
.413	10.49	95
.414	10.52	96

SPECIMEN # 6-49 (cont.)

Crack Length 2a (in)	Crack Length 2a (mm)	Number of kilocycles
.420	10.67	97
.422	10.72	98
.424	10.77	99
.428	10.87	101
.431	10.95	102
.435	11.05	103
.436	11.07	104
.438	11.13	105
.443	11.25	106
.448	11.38	107
.452	11.48	108
.455	11.56	109
.458	11.63	110
.462	11.73	111
.463	11.76	113
.470	11.94	114
.475	12.07	115
.482	12.24	116
.487	12.37	117
.489	12.42	117.5
.492	12.50	118
.495	12.57	119

SPECIMEN # 6-49 (cont.)

Crack Length 2a (in)	Crack Length 2a (mm)	Number of kilocycles
.497	12.62	119.5
.499	12.67	120.5
.501	12.73	121
.504	12.80	121.5
.507	12.88	122
.510	12.95	122.5
.512	13.00	123
.516	13.11	123.5
.519	13.18	124
.521	13.23	124.5
.522	13.26	125
.524	13.31	125.5
.528	13.41	126
.529	13.44	126.5
.533	13.54	127
.536	13.61	127.5
.537	13.64	128
.541	13.74	128.5
.542	13.77	129
.548	13.92	130
.552	14.02	130.5
.556	14.12	131

SPECIMEN # 6-49 (cont.)

Crack Length 2a (in)	Crack Length 2a (mm)	Number of kilocycles
.560	14.22	131.5
.563	14.30	132
.565	14.35	132.5
.568	14.43	133
.574	14.58	133.5
.576	14.63	134
.577	14.66	134.5
.580	14.73	135
.586	14.88	135.5
.588	14.94	136
.590	14.99	136.5
.595	15.11	137
.601	15.27	137.5
.603	15.32	138
.608	15.44	138.5
.612	15.54	139
.615	15.62	139.5
.621	15.77	140
.624	15.85	140.5
.628	15.95	141
.634	16.10	141.5
.641	16.28	142

SPECIMEN # 6-49 (cont.)

Crack Length 2a (in)	Crack Length 2a (mm)	Number of kilocycles
.644	16.36	142.5
.649	16.48	143
.654	16.61	143.5
.660	16.76	144
.665	16.89	144.5
.667	16.94	145
.676	17.17	145.5
.682	17.32	146
.691	17.55	146.5
.696	17.68	147
.701	17.81	147.5
.710	18.03	148
.717	18.21	148.5
.726	18.44	149
.735	18.67	149.5
.745	18.92	150
.754	19.15	150.5
.767	19.48	151
.785	19.94	151.5
.808	20.52	152

University Libraries
University of Missouri

Digitization Information Page

Local identifier Reeves1977

Source information

Format	Book
Content type	Text
Source ID	Gift copy from department; not added to MU collection.
Notes	

Capture information

Date captured	December 2023
Scanner manufacturer	Fujitsu
Scanner model	fi-7460
Scanning system software	ScandAll Pro v. 2.1.5 Premium
Optical resolution	600 dpi
Color settings	8 bit grayscale
File types	tiff
Notes	

Derivatives - Access copy

Compression	Tiff: LZW compression
Editing software	Adobe Photoshop
Resolution	600 dpi
Color	grayscale
File types	pdf created from tiffs
Notes	Images cropped, straightened, brightened Page 155 is missing. Page numbers are slightly cut off on pages 222, 224, 226, 228, 233, 236-238, 241-242, 244-245, 250-251, 253. This reflects the original thesis.